

# Fuoidan degradation by marine bacteria

Andreas Sichert

**Dissertation**

Zur Erlangung des akademischen Grades eines Doktors der Naturwissenschaften

-Dr. rer. Nat.-

Im Fachbereich Geowissenschaften der Universität Bremen

Bremen, Oktober 2019



Die vorliegende Arbeit wurde in der Zeit von November 2016 bis Oktober 2019 an der Universität Bremen durchgeführt. Die Ergebnisse der Arbeit wurden am MARUM Zentrum für marine Umweltwissenschaften und am Max-Planck-Institut für Marine Mikrobiologie erarbeitet und im Rahmen des Programms „International Max Planck Research School for Marine Microbiology“ (MarMic) angefertigt.

Gutachter: Dr. Jan-Hendrik Hehemann

Gutachter: Prof. Dr. Carol Arnosti

## Summary

The oceans are an important carbon sink that have sequestered about half of all anthropogenic CO<sub>2</sub> emissions. Marine carbon cycling is driven by the deposition of photosynthetic micro- and macroalgae in ocean sediments, where carbon is stored over thousands of years. The algal polysaccharide fucoidan is a central molecule in the marine carbon cycle. Fucoidans are considered to be recalcitrant to microbial degradation and may therefore facilitate long-term carbon storage. Yet, factors that render fucoidan recalcitrant against microbial degradation remain unidentified, hampering our understanding of fucoidans in the carbon cycle.

Fucoidans originating from the cell wall of brown algae are often co-extracted with other cell wall components. Those impurities challenge molecular work with fucoidans such as defined enzyme assays. In **Chapter I**, I develop a simple step-wise protocol to purify fucoidans from different brown algae. Contaminating proteins and polysaccharides can be efficiently removed by anion-exchange chromatography. Using mass spectrometry and nuclear magnetic resonance (NMR) analyses, I describe the highly diverse and branched structures of different fucoidans.

In **Chapter II**, I examine how marine bacteria degrade those complex branched polysaccharides. Using genomics, proteomics and biochemistry, I characterize the newly isolated *Verrucomicrobium* ‘*Lentimonas*’ sp. CC4 and show that fucoidan degradation requires highly dedicated pathways of over 100 enzymes covering 20% of the ‘*Lentimonas*’ sp. CC4 proteome. The complexity of these pathways implies that only highly specialized bacteria can effectively degrade fucoidans and gives a clue why it may be recalcitrant.

The proteomic analysis of ‘*Lentimonas*’ sp. CC4 in chapter II suggested that two protein families, S1\_15 and GH29, are key in fucoidan degradation. In **Chapter III**, I biochemically and structurally characterize one S1\_15 sulfatase and one GH29 fucosidase, revealing their exo-enzyme activity and a novel catalytic pair of two aspartate residues. This provides insights into the molecular mechanism of exo-enzymatic fucoidan degradation.

In **Chapter IV**, I trace the dynamics of different polysaccharides during a diatom spring bloom in Helgoland. I found that the dominant bloom-forming diatom *Chaetoceros socialis* secretes fucoidan in dissolved form, which aggregates and accumulates in particles at the end of the bloom. Known enzymes to degrade this polysaccharide are not expressed in the microbial community which indicates that fucoidans are not microbially degraded and act as vector for organic carbon drawdown.

## Summary

To summarize, fucoidans are diverse, highly branched polysaccharides whose degradation requires a large set of enzymes found in very few specialized marine bacteria. Their stability-enhancing properties lead to increased brown algal deposition in coastal sediments and in the open ocean they may act as aggregation nuclei that enhance aggregation and settling of phytoplankton aggregates. Their abundance, recalcitrant nature and stickiness make fucoidans a likely key player in oceanic carbon sequestration.

## Zusammenfassung

Die Ozeane spielen eine wichtige Rolle als Kohlenstoffsенke und haben etwa die Hälfte aller anthropogenen CO<sub>2</sub>-Emissionen dauerhaft gespeichert. Der Kohlenstoffkreislauf im Meer wird durch die Ablagerung von photosynthetischen Mikro- und Makroalgen in Ozeansedimenten angetrieben, in denen Kohlenstoff über Jahrtausende gespeichert werden kann. Das Algenpolysaccharid Fucoïdan ist ein zentrales Molekül im marinen Kohlenstoffkreislauf. Fucoïdane gelten als schwer von Mikroben abbaubar („rekalzitran“t“) und können daher die Langzeitspeicherung von Kohlenstoff erleichtern. Die Faktoren, die Fucoïdan rekalzitran“t machen, sind jedoch groÙtenteils unbekannt, was unser Verständnis der Rolle von Fucoïdanen im Kohlenstoffkreislauf erschwert.

Fucoïdane aus den Zellwänden von Braunalgen werden oft gemeinsam mit anderen Zellwandkomponenten extrahiert. Diese Verunreinigungen erschweren die molekulare Arbeit mit Fucoïdanen, wie zum Beispiel definierte enzymatische Analysen. In **Kapitel I** entwickle ich ein einfaches, schrittweises Protokoll zur Aufreinigung von Fucoïdanextrakten aus diversen Braunalgen. Protein- und Polysaccharidverunreinigungen werden durch Anionenaustauschchromatographie wirksam entfernt. Mithilfe von Massenspektrometrie und Kernspinresonanzanalyse charakterisiere ich verschiedene Fucoïdane und beschreibe ihre diverse und verzweigte Struktur.

In **Kapitel II** untersuche ich, wie marine Bakterien diese komplex verzweigten Polysaccharide abbauen. Basierend auf genomischen, proteomischen und biochemischen Analysen charakterisiere ich das neu isolierte Verrucomicrobium ‘*Lentimonas*’ sp. CC4 und zeige, dass der Fucoïdanabbau hochspezifische Reaktionswege von über einhundert Enzymen erfordert, die 20% des Proteoms von ‘*Lentimonas*’ sp. CC4 ausmachen. Die Komplexität dieser Reaktionswege hat zur Folge, dass nur hochspezialisierte Bakterien Fucoïdane effektiv abbauen können, was die Rekalzitran“z von Fucoïdan erklärt.

Die Proteomanalyse von ‘*Lentimonas*’ sp. CC4 in Kapitel II ergab, dass zwei Proteinfamilien, S1\_15 und GH29, eine Schlüsselrolle im Abbau von Fucoïdan spielen. In **Kapitel III** führe ich die biochemische und strukturelle Charakterisierung einer S1\_15-Sulfatase und einer GH29-Fucosidase durch. Hauptergebnisse dieser Charakterisierung sind die exoenzymatische Aktivität der Enzyme und die Entdeckung von zwei Aspartat-Resten als neuartige katalytische Reste. Dies liefert Einblicke in den molekularen Mechanismus des exoenzymatischen Fucoïdan-Abbaus.

## Zusammenfassung

In **Kapitel IV** verfolge ich die Dynamik verschiedener Polysaccharide während einer Diatomeenblüte bei Helgoland. Die dominante, blütenbildende Kieselalge *Chaetoceros socialis* sondert Fucoidan in gelöster Form ab, das sich zum Ende der Blüte hin in Partikelform aggregiert. Bekannte Enzyme zum Abbau dieses Polysaccharids werden in der mikrobiellen Gemeinschaft nicht exprimiert, was darauf hinweist, dass Fucoidane nicht mikrobiell abgebaut werden und als Vektoren für den organischen Kohlenstoffabbau fungieren.

Zusammenfassend sind Fucoidane diverse, hochgradig verzweigte Polysaccharide, deren Abbau eine große Anzahl von Enzymen erfordert, die in nur sehr wenigen spezialisierten marinen Bakterien zu finden sind. Ihre stabilitätsverbessernden Eigenschaften führen zu einer verstärkten Ablagerung von Braunalgen in Küstensedimenten. Im offenen Ozean können sie als Aggregationsnuklei wirken, die die Aggregation und Ablagerung von Phytoplanktonaggregaten fördern. Ihre Abundanz, Rekalzitranz und Klebrigkeit machen Fucoidane zu einem wahrscheinlichen Hauptakteur der Kohlenstoffbindung im Meer.

### Acknowledgments

First of all, I would like to thank my supervisor Jan-Hendrik Hehemann for mentoring me and for giving me the space to approach this fascinating project in my own way. My sincere thanks to Carol Arnosti for reviewing my thesis and the common passion for polysaccharides and Verrucomicrobia. I am also grateful to Finn Aachmann, H el ene Rogniaux, Marcel Kuypers, Martin Polz for their great advice in my thesis committee meetings.

Many thanks to the members of the Marine Glycobiology group, Stefan, Agata, Tao, Silvia, Nadine, Craig, Melissa, Alek, Tina, Hagen, Jaagni, Mikkel, Nicola, and Guoyin, who were not only very supporting colleagues, but also became friends during the last three years. Also, I have learned to enjoy teaching and closely working with my students Tatjana, Alek, Gregor and Tina. It was great fun teaching you.

I wish to thank Assaf Vardi, who invited me to the mesocosm project in Bergen, where I met Otto Cordero, who invited me to a research stay at MIT. Thanks to funding from “Bremen Idea Out” and the DAAD, I had an amazing time in the Cordero lab and I wish to thank Otto and his entire group for their hospitality.

Thank you to all my co-workers, in particular Manuel Liebeke, Morten Iversen and Bram Vekeman, for all the help and discussions.

Finally, special thanks go to my dear friends and MARMIC class members, Clara, Greta, Dolma, Nina and Candice who made my time in Bremen fun, were always available for a cup of coffee and supported me in every aspect. And of course, thanks to my loving wife Alexandra for your patience and endurance during my PhD times! I am lucky to have you!

## Table of Contents

Summary .....	i
Zusammenfassung.....	iii
Acknowledgments.....	v
Table of Contents .....	vi
Abbreviations.....	viii
List of Figures .....	x
Introduction.....	13
Coastal brown macroalgae as carbon sink .....	13
Phytoplankton and the biological carbon pump.....	14
Bacterial control of carbon export .....	15
The polyanionic polysaccharide fucoidan .....	16
The chemical complexity of polysaccharides challenges their analysis ....	18
Glycoside hydrolases and sulfatases drive the carbon cycle .....	20
The knowledge gap: fucoidan degrading microbes and their enzymes .....	23
Aims and objectives.....	25
Contributions to manuscripts .....	27
Chapter I. Ion-exchange purification and structure of five sulfated fucans from brown algae .....	29
Chapter II. Verrucomicrobia use hundreds of enzymes to digest the algal polysaccharide fucoidan.....	45
Chapter III. Aspartate as novel acid/base catalyst in a marine GH29 fucosidase from ' <i>Lentimonas</i> ' sp. CC4 .....	79



## Table of Contents

Chapter IV. Fuco­se polysaccharide from diatoms may sequester carbon in the ocean .....	101
General Discussion .....	127
Verrucomicrobia are important polysaccharide degraders .....	127
Biotechnological potential of ‘ <i>Lentimonas</i> ’ sp. CC4.....	128
Complete degradation of fucoidan is community controlled.....	130
Fucoidan forms particles in the environment.....	131
Concluding remarks .....	132
Appendix.....	133
Supplementary Figures and Tables for Chapter I .....	133
Supplementary Figures and Tables for Chapter II.....	138
Supplementary Figures and Tables for Chapter III.....	141
Supplementary Figures and Tables for Chapter IV .....	147
References.....	153
Eidesstattliche Erklärung .....	181

## Abbreviations

### Abbreviations

AA	Auxiliary activity
CAZyme	Carbohydrate active enzyme
CBM	Carbohydrate binding domain
CE	Carbohydrate esterase
DOC	Dissolved organic carbon
DOM	Dissolved organic matter
DP	Degree of polymerization
EPS	Extracellular polymeric substance
FCSP	Fucose-containing sulfated polysaccharide
FGE	Formyl-glycine-generating enzyme
FGly	Formyl-glycine
FT-ICR-MS	Fourier-transform ion cyclotron resonance
GC-MS	Gas chromatography with mass spectrometry detection
GDP-fucose	Guanosine diphosphate fucose
GH	Glycoside hydrolase
HMW	High molecular weight
HPAEC-PAD	High performance anion exchange chromatography with pulsed amperometric detection
HPLC	High performance liquid chromatography
IMAC	Immobilized metal affinity chromatography
IM-MS	Ion-mobility mass spectrometry
IPTG	Isopropyl- $\beta$ -D-thiogalactopyranosid

## Abbreviations

IR	Infrared spectroscopy
MAG	Metagenome-assembled genome
Mbp	Megabasepair (unit of length of DNA)
MS/MS	Tandem mass spectrometry
NMR	Nuclear magnetic resonance spectroscopy
NPP	Net primary production
PAPS	3'-Phosphoadenosin-5'-phosphosulfate
pK <sub>a</sub>	Acid dissociation constant
PL	Polysaccharide lyase
PMAA	Partially methylated alditol acetate
pNP- $\alpha$ -L-Fuc	4-Nitrophenyl- $\alpha$ -L-fucopyranoside
pNP-S	4-Nitrophenyl sulfate potassium salt
POC	Particulate organic carbon
POM	Particulate organic matter
TEP	Transparent exopolymer particle

## List of Figures

Figure 1: <b>Fucoidan from the cell wall of brown algae.</b> .....	17
Figure 2: <b>Polysaccharides are the most diverse macromolecule in nature.</b> .....	20
Figure 3: <b>Inverting and retaining mechanism of glycoside hydrolases.</b> .....	22
Figure 4: <b>The transesterification-elimination reaction mechanism of sulfatases.</b> .....	23
Figure 5: <b>Distribution of putative fucoidan-active enzymes in marine bacteria.</b> .....	24
Figure 6: <b>Ion exchange chromatography separates fucoidans according to their sulfate content.</b> .....	42
Figure 7: <b>Quantitative glycan profiling during purification of four different fucoidans.</b>	42
Figure 8: <b>The composition of purified fucoidans is enriched in fucose and sulfate.</b> .....	43
Figure 9: <b>Linkage analysis of five different fucoidans.</b> .....	43
Figure 10: <b>Degradation of complex fucoidans by specialized ‘<i>Lentimonas</i>’ spp.</b> .....	72
Figure 11: <b>‘<i>Lentimonas</i>’ sp. CC4 has a megaplasmid and distinct genetic loci for the degradation of sulfated polysaccharides.</b> .....	73
Figure 12: <b>Differential proteomics reveal pathways for fucoidan degradation.</b> .....	74
Figure 13: <b>Genetic and enzymatic specificity of pathway for diverse fucoidans.</b> .....	75
Figure 14: <b>High metabolic burden to express dedicated pathways for fucoidans including a fucose-specific bacterial microcompartment.</b> .....	76
Figure 15: <b>Verrucomicrobia are abundant and specialized polysaccharide degraders.</b> ...77	
Figure 16: <b>Operon structure for the degradation sulfated fucans.</b> .....	94
Figure 17: <b>Biochemical characterization of 22_GH29.</b> .....	95
Figure 18: <b>Activity of 22_GH29 on fucoidan.</b> .....	97
Figure 19: <b>Size and stability of 22_S1_15.</b> .....	97
Figure 20: <b>Overall structure of 22_GH29 and 21_S1_15.</b> .....	98

Figure 21: **New catalytic pair of 22\_GH29.** .....99

Figure 22: **Schematic overview of the polysaccharide sampling, extraction and analysis.**  
..... 121

Figure 23: **Different polysaccharide structural types are present in HMWDOM and POM and show fluctuations in their abundance during the diatom bloom.** ..... 122

Figure 24: **Enzymatic epitope deletion, substrate concentration effect and reproducibility.**..... 124

Figure 25: **Content and expression of particular CAZymes by marine bacteria during the bloom.**..... 125

Figure 26: **FCSP is produced by diatoms and increases abundance in POM during the bloom.**..... 126



## Introduction

### Coastal brown macroalgae as carbon sink

Commonly known as seaweeds, brown macroalgae form vital and productive ecosystems along the oceans' shores. Most brown algae are sessile on sandy or rocky surfaces, including the bladder wrack *Fucus vesiculosus* which dominates along German coasts. In the Pacific, the giant kelp *Macrocystis pyrifera* forms underwater forests of up to 45 m height. Covering only ~0.4% of the oceans' area, macroalgae account for ~3% of total oceanic production fixing up to 4 g carbon m<sup>-2</sup> day<sup>-1</sup> via photosynthesis, which is equally productive as a terrestrial pine forest (5 g carbon m<sup>-2</sup> day<sup>-1</sup>) (Jackson, 1987; Baldocchi et al., 1997; Field, 1998; Carlos M. Duarte, 2017). Yet, brown algal ecosystems are overlooked, since deep-water macroalgae growing between 60 to 200 m water depth were only recently discovered and their biomass and productivity is largely unknown (Graham et al., 2007). Despite their high productivity and wide distribution, the fate of carbon assimilated by macroalgae is poorly quantified, limiting our understanding of the marine carbon cycle (Krause-Jensen & Duarte, 2016).

Besides sessile brown algae, *Sargassum fluitans* and *S. natans* are prominent free-floating brown algae with an ambivalent ecological role. On the one hand, they are key-stone species that fulfils important roles in their ecosystem, e.g., acting as a nursing home for young turtles. On the other hand, they can form gigantic blooms with detrimental effects on coastal ecosystems (Smetacek & Zingone, 2013). Between 2014 and 2018, eutrophication by run-offs from the Amazon River triggered *Sargassum* blooms spanning almost 9000 km from the Caribbean Sea to the coast of Africa (M. Wang et al., 2019). *Sargassum* uses gas-filled vesicles to float in surface waters and circulates along the Gulf Stream, North Atlantic Current, Azores Current, Canary Current and North Equatorial Current. How the increasing blooms affect the Atlantic ecosystems is barely known. Additionally, currents and storms wash thousands of tons of *Sargassum* biomass onto Caribbean shores clogging fishing nets and requiring extensive clean-up of beaches. This urgently calls for practical solutions to handle increasing bloom biomass such as biorefinement of algal biomass with microbial enzymes into valuable chemicals (Reisky et al., 2019).

In the face of rising atmospheric CO<sub>2</sub> concentrations, brown algae are a comparatively effective carbon sink and are discussed as Blue Carbon strategy to store carbon in the ocean and mitigate climate change (SMITH, 1981; C M Duarte et al., 2005; Krause-Jensen & Duarte,

## Introduction

2016). A aquaculture of *Ecklonia radiata* can sequester 1 kg CO<sub>2</sub> m<sup>-2</sup> yr<sup>-1</sup> and therefore, the active management of macroalgal vegetation would provide a mean to store carbon (Chung et al., 2013). About 50% of macroalgal net primary production (NPP) is stored in coastal shelf areas and 10% of their NPP (a total of 173 TgC yr<sup>-1</sup>) is exported to the deep ocean where carbon is stored for thousands of years (Krause-Jensen & Duarte, 2016). Mechanistically, macroalgae secrete about 20 to 40% of their NPP as dissolved organic matter (DOM) and uprooted thalli can be transported for hundreds of kilometres and directly sink to the deep sea. As a result, *Sargassum spp.* and other brown algae are frequently found below 1000 m in marine sediments. Altogether, macroalgae potentially sequester as much carbon as seagrasses, tidal marches and mangrove forests combined and are therefore integral to future Blue Carbon strategies (Carlos M. Duarte, 2017).

## Phytoplankton and the biological carbon pump

In the open ocean, carbon sequestration is mediated by the growth, aggregation and sinking of phytoplankton cells. Between 25 and 40% of total emitted anthropogenic CO<sub>2</sub> has been transported by phytoplankton from the atmosphere to depths below 1000 m where carbon is stored on a millennial scale (Maier-Reimer et al., 1996; Le Quéré et al., 2018). The major transport process is the so called biological carbon pump, accounting for about 70% of the annual carbon export (Sarmiento & Gruber, 2002; Uta Passow & Carlson, 2012). In the ocean surface, small unicellular phytoplankton photosynthetically fix 50 Gt CO<sub>2</sub> yr<sup>-1</sup> into biomass, of which 2% is exported to the seafloor through phytoplankton aggregation and sinking (Field, 1998; Tréguer et al., 2003). Phytoplankton includes diatoms, and other phototrophic pro- and eukaryotes such as cyanobacteria (*Synechococcus*, *Trichodesmium*), haptophytes (*Emiliania*, *Phaeocystis*) and green algae (*Ostreococcus*). Compared to macroalgae which sequester 10-50% of their NPP, phytoplankton only sequester a minor fraction (2%) of their NPP making the biological carbon pump an inefficient process (Boyd et al., 2019). The factors controlling the growth and sinking of phytoplankton are key to predict carbon export via the biological carbon pump.

The growth of phytoplankton is controlled by the available nutrients, temperature and irradiance resulting in a high spatiotemporal variation of phytoplankton growth. The largest parts of the ocean are referred to as “ocean deserts” as they do not support the growth of phytoplankton due to the lack of essential nutrients such as nitrogen, phosphorus, iron and silica. Often, at least one factor limits the growth of phytoplankton, e.g., iron in the southern



ocean (de Baar et al., 1995). If temperature and nutritional requirements are met, distinct species of phytoplankton begin to bloom (Sverdrup, 1953; Needham & Fuhrman, 2016). For example, in the Northern Atlantic, diatoms bloom when temperatures rise in spring and nutrients like silicate, essential to build up their frustules. Due to the high cell concentration, phytoplankton blooms promote collision and aggregation of cells resulting in high spatiotemporal variability of carbon export.

Sinking of phytoplankton is driven by sticky anionic polysaccharides acting as nucleus for the formation of marine particles. In surface waters, marine particles assemble from the encounter of algal cells, proteins and polysaccharides driven by turbulence or Brownian motion (Chin et al., 1998; Verdugo et al., 2004). Upon reaching a certain density or size, these particles sink and transport fresh photosynthetic material into the deep ocean. Aggregation heavily depends on the ‘stickiness’ of the organic material because increasing stickiness increases the probability of two particles to stick together upon collision (Thomas Kiørboe & Hansen, 1993). Many phytoplankton species, e.g., *Emiliania huxleyi* produce mucus-like transparent exopolymer particles (TEP) (Engel et al., 2004). These TEPs are rich in sticky, hydrogel-forming anionic polysaccharides and act as glue between cells that promotes aggregation and sinking (U. Passow, 2002).

## Bacterial control of carbon export

Bacteria are the master recyclers of phytoplankton derived organic matter, turning the ocean into a big heterotrophic digester (Hedges et al., 2001; Buchan et al., 2014). Bacteria recycle between 30% and 50% of algal NPP, underpinning their importance in the global carbon cycle (Azam & Graf, 1983; Cole et al., 1988; Ducklow et al., 1993). An important food source for bacteria is dissolved organic matter (DOM), which is actively secreted by phytoplankton up to 20 – 50% of their NPP (Mykkestad, 1995; Lihini I. Aluwihare et al., 1997; Biersmith & Benner, 1998). Other mechanisms of DOM release include sloppy feeding by copepods and viral lysis (Lampert, 1978; Strom et al., 1997; T. Kiørboe & Thygesen, 2001; Suttle, 2007).

Bacterial degradation controls the concentration of algal polysaccharides and thus indirectly regulates aggregation and export dynamics. Phytoplankton synthesize a range of different polysaccharides, which constitute between 20-40% of DOM (McCarthy et al., 1996; L I Aluwihare & Repeta, 1999). Following a spring diatom bloom, heterotrophic bacteria express hydrolytic enzymes to degrade algal polysaccharides and additionally, bacteria evolved sophisticated enzymatic machineries to sense, swim towards, colonize and degrade marine

## Introduction

particles (Stocker, 2012; Teeling et al., 2012, 2016; Datta et al., 2016; Unfried et al., 2018). However, polysaccharides are degraded with varying speed by bacterial communities, for example the storage-polysaccharide laminarin is quickly hydrolysed, whereas the sulfated cell-wall polysaccharide fucoidan is hardly hydrolysed (C. Arnosti et al., 2005; Carol Arnosti, 2011; Carol Arnosti et al., 2011). Only polysaccharides that escape fast bacterial degradation such as fucoidan can accumulate in the marine environment. Yet, the factors determining the turn-over of specific polysaccharides are unknown.

## The polyanionic polysaccharide fucoidan

In brown algae, fucoidan is the major component their cell walls conferring their sturdiness, which likely contributes to their potential to sequester carbon. The cell wall of brown algae is a tight network of proteins, minerals, phenolic compounds and different polysaccharides (Deniaud-Bouët et al., 2017). Being constantly exposed to strong forces of waves, brown macroalgae need to balance flexibility and rigidity of their cell walls. Rigid cellulose fibrils are connected via a network of fucoidans and are loosely embedded in a jelly-like matrix of alginate (Figure 1 a,b). Alginate forms hydrogels in combination with calcium ions and regulates the rigidity of the cell wall, likely by cross-linking with phenolic compounds, i.e. phlorotannins. Together, fucoidans and alginate account in approximately equal proportions for up to 45% of the algal dry weight, making them the major structural polysaccharides of brown algae (Deniaud-Bouët et al., 2014). Bacteria such as *Zobellia galactanivoans* can directly digest alginate from the algal tissue, but not fucoidan (Barbeyron, Thomas, et al., 2016; Zhu et al., 2017). Additionally, fucoidan confers a high stability to brown algal cell wall in combustion experiments and thus, fucoidan potentially facilitates export of macroalgal tissue to the deep-sea (Trevathan-Tackett et al., 2015).

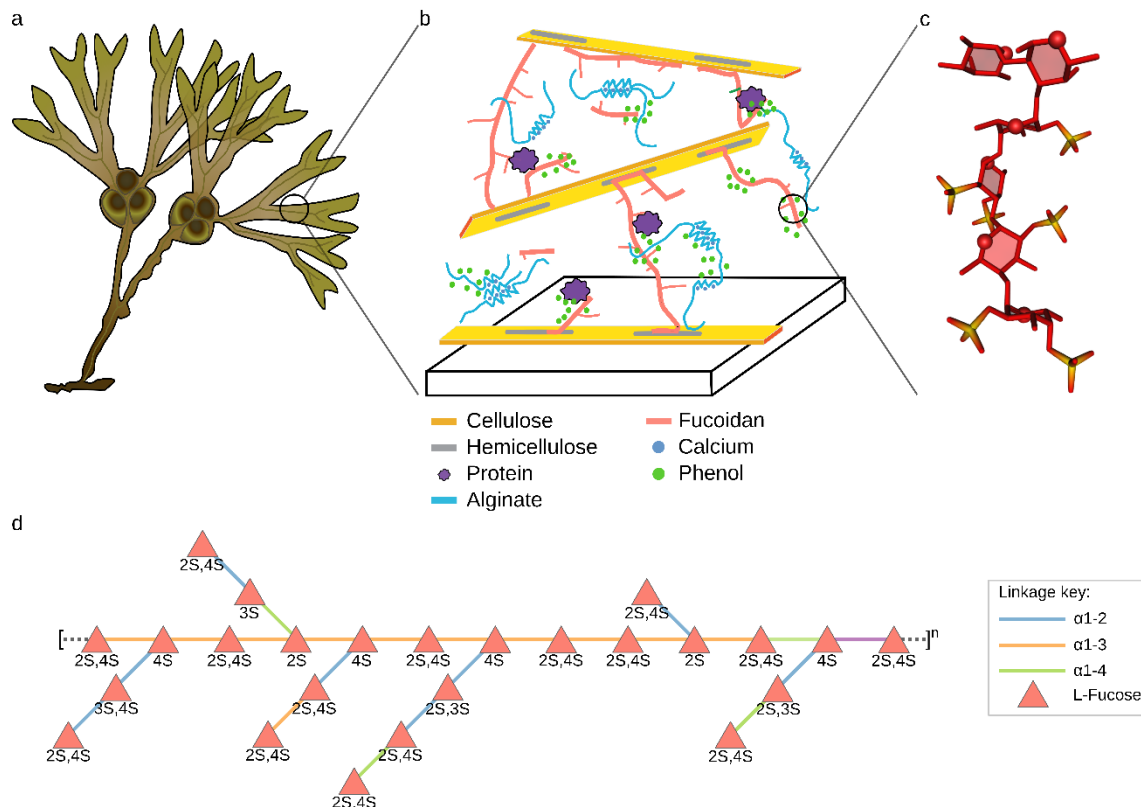


Figure 1: **Fucoindan from the cell wall of brown algae.** **a.** Schematic drawing of the brown algae *Fucus vesiculosus*. **b.** Model of the cell wall architecture from *F. vesiculosus* (Deniaud-Bouët et al., 2014). **c.** The main repeating unit fucoindan from *F. vesiculosus*, the backbone consists of alternated  $\alpha$ -1,3/  $\alpha$ -1,4 linked L-fucose with  $\alpha$ -1,4 L-fucose at C-2 and sulfate at C-2 and/or C-4 (Chevolot et al., 2001). **d.** Model of the macromolecular structure of fucoindan from *Laminaria hyperborea* (Kopplin et al., 2018).

The structure of fucoindan from different brown algae is highly variable making them a diverse class of sulfated polysaccharide. Fucoindans are broadly grouped into homofucans with a purely fucose containing backbone and hetero-polysaccharides with a non-fucose backbone, but side-branches of fucose. The main repeating unit of homofucans from the order of *Laminariales* and *Ectocarpales* such as *Laminaria hyperborea* or *Cladophora okamurans* is  $\alpha$ -1,3 linked L-fucose with sulfate esters at C-4 (Figure 1d) (Nagaoka et al., 1999; Kopplin et al., 2018). Fucoindans from *Fucales* have an alternating  $\alpha$ -1,3/ $\alpha$ -1,4 linked L-fucose backbone with sulfate at C-2 and C-4 (Chevolot et al., 2001). The hetero-fucoindan from *Sargassum fusiforme* has a complex backbone of glucuronic acid, sulfated mannose and sulfated galactose (Bilan et al., 2010). Fucoindans have branches of sulfated fucose and other monosaccharides such as galactose, mannose or glucuronic acid. Additionally, the monosaccharide composition of fucoindans varies between species and season and thus fucoindans comprise a pool of diverse molecules. Due to their complexity, the exact molecular structure of fucoindans is difficult to characterize and most fucoindans are poorly characterized

## Introduction

Not only brown algae produce fucoidans, but also diatoms secrete compounds similar to fucoidan as extracellular polymeric substance (EPS), which increases their stickiness similar to TEP. Diatoms and brown algae are phylogenetic sister groups belonging to the *Stramenopile* and share the production of similar polysaccharides such as the storage glucan (chryso-) laminarin (Paulsen & Myklestad, 1978; Popper et al., 2011; Kadam et al., 2015). Diatoms and brown algae secrete as mucus-like EPS, which is rich in fucose (Jian Zhou et al., 1998; Gogou & Repeta, 2010; Nelson et al., 2013; BP et al., 2015; Gügi et al., 2015; Koch et al., 2019). This EPS is surface active and likely charged, as it can be extracted from diatom cultures with bubble adsorption (Gogou & Repeta, 2010). Yet, the exact structure of diatom fucoidan is not well characterized at a molecular level and might differ from the fucoidan structure of brown algae.

Strictly speaking, it was proposed to use the term fucoidan to denote heteropolysaccharides and to use fucose-containing sulfated polysaccharide (FCSP) as collective term for hetero- and homofucans (Deniaud-Bouët et al., 2017). But a google scholar search (accessed on October 3rd 2019) yielded forty-times more hits for ‘fucoidan’ than for ‘fucose-containing sulfated polysaccharides’ suggests that ‘fucoidan’ as a more effective mean of communication, since it is a more widely hold term. Therefore, I use fucoidan equivalent to FCSP and when appropriate, point out to the reader when I use ‘fucoidan’ to refer to heteropolysaccharides.

## The chemical complexity of polysaccharides challenges their analysis

Polysaccharides are the most diverse macromolecules in nature due to the unique chemistry of monosaccharides. Compared to the 4-letter alphabet of DNA and the 20-letter alphabet of proteins, polysaccharides are build-up from a much larger alphabet of 776 different monosaccharide building blocks (<http://www.monosaccharidedb.org/>, accessed September 27<sup>th</sup> 2019) (Böhm et al., 2019). Many monosaccharides contain additional chemical groups such as carboxyl groups (e.g., glucuronic acid), amino groups (e.g., glucosamine) and acetylation (e.g., N-acetylglucosamine). Usually, hexose sugars have four or five chiral centres and different hexoses can be regarded as permutation of their stereochemical configuration of hydroxy-groups at their chiral centres. For example,  $\alpha$ -L-rhamnose and  $\alpha$ -L-fucose differ in the configuration of the hydroxy groups at C2 and C4, which can be axial or equatorial position of the (Figure 2 a). Glycosidic linkages connect the reducing end i.e. the anomeric carbon with an aldehyde-group to any hydroxy-group of another carbohydrate (Figure 2b). Therefore,

polysaccharides have a directionality from the non-reducing end to the reducing end. The linkage between two monosaccharides can either be in the  $\alpha$ - or  $\beta$ -configuration (Figure 2c) resulting in 12 different possible isomers. Most notable feature of polysaccharides is their ability to form branches, where a monosaccharide is linked to multiple other monosaccharides. As a result, compared to the linear structure of DNA and proteins, carbohydrates are more diverse since they can form orders of magnitudes more different isomers (Figure 2d).

Owing to their chemical complexity, the structure of polysaccharides can only be elucidated by a combination of different methods. The composition of polysaccharides is usually determined via acid hydrolysis, which randomly cleaves polysaccharides into its building blocks such as different monosaccharides, sulfate or acetate for subsequent quantification via HPLC or GC-MS based methods. For example, HPAEC-PAD takes advantage of different  $pK_a$  values of monosaccharides under basic conditions, which enables their separation on an ion-exchange column. Different monosaccharides can be identified and quantified by known reference standards down to 1 to 10  $\mu\text{g L}^{-1}$  (Engel & Händel, 2011). To identify the glycosidic linkages, free hydroxy groups are permethylated, followed by acid hydrolysis and peracetylation (Harris et al., 1984; Morelle et al., 2009). This results in partially methylated alditol acetates (PMAA), where unlinked hydroxy-groups are methylated and hydroxy-groups that originated from a glycosidic linkage are acetylated. Those PMAAs can then be identified by retention time and fragmentation ions ( $m/z$ ) in GC-MS. Notably, both methods are invasive and can neither resolve which monosaccharides are actually linked nor their  $\alpha/\beta$  configuration. The absolute configuration of a glycosidic linkage can only be identified by Nuclear magnetic resonance spectroscopy (NMR) experiments requiring highly pure oligo- or polysaccharides as input.

Due to their high sulfate content, the structural analysis of fucoidans is particularly challenging. Mild acid treatment is frequently used to cleave polysaccharides into smaller oligosaccharides for MS/MS or NMR analysis (Amicucci et al., 2019). However, sulfate esters are more unstable than glycosidic linkages resulting in a de-sulfation of the molecule and loss of chemical information. Also, the common electrospray ionization (ESI) results in loss of sulfate and only soft ionization techniques keep the structure intact (Ropartz et al., 2017). Additionally, sulfate groups mask the signal of the anomeric carbon in NMR experiments, thus, fucoidans are typically chemically desulfated by processes such as solvolytic desulfation which remove the sulfate groups, but leave the glycosidic linkage intact (Usov et al., 1971; Kopplin et al., 2018). Due to this analytical challenge, fucoidan cannot be quantified directly in the

## Introduction

environment, which hampers our understanding of the contribution of fucoidans to the marine carbon cycle.

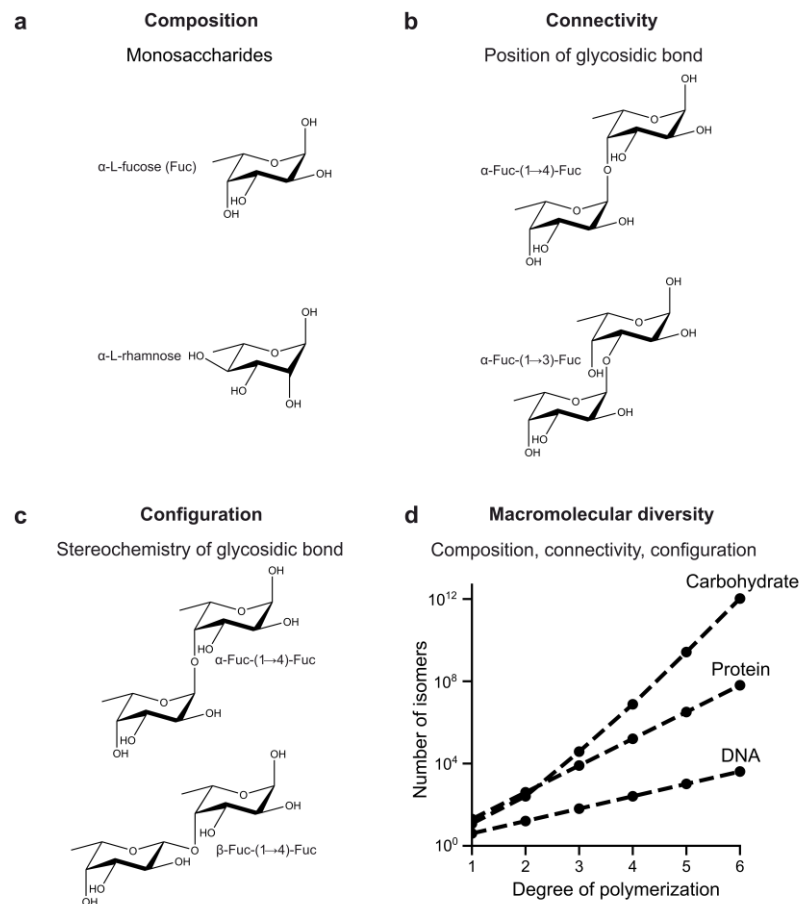


Figure 2: **Polysaccharides are the most diverse macromolecule in nature.** **a.** Polysaccharides are composed of different monosaccharides which differ in the stereochemical orientation of at least one of their carbon atoms as seen for fucose and rhamnose. **b.** A glycosidic linkage connects the keto- or aldehyde of one monosaccharide to one of the hydroxy-group of another monosaccharide. **c.** The glycosidic bond can be configured in  $\alpha$  or  $\beta$ . **d.** Combined, these structural possibilities result in high molecular diversity. Adapted from (Laine, 1994; Hofmann et al., 2015)

## Glycoside hydrolases and sulfatases drive the carbon cycle

Enzymes that cleave glycosidic linkages such as glycoside hydrolases (GH) ‘read’ the structural information of polysaccharides by accommodating specific carbohydrate structures in substrate binding sites. Amino acids with delocalized  $\pi$ -electrons such as histidine and tryptophan form binding sites to bind specific residues of a target carbohydrate structure. Depending on the point of cleavage, substrate binding sites are named from -n to -1 (the new reducing end) and +1 to +n in direction to reducing end (G. J. Davies et al., 1997). Since GHs evolved different substrate binding pockets to accommodate different carbohydrate structures,

GHs are highly substrate specific. Therefore, GHs process polysaccharides in a sequence-specific manner and can be used as tool to produce defined oligosaccharides equivalent to the use of restriction enzymes in molecular biology. For example, heparinases were used to dissect bikunin (a human proteo-polysaccharide) into different oligosaccharides and as result, bikunin could be fully sequenced via FT-ICR-MS/MS (Ly et al., 2012). Furthermore, sequence specific laminarinases can be used to quantify laminarin in environmental samples (Becker et al., 2017). Therefore, glycoside hydrolases are highly relevant for biotechnological applications.

GHs use a conserved hydrolytic mechanism to cleave glycosidic bonds. In their active side, GHs have one catalytic acid/base residue and one base/nucleophile residue, which are typically aspartates or glutamates (G. Davies & Henrissat, 1995). Two slightly different catalytic mechanism hydrolyse the glycosidic linkage (Figure 3). The retaining mechanism has an enzyme-glycosyl intermediate, which dissociates by the attack of a water molecule keeping the original configuration at the anomeric carbon. In an inverting mechanism, a water molecule coordinates a non-covalent enzyme-substrate transition state. Since this water molecule attacks the linkage, the configuration of the anomeric carbon is inverted (Koshland, 1953; Vasella et al., 2002). Depending on the structure of the active side, exo-acting enzymes cleave at the end of a polysaccharide, whereas endo-enzymes cleave in the middle of the chain.

Carbohydrate active enzymes (CAZymes) including the GH are grouped into homologous enzyme families (Lombard, Ramulu, et al., 2014). This differs from the classification by activity, e.g., the E.C. classification. The reason is the complex evolutionary origin of CAZymes. For example, known endo-glucanases have at least nine different folds, suggesting that the endo-glucanase activity evolved independently multiple times in different enzyme super-families (convergent evolution). In contrast, highly identical homologs with the same structure can have different activities and form poly-specific enzyme families (divergent evolution). Poly-specific enzyme families can be further split into monophyletic subfamilies each with a different specificity. For examples, the GH16 comprises 23 different subfamilies including laminarinases, porphyranases and carrageenases (Viborg et al., 2019).

## Introduction

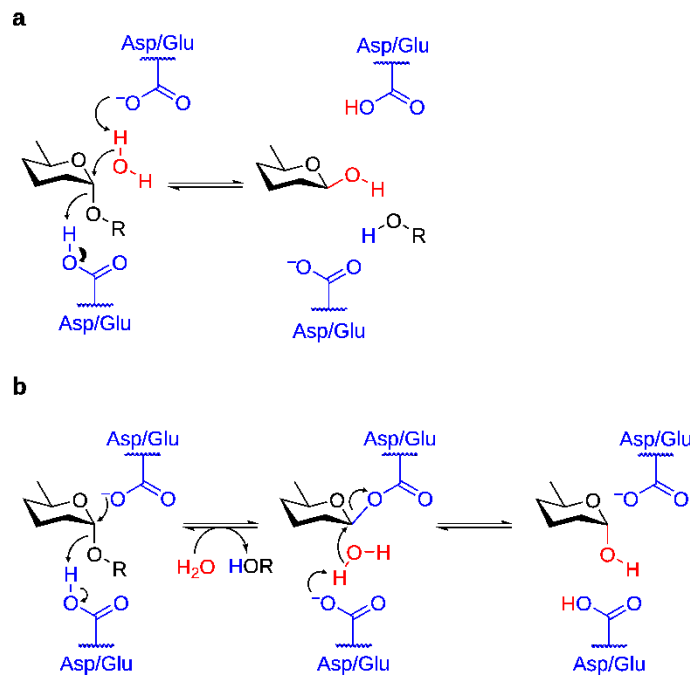


Figure 3: **Inverting and retaining mechanism of glycoside hydrolases.** Both mechanisms use two acidic amino acids as nucleophile or general acid/base. The inverting mechanisms is a one-step reaction in which a water molecule directly attacks the anomeric carbon inverting its configuration. In the retaining mechanism, a covalently bound glycosyl-enzyme intermediate is formed and thus, the subsequent attack of the water molecule retains the original configuration of the anomeric carbon. Adapted from (Koshland, 1953; Vasella et al., 2002).

Next to cleavage of glycosidic linkages, the degradation of sulfated polysaccharides also requires sulfatases to remove sulfate esters from the carbohydrate backbone. In the active site, acidic amino acids such as aspartate and glutamate coordinate a Ca<sup>2+</sup>-ion, which together with positive charge amino acids such as lysine bind the sulfate group. The catalytic residue is a formyl-glycine (FGly) residue, which forms by posttranslational modification of a serine or cysteine. This is catalysed by FGly-generating enzymes (FGE), which also need to be co-expressed for heterologous production of active sulfatases in *E.coli*. Now, it is commonly accepted that the reaction mechanism of sulfatases is a transesterification-elimination and not a hydrolytic mechanism (Chai et al., 1992; Hanson et al., 2004). FGly is a reactive aldehyde and stabilized by two histidine residues to directly attack sulfate ester producing covalently bound sulfate and releasing the carbohydrate. In a second step the intermediate dissociates and a water molecule then restores the hydration state of FGly.

Similar to CAZymes, sulfatases have substrate binding sites to accommodate different carbohydrate backbone structures. In addition to GHs, sulfatases have a 0 subsite that accommodates the carbohydrate carrying the sulfate group (Hettle, Vickers, Robb, Liu, Withers, Hehemann, & Boraston, 2018). With more and more biochemically and structurally



characterized sulfatases, it is now established that sulfatases are as specific to the carbohydrate structures as glycoside hydrolases (Ficko-Blean et al., 2017; Reisky et al., 2019). But unlike CAZymes, most sulfatases share about 20% sequence identity and likely evolved from one ancestral gene and diversified to accommodate different carbohydrate structures (Peters et al., 1990; Barbeyron, Brillet-Guéguen, et al., 2016). Analogous to CAZyme families, sulfatases are split into 74 families based on sequence homology (Barbeyron, Brillet-Guéguen, et al., 2016).

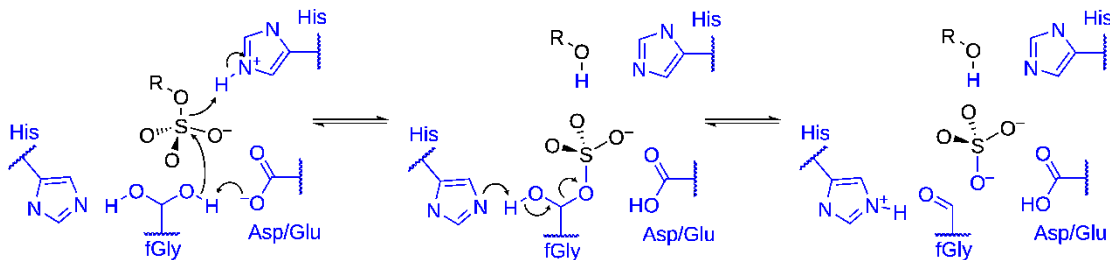


Figure 4: **The transesterification-elimination reaction mechanism of sulfatases.** Hydrated formylglycine (FGly) attacks the sulfate ester cleaving the S-OR bonds and forming a covalently bound sulfate intermediate. The sulfate ion is released after proton transfer from histidine and a water molecule restores the hydration state of FGly. For simplicity, only amino acids residues involved in the catalytical mechanism are shown, modified after (Hanson et al., 2004).

## The knowledge gap: fucoidan degrading microbes and their enzymes

The degradation of fucoidan is a rare trait among marine heterotrophic bacteria. Endo-lytic enzymes that initiate the degradation of fucoidan are almost absent in marine metagenomes (Teeling et al., 2012, 2016). Metagenome-assembled genomes (MAG) of free-living Bacteroidetes are devoid of any capability to process fucoidan, and only a few particle-associated Bacteroidetes encode genes that could be involved in fucoidan degradation (Kappelmann et al., 2019; Krüger et al., 2019). However, successful growth assays of isolated Bacteroidetes on fucoidan are scarce (Barbeyron et al., 2008; A. Silchenko et al., 2013; F Chen et al., 2016). In contrast, reports of fucoidan degrading bacteria from the Planctomycetes-Verrucomicrobia-Chlamydia (PVC) superphylum are surprisingly frequent (Sakai et al., 2003; Ohshiro et al., 2012; van Vliet et al., 2019a). PVC bacteria are thought to be specialized for the degradation of sulfated polysaccharides and it was hypothesized that fucoidan is only accessible to highly specialized bacteria (Glöckner et al., 2003; Wegner et al., 2013; Spring et al., 2016). Yet, none of these bacteria were thoroughly characterized and therefore, we lack a model organism to study fucoidan degradation.

## Introduction

Known CAZymes and sulfatases that act on fucoidan belong to the families CE4, GH29, GH107, S1\_17 and S1\_25. The GH107 is a sulfated fucan endo-1,4-fucanase and produces oligosaccharides from fucoidan (Colin et al., 2006; A. S. Silchenko et al., 2017; Vickers et al., 2018). These are desulfated by S1\_17 and S1\_25, which are exo-2O-sulfatases and exo-3O-sulfatases sequentially acting on 2,3-di-O-sulfated fucose-oligosaccharides (A. S. Silchenko et al., 2018). Acetylation of fucoidan from *Cladosiphon okamurans* are removed by a CE7, yet, the exact linkage of the acetylation was not determined (Nagao et al., 2017). GH29 is an exo-fucosidase using a retaining mechanism to remove fucose from the non-reducing end. The current degradation scheme of fucoidan assumes that the GH107 endo-enzyme produces oligosaccharides which are processed by a series of exo-enzymes.

The recent structure of fucoidan from *Laminaria hyperborea* (Figure 1d) revealed that the degradation of fucoidan must be more complex than previously thought. The backbone is heavily branched and thus, endo-enzymes such as GH107 cannot initiate the degradation. Therefore, exo-acting enzymes must de-branch the substrate. Fucoidan degrading bacteria encode many copies of exo-fucosidases such as GH29, GH95 and GH141 (Figure 5), suggesting that these are involved in debranching fucoidan. Yet, most GH29, GH95 and GH141 are characterized acting on unsulfated plant or human carbohydrates and leaving their exact function for fucoidan degradation unknown.

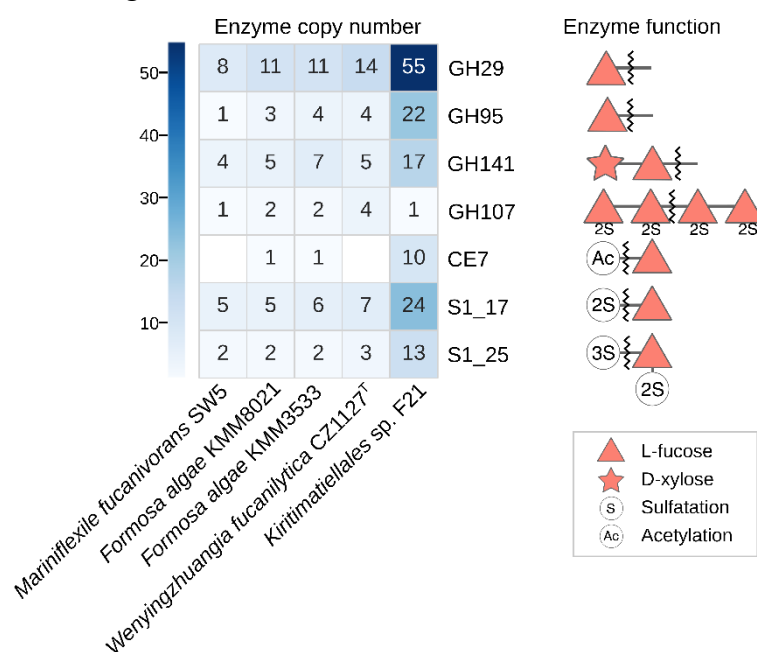


Figure 5: **Distribution of putative fucoidan-active enzymes in marine bacteria.** Currently, only five genome sequenced bacteria are confirmed to degrade fucoidan. The heatmap shows the number of CAZymes and sulfatases that are associated with the degradation of fucoidans in those bacteria. The schematic drawing on left illustrates the putative enzymatic function.

## Aims and objectives

In this thesis, I want to understand the role of the algal polysaccharide fucoidan in the global carbon cycle. More specifically:

### 1. Establish purification methods for fucoidan

Impurities of commercially available fucoidan products hamper defined molecular work. Therefore, we developed a simple protocol for medium scale purification of fucoidans from different brown algae. This would enable standardized work with fucoidan.

### 2. Fucoidan metabolism of '*Lentimonas*' sp. CC4

Here, I aim to identify the factors that render fucoidans recalcitrant to bacterial degradation. Therefore, I characterized the newly isolated *Verrucomicobium* '*Lentimonas*' sp. CC4 and use a combination of genomics, proteomics, metabolomics and biochemical experiments to characterize fucoidan degradation pathways. These insights will explain the recalcitrant of fucoidan to microbial degradation in the environment.

### 3. Structural and biochemical characterization of fucoidan degrading enzymes

Detailed understanding of enzymes of degrading algal polysaccharide is still scarce and currently, only few fucoidan active enzymes are characterized with limiting insights into the molecular mechanisms. Here, I use biochemical and structural analyses to characterize a fucosidase and sulfatase from '*Lentimonas*' sp. CC4. This enables us to understand the molecular details how bacteria recycle polysaccharides in the ocean.

### 4. Environmental dynamics of fucoidans during a diatom spring bloom

Production, aggregation and degradation of polysaccharides control the dynamic equilibrium between DOM and POM and thus carbon export. Yet, resolving individual polysaccharides in a complex environmental sample poses an analytical challenge. We used carbohydrate microarrays to trace individual polysaccharide structures over the course of a diatom spring bloom. This enables us to classify different polysaccharide into labile and stable polysaccharides and assess their potential to sequester carbon in the ocean.



## Contributions to manuscripts

### **Chapter I: Ion-exchange purification and structure of five sulfated fucans from brown algae**

Andreas Sichert, Sophie Le Gall, Leesa Klau, David Ropartz, H el ene Rogniaux, Finn Lillelund Aachmann, Jan-Hendrik Hehemann.

J.-H.H. and A.S. initiated the study and coordinated the project. A.S. purified the fucoidans and analyzed their composition. F.L.A. and L.K. conducted the NMR and SEC-MALS analysis and interpretation. D.P., S.L.G and H.R. conducted the linkage analysis. A.S and J.-H.H. prepared the manuscript and received input from all co-authors.

*Manuscript in preparation.*

### **Chapter II: Verrucomicrobia use hundreds of enzymes to digest the algal polysaccharide fucoidan**

Andreas Sichert<sup>#</sup>, Christopher H. Corzett<sup>#</sup>, Matthew S. Schechter, Frank Unfried, Stephanie Markert, D orte Becher, Antonio Fernandez-Guerra, Manuel Liebeke, Thomas Schweder, Martin F. Polz, Jan-Hendrik Hehemann.

<sup>#</sup> These authors contributed equally

JHH and MFP initiated the study and directed the project. CHC and AS conducted the experiments. The strains were isolated by CHC. FU and SM conducted the proteome analysis for which TS and DB provided resources. MSS and AFG analyzed the OSD and TARA. ML conducted GC-MS measurements and provided resources for metabolomics. AS, JHH, MFP prepared the manuscript and received input from all authors.

*Manuscript under review in Nature Microbiology.*

## Contributions to manuscripts

### **Chapter III: Aspartate as novel acid/base catalyst in a marine GH29 fucosidase from ‘*Lentimonas*’ sp. CC4**

Andreas Sichert<sup>#</sup>, Nadine Gerlach<sup>#</sup>, Tatjana von Rosen, Craig S. Robb, Jan-Hendrik Hehemann.

<sup>#</sup> These authors contributed equally

JHH and AS initiated the study. Protein crystallization was done by AS, NG and TvR. The crystal structure was determined by CR and NG. Primer design and cloning was conducted by AS, NG and TvR. Biochemical experiments were carried out by AS and NG. AS, NG and JHH wrote the manuscript and received input from all authors.

*Manuscript in preparation.*

### **Chapter IV: Fucose polysaccharide from diatoms may sequester carbon in the ocean**

Silvia Vidal-Melgosa, Andreas Sichert, Ben Francis, Daniel Bartosik, Pier Luigi Buttigieg1 Jutta Niggemann, Antje Wichels, Thomas Schweder, Dörte Becher, Rudolf Amann, Hanno Teeling, Jan-Hendrik Hehemann.

S.V.-M. and J.-H.H. designed the study. S.V.-M performed the polysaccharide extractions, microarray analyses, immunolabeling and epitope detection chromatography. A.S. performed monosaccharide analysis and statistical analyses. J.N. executed DOC measurements. A.W. supported with the TFF processing during the sampling campaign. B.F. performed metagenome analysis. D.B. performed metaproteome analysis. P.L.B. executed the filter classification analysis to the microarray data. S.V-M, A.S. and B.F. prepared graphical illustrations. All authors discussed the results. SV-M and J-HH wrote the manuscript. All authors commented and approved the manuscript.

*Manuscript in preparation.*

## **Chapter I.**

# **Ion-exchange purification and structure of five sulfated fucans from brown algae**

Andreas Sichert<sup>1,2</sup>, Sophie Le Gall<sup>4</sup>, Leesa Klau<sup>3</sup>, David Ropartz<sup>4</sup>, H el ene Rogniaux<sup>4</sup>, Finn Lillelund Aachmann<sup>3</sup>, Jan-Hendrik Hehemann<sup>1,2</sup>

<sup>1</sup> Max Planck Institute for Marine Microbiology, 28359 Bremen, Germany

<sup>2</sup> University of Bremen, Center for Marine Environmental Sciences, 28359 Bremen, Germany

<sup>3</sup> Norwegian Biopolymer Laboratory, Department of Biotechnology, NTNU, 7491 Trondheim, Norway

<sup>4</sup> INRA UR1268 Biopolymers Interactions Assemblies, 44316 Nantes, France

\*Correspondence: [jhhehemann@marum.de](mailto:jhhehemann@marum.de)





## Abstract

Fucoidans are a diverse class of sulfated polysaccharides integral to the cell wall of brown algae and due to their various bioactivities, fucoidans are potential marine drugs. Standardized work with fucoidans is required for structure-function studies, but remains challenging since available fucoidan preparations are often contaminated with other algal compounds. Additionally, fucoidans are structurally diverse depending on species and season, stressing the need for standardized purification protocols. Here, we use ion exchange chromatography to purify different fucoidans and elucidate their structure showing a high molecular diversity and novel structural features. A wash step with 0.5 M NaCl efficiently removes contaminating polysaccharides such as alginate and laminarin. Subsequently, we developed a simple stepwise protocol to purify fucoidans from different brown algae. Linkage analysis and NMR characterization of the purified fucoidans confirms their high purity and reveals novel structural features such as acetylation and high amount of  $\beta$ -linked galactose. This study emphasizes the use of standardized IEX to obtain fucoidans for subsequent molecular studies.

## Introduction

Fucoidans are the major cell wall polysaccharide of brown algae accounting for up to 23% of algal dry weight (Deniaud-Bouët et al., 2014). Humans have used brown algae for food and medical purposes for at least 14,000 years (Dillehay et al., 2008). Nowadays, fucoidans are well established as a major algal molecule that displays various bioactivities such as anticoagulant, antiviral, antitumor and immune-inflammatory actions and thus, fucoidans are of high medical interest (Synytsya et al., 2010; Ale et al., 2011; Vishchuk et al., 2011; Fitton et al., 2015). However, fucoidans originating from the cell wall of brown algae tightly interact and are co-extracted with proteins, phenols and alginates (Deniaud-Bouët et al., 2014, 2017). Consequently, fucoidans are inherently difficult to purify, which hampers further structure function studies of this potential marine drug.

Fucoidans are a diverse class of polysaccharides and are broadly classified into homofucans and heterofucans. Homofucans from the brown algal order *Laminariales* and *Ectocarpales* have a backbone of  $\alpha$ 1,3 with sulfate groups mainly at C2 and C4, whereas homofucans from the order *Fucales* have an alternating  $\alpha$ 1,3/  $\alpha$ -1,4 linked L-fucose sulfated at C2 and C3 (Chevolot et al., 2001; Deniaud-Bouët et al., 2017; Kopplin et al., 2018). Homofucans have branches of fucose or other building blocks such as galactose, glucuronic acids, xylose, mannose and acetate (Nishino et al., 1991; Nagaoka et al., 1999; Shimanaka et

## Chapter I

al., 2003; Bilan et al., 2013, 2014). Heterofucans have a non-fucose backbone, e.g., of galactose or glucuronic acid with side branches of sulfated fucose (Bilan et al., 2010, 2017; Deniaud-Bouët et al., 2017). Owing to their diversity, most fucoidans are structurally poorly characterized. Especially, the high sulfate content requires a combination of different analytical methods such as chemical desulfation, mass spectrometry and NMR analysis (Usov et al., 1971; Kopplin et al., 2018). As sulfate groups are the major factor responsible for the bioactivity of fucoidans, we require a more detailed understanding of the molecular diversity of highly sulfated fucoidans (Haroun-Bouhedja et al., 2000; Kopplin et al., 2018).

Due to variation in existing sampling, extraction and purification methods, current fucoidan preparations are molecularly poorly defined and often contaminated with other algal compounds. Often, brown algal biomass is harvested, not taking into account that its composition varies between seasons (Rioux et al., 2009; Skriptsova et al., 2010; Mak et al., 2013; Fletcher et al., 2017). To extract fucoidan, a variety of different extraction methods such as chemical fractionation, enzyme-assisted extractions or microwave-assisted extraction are used, which result in different fucoidan preparations, even when using the same starting material (Hahn et al., 2012; Deniaud-Bouët et al., 2017). For higher yields, algal biomass is for example pretreated with acid, which also results in the desulfation of fucoidan (Hahn et al., 2012). This variation in extraction protocols poses the question if reported structural data or biological activities can be compared between different extraction protocols. One possibility to circumvent this are additional chromatographic purification steps such as the recently developed dye affinity chromatography capturing fucoidans with a relatively low molecular weight and sulfate content (Hahn et al., 2016; Zayed et al., 2016). To enrich highly sulfated fucoidans, ion-exchange chromatography takes advantage of the negative charge of sulfated fucans, which can potentially be exploited to purify fucoidans.

In this study, we use ion-exchange chromatography to purify highly sulfated fucoidans and provide a detailed structural characterization. First, we develop a simple stepwise protocol to remove contaminating polysaccharides from fucoidan preparations. Next, we obtained eight highly sulfated fucoidans from major brown algal orders including *Ectocarpales*, *Laminariales* and *Fucales*. As our collection covers most of brown algal diversity, we conduct a comparative structural analysis of five different fucoidans using NMR and mass spectroscopy. Thereby, we confirmed their purity and identified novel structural features providing a basis for further bioactivity assays.

## Materials and Methods

### Compositional analysis of carbohydrates

#### Phenol sulfuric acid method

Total carbohydrate content (TCHO) was measured using the phenol-sulfuric acid method (Dubois et al., 1956) adapted to a microtiter plate format. 100  $\mu\text{L}$  of concentrated sulphuric acid and 15  $\mu\text{L}$  5% phenol were added to 25  $\mu\text{L}$  of samples in a microtiter plate. A standard curve of L-fucose in deionized water was used for subsequent quantification. The plate was heated to 60°C for 10 minutes and the absorbance at 490 nm was measured using a plate reader. The amount of TCHO (in  $\text{mg mL}^{-1}$ ) was calculated from the slope and intercept of a linear fit of the standards (x-axis amount and y-axis absorbance).

#### Sulfate content

The sulfate released by acid hydrolysis was measured on a Metrohm 761 compact ion chromatograph with a Metrosep A SUPP 5 column and suppressed conductivity detection with  $\text{H}_2\text{SO}_4$ . Ions were separated by an isocratic flow of carbonate buffer (3.2 mmol  $\text{Na}_2\text{CO}_3$  and 1 mmol  $\text{NaHCO}_3$ ) and the duration of a run was 20 min, with sulfate eluting at 16 minutes.

#### Quantification of monosaccharides via HPAEC-PAD

Monosaccharides in samples were quantified in a HPAEC-PAD system. This takes advantage of monosaccharides being partially charged in basic conditions and thus can be separated according to their pKa. We adapted a protocol for neutral and acidic sugars described previously (Engel & Händel, 2011). In short, a Dionex 5000+ system with pulsed amperometric detection (PAD) was equipped with a CarboPacPA10 anion exchange column. Neutral and amino monosaccharides were separated by an isocratic flow of 18 mM NaOH for 20 minutes, followed by a gradient of 500 mM NaAcetate to separate acidic sugars. Standard substances (fucose, rhamnose, galactosamine, arabinose, glucosamine, galactose, glucose, mannose, xylose, muramic acid, galacturonic acid, glucuronic acid and mannuronic acid) were used to identify peaks by retention time. A standard mix ranging from 1-10 to 1000  $\mu\text{g L}^{-1}$  was used to quantify the amount of monosaccharide (x-axis amount and y-axis peak area).

#### Solvolytic desulfation of sulfated fucans

Fucoidans were desulfated according to a previously published protocol (Torode et al., 2015). Dowex 50 W cation exchange resin ( $\text{H}^+$  200–400 mesh, Sigma-Aldrich) was slurred in ddH<sub>2</sub>O

## Chapter I

and ~10 mL were packed into a disposable PD-10 column (Sigma-Aldrich) and mounted above a glass bottle containing 25 mL 20 % (v/v) pyridine (Sigma-Aldrich). 100 mg of fucoidans were dissolved in 10 mL ddH<sub>2</sub>O and passed over the column to remove all counter ions. The solution was dialyzed against ddH<sub>2</sub>O (Spectra/Por 7 Dialysis Tubing, 8 kD MWCO, 18 mm flat width). The solution was lyophilized and resuspended to 1% (w/v) in anhydrous pyridine. Chlorotrimethylsilane (Sigma-Aldrich) was added to a final of 10% (v/v) and incubated at 100°C for 3h with a reflux condenser under constant cooling in the fume hood. The reaction was stopped by the dropwise addition of ddH<sub>2</sub>O. The solution was stepwise dialyzed to remove all traces of pyridine with tap water, 0.1 M NaCl and a final ddH<sub>2</sub>O step and then lyophilized.

### Ion-exchange chromatography of sulfated and desulfated fucoidan from *F. vesiculosus*

Ion-exchange chromatography (IEX) was carried out on an ÄKTA start chromatography system (GE Healthcare Life Sciences) with two serial 5 mL HiTrap ANX Sepharose FF columns (GE Healthcare Life Sciences) equilibrated in Buffer A (20 mM Tris pH 7.5) at a constant flow rate of 5 mL min<sup>-1</sup>. 100 mg of fucoidan from *F. vesiculosus* and 100 mg of its desulfated derivative were dissolved in 100 mL Buffer A and applied onto the columns by circulating the solution three times over the columns. After a wash with 50 mL Buffer A, a linear gradient from 0 – 100 % Buffer B (20 mM Tris pH 7.5, 5 M NaCl) was used to elute charged carbohydrates with 30 fractions à 2 mL (60 mL gradient volume). The fractions were analyzed for TCHO and fractions 5 - 11, 12 - 16 and 17-21 were pooled for analysis of monosaccharide composition and sulfate content.

### Purification of sulfated fucans

Sulfated fucan extracts were further purified using a custom medium-scale ion-exchange chromatography setup. We created a detailed stepwise protocol at protocol.io under <https://www.protocols.io/private/BDC1EAD2F01511E99D8F0242AC110004>. A MasterFlex L/S peristaltic pump was used to operate a XK50/20 column (GE Healthcare) packed with 200 mL ANX FF ion-exchange resin (GE Healthcare) at a flow of 50 mL min<sup>-1</sup> (Supplement Figure 1). Fucoidans (Table 1) were solubilized in 50 mM TRIS pH 7.5 and centrifuged for 30 minutes at 5000 rpm. For binding, the supernatant was circulated three times over the column. Next, the column was washed with three column volumes of 50 mM TRIS pH 7.5 and three column volumes 50 mM TRIS pH 7.5 with 500 mM NaCl. Highly charged molecules were eluted with 100 mL of 50 mM TRIS pH 7.5 with 5 M NaCl. After each run, the column was washed with 50 mM TRIS pH 7.5 with 5 M NaCl, deionized water, 250 mM NaOH and deionized water. The elution was then dialyzed against ddH<sub>2</sub>O and lyophilized. 50 µg of each polysaccharide

were acid hydrolyzed in triplicates and released sulfate and monosaccharides were quantified via HPAEC-PAD and IC.

Table 1: *List of fucoidans used in this study.*

<b>Fucoidan</b>	<b>Supplier</b>	<b>Ordering number</b>	<b>Comment</b>
<i>Undaria pinnatifida</i>	Carbosynth	YF145110	IEX-purified
<i>Sargassum fusiforme</i>	Carbosynth	YF157167	IEX-purified
<i>Fucus serratus</i>	Carbosynth	YF09360	IEX-purified, linkage, NMR
<i>Macrocystis pyrifera</i>	Carbosynth	YF145109	IEX-purified
<i>Ecklonia maxima</i>	Carbosynth	YF157166	IEX-purified, linkage, NMR
<i>Cladosiphon okamurans</i>	Carbosynth	YF146834	IEX-purified, linkage, NMR
<i>Durvillea potatorum</i>	Carbosynth	YF157165	IEX-purified, linkage, NMR
<i>Lessonia nigrescens</i>	Carbosynth	YF146833	IEX-purified
<i>Fucus vesiculosus</i>	Sigma-Aldrich	F5631	linkage, NMR

## Chapter I

### Quantitative profiling of the purification process

During the purification process, aliquots of the starting material, flow through, 0.5 M NaCl wash and 5 M NaCl elution were subjected to TCHO and monosaccharide analysis. This enables us to track the compositional change over the course of the purification. Let  $S_j$  denote the starting amount of each monosaccharide ( $j \in \{\text{fucose, rhamnose, ... mannuronic acid}\}$ ). Per purification step  $i$  ( $i \in \{\text{flow through, wash, elution}\}$ ), the absolute loss of each monosaccharide can be derived from the absolute concentration ( $TCHO_i$ ) and relative monosaccharide composition ( $Mono_i^j$ ). Therefore, the composition of the remaining material of interest ( $R_{i,j}$ ) can be calculated from:

$$R_{i,j} = S_j - \sum_{i=1}^3 TCHO_i \times Mono_i^j$$

### SEC-MALS

The molecular weight of fucoidan was measured by size exclusion chromatography (SEC) using an HPLC system fitted with online multi-angle static light scattering (MALS) and with viscometry (VISC) detectors. The measurements were performed at ambient temperature using two serially connected columns of TSKG 6000 PWXL and 5000 PWXL or TSK 4000 PWXL and 2500 PWXL. The column outlet was connected to a Dawn HELEOS-II multi-angle laser light scattering photometer (Wyatt, USA) ( $\lambda = 663.8$  nm) followed by an Optilab T-rEX differential refractometer and finally a ViscoStar II differential viscometer. The eluent was 0.15 M  $\text{NaNO}_3$  and 0.01M EDTA at pH 6 and the flow rate was  $0.5 \text{ mL min}^{-1}$ . Samples were filtered (pore size =  $0.8 \mu\text{m}$ ) before injection. The injection volume was 100–500  $\mu\text{L}$ , and the sample concentration was adjusted to obtain the best possible light scattering signal without influencing the RI profile.

### Linkage analysis

Methylation analysis was performed as described previously (Buffetto et al., 2015). Samples were dissolved in dimethylsulfoxide (DMSO; 0.2 ml), sonicated for 2 min and incubated at ambient temperature for 30 minutes. Permethylation was performed by adding 0.2 ml of NaOH-DMSO reagent and 0.1 ml of methyl iodide followed by sonication and vortexing. The reaction was stopped after 10 min by the addition of water (2 ml) and the methylated products were extracted with chloroform (2 ml). The solutions were vigorously vortexed before a brief centrifugation to allow phase separation. The organic phase was washed three times with water (2 ml) and dried under a stream of  $\text{N}_2$ . Methylated carbohydrates were hydrolyzed with 2 M

trifluoroacetic acid and converted to their alditol acetates. The partially methylated alditol acetates were analyzed by gas chromatography–mass spectrometry (TRACE-GC-ISQ, Thermo™) on a non-polar thermo scientific™ TraceGOLD™ TG-1MS GC Column (30 m x 0.25 mm x 0.25 μm) using H<sub>2</sub> as carrier gas at a flow rate of 1.5 ml min<sup>-1</sup>. The samples were injected at 240 °C. The column oven temperature was constant for 5 min at 60 °C followed by 3 °C min<sup>-1</sup> ramp to 315 °C and a hold for 2 min. The ion source temperature of the electron impact (EI) mass spectrometer was 230 °C. Masses were acquired with a scan range from m/z 100 to 500. Identification of partially methylated alditol acetates was based on their retention time combined with mass spectra fragmentation and compared with a home-made library. The identified glycosidic linkages are abbreviated as e.g., 3-fucose, which denotes a fucose with a glycosidic linkage at the C3-hydroxy group.

### NMR spectroscopy

The purified fucoidan (10 mg) was dissolved in 1 mL of 99.9% D<sub>2</sub>O (Chiron) and lyophilized in order to reduce the residual water signal. Subsequently, the sample was dissolved in 595 μL of D<sub>2</sub>O, and 5 μL of 1% 3-(trimethylsilyl)-propionic-2,2,3,3-d<sub>4</sub> acid sodium salt (Sigma-Aldrich) was added for a chemical shift reference. The desulfated fucoidan (25 mg) was dissolved in 1 mL of 99.9% D<sub>2</sub>O, and the solution was lyophilized. Residual DMSO from the desulfation procedure (see above) was used as a chemical shift reference. All homo- and heteronuclear NMR experiments were recorded on a Bruker Avance 600 MHz or Bruker AVIIIHD 800 MHz (Bruker BioSpin AG, Fälladen, Switzerland) equipped with a 5 mm cryogenic CP-TCI z-gradient probe. All NMR recordings were performed at 25°C.

For the chemical shift assignment of desulfated fucoidan, the following spectra were recorded: 1D proton, 2D double quantum filtered correlation spectroscopy (DQF-COSY), 2D total correlation spectroscopy (TOCSY) with a 70 ms mixing time, 2D <sup>13</sup>C heteronuclear single quantum coherence (HSQC) with multiplicity editing, 2D <sup>13</sup>C heteronuclear 2 bond correlation (H2BC), 2D <sup>13</sup>C HSQC-[1H,1H]TOCSY with a 70 ms mixing time on protons, and 2D heteronuclear multiple bond correlation (HMBC) with BIRD filter to suppress first-order correlations. The spectra were recorded, processed, and analyzed using the TopSpin 3.5 software (Bruker BioSpin AG).

# Results

### Ion-exchange purification of highly sulfated fucoidans

The high sulfate content of fucoidans results in strong binding to an anion exchange column, which we exploited to develop a simple stepwise purification protocol. Since the sulfate groups confer a strong negative charge at a neutral pH, fucoidans bind to a positively charged column and can subsequently be eluted with a salt gradient. To test if IEX chromatography can be used to separate polysaccharides according to their sulfate content, we separated fucoidan from *Fucus vesiculosus* and its desulfated derivative using an anion exchange column at a pH of 7.5 and a salt gradient from 0 to 5 M NaCl (Figure 6). The native fucoidan eluted between 2 and 5 M NaCl, whereas the desulfated fucoidan eluted between 0.5 M and 2 M NaCl. Analysis of the sulfate content linearly correlated with the retention time showing the strong binding of sulfate groups to the resin. Notably, we observed the elution of proteins in the UV detector below a salt concentration of 0.5 M NaCl (data not shown), suggesting a wash step with 0.5 M NaCl sufficiently removes contaminating proteins. Additionally, brown phenolic compounds such as phlorotannins (Koivikko et al., 2005) strongly stuck to the column and could only be eluted with a NaOH wash step. Together, we suggest to use a 0.5 M NaCl wash step to remove less charged biomolecules, followed by an elution with 5 M NaCl to purify fucoidans.

Next, we demonstrate that IEX is sufficient to remove impurities from eight different commercially available fucoidan extracts. For this, we purified 500 mg of each fucoidan (Table 1) using a medium-scale IEX setup and a detailed workflow is publicly available (<https://www.protocols.io/private/BDC1EAD2F01511E99D8F0242AC110004>). Over the course of the purification, we quantified the yield of carbohydrates and their monosaccharide composition (Figure 7). Overall, non-fucose monosaccharides such as glucose, mannose or mannuronic acid decreased, suggesting multiple types of polysaccharides within the samples that could be separated from fucoidans during purification. These polysaccharides could be alginate, mannans or laminarin. In fact, the preparation of *Fucus serratus* contained more than 99% glucose illustrating the high degree of contaminations in commercial fucoidan preparations.

The purified fucoidans are large and highly sulfated. The molecular weight of fucoidans ranged from 95 kDa to up to 418 kDa (Table 2). Over the course of the purification, the sulfate content significantly increases (two-sided paired t-test, p-value<0.01) ranging from 10 to 45% of the dry weight (Figure 8, Supplement Table 1). The molar ratio of fucose:sulfate suggest an



average of 1.8 sulfate groups per fucose. This agrees well with previous studies on fucoidan from *Laminaria hyperborea* with an average of 1.7 sulfate groups per fucose (Kopplin et al., 2018). In contrast to fucoidan from *Laminaria hyperborea*, the IEX-purified fucoidans are rich in other monosaccharides such as galactose and glucuronic acid, which are as abundant as fucose. This poses the question, whether these are homo- or heterofucans.

Table 2: Molecular weight of fucoidans measured with SEC-MALS. The molecular weight is represented as mean of replicates.

Fucoidan	Molecular weight (kDa)
<i>Fucus vesiculosus</i>	105.4
<i>Ecklonia maxima</i>	123.5
<i>Fucus serratus</i>	204.4
<i>Durvillea potatorum</i>	418.9
<i>Cladosiphon okamurans</i>	95.7

### Glycosidic linkages of purified fucoidans

For structural elucidation, we focused on IEX-purified fucoidans from *Cladosiphon okamurans*, *Fucus serratus*, *Ecklonia maxima* and *Durvillea potatorum* and fucoidan from *Fucus vesiculosus* as a reference. Via methylation analysis, we identified 15 different linkages (Figure 9). Based on their relative peak area, we derived the relative abundance of each linkage per fucoidan. The structurally simplest fucoidan is *C. okamurans*, since it mainly composed of 3-linked (60%) and 2,3-linked fucose (25%). All other fucoidans have a surprisingly high amount of terminal fucose (26 to 34%), which is indicative for many short branches as reported by Kopplin et al., 2019. *E. maxima* and *F. serratus* are also rich in 3-linked fucose (41 and 17%). In contrast, fucoidans from *F. vesiculosus* and *D. potatorum* are rich in 4-linked and 3,4-linked fucose. Additionally, we found 2,3,4-linked fucose (that is a fucose with a glycosidic linkage on each hydroxy group) with 1% abundance in fucoidan from *F. vesiculosus*, pointing towards a high structural complexity of this fucoidan. Furthermore, we identified terminal xylose in *F. vesiculosus* and various galactose linkages in fucoidans from *F. serratus*, *E.*

## Chapter I

*maxima* and *D. potatorum*. Overall, the relative abundances of each linkage agree with the monosaccharide composition for those sugars.

### NMR Spectroscopy

To resolve the configuration of glycosidic linkages we recorded two-dimensional  $^{13}\text{C}$  HSQC NMR spectra (Supplement Figure 2-6). We identified the anomeric carbon based on chemical shifts from reference NMR spectra of fucoidans (Chevolot et al., 2001; Shimanaka et al., 2003; Pomin et al., 2005; Rocha et al., 2005; Grachev et al., 2006; Clément et al., 2010; Bilan et al., 2013; Usoltseva et al., 2017, 2018). Thereby, we could assign the majority of peaks in the NMR spectra originating from fucopyranose and galactopyranose. Mainly, we found that all fucose linkages are in the  $\alpha$ -configuration, whereas most galactose linkages are in the  $\beta$ -configuration. Currently, it is unclear if signals originate from the backbone or branches, which could potentially be resolved by a comparison of the native fucoidan to the desulfated derivative.

Additionally, we found that O-acetylation (at 2.1 ppm/20 ppm) is a feature common of all fucoidans with the exception of fucoidan from *Fucus vesiculosus*. Furthermore, we identified an  $\alpha$ -1,2-linked hexose (5.2 ppm/100 ppm) on fucoidan from *C. okamurans*, which overlaps with signals from  $\alpha$ -1,2-linked glucuronic acid as previously reported (Shimanaka et al., 2003). These structural insights underpin the purity of fucoidans, since structural features can be resolved without further chemical or enzymatic treatment of the fucoidans.

### Discussion

This study shows that ion exchange chromatography efficiently removes contaminating polysaccharides from fucoidan preparations. We developed a simple stepwise protocol to remove alginate and laminarin contaminations resulting in highly pure fucoidan preparations. Subsequently, we assessed their structure using NMR and mass spectrometry and provide a comprehensive structural characterization of fucoidans from different algal species.

The fucoidan structure obtained from *Durvillea potatorum* is the first reported structure for the important genus *Durvillea*. Large *Durvillea* populations grow mainly around Chile, New Zealand, Tasmania and sub-Antarctic islands, since their sporophytes are dispersed with the Antarctic Circumpolar Current (Rothäusler et al., 2012). In these regions, *Durvillea* has long tradition in food and medicine (Dillehay et al., 2008). The fucoidan from *Durvillea potatorum* is a 400 kDa large fibre containing 30% fucose, 10% galactose and 20% (w/w)

sulfate. NMR and methylation analysis show a high content of 1,3 and 1,4 linked fucose which are likely in the  $\alpha$ -configuration, which points towards the alternating  $\alpha$ 1,3/1,4-linked fucose backbone typical for the order *Fucales* (Chevolot et al., 2001; Bilan et al., 2006). Additionally, we identified high amount of galactose, which is likely  $\beta$ 1,4 and  $\beta$ 1,3 linked. This large and sulfated structure provides opportunities to further investigate potential bioactivities of this molecule.

Previously, it was thought that fucoidans from the order *Fucales* have a backbone of alternating  $\alpha$ 1,3 and  $\alpha$ 1,4 linkages. This alternating backbone structure was characterized in *Fucus distichus*, *Fucus serratus*, *Fucus vesiculosus* and *Ascophyllum nodosum* and proposed to be the main repeating unit of fucoidans from *Fucales* (Chevolot et al., 2001; Bilan et al., 2004, 2006). It was then noted that fucoidan from *Himantalia elongata* has an  $\alpha$ 1,3-backbone resembling the backbone structure of *Laminariales* and *Ectocarpales* (Deniaud-Bouët et al., 2014). In this study, we observed that fucoidan from *Fucus serratus* is rich in 3-linked fucose, which together with NMR spectra suggests a backbone of  $\alpha$ 1,3-linked L-fucose similar to *Laminariales* and *Ectocarpales*. In contrast, fucoidans from *F. vesiculosus* and *D. potatorum* are rich in 4-linked and 3,4-linked fucose and likely those algae have the alternating  $\alpha$ 1,3/ $\alpha$ 1,4-linked backbone structure of *Fucales*. This suggests that the canonical backbone of alternating  $\alpha$ 1,3 and  $\alpha$ 1,4 linkages is less conserved in *Fucales* than previously thought.

### Author contributions

J.-H.H. and A.S. initiated the study and coordinated the project. A.S. purified the fucoidans and analyzed their composition. F.L.A. and L.K. conducted the NMR and SEC-MALS analysis and interpretation. D.P., S.L.G and H.R. conducted the linkage analysis. A.S and J.-H.H. prepared the manuscript and received input from all co-authors.

### Acknowledgements

AS is member of the International Max Planck Research School of Marine Microbiology (MarMic). JHH, AS and NG acknowledges funding from the Max-Planck-Gesellschaft and from the Emmy Noether Program of the DFG, grant number HE 7217/1-1

### Declaration of interests

The authors declare no competing interests.

Figures

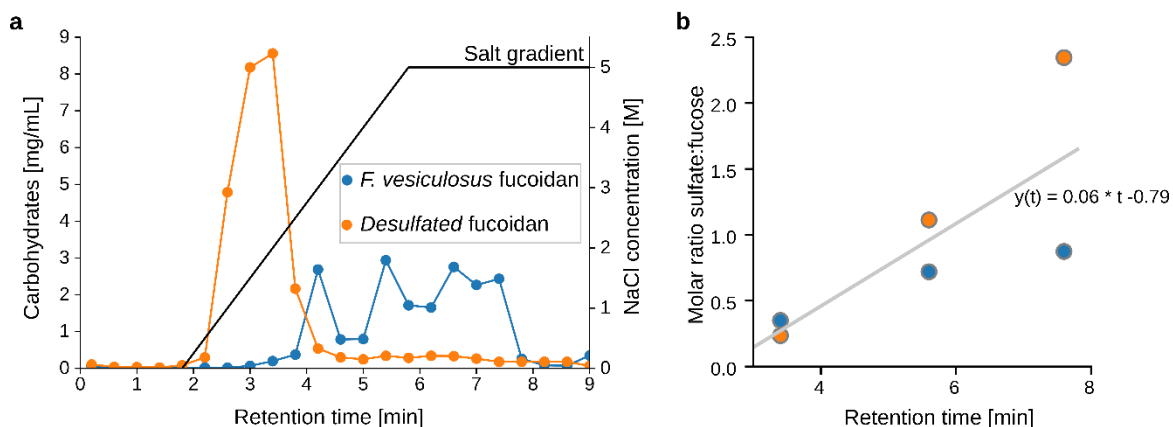


Figure 6: **Ion exchange chromatography separates fucoidans according to their sulfate content.** **a.** Comparison of elution profiles from *Fucus vesiculosus* and its desulfated derivative. **b.** The sulfate content of obtained fractions correlates with the retention time.

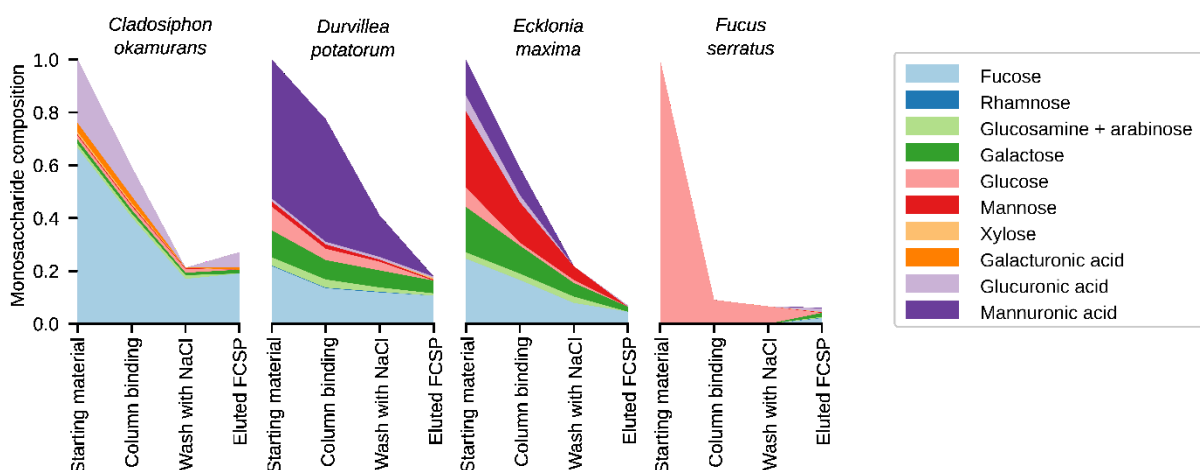


Figure 7: **Quantitative glycan profiling during purification of four different fucoidans.** The change in absolute amount and relative composition shows that contaminating polysaccharides are removed by ion exchange chromatography.

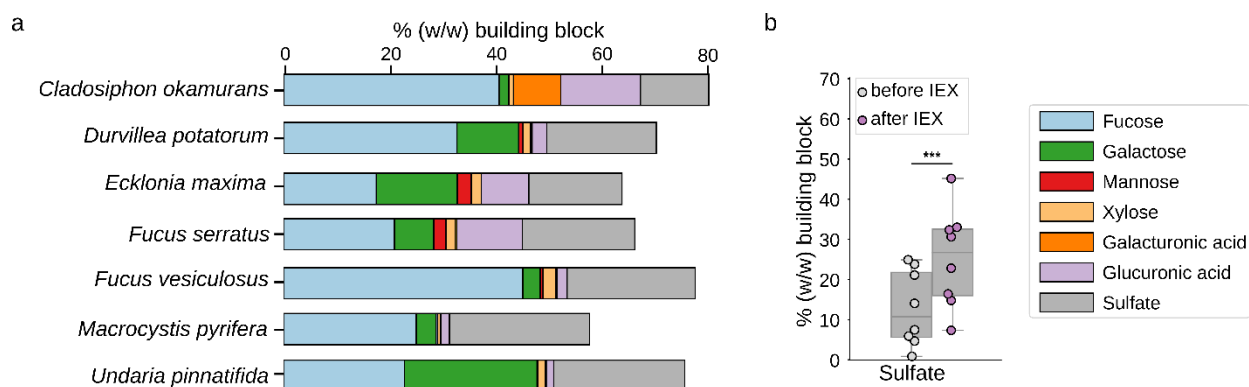


Figure 8: **The composition of purified fucoidans is enriched in fucose and sulfate.** **a.** Monosaccharide and sulfate content of fucoidan from various brown algae. **b.** Comparison of fucose and sulfate content before and after IEX purification. The three asterisks denote a significant difference ( $p < 0.01$ ) of a paired t-test.

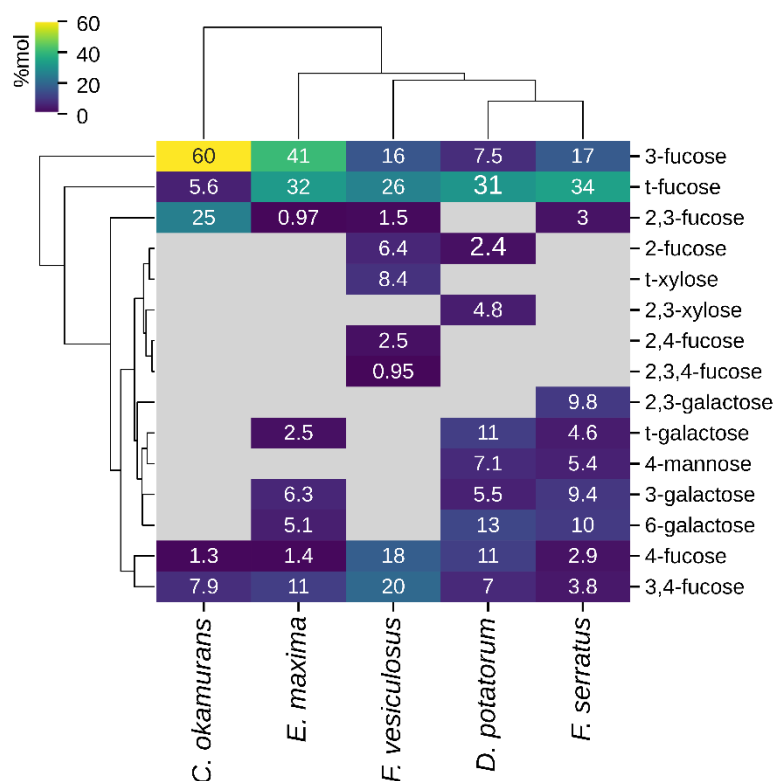


Figure 9: **Linkage analysis of five different fucoidans.** The heatmap show the molecular percentage of different glycosidic linkages of fucoidan from different brown algae. Rows and columns are ordered by a hierarchical clustering based on the Euclidean distance metric.



## Chapter II.

### **Verrucomicrobia use hundreds of enzymes to digest the algal polysaccharide fucoidan**

Andreas Sichert<sup>1,2#</sup>, Christopher H. Corzett<sup>3,7#</sup>, Matthew S. Schechter<sup>1</sup>, Frank Unfried<sup>4,5</sup>, Stephanie Markert<sup>4,5</sup>, Dörte Becher<sup>6</sup>, Antonio Fernandez-Guerra<sup>1,2,8</sup>, Manuel Liebeke<sup>1</sup>, Thomas Schweder<sup>4,5</sup>, Martin F. Polz<sup>3</sup>, Jan-Hendrik Hehemann<sup>1,2</sup>

<sup>1</sup> Max Planck Institute for Marine Microbiology, 28359 Bremen, Germany

<sup>2</sup> University of Bremen, Center for Marine Environmental Sciences, 28359 Bremen, Germany

<sup>3</sup> Department of Civil and Environmental Engineering, Massachusetts Institute of Technology, Cambridge, MA 02139, USA

<sup>4</sup> Pharmaceutical Biotechnology, Institute of Pharmacy, University Greifswald, 17487 Greifswald, Germany

<sup>5</sup> Institute of Marine Biotechnology, 17489 Greifswald, Germany

<sup>6</sup> Microbial Proteomics, Institute of Microbiology, University Greifswald, 17487 Greifswald, Germany

<sup>7</sup> Present address: Molecular and Computational Biology Section, Department of Biological Sciences, University of Southern California, Los Angeles, CA 90089, USA

<sup>8</sup> Present address: Lundbeck Foundation GeoGenetics Centre, GLOBE Institute, University of Copenhagen, 1350 Copenhagen K, Denmark

# These authors contributed equally

\*Correspondence: [jhhehemann@marum.de](mailto:jhhehemann@marum.de)





## Abstract

Brown algae are important players in the carbon cycle by fixing carbon dioxide into 1 Gt ton of biomass annually, yet the fate of fucoidan, their major cell wall polysaccharide, remains poorly understood. Previous evidence suggests that fucoidans are recalcitrant to microbial degradation due to their structural complexity, suggesting they play an important role in sequestering carbon in the ocean. Here we show that ‘*Lentimonas*’ sp. CC4 belonging to the Verrucomicrobia acquired an extraordinarily complex degradation machinery for the degradation of at least six different types of fucoidans. The strain accumulated over 200 different glycoside hydrolases and sulfatases, which are located on a 0.89 Mbp plasmid. Proteomics shows that these enzymes assemble into substrate-specific pathways with about 100 enzymes per type of fucoidan. Exo-enzymes are primarily responsible for depolymerization of fucoidans in a stepwise fashion into fucose, which is metabolized in a proteome-costly bacterial microcompartment. Marine genomes and metagenomes demonstrate that ‘*Lentimonas*’ and other members of the Verrucomicrobia are abundant and highly specialized degraders of fucoidans and other complex polysaccharides. Overall, the complexity of the pathways underscores why these polysaccharides are likely recalcitrant since only highly specialized organisms with a costly proteome can effectively degrade fucoidans in the oceans.

## Introduction

Brown macroalgae such as *Macrocystis* form productive kelp forests along the coasts and planktonic *Sargassum* grow into algal blooms covering the Atlantic from west to east (Field, 1998; M. Wang et al., 2019). With these blooms occurring in greater size and frequency, macroalgae play an increasingly important role in the carbon cycle acting as carbon sink of about 173 TgC yr<sup>-1</sup> (Krause-Jensen & Duarte, 2016; M. Wang et al., 2019). Carbon sequestration may be facilitated by the unique chemical structures of their cell walls – a tight network of proteins and polysaccharides including primarily alginate and fucoidans (Deniaud-Bouët et al., 2014; Trevathan-Tackett et al., 2015). Specifically, fucoidans have been hypothesized to play an important role in carbon sequestration as they are recalcitrant, i.e. they resist microbial degradation (Carol Arnosti, 2011). Fucoidans, which make up 23% of algal dry weight, are highly branched and sulfated, and have variable structure and composition depending on algal species and even season of production (Figure 10a) (Deniaud-Bouët et al., 2017). The backbone of fucoidans is either  $\alpha$ -1,3 or alternating  $\alpha$ -1,3/  $\alpha$ -1,4 linked L-fucose with sulfate esters on O-2, O-3 or O-4. Free hydroxy groups are decorated with acetate, sulfate

## Chapter II

or monosaccharides to the extent that only every third fucose has a free hydroxy-group in fucoidans from *Laminaria hyperborean* (Kopplin et al., 2018). This heavily chemically decorated structure sterically shields glycosidic linkages from enzymatic hydrolysis since dismantling enzymes such as sulfatases and carbohydrate esterases need to act first. Because of this complexity and variation in structure, it remains an open question whether microbes can effectively degrade and consume fucoidans.

The view that sulfated fucans are recalcitrant is further supported by the lack of any microbial isolates that can fully enzymatically degrade sulfated fucans and the apparent low activity of biochemically characterized fucoidanases. Although a few Bacteroidetes, Gammaproteobacteria or Planctomycetes-Verrucomicrobia-Chlamydia isolates can hydrolyze sulfated fucans, they can only produce oligomers yielding about 60% degradation (Sakai et al., 2003; Barbeyron et al., 2008; A. Silchenko et al., 2013; Feng Chen et al., 2016; Schultz-Johansen et al., 2018; van Vliet et al., 2019a). Moreover, most of the enzymes and pathways used for fucoidan degradation remain unknown. Current partial degradation pathways of fucoidans involve a combination of glycoside hydrolases (GH), carbohydrate esterases (CE) and sulfatases. These enzymes are specific to the targeted carbohydrate structure and grouped into homologous families of carbohydrate-active enzymes (CAZymes) with similar enzymatic activity (Lombard, Golaconda Ramulu, et al., 2014; Barbeyron, Brillet-Guéguen, et al., 2016; Hettle, Vickers, Robb, Liu, Withers, Hehemann, & Boraston, 2018). GH family 107 (GH107) are endo-enzymes producing sulfated fucose oligosaccharides, which are processed by GH29 exo-fucosidases producing fucose, and sulfatases such as S1\_17 and S1\_25 removing sulfate esters (Colin et al., 2006; A. S. Silchenko et al., 2017, 2018; Schultz-Johansen et al., 2018; Vickers et al., 2018). In some cases, degradation increased by adding carbohydrate esterases or sulfatases (Berteau et al., 2002; Nagao et al., 2017; A. S. Silchenko et al., 2018), suggesting fucoidans are degraded by combinations of exo-sulfatases and exo-GH similar to ulvan or pectin degradation by Bacteroidetes (Ndeh et al., 2017; Reisky et al., 2019). Therefore, any complete pathway for fucan degradation should involve a substantial number of enzymes either distributed within a microbial community or housed within highly specialized bacteria.

Candidates for degradation of highly sulfated polysaccharides are members of the Planctomycetes-Verrucomicrobia-Chlamydia (PVC) superphylum, which have been suggested to be specialists for sulfated polysaccharides due to their genomes being enriched in sulfatases. *Rhodopirellula baltica* SWK7 has 181 sulfatases, *Lentisphaera araneosa* HTCC2155<sup>T</sup> has 267 sulfatases and *Kiritimatiellales* F1 has 521 sulfatases (Thrash et al., 2010; Wegner et al., 2013; van Vliet et al., 2019a). However, their putative function as polysaccharide degraders is

primarily based on genomic predictions and a few physiological characterizations. With only a handful of characterized sulfatases specific for algal polysaccharides, it is puzzling why these organisms encode hundreds of sulfatases in their genomes and yet to be tested whether they are involved in desulfation of fucoidans.

Here, we characterize the newly isolated marine '*Lentimonas*' sp. CC4 from the phylum Verrucomicrobia and demonstrate how it adapted to overcome the complexity of fucoidans. The strain accumulated over 200 fucose-specific enzymes, and proteomics suggests that these enzymes are combined into substrate-specific pathways with about 100 GH and sulfatases expressed per fucoidan. Primarily, these enzymes liberate fucose, but not other monosaccharides of fucoidans. We then show that a few families of exo-fucosidases and sulfatases have diversified forming unique operons for step-wise depolymerization of the substrate. Liberated fucose is then metabolized in a bacterial microcompartment. Through analyzing available metagenomes and genomes, we further explore the ecology of Verrucomicrobia as specialized degraders of complex polysaccharides especially in the coastal ocean. The results highlight an effective specialization of '*Lentimonas*' spp. towards fucoidans and support the recalcitrance of fucoidans to most marine, heterotrophic bacteria.

### Results

#### **‘*Lentimonas*’ isolates are specialized degraders of fucoidans**

The isolation of bacterial strains capable of degrading fucoidan proved particularly challenging due to the presence of fast-growing cross-feeders within the bacterial community. We sampled a coastal microbial community at Nahant beach (Nahant, Massachusetts, USA) and first carried out enrichments in liquid medium, followed by plating to isolate colonies and to screen for visible growth on fucoidans in liquid medium. The majority of over 1000 tested colonies did not grow on fucoidan or positive growth tests turned out to be a mixture of different morphotypes on the plate. After several rounds of re-growth and re-plating, we isolated seven fucoidan degrading appeared only after weeks of incubation as tiny, colorless colonies. Due to their slow growth rates, those strains were likely overgrown in liquid by cross-feeders did not degrade the polymer but rather fed on degradation products later identified as fucose, lactate and propanediol. The isolates shared >99.8% identity of the 16S rRNA gene and we identified them as ‘*Lentimonas*’ with 97.4% to ‘*Lentimonas*’ *marisflavi* (EF157839). The genus ‘*Lentimonas*’ is taxonomically not validly described and contains the strain *Fucophilus fucoidanolyticus* (AB073978) which was described as a partial degrader of fucoidans from the brown algae *Cladosiphon okamurans*, but is unavailable via culture collections (Sakai et al., 2003). Therefore, we refer to the strains as ‘*Lentimonas*’ sp. CC4, CC6, CC8, CC10, CC11, CC19 and CC21 and deposited strain CC4 at the DSMZ under accession number DSM 110005.

Growth assays with various carbon substrates suggest that ‘*Lentimonas*’ strains are highly specialized for degradation of sulfated cell wall polysaccharides of specific red and brown algae (Figure 10a,b). ‘*Lentimonas*’ strains grew on iota-carrageenan from red algae and six fucoidans from brown algae with the notable exception of polysaccharides from *Sargassum fusiforme* and *Undaria pinnatifida*, which although containing sulfated fucose have a different structure due to a non-fucose backbone. Moreover, ‘*Lentimonas*’ strains neither grew on other sulfated polysaccharides (e.g., porphyran, agar and heparin) nor on non-sulfated polysaccharides (laminarin, alginate, xylan) that co-occur in fucoidan-producing macroalgae. Even simple  $\beta$ -1,3 or  $\beta$ -1,4 glucose oligosaccharides such as Pachyman or cellobiose were not degraded, which contrasts the wide-spread ability to hydrolyze beta-glucans in other marine polysaccharide degraders (Corzett et al., 2018; Kappelmann et al., 2019). Hence, ‘*Lentimonas*’ appears to have a narrow metabolic niche restricted to sulfated cell wall polysaccharides of red and brown algae.

'*Lentimonas*' sp. CC4 is unique among known fucoidan degraders as it catalyzes near complete depolymerization of multiple fucoidans into monomers. We analyzed the change of molecular weight, the production of oligosaccharides and the release of monosaccharides during the growth of '*Lentimonas*' sp. CC4 on different fucoidans and iota-carrageenan. High molecular weight iota-carrageenan is almost completely degraded with a minor fraction of stable oligosaccharides accumulating. In contrast, a fraction ( $\approx 26\% \pm 10\%$  of initial fucose content) of high-molecular weight fucoidans resisted degradation and no oligosaccharides were observed (Supplement Figure 7). We also noticed that during polymer degradation, '*Lentimonas*' sp. CC4 releases high concentrations of extracellular free monosaccharides (Figure 10c). In mid-exponential phase, peak concentrations of released monosaccharide reached up to 110  $\mu\text{M}$  free fucose and 71  $\mu\text{M}$  free glucuronic acid. This excess production of monosaccharide in the supernatant suggests that extracellular enzymes depolymerize fucoidans into monosaccharides, which are taken up into the cell. In addition, those high amount of liberated fucose explains the difficulties in isolating '*Lentimonas*' as cross-feeders can use fucose in our enrichments as well as in a natural community.

The release of high quantities of monosaccharides poses the question whether all of these can serve equally well as growth substrates for '*Lentimonas*' sp. CC4. To explore this question, we acid hydrolyzed polymeric carbohydrates into their building blocks and profiled their change during growth (Figure 10c). These assays showed that '*Lentimonas*' primarily uses almost exclusively fucose, which decreased by 5-10 mM to 20-40% of the starting concentration, consistent with the efficiency of other fucoidan degrading bacteria (Barbeyron et al., 2008; A. Silchenko et al., 2013; Feng Chen et al., 2016; Schultz-Johansen et al., 2018; van Vliet et al., 2019a). In contrast, other monosaccharides were only used in exceptions. For example, glucuronic acid is present in fucoidans from *Fucus serratus*, *Ecklonia maxima* and *Cladosiphon okamurans* but only decreased in fucoidans from *C. okamurans*. Moreover,  $\beta$ -1,4-linked xylose slightly decreased when obtained from *F. serratus* but not from *F. vesiculosus* (Chevolot et al., 2001; Bilan et al., 2006). This indicates that fucoidans have subtle structural differences in monosaccharide decoration and '*Lentimonas*' sp. CC4 primarily degrades undecorated parts of fucoidans as it cannot remove all decorations equally well.

### **'*Lentimonas*' sp. CC4 has a megaplasmid for the degradation of fucoidans**

The genetic makeup of '*Lentimonas*' sp. CC4 reflects its extraordinary specialization for hydrolysis of fucoidans and mannans as well as iota-carrageenans. In fact, 8.5% of all genes

## Chapter II

are devoted to the degradation of these complex polysaccharides (Figure 11). The most notable feature of '*Lentimonas*' sp. CC4 is a megaplasmid of 0.89 Mbp that contains 552 genes including 100 GH, 113 sulfatases and 20 pairs of histidine kinase and response regulator. This plasmid is likely involved in the degradation of fucoidans since we identified 50 copies of exo-acting fucosidases from families GH29, GH95 and GH141 and four copies of the sulfated fucan endo-1,4-fucoidanase GH107. The 3.98 Mbp genome contains 3,506 genes that include 75 sulfatases and 63 GH primarily distributed among five regions, which we refer to as polysaccharide utilization loci (PUL) (Martens et al., 2008). We detected two PULs for fucoidan with sulfatases and fucosidases (GH29, GH95 and GH141), two PULs for sulfated mannan separated by only 47kbp with sulfatases and mannosidases (GH38 and GH105) and one PUL for iota-carrageenan with sulfatases, GH16, GH82 and GH127 carrageenases. Mannan and fucoidan PULs are flanked with mobile elements such as integrases or transposases indicating acquisition of those islands via horizontal gene transfer. The chromosome also contains several other notable metabolic genes including an operon for nitrogen fixation, various monosaccharide pathways such as fucose and uronic acids, and a complete TCA cycle and respiratory chain with terminal cbb3-type oxidase. Finally, consistent with the growth data, we did not observe enzymes for the degradation of unsulfated polysaccharides like chitin, laminarin or alginate. Hence '*Lentimonas*' sp. CC4 appears highly specialized for, and perhaps even restricted to, three classes of sulfated polysaccharides: sulfated mannans, iota-carrageenan and different types of fucoidans.

The overall genomic architecture of '*Lentimonas*' sp. CC4 is preserved in the related isolates CC6 to CC21, which share >95% sequence identity to the CC4 genome and plasmid. However, the plasmid is absent from *Coralimargarita akajimensis* DSM 45221, which still shares ~70% genome identity with CC4 (Supplement Figure 8), suggesting that the plasmid is a key feature of the '*Lentimonas*' isolates and that its acquisition greatly enhanced the ability to degrade the fucoidans.

### Degradation of fucoidans requires over 100 GHs and sulfatases

Fucoidan from *C. okamurans* and *F. vesiculosus* induced the expression of 78 CAZymes and 76 sulfatases from 44 enzyme families representing an order of magnitude more enzymes than required for the degradation of pectin (21 enzymes), the most complex terrestrial cell wall polysaccharide (Ndeh et al., 2017). Using proteome analysis during growth on fucose, galactose, iota-carrageenan and two fucoidans from *C. okamurans* and *F. vesiculosus*, we

identified 566 differentially expressed proteins which we grouped into eight clusters based on their standardized z-score expression vector (Figure 12a). These analyses showed that 46 GH and 53 sulfatase enzymes are specifically induced by fucoidans from *C. okamurans* and *F. vesiculosus* in cluster 1 and 2, respectively (Figure 12b). Additionally, both fucoidans co-regulate the expression of 55 enzymes of cluster 3, 4 and 5, suggesting that those enzymes are generally involved in the degradation of both fucoidans. Also, both fucoidans only induced 154 out of 262 enzyme encoding genes of the fucoidan PULs, suggesting that those additional enzymes are required to degrade other fucoidans. Along with enzyme families GH29, GH107, S1\_17, S1\_25 and CE7 with known function for fucoidan degradation, fucoidans induced genes of enzyme families that were previously not known to be involved in fucoidan degradation such as S1\_15, S1\_16, GH28, GH36, GH95, GH115, GH116, GH117 and GH141. The high number of substrate specific expressed enzymes and enzyme families suggests a remarkably complex pathway for fucoidans. For comparison, iota-carrageenan induced the expression of 13 enzymes from 8 families (GH82, GH127, GH16, S1\_7 and S1\_19), which degrade iota-carrageenan by the previously described mechanism (Ficko-Blean et al., 2017). Importantly, we did not observe cross-induction between iota-carrageenan and fucoidans, underlining the substrate specific genetic response of glycoside hydrolase and sulfatase encoding genes and the corresponding specific enzyme activities on the different sulfated polysaccharides.

### **Structurally different fucoidans are degraded by specific pathways**

The enzymes for degrading fucoidans are organized in operons with unique combinations of different enzymes to target different substructures of fucoidans. Enzymes that are mutually dependent to act in synergy on a substrate are often co-regulated in operons and thus the gene arrangement in operons reflects the structure of the targeted polysaccharide. Using RNAseq, we identified 90 operons with 2 to 16 sulfatases or GHs (Supplement Figure 10). The gene expression of those operons is likely to be orchestrated by 25 pairs of histidine kinase and response regulators that are co-located in the PULs. None of the operons are identical in their enzyme content. For example, most GH29 are often co-regulated with at least one enzymatic partner such as S1\_15, S1\_16, S1\_17, S1\_22, S1\_25, S1\_46, CE6, CE7, CE10, GH116, GH117 or GH141. This variety of different enzyme combination suggests that different operons target different substructures of fucoidans. Additionally, we observed that similar enzymes (>50% identity) are combined with different enzymes into operons that respond differently to

## Chapter II

fucoidans from *C. okamurans* or *F. vesiculosus* (Figure 13a). This shows that the same enzyme homolog can be involved in degrading different fucoidans and the enzyme combination within the operon determines its substrate specificity.

The induced enzyme families are remarkably diverse with a fine-tuned expression indicating different functions such as the recognition of subtle different oligosaccharide structures. For example, phylogenetic analysis of GH29 from '*Lentimonas*' sp. CC4 shows the most distant GH29 homologs share below 20% identity and the most similar share 90% identity (Supplement Figure 9). Furthermore, based on a 40% identity clustering, we identified 20 clades of GH29 and most have at least one differentially regulated homolog. Enzyme families S1\_15, S1\_16, S1\_17, GH95 and GH141 show similar diversity and regulation posing the question whether the different homologs have different functions for fucoidan degradation. Primarily, the activity of GHs is determined by the accommodation of glycan structures in the active site and even within one GH family, homologs differ in their substrate specificity (G. J. Davies et al., 1997; Stam et al., 2006; Mewis et al., 2016). The subtle details of substrate recognition of GH29 and other induced enzyme families remain largely unknown, but recent studies show that GH29 are highly selective for accommodating different oligosaccharide structures in their active side. For example, SpGH29C (AAK76203.1) removes  $\alpha$ -1,3 or  $\alpha$ -1,4-linked fucose from a trisaccharide, but the activity depends on the accommodation of galactose in the +2 subsite and therefore this enzyme cannot cleave disaccharides (Hobbs et al., 2019). Also, TfFuc1 (AEW21393.1) only cleaves  $\alpha$ -1,2-linked fucose from a linear but not a branched oligosaccharide (Megson et al., 2015). Since fucoidans have a complex structure with variable position of branches or sulfate groups, these examples suggest that fucoidan degradation requires multiple homologs of highly substrate-specific exo-enzymes such as GH29.

Because our omic analysis suggests highly specific enzymes and operons for fucoidans, we asked whether this specificity can be reproduced on an enzymatic level. To test if the expressed pathways depolymerize fucoidan in a stereo-specific manner, we measured the cross-reactivity between expressed sub-proteomes and fucoidans using enzyme assays (Figure 13b,c). We extracted the expressed enzymes during mid-exponential growth on five different fucoidans and fucose, assayed the enzyme extracts against all growth substrates and derived the rate of hydrolysis of polysaccharides. The control, enzyme extracts from fucose grown cells, did not show activity on any of the substrates, underlining that the few enzymes expressed during growth on fucose are not sufficient to degrade fucoidans (Figure 12). Enzyme extracts from fucoidan grown cells have the following activity pattern: enzyme extract from *D.*



*potatorum* and *F. vesiculosus* grown cells showed the highest activity rate on *D. potatorum* and *F. vesiculosus*, respectively. Enzyme extract from *E. maxima*, *C. okamurans* and *F. serratus* grown cells have high cross activity on each other. This shows at least three different pathways for three types of fucoidans: *E. maxima*, *C. okamurans* and *F. serratus* are acetylated and rich in glucuronic acid, *F. vesiculosus* has a unique O-2 sulfate and *D. potatorum* has a high galactose content. Those structural features require unique enzymes for their degradation and also shield the substrate from unspecific hydrolysis since the cross-activity between structural types drops by about 66%. These assays show that the high number of induced enzymes is needed to hydrolyze the complex structure of fucoidans and changes in the structure lead to different pathways.

### High metabolic burden for degradation of fucoidans

The degradation of fucoidans is complicated by a 3-fold higher protein demand for fucoidan metabolism compared to iota-carrageenan utilization. To quantify the proteome fraction that changed in response to fucoidans, we summed up the relative expression (%iBAQ) of each differential expressed proteins per cluster and growth condition (Figure 14). During growth on iota-carrageenan, the expression level of GHs, sulfatases and monosaccharide pathway in cluster 8 contributes 3% of the proteome and in total 7% of the proteome are actively overproduced. In contrast, 21% and 18% of the proteome are allocated to fucoidans from *F. vesiculosus* and *C. okamurans*. GHs and sulfatases contribute ~3%, fucose metabolic enzymes and proteins of a bacterial microcompartment contribute 3% and a bacterial porin (BBP\_2, LCC\_1\_1313) contributes 8% of the proteome. A homolog was also highly expressed in marine Bacteroidetes during growth on the beta-glucan laminarin and associated with the acquisition of nitrogen (Unfried et al., 2018). The putative porin LCC\_1\_1313 might have a similar role as it is co-located with a constitutively expressed argininosuccinate synthase (EC 6.3.4.5). Notably, the average protein abundance of individual fucosidases is about ten-times lower than iota-carrageenases and consequently, higher initial cell concentration would be needed for sufficient enzyme titer to initiate fucoidan degradation (Enke et al., 2018). The large proteome fractions that are allocated to the metabolism of complex fucoidan represent a metabolic burden (Shachrai et al., 2010; Basan et al., 2015), which potentially constrains the growth of '*Lentimonas*' sp. CC4 on fucoidans.

## Chapter II

### **Fucose is metabolized in a bacterial microcompartment**

Proteins of a bacterial microcompartment (BMC) are highly expressed during growth on fucose and fucoidans and have previously been shown to metabolize fucose or rhamnose (Axen et al., 2014; Erbilgin et al., 2014; He et al., 2017). Fucose and rhamnose have a similar pathway producing the highly reactive and thus toxic lactaldehyde as intermediate which is then detoxified by a fermentation reaction inside the BMC. In '*Lentimonas*' sp. CC4, we identified key enzymes for fucose metabolism and a gene cluster encoding the BMC proteins (Figure 14b). The BMC shell proteins assemble into a protein shell and metabolic enzymes therein catabolize lactaldehyde (Figure 14c). Yet, the specificity of the BMC for fucose or rhamnose is ambiguous since key metabolic enzymes such as the kinase and aldolase genes share 30-40% identity with characterized enzymes specific to fucose or rhamnose.

To identify whether a BMC-fucose pathway is active in '*Lentimonas*', we quantified metabolites in the culture supernatant (Figure 14d). The signature end product of BMC is 1,2-propanediol (Baldomà & Aguilar, 1988; Petit et al., 2013), which we detected together with lactate in fucose grown cultures. 1,2-propanediol was not detected in cultures with rhamnose, glucose, mannose or galactose (data not shown) showing that the pathway is specific for fucose. Interestingly, the cells secrete propanediol and lactate which we measured to estimate their metabolic fluxes. Theoretically, the pathway produces 0.5 mole dihydroxyacetone phosphate, 0.25 mole of lactate and 1,2-propanediol per 1 mole consumed fucose. We measured the degradation of 0.352 mM fucose/h with a production of 0.101 mM lactate/h and 0.075 mM 1,2-propanediol/h which corresponds to a stoichiometric ratio of 1:0.28:0.21 (fucose:lactate:propanediol). This shows that '*Lentimonas*' actively uses the BMC to metabolize fucose and converts about 25% of the carbon into lactate and 1,2-propanediol.

### **'*Lentimonas*' are globally relevant degraders of fucoidans**

Next, using marine metagenomes, we found up to 8% relative abundance and highly conserved proteins of '*Lentimonas*' in coastal, macroalgae rich environments suggesting an important ecological role as a degrader of algal polysaccharides. We analyzed the relative abundance of '*Lentimonas*' in the oceans using miTAGs from TARA ocean and Ocean Sampling Day (OSD) (Kopf et al., 2015; Sunagawa, Coelho, Chaffron, Kultima, Labadie, et al., 2015). The relative abundance of '*Lentimonas*' did not reach more than 1% in open ocean samples of the Atlantic or Pacific but reached up to 8% in coastal samples of OSD i.e. the OSD113 sample (Figure

15a,b). This enrichment of *Lentimonas* in coastal, macroalgae-rich regions accords with previous studies that found up to 32% of *Lentimonas* in particle-associated microbial communities (Freitas et al., 2012; Bachmann et al., 2018; Needham et al., 2018). Yet, although abundant in marine samples, the ecological function of *Lentimonas* is poorly understood. To this end, we assembled 173,215 proteins of the OSD113 sample and found homologs to half of all proteins of *Lentimonas* (Figure 15). About 1000 proteins shared between 80 and 100% identity with *Lentimonas* sp. CC4 including all proteins of the BMC-fucose pathway, 26 sulfatases, three GH29, and one GH95, which indicates that the characterized, fucoidan metabolism of *Lentimonas* sp. CC4 occurs in the ocean. Notably, we detected one additional homolog for each microcompartment protein with about 60% identity, suggesting *Lentimonas* is one out of two microbes that actively use this pathway in this sample.

*Lentimonas* sp. CC4 uses an expanded enzyme repertoire of a few families to specialize on the degradation of a single complex polysaccharide, a theme common to other Verrucomicrobia. For example, the human gut commensal *Akkermansia* specialized in the degradation of mucins (Seekatz et al., 2016) and *Akkermansia glycaniphila* accumulated 15 GH20 to degrade mucin. Analyzing the GH content of annotated microbial genomes ([www.cazy.org/b.html](http://www.cazy.org/b.html)), we observed that Verrucomicrobia often encode the highest copy number from one family of exo- and endo-enzymes (Figure 15d), e.g., *Opitutaceae* bacterium TAV5 has 47 GH39, *Ereboglobus luteus* Ho45 has 11 GH106 and *Coralimargarita akajimensis* has 16 GH86 (Mavromatis et al., 2010; Kotak et al., 2015; Tegtmeier et al., 2018) indicating specialization for unique types of polysaccharides. Those enzymes are involved in the degradation of complex polysaccharides such as hemicellulose, rhamnogalacturonan I or porphyran and the genomes are depleted in enzymes that target other types of polysaccharide. Notably, this specialization occurred in host-associated Verrucomicrobia such as *Akkermansia*, *Ereboglobus* and *Opitutaceae* bacterium TAV5 as well as free-living Verrucomicrobia such as *Lentimonas*, *C. akajimensis* and *Opitutus terrae*. This concentration of GH from one family generally contrasts the CAZyme pattern in Bacteroidetes, which often are generalists with multiple PULs for multiple different polysaccharides, whereas Verrucomicrobia appear to specialize each on their own narrow range of complex polysaccharides.

## Discussion

In this study, we characterize the newly isolated marine *Lentimonas* sp. CC4 as a specialized degrader of fucoidans – a class of structurally complex cell wall polysaccharides from brown algae. Using genomics, proteomics, carbohydrate analysis and enzyme assays, we uncovered a

## Chapter II

remarkably complex pathway for fucoidan degradation: at least 100 enzymes are required to liberate fucose, which is then metabolized via a bacterial microcompartment. The requirement of such a complex catabolic pathway underpins the recalcitrance of fucoidans for most marine bacteria.

Our proteomic analysis shows that fucoidans are degraded by an expanded repertoire of 100 exo-acting enzymes from families GH29, GH95, GH141, S1\_15, S1\_16 and S1\_17. Such an expansion of enzyme copy number is a signature of microbial specialization. For example, plant or animal pathogens expand their hydrolytic repertoire to lyse their host tissue, or *Vibrio breoganii* specialized on alginate degradation encodes 10 PL7 compared to the 3-5 PL7 of generalists vibrios (Sprockett et al., 2011; Aranda-Martinez et al., 2016; Corzett et al., 2018). Gene dosage, i.e. the linear correlation between copy number and hydrolytic activity, could be one factor driving the enzyme expansion (Hehemann et al., 2016). However, in '*Lentimonas*' gene dosage plays a minor role. Instead, these homologs vary in their specificity for different oligosaccharide structures since we observed that these homologs are diverse, actively regulated in complex operons and the expressed pathways are substrate specific. We hypothesize that the branched and heavily decorated structure of fucoidans requires highly specific exo-enzymes. Typically, linear (sulfated) polysaccharides such as iota-carrageenan, agar or ulvan are cleaved by endo-enzymes into regular oligosaccharides for processing by only a few exo-enzymes (Ficko-Blean et al., 2017; Pluvinage et al., 2018; Reisky et al., 2019). This concept of metabolic funneling into regular intermediates is common for biodegradation pathway such as isomerases in lignin degradation, but might not be applicable to fucoidans (Linger et al., 2014). For example, random variations in backbone decorations block the substrate recognition of endo-enzymes (Hehemann et al., 2012; Labourel et al., 2016). Also, whenever two or more modifications such as sulfate, acetate or branches co-occur on the same monosaccharide, these structures can only be recognized and degraded by highly specific exo-enzymes. For example, xylose with two arabinose or two acetate decorations shield xylans from unspecific degradation and requires highly substrate specific arabinosidases and esterases (Rogowski et al., 2015; Razeq et al., 2018). Similarly, sulfatases display high subsite specificity (Hettle, Vickers, Robb, Liu, Withers, Hehemann, & Boraston, 2018; Reisky et al., 2019) and therefore, we hypothesize that the heavily decorated structure of fucoidans requires multiple homologs of exo-enzymes that vary in their substrate recognition.

In the environment, '*Lentimonas*' is a particle-associated degrader of fucoidans and may enable social interactions within the microbial community. Marine particles are a complex matrix of debris, cells, proteins and carbohydrates and can form by the aggregation of charged

algal exudates which are often rich in fucose and rhamnose (Engel et al., 2004; J. Zhou et al., 2011; Koch et al., 2019). Due to their complex origin, particles likely contain a variety of polysaccharides from different algae or time of production. To exploit the diversity of fucoidans in the environment, the plasmid of *Lentimonas* with over 200 enzyme encoding genes facilitates transfer of new enzymatic tools, or may even provide a convenient way to get rid of genetic burden when fucoidan is rare in the environment. Additionally, particles are concentrated hot spots of food for *Lentimonas* and also provide a matrix enabling biofilm formation and reducing diffusive losses of secreted enzymes and liberated monosaccharides (Drescher et al., 2014). Even with more than 100 hydrolytic enzymes, *Lentimonas* is only capable of breaking down undecorated parts of fucoidans by 75% and as a result the composition of fucoidans is depleted in fucose but enriched in xylose and galactose. Other particle associated polysaccharide degraders such as Bacteroidetes could further deconstruct the fucose depleted rest rendering complete degradation of fucoidans a community effort. Additionally, microbes without any hydrolytic enzymes could directly profit from the liberated fucose, lactate or propanediol (Enke et al., 2018). The ability of *Lentimonas* to grow on various fucoidans incurs a high cost of maintaining a large genome and proteome, which potentially reduces its competitiveness. Consequently, interactions within a microbial community might control the growth dynamics of *Lentimonas* and the turnover of fucoidans in the environment.

Our results highlight the role of specialized *Verrucomicrobia* in degrading complex polysaccharides. A single bacterium uses 76 sulfatases and 78 CAZymes to degrade one class of sulfated polysaccharides, which shows that pathways for sulfated polysaccharides are more complex than previously thought. Despite the complexity of the pathway, the highly dedicated pathways of *Lentimonas* achieve fast growth rates on fucoidans demonstrating that highly specialized microbes can catalyze the turn-over of complex fucoidans in the ocean.

## Materials and Methods

### Medium and growth conditions

*Verrucomicrobia* isolates were either grown in Tibbles and Rawling medium (Tibbles & Rawlings, 1994) or MOPS-buffered minimal medium (MMM) which is derived from Tibbles Rawling medium by reducing the phosphate to 1 mM and 20 mM MOPS buffer at pH 8 instead of Tris buffer. Unless otherwise stated, we used 0.2% (w/v) of carbohydrates.

## Chapter II

### Sampling and isolation of marine Verrucomicrobia

Coastal ocean surface water and sediments were sampled on 18 July 2013 from a site located near Northeastern University's Marine Science Center (Canoe Beach, Nahant, MA, USA; 42°25'01.500 N, 70°54'02.600 W). Enrichments were performed in Tibbles-Rawling medium supplemented with 1g/L fucoidan (Fucoidan from *Fucus vesiculosus*, Sigma F8190) as sole carbon source. Briefly, environmental samples were inoculated 1:100 (v/v) into 200 µl filter-sterilized fucoidan minimal media within 96-well plates and monitored for changes in optical density during static growth. Cultures exhibiting an increase in optical density were passaged through subsequent re-enrichment cultures and plated on MB2216 agar to isolate colonies. Putative fucoidan-degrading isolates were reinoculated into fucoidan minimal media to confirm growth then stored in 20% glycerol stocks at -80°C. Strain '*Lentimonas*' sp. CC4 has been deposited at the DSMZ (Braunschweig, Germany) under the accession number DSM110005.

### Genome and transcriptome sequencing

The isolates '*Lentimonas*' sp. CC4 to CC21 were sequenced using the Illumina HiSeq 2000 system. The genome of '*Lentimonas*' sp. CC4 was additionally sequenced using the PacBio RSII platform. Sequence data was deposited in the European Nucleotide Archive (ENA) using the data brokerage service of the German Federation for Biological Data (GFBio), in compliance with the Minimal Information about any (X) Sequence (MIxS) standard (Yilmaz et al., 2011; Diepenbroek & Glöckner, 2014; Harrison et al., 2019). All sequencing data will be made publicly available upon review.

#### Closed reference genome of '*Lentimonas*' sp. CC4 with PacBio.

PacBio sequencing of '*Lentimonas*' sp. CC4 was carried out in collaboration with the Max Planck-Genome-centre Cologne of the Max Planck Institute for Plant Breeding Research. Genomic DNA was size selected for fragments larger than 11 kbp with Blue Pippin (SAGE Science) and library was prepared using the SMRTbell Template Prep Kit and SMRTbell Damage Repair Kit (Pacific Biosciences). Sequencing was performed using a PacBio RS II platform resulting in 56,812 raw reads and with a total of 869,712,267 bp. After quality trimming reads were assembled via the PacBio software into two closed contigs with 4,016,414 bp and 907,129 bp with a coverage of 157.79 and 150.12.

### Genome alignment and whole genome identity.

For genome comparison between the Illumina genomes and the PacBio reference genome of '*Lentimonas*' sp. CC4, the contigs were aligned with the "move contig" function of Mauve(Darling, 2004). The contigs were then grouped based on their alignment to either the genome or the plasmid of CC4. Then, we computed the pairwise average nucleotide identity based on BLAST (ANIb) via the JSPECIES web and *Coralimarkarita akajimensis* DSM 45221 (GCA\_000025905.1) as an outgroup (Richter et al., 2016).

## Chapter II

### Functional gene prediction and annotation.

Open reading frames were predicted using prodigal v2.6.3 and annotated using The Seed, COG and Pfam v.31 (Overbeek, 2005; Galperin et al., 2015; El-Gebali et al., 2019).

### Annotation of CAZymes and sulfatases.

Proteins of '*Lentimonas*' sp. CC4 were assigned to CAZyme families on a combined approach using DIAMOND blastp and HMMer v3.0. ORFs were scanned for CAZyme domains using hmmer modules provided by dbCAN (v6). Hits were then searched against a database of known CAZymes ([www.cazy.org](http://www.cazy.org)) using BLAST diamond. Only if HMMer domain and BLAST alignment overlapped, we assigned CAZyme families the respective enzyme family.

Proteins of '*Lentimonas*' sp. CC4 with annotated sulfatase domain (PF00884) were filtered by e-value  $< e^{-10}$  and length  $> 50$  amino acids and then blasted against a database of classified sulfatases (<http://abims.sb-roscoff.fr>) (Barbeyron, Brillet-Guéguen, et al., 2016). The sulfatase subfamily was assigned based on the highest scoring blast hit.

### Transcriptome analysis.

'*Lentimonas*' sp. CC4 and '*Lentimonas*' sp. CC6 were cultured in Tibbles-Rawling medium with 0.2% (w/v) iota-carrageenan, mannose, pure fucoidan or crude fucoidan. After 20 h or 40 h of growth, cells were harvested and RNA was preserved with RNA Protect Bacterial Reagent (Quiagen). RNA was extracted using the RNeasy Mini Kit (Quiagen) and treated with Turbo DNA-free DNase (Thermo Fisher). rRNA was depleted using RiboZero (Epicentre) and libraries were prepared using the ScriptSeq v2 RNA-Seq Library Preparation Kit (Epicentre). Libraries were single-end sequenced on an Illumina HiSeq 2000 system at the BioMicroCenter at MIT, Cambridge.

### Prediction of operons.

To extract genes that are regulated as an operon we used Rockhopper v 2.0.3 which uses a definition of operons as consecutive genes with low gene distance and high transcription similarity (McClure et al., 2013). For this analysis we used the '*Lentimonas*' sp. CC4 RNAseq data of the 20 h timepoint of iota-carrageenan and the 40h timepoint of pure fucoidan.

## Compositional analysis of carbohydrates

### Acid hydrolysis.



Polysaccharides were hydrolyzed in pre-combusted glass vials with 1 M HCl at 100 °C for 24 h.

### Phenol sulfuric acid method.

Total carbohydrate content (TCHO) was measured using the phenol-sulfuric acid method (Dubois et al., 1956) adapted to a microtiter plate format. 100 µL of concentrated sulphuric acid and 15 µl 5% phenol were added to 25 µL of samples in a microtiter plate. A standard curve of L-fucose in deionized water was used for subsequent quantification. The plate was heated to 60 °C for 10 minutes and the absorbance at 490 nm was measured using a plate reader.

### Sulfate content.

The released sulfate by acid hydrolyzed of fucoidans was measured on a Metrohm 761 compact ion chromatograph with a Metrosep A SUPP 5 column and suppressed conductivity detection with 0.5 M H<sub>2</sub>SO<sub>4</sub>. Ions were separated by an isocratic flow of carbonate buffer (3.2 mM Na<sub>2</sub>CO<sub>3</sub> and 1 mM NaHCO<sub>3</sub>) and the duration of a run was 20 minutes, with sulfate eluting at 16 minutes.

### Quantification of monosaccharides via HPAEC-PAD.

Monosaccharides in samples were quantified in a HPAEC-PAD system. This takes advantage of monosaccharides being partially charged in basic conditions and thus can be separated according to their pKa. We adapted a protocol for neutral and acidic sugars described previously (Engel & Händel, 2011). In short, a Dionex 5000+ system with pulsed amperometric detection (PAD) was equipped with a CarboPacPA10 anion exchange column. Neutral and amino monosaccharides were separated by an isocratic flow of 18 mM NaOH for 20 min, followed by a gradient of 500 mM NaAcetate to separate acidic sugars. Standard substances were used to identify peaks by retention time and a standard mix ranging from 1-10 to 1000 µg/L was used to quantify the amount of monosaccharide (x-axis amount and y-axis peak area).

## Chapter II

Table 3: Monosaccharide standards and their retention time used in the HPAEC-PAD system.

Monosaccharide	Abbreviation	Retention time [min]	Sigma Order number
Fucose	Fuc	5.6	F2252
Rhamnose	Rha	8	R3875
Galactosamine	GalN	9	G0500
Arabinose	Ara	10	A3256
Glucosamine	GlcN	12	G4875
Galactose	Gal	16	G0750
Glucose	Glc	17	G8270
Mannose	Man	18	M8574
Xylose	Xyl	19	W360600
Gluconic acid	GulA	28	G9005
Muramic acid	MurA	29	M2503
Galacturonic acid	GalA	30	G48280
Glucuronic acid	GlcA	33	G5269
Mannuronic acid	ManA	34	SMB00280

### Purification of fucoidans

Fucoidan extracts were further purified using a custom medium-scale ion-exchange chromatography setup. A MasterFlex L/S peristaltic pump was used to operate a XK50/250 column (GE healthcare) packed with 200 mL ANX FF ion-exchange resin (GE healthcare) at a flow of 50 ml/min. Fucoidans were solubilized in 50 mM TRIS pH 7.5 and centrifuged for 30 min at 5,000 rpm. For binding, the supernatant was circulated three times over the column. Next, the column was washed with three column volumes of 50 mM TRIS pH 7.5 and three column volumes 50 mM TRIS pH 7.5 with 500 mM NaCl. Highly charged molecules were eluted with 100 mL of 50 mM TRIS pH 7.5 with 5 M NaCl. After each run, the column was washed with 50 mM TRIS pH 7.5 with 5 M NaCl, deionized water, 250 mM NaOH and deionized water. The elution was then extensively dialyzed against deionized water and then freeze dried. The composition of IEX-purified fucoidans was determined with a combination of HPAEC-PAD, ion-chromatography and phenol-sulfuric acid method. 100 µg of

polysaccharide were acid hydrolyzed and released sulfate and monosaccharides were quantified via HPAEC-PAD and IC. To account for incomplete hydrolysis of glycosidic linkages, monosaccharides were normalized to the carbohydrate content of the fucoidans was measured using the phenol-sulfuric acid method. The monosaccharide composition and sulfate content were then normalized to 1. Measurements were done in duplicates (n=2) and the mean is shown in Figure 1a.

Table 4: *List of fucoidans used in this study.*

Source of fucoidan	Supplier	Ordering number	Purified via IEX
<i>Undaria pinnatifida</i>	Carbosynth	YF145110	yes
<i>Sargassum fusiforme</i>	Carbosynth	YF157167	yes
<i>Fucus serratus</i>	Carbosynth	YF09360	yes
<i>Macrocystis pyrifera</i>	Carbosynth	YF145109	yes
<i>Ecklonia maxima</i>	Carbosynth	YF157166	yes
<i>Cladosiphon okamurans</i>	Carbosynth	YF146834	yes
<i>Durvillea potatorum</i>	Carbosynth	YF157165	yes
<i>Fucus vesiculosus</i>	Sigma-Aldrich	F5631	no

### Glycan profiling during fucoidan degradation

'*Lentimonas*' sp. CC4 was grown in triplicates (n=3) in MMM with fucoidans from *Fucus vesiculosus*, *Fucus serratus*, *Cladosiphon okamurans*, *Durvillea potatorum* and *Ecklonia maxima* and fucose (0.2% w/v) and iota-carrageenan (0.1% w/v) as control. The concentration of fucoidans was set to a final concentration of 0.2% w/v fucose. Over up to 5 days of growth, we sampled the cultures with an interval between 3 and 10 h. 1 mL samples were taken for OD<sub>600</sub> measurement and were subsequently filtered through 0.2 µm filter to generate a cell-free culture supernatant. The supernatant was stored at -80°C until analysis. We fitted the OD<sub>600</sub> of all replicates to a logistic growth function and derived the average maximum growth rate in mid-exponential phase.

Quantification of free monosaccharides.

## Chapter II

Released free monosaccharides during growth, were quantified via the HPAEC-PAD system. For this, supernatant samples were diluted 1:25 in distilled water to reduce the salt concentration and then quantified by HPAEC-PAD.

### Quantification of polymeric monosaccharides.

To quantify the monosaccharides that are part of an oligo- or polysaccharide, we used acid hydrolysis to cleave glycosidic linkages into monosaccharides. 500  $\mu$ L of supernatant sample were acid hydrolyzed and then diluted 1:1000 and quantified via HPAEC-PAD. From this we subtracted the amount of free monosaccharide to obtain the amount of monosaccharides that were produced by the acid treatment.

### Analysis of produced oligosaccharides.

Released oligosaccharides during growth, were profiled via the HPAEC-PAD system with using a protocol for larger oligosaccharides (Unfried et al., 2018). In short, a 1:25 dilution of samples was analysed on a Dionex CarboPac PA100 analytical column (2 $\times$ 250 mm) coupled with a Dionex CarboPac PA100 guard column (2 $\times$ 50mm). Separation at 35 °C was achieved by 150 mM NaOH and a linear gradient from 0 to 500 mM NaAc over 19.5 min at a constant flow rate of 0.25 mL/min.

### C-PAGE analysis of molecular weight.

The change of molecular weight over growth was profiled using carbohydrate polyacrylamide gel electrophoresis (C-PAGE). 15  $\mu$ L of sample were loaded into a 4–20% Mini-PROTEAN TGX Precast Protein Gel (Bio Rad). The running buffer consisted of 25 mM Tris-base and 0.2 M glycine and was chilled to 4 °C before use. Gels were run on ice for 30 minutes at 100 V followed by 1 hour at 300 V. Gels were stained for 2h in 0.025% Stains-All (Sigma) in 25% 2-propanol and 50 mM TRIS pH 7.5. Gels were de-stained with 25% 2-propanol until the background was clear.

## Quantification of cross-reactivity between expressed fucoidan pathways

### Preparation of enzyme cocktails.

'*Lentimonas*' sp. CC4 was grown in quadruplicates (n=4) MMM with fucoidans from *Fucus vesiculosus*, *Fucus serratus*, *Cladosiphon okamurans*, *Durvillea potatorum* and *Ecklonia maxima* and fucose (0.2% w/v) as control. The concentration of fucoidans was set to a final concentration of 0.2% w/v fucose. Cells were grown until mid-exponential phase (OD<sub>600</sub>

between 0.25 and 0.35) and 50 mL of culture were harvested by centrifugation for 15 min at 4,000 x g. The supernatant was discarded and excess liquid removed by pipetting to determine the wet weight of the cell paste. Per mg cell paste, the pellet was resuspended in 10  $\mu$ L protein extraction buffer containing 80% v/v Bug Buster protein extraction reagent (Merck) supplemented with lysozyme (1 mg/mL), DNase (0.1 mg/mL), 3.3 mM MgCl<sub>2</sub>, cOmplete Protease Inhibitor (Roche), 1 mM TCEP and 8 mM MOPS buffer pH 7.9. The cell suspension was mixed for 10 minutes then centrifuged for 5 minutes at 10,000 x g and 4 °C. The supernatant containing the soluble extracted proteins was sterile filtered using centrifugal filter and directly used to start enzyme assays.

### Enzyme reaction.

As substrates, fucoidans from *Fucus vesiculosus*, *Fucus serratus*, *Cladosiphon okamurans*, *Durvillea potatorum* and *Ecklonia maxima* and fucose were solubilized to 0.5 g/L in 35 g/L sea salts (Sigma) with 10 mM MOPS pH 7.9 and 1 mM TCEP. The solution was sterile filtered and stored in aliquots at -80°C until analysis. 1.8 ml of each substrate was mixed with 40  $\mu$ L of enzyme extract and a negative control of heat inactivated (80 °C, 10 min) enzyme extract. Each of the reactions was sampled over 24 h; a 150  $\mu$ L subsample was heat inactivated and stored at -80°C until analysis. In total, 1,764 samples were collected and 50  $\mu$ L were used to quantify the reducing ends using the PAHBAH assay. Additionally, the first and the last timepoint of each enzyme reaction was diluted 1:25 with de-ionized water and liberated monosaccharides were quantified via HPAEC-PAD.

### Reducing sugar assay.

Reducing sugar equivalents of a sample were quantified with the para-hydroxybenzoic acid hydrazide (PAHBAH) assay. Reducing equivalents are carbohydrates in the open, hemi-acetal or hemi-ketal form which includes monosaccharides and the terminal carbohydrate of oligo- or polysaccharides. Working reagent was freshly prepared as a 9:1 mixture of reagent A (0.3 M 4-hydroxybenzhydrazide, 0.6 M HCl) and reagent B (48 mM trisodium citrate, 10 mM CaCl<sub>2</sub>, 0.5 M NaOH). 1 mL of working reagent was added to 50  $\mu$ L of sample. A standard curve of L-fucose in deionized water was used for subsequent quantification. The mixture was heated for 6 minutes at 100 °C under constant mixing and the absorbance at 410 nm was measured. The amount of reducing sugar equivalents (in mg/mL) was calculated from the slope and intercept of a linear fit of the standards (x-axis amount and y-axis absorbance).

### Data analysis.

## Chapter II

The amount of reducing end were fitted to an enzymatic saturation curve ( $\frac{a*x}{b+x} + C$ ) and the rate of released reducing ends was derived from the slope after 30 min of each reaction. For enzyme reaction without any activity, i.e. the negative controls or enzyme extracts from fucose grown cells, we set the slope to 0 for further analysis. As we observed substrate specific differences in the maximum amount of released reducing end, we normalized the rate per substrate to 1. The activity data were then hierarchical clustered (rows: growth substrate, columns: reaction substrate) based on the Euclidean distance metric.

### Whole-cell proteome analysis

For proteome analysis, '*Lentimonas*' sp. CC4 was cultured in triplicates (n=3) in MMM with 0.1% iota-carrageenan, 0.2% galactose, 0.2% fucose, 0.2% fucoidan from *Cladosiphon okamurans* or 0.2% fucoidan from *Fucus vesiculosus*. Pre-cultures with the same carbon source were used to set the starting OD<sub>600</sub> of the main culture to 0.05. Cells were harvested in mid-exponential phase (OD<sub>600</sub> = ~0.25) by centrifugation at 4,000 x g for 10 min at 4 °C and stored at -80 °C until analysis. Cell pellets were washed in TE buffer (10 mM Tris-HCl pH 7.5, 10 mM EDTA pH 8.0) containing cOmplete Protease Inhibitor (Roche). Soluble proteins were extracted by sonication (2 x 25 s), and the protein concentration was determined with the Bradford assay. Then, 15 ug of protein separated (60 min, 150 V) in a 10% SDS gel and stained with Roti-Blue quick (Carl Roth). Subsequently, entire gel lanes were sliced into ten equal pieces and digested with a 1 µg mL/L trypsin solution. Peptides were separated on a C18 column and reversed-phase chromatography on a nano-ACQUITY-UPLC (Waters Corporation). Mass spectrometry (MS) and MS/MS data were determined using an online-coupled LTQ-Orbitrap mass spectrometer (Thermo Fisher) (Otto et al., 2010). MS spectra were searched against a protein sequence database, including '*Lentimonas*' sp. CC4 and common laboratory contaminants. Protein searches were performed using MaxQuant with a peptide level false discovery rate of 0.01 (Tyanova et al., 2016). Only proteins with at least two unique peptides detected were considered positively identified. In total 2,059 proteins were quantified. For comparisons between samples the automatically calculated iBAQ values (intensity-based absolute quantification; i.e., peak area divided by the sum of all theoretical peptides) were normalized to 100% in each sample to obtain %iBAQ values giving the relative protein expression in % of the total proteome (Shin et al., 2013). Mass spectrometry data were

deposited to the ProteomeXchange Consortium via the PRIDE partner repository with the dataset identifier PXD015328 (Username: reviewer29900@ebi.ac.uk Password: YPdHjzis).

### Proteome data analysis.

Prior to statistical analysis, the proteome dataset was imputed with the LSA-method(Bo et al., 2004). Then, differentially expressed proteins (566 proteins, fold change >10, p-value < 0.05 and q-value <0.05) were identified using a version of Linear Models for Microarray Data (LIMMA) optimized for proteome data with correction for false discovery by the Benjamin-Hochberg procedure (Kammers et al., 2015). The expression data were normalized using the z-score and differentially expressed proteins were subjected to kmean-clustering to group into clusters of co-expressed proteins. From the sum of squared distances to the closest cluster center, we estimated that eight k-mean clusters are a reasonable number to capture major patterns of differentially expressed proteins. The results of the LIMMA analysis and clustering are summarized in Supplementary Table 3.

### Metabolomics of the bacterial microcompartment

*Lentimonas* sp. CC4 was grown in triplicates (n=3) MMM with 0.2% of fucose, rhamnose, glucose, mannose or galactose. During growth, the cultures were sampled with an interval between 3 and 10 h. 1 mL samples were taken for OD<sub>600</sub> measurement and were subsequently filtered through 0.2 µm filter to generate a cell-free culture supernatant. The supernatant was stored at -80 °C until analysis. First, samples were screened for metabolite production using a derivatization method adapted to salty samples on a 7890B GC System equipped with a 5977 MS detector (Agilent Technologies) (Sogin et al., 2019). Next, lactate was quantified using the lactate assay kit (Sigma) and 1,2-propanediol using a GC-MS protocol based on a DB-WAX Ultra Inert capillary column (Agilent Technologies, part no 122-7033UI) and following temperature settings: start temperature 100 °C, hold 1 min, ramp 10 °C /min to 180 °C, hold 6 min, ramp 10 °C /min to 250 °C and final hold for 4 min. We used a logistic growth function to fit the OD<sub>600</sub> data, and aligned the growth curve of replicates to intersect at OD<sub>600</sub>=0.25. To obtain the rate of metabolite production or consumption, fitted the metabolite concentrations to a logistic function and derived the maximum slope (at around 50 h).

## Chapter II

### Protein and 16S mapping of ‘*Lentimonas*’ to OSD and TARA metagenomes

We used the aligner SINA (Pruesse et al., 2012) to identify reads belonging to the 16S rRNA gene (miTAGs) in TARA Oceans prokaryotic, surface fraction (Sunagawa, Coelho, Chaffron, Kultima, Bork, et al., 2015) and Ocean Sampling Day 2014 (Kopf et al., 2015). The reads were then classified using a Bayesian classifier in combination with the SILVA 132 database (Q. Wang et al., 2007; Quast et al., 2013) and the relative abundance of miTAGs per genus was derived from the ratio of aligned reads to total 16S rDNA reads. Metadata and relative abundances from the samples are provided in Supplementary Table 5 and the detailed workflow for analyzing the metagenomic and miTAG data can be found at [https://figshare.com/articles/16S\\_miTAGs\\_Sichert\\_et\\_al\\_2019/9904793](https://figshare.com/articles/16S_miTAGs_Sichert_et_al_2019/9904793) and [https://github.com/mschecht/lentimonas\\_env\\_analysis/](https://github.com/mschecht/lentimonas_env_analysis/).

The OSD samples with the highest proportion of ‘*Lentimonas*’ (OSD6, OSD13, OSD46, OSD113, OSD131, OSD170, OSD173, SD174, OSD176, OSD177) were assembled using Plasm 2.c7e35 (Steinegger et al., 2019). The resulting open reading frames were aligned to genome of ‘*Lentimonas*’ sp. CC4 using mmseqs search (‘--cov-mode 1 -c 0.6’) (Steinegger & Söding, 2017). Next, aligned proteins were filtered for the most confident hit and to account for multiple hits, we only allowed one alignment per metagenomic protein to a genomic protein.

### Acknowledgments

We thank Kristoffer Caspersen for his help with GC-MS measurements, Timothy Ferdelman and Kirsten Imhoff for their expertise in sulfate quantification, Marie-Katherin Zühlke for submission of the proteome data to PRIDE, Ivaylo Kostadinov of GFBio (<http://www.gfbio.org>) for sequence data deposition and Bruno Hüttel from the Max-Planck-Genome-Center Cologne. AS and MSS are members of the International Max Planck Research School of Marine Microbiology (MarMic). JHH acknowledges funding from the Max-Planck-Gesellschaft and from the Emmy Noether Program of the DFG, grant number HE 7217/1-1. MFP acknowledges support by the U.S. Department of Energy (DE-SC0008743). The work of SM, TS and DB was financially supported by grants (BE 3869/4-1, SCHW 595/10-1) of the DFG in the framework of the research unit FOR2406 “Proteogenomics of Marine Polysaccharide Utilization” (POMPU). FU was supported by a scholarship from the Institute of Marine Biotechnology e.V.



### **Author contributions**

JHH and MFP initiated the study and directed the project. CHC and AS conducted the experiments. The strains were isolated by CHC. FU and SM conducted the proteome analysis for which TS and DB provided resources. MSS and AFG analyzed the OSD and TARA. ML conducted GC-MS measurements and provided resources for metabolomics. AS, JHH, MFP prepared the manuscript and received input from all authors.

### **Declaration of interests**

The authors declare no competing interests.

Figures

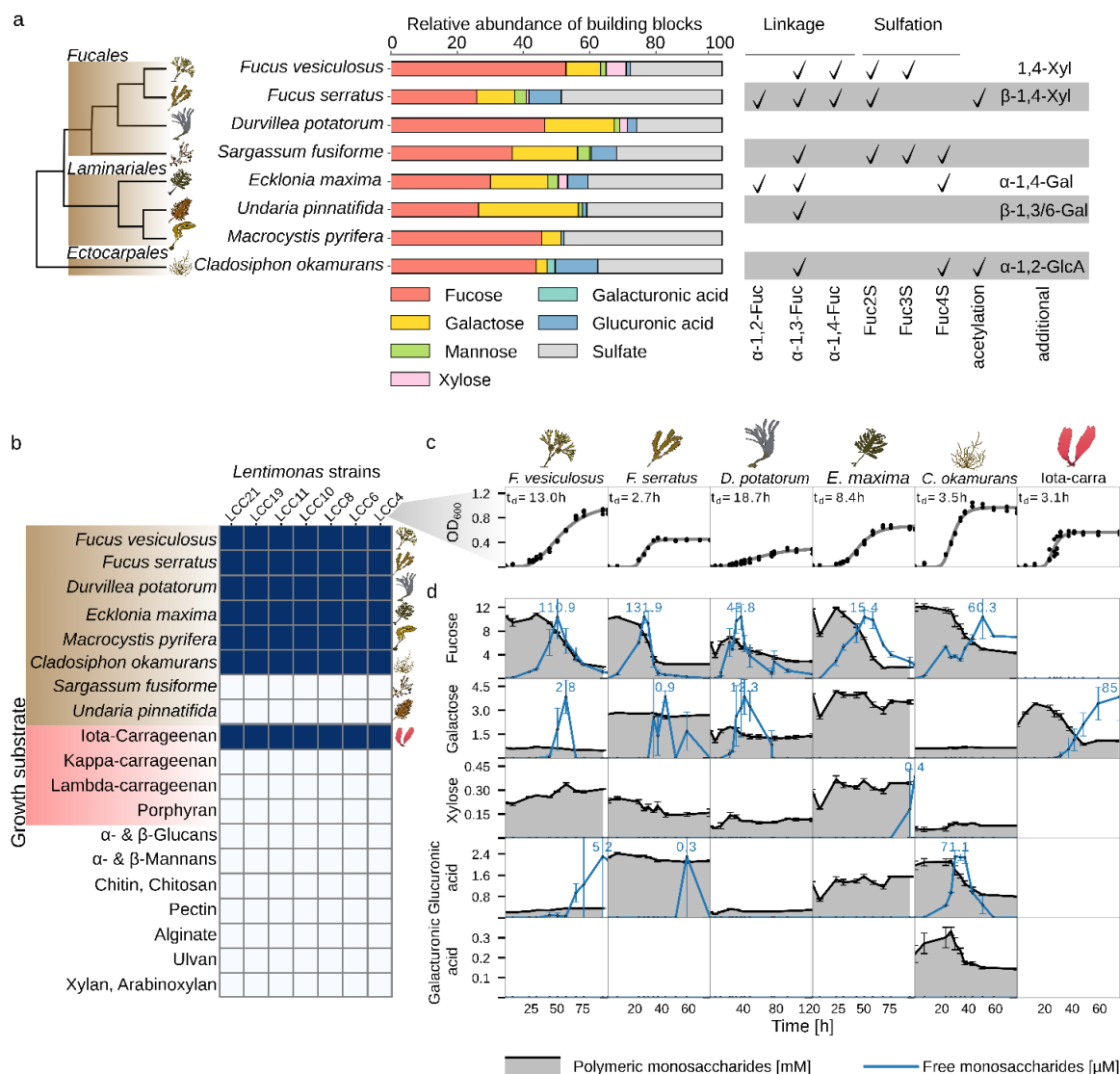


Figure 10: **Degradation of complex fucoidans by specialized ‘Lentimonas’ spp.** **a**, Overview of the fucoidans used in this study. From left to right: cladogram of the phylogenetic relationship between species of brown algae from (Silberfeld et al., 2010), mean (n=2) relative abundance of building blocks and known structural features obtained from literature (Nishino et al., 1991; Nagaoka et al., 1999; Chevlot et al., 2001; Bilan et al., 2006; Hemmingson et al., 2006; Cong et al., 2016). **b**, Substrate utilization of polysaccharides by different ‘Lentimonas’ sp. CC4 to CC21 represented as a heatmap. **c**, Growth of ‘Lentimonas’ sp. CC4 on five different fucoidans and iota-carrageenan (n=3). The black dots represent the measured OD<sub>600</sub> values and the text denotes the doubling time derived from a fitted growth function (grey line). **d**, Monosaccharide profiling over growth of ‘Lentimonas’ sp. CC4 on different sulfated polysaccharides. The blue line represents free monosaccharides measured in the culture supernatant and the grey shaded area and solid black line represent monosaccharides of oligo- or polymers measured after acid hydrolysis. For comparison, free monosaccharides are plotted on an arbitrary scale from zero to the maximum value, which included in the graph. Data points represent the mean and error bars the standard deviation (n=3).

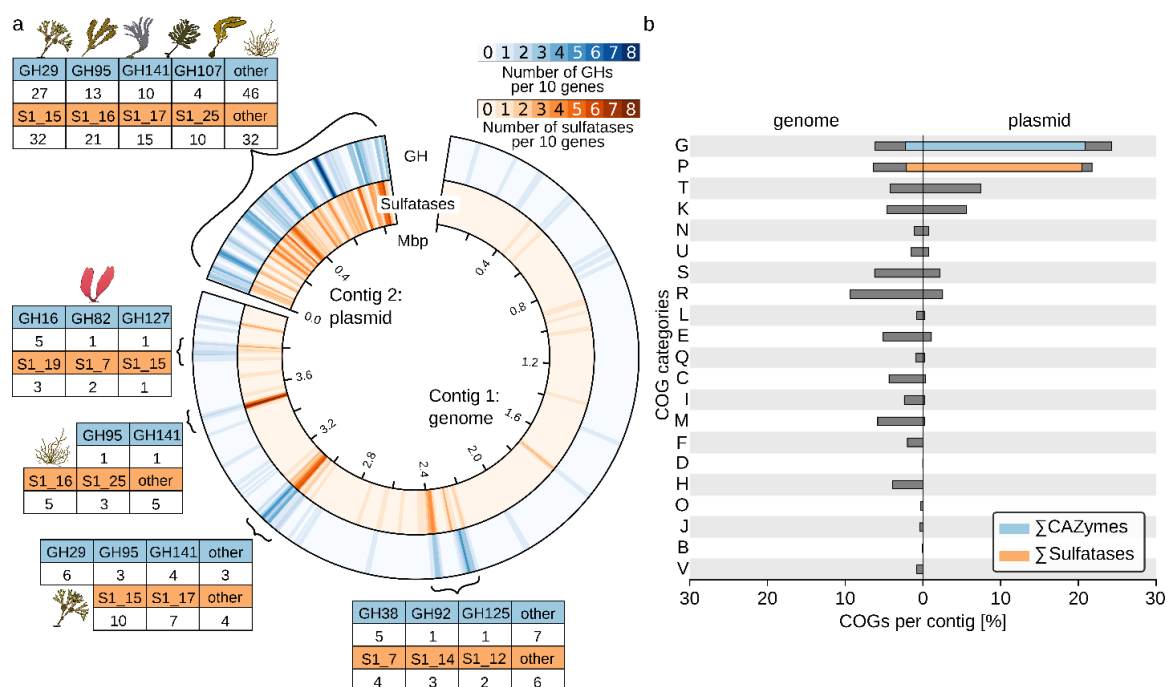
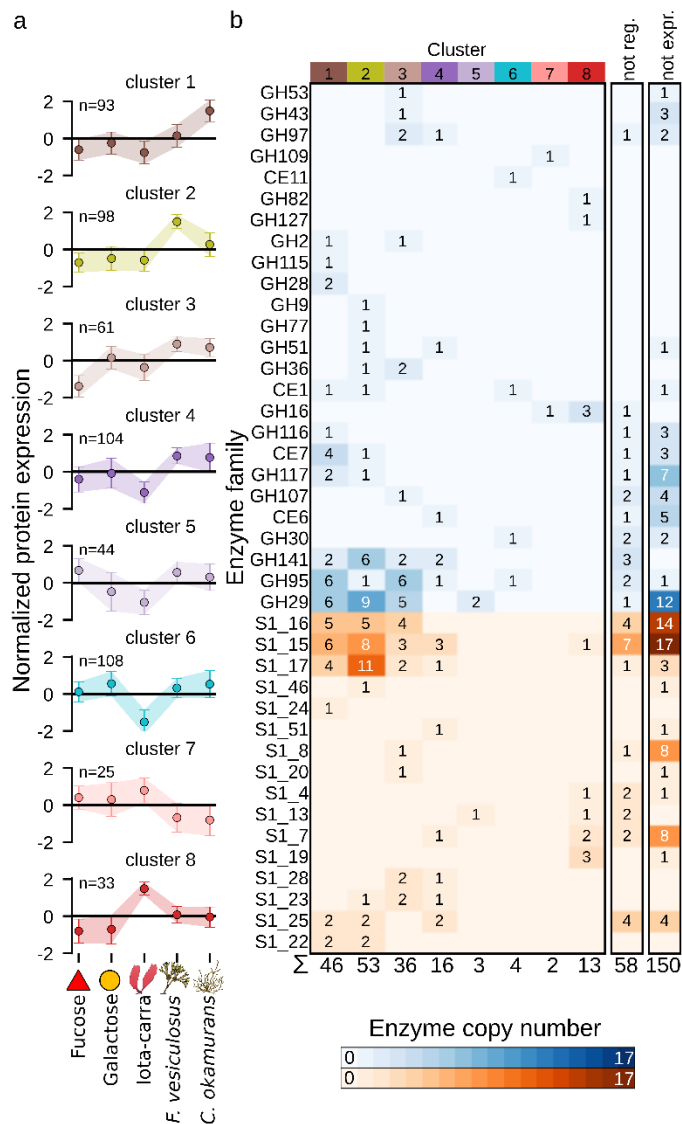
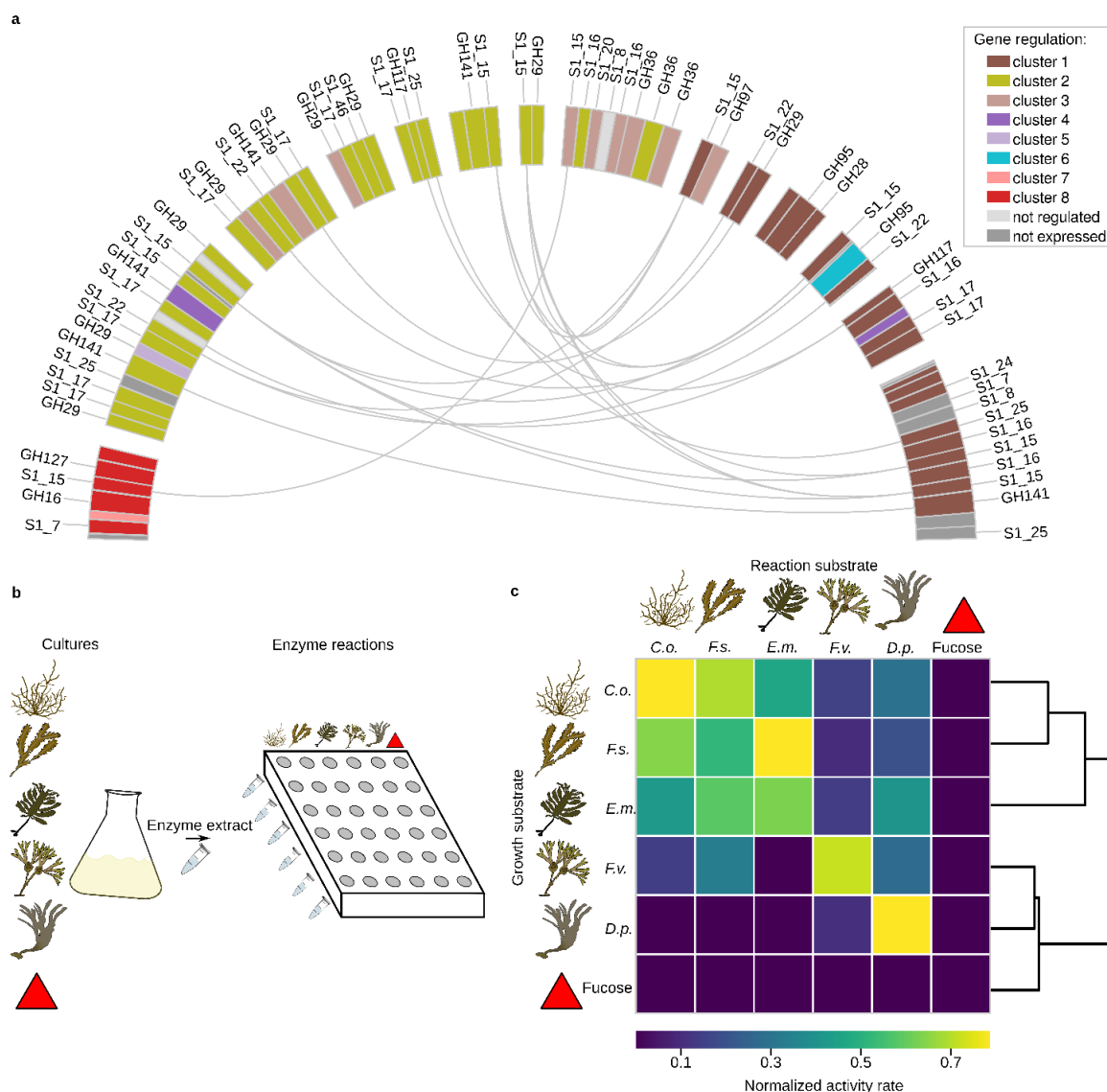


Figure 11: '*Lentimonas*' sp. CC4 has a megaplasmid and distinct genetic loci for the degradation of sulfated polysaccharides. **a**, Genome overview of '*Lentimonas*' sp. CC4; from inside to outside: genome scale in Mbp, circular heatmap of density of sulfatase genes (orange) and glycoside hydrolases (GH) genes (blue), curly brackets mark the genomic loci and the tables their enzyme content. **b**, Functional profile of each contig based on clusters of orthologous groups (COG) annotation normalized to the gene content. Abbreviations for COG categories: Carbohydrate transport and metabolism (G), inorganic ion transport and metabolism (P), signal transduction mechanisms (T), transcription (K), cell motility (N), intracellular trafficking, secretion and vesicular transport (U), function unknown (S), general functional prediction only (R), Energy production and conversion (C), replication, recombination and repair (L), amino acid transport and metabolism (E), secondary metabolites biosynthesis, transport and catabolism (Q), energy production and conversion (C), lipid transport and metabolism (I), cell wall/membrane/envelope biogenesis (M), nucleotide transport and metabolism (F), cell cycle control, cell division, chromosome partitioning (D), coenzyme transport and metabolism (H), posttranslational modification, protein turnover, chaperones (O), translation, ribosomal structure and biogenesis (J), chromatin structure and dynamics (B) and defense mechanisms (V).

## Chapter II



**Figure 12: Differential proteomics reveal pathways for fucoidan degradation.** **a**, Protein expression of clusters of co-expressed enzymes. 566 differentially expressed proteins were clustered using the kmean-algorithm based on their normalized expression vector (zscore). The number of proteins in each cluster is denoted by n and the mean and standard deviation of their zscore is denoted by data points and error bar. Enzyme expression was quantified in three replicates (n=3). **b**, Heatmap representing enzyme copy number families with at least one differential regulated protein together with not-regulated and not-expressed enzymes for comparison.



**Figure 13: Genetic and enzymatic specificity of pathway for diverse fucoidans.** **a**, Assembly of substrate specific operons by combining different enzyme homologs. Genes from representative operons of ‘*Lentimonas*’ are shown as coloured bars denoting their regulation according to the colour scheme used from the cluster of co-expressed enzymes (Figure 13). Numeric identifier for operons (from Supplementary Table 4) from left to right: 734, 607, 793, 829, 790, 878, 786, 897, 894, 871, 850, 840, 813 and 688. Grey links are drawn between enzymes in different operons with more than 50% identity. **b**, Experimental design to measure cross-activity between expressed pathways and fucoidans. **c**, Heatmap showing the normalized rate of released reducing end after 30 min (n=4). Substrates are arranged according to a hierarchical clustering based on the Euclidean distance.

## Chapter II

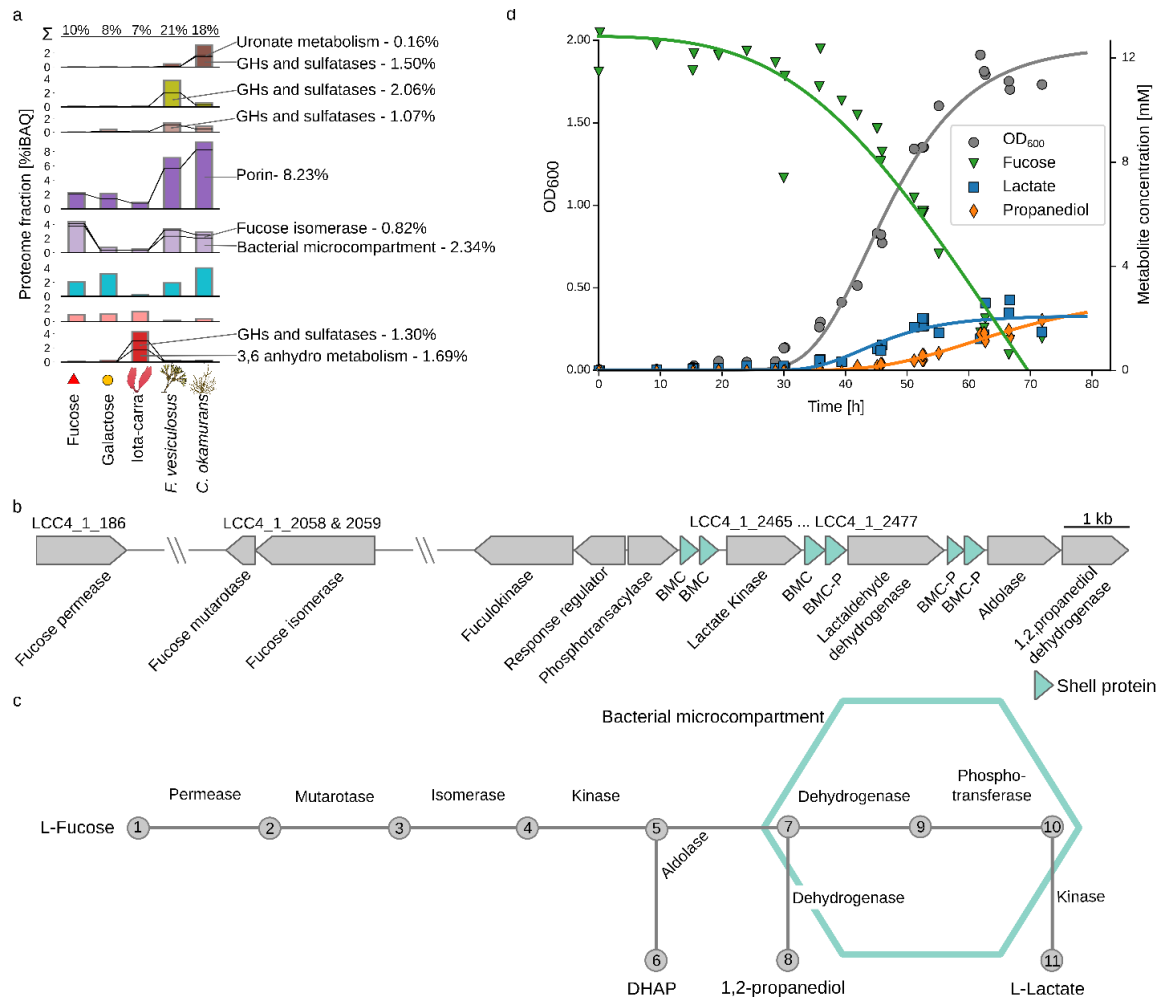


**Figure 14: High metabolic burden to express dedicated pathways for fucoidans including a fucose-specific bacterial microcompartment.** **a**, Proteome fractions of during growth on different carbohydrates. The bar graph shows the sum of protein expression per cluster of co-expressed enzymes and the text label denotes the proteome fraction of selected enzymes or enzyme families. **b**, Gene organization encoding the fucose metabolic pathway of ‘*Lentimonas*’ sp. CC4. **c**, Reaction scheme of the fucose monosaccharide pathway. Key for the compounds: 1) extracellular  $\alpha$ -L-fucose, 2) intracellular  $\alpha$ -L-fucose, 3)  $\beta$ -L-fucose, 4) L-fuculose 5) L-fuculose-1-P, 6) Dihydroxyacetone phosphate, 7) L-lactaldehyde, 8) 1,2-propanediol, 9) lactyl-CoA, 10) lactyl-phosphate 11) L-lactate. **d**, Production of L-lactate and 1,2-propanediol during growth (n=3) of ‘*Lentimonas*’ sp. CC4 on L-fucose.

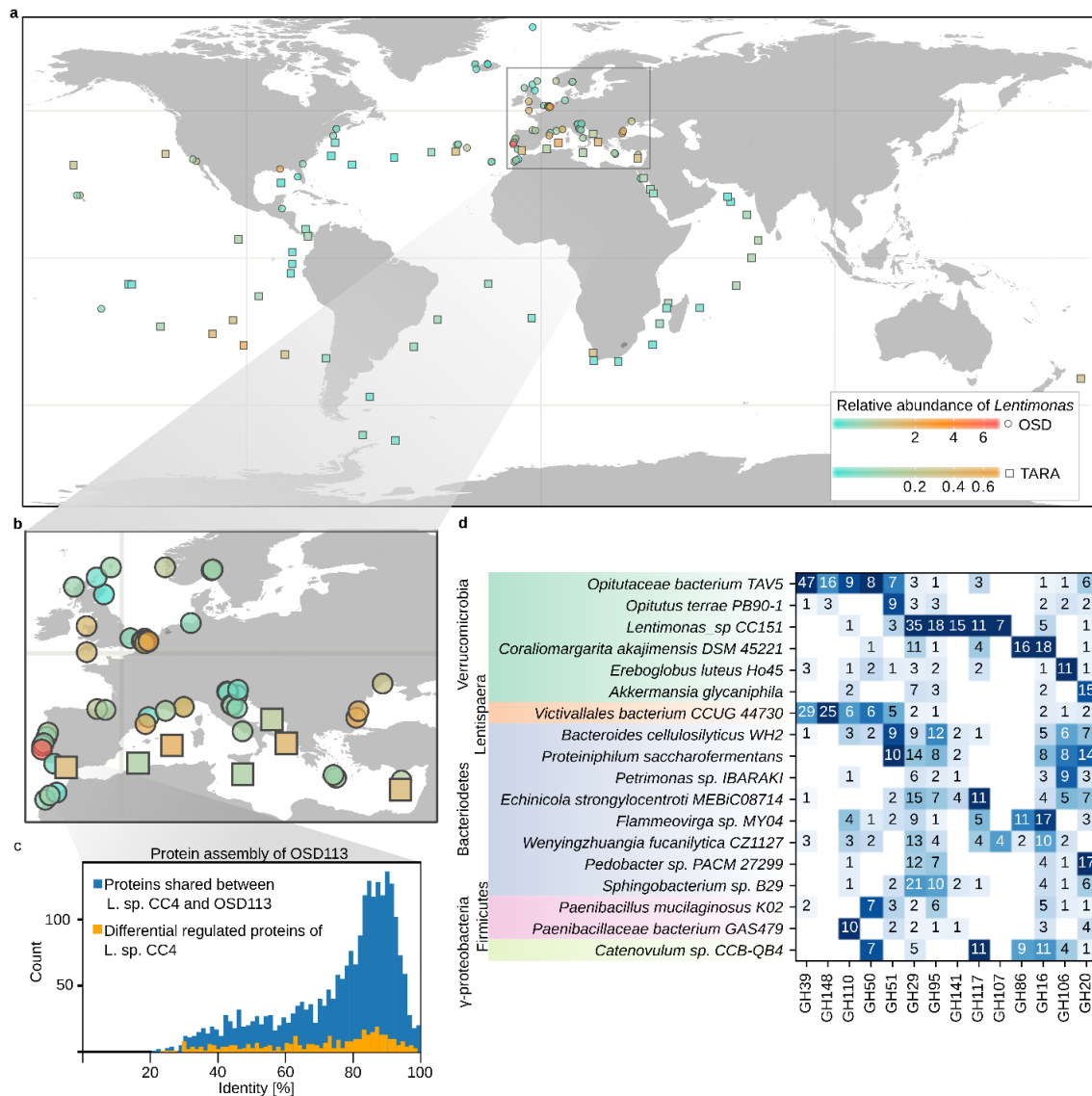


**Figure 15: Verrucomicrobia are abundant and specialized polysaccharide degraders. a.** Relative abundance of the genus ‘*Lentimonas*’ in miTAGs of the Ocean Sampling Day 2014 and TARA ocean. **b.** Zoom into coastal samples around Europe with high abundance of ‘*Lentimonas*’ **c.** Protein comparison of the OSD113 sample with the highest relative abundance and ‘*Lentimonas*’ sp. CC4. The histogram shows the pairwise identity of assembled proteins of the OSD113 sample compared with ‘*Lentimonas*’ sp. CC4. **d.** Heatmap showing the copy number of enzymes in Verrucomicrobia compared to other bacterial phyla.





## Chapter III.

### **Aspartate as novel acid/base catalyst in a marine GH29 fucosidase from '*Lentimonas*' sp. CC4**

Andreas Sichert<sup>1,2,#</sup>, Nadine Gerlach<sup>1,2,#</sup>, Tatjana von Rosen<sup>1,2,3</sup>, Craig S. Robb<sup>1,2,4</sup>, Jan-Hendrik Hehemann<sup>1,2\*</sup>

<sup>1</sup> MARUM - Center for Marine Environmental Sciences, University Bremen, 28359 Bremen, Germany

<sup>2</sup> Max Planck Institute for Marine Microbiology, 28359 Bremen, Germany

<sup>3</sup> Current address: Department of Biology, ETH Zurich, 8093 Zurich, Switzerland

<sup>4</sup> Current address: University of British Columbia, BC V6T 1Z4 Vancouver, Canada

\*Correspondence: [jhhehemann@marum.de](mailto:jhhehemann@marum.de)

# The authors contributed equally.



## Abstract

Fucoidans are a diverse class of sulfated polysaccharides from the cell wall of brown algae. Owing to their structural diversity, fucoidans are only degraded by highly specialized bacteria such as the marine Verrucomicrobium ‘*Lentimonas*’ sp. CC4 with approximately 100 enzymes. Since these enzymes are interlocked in a complex degradation cascade, each single enzyme may only yield minuscule amounts of product challenging the characterization of fucoidan active enzymes without their cognate partner. To circumvent this, we biochemically and structurally characterize the 22\_GH29 fucosidase and 21\_S1\_15 sulfatase originating from a two gene operon of ‘*Lentimonas*’ sp. CC4. We solved the monomeric structure of GH29 and S1\_15 by X-ray crystallography to 1.8 and 1.7 Å, revealing an active site typical for exo-acting enzymes. Unlike in other GH29s, the catalytic residues of 22\_GH29 involved two Asp instead of one Asp and one Glu acting as Brønsted acid/base. Furthermore, the GH29 is specific to  $\alpha$ 1,3-linked L-fucose producing a yet unidentified component from fucoidan. Our findings provide insights into the microbial remineralisation of fucoidan and underscore ‘*Lentimonas*’ sp. CC4 as a resource for novel fucoidan active enzymes.

## Introduction

Fucoidans are diverse class of sulfated cell wall polysaccharide from brown algae with complex degradation pathways and a high environmental importance. Fucoidans, which make up to 23% of algal dry weight, are highly branched and sulfated and their structure varies depending on algal species and growth season (Skriptsova et al., 2010; Deniaud-Bouët et al., 2014, 2017). For example, fucoidan from *Fucus vesiculosus* has a backbone of alternating  $\alpha$ -1,3/ $\alpha$ -1,4 linked L-fucose with sulfate esters on O-2 or O-3 with additional mannose and xylose residues (Nishino et al., 1994; Chevolut et al., 2001). Due to this structural complexity, fucoidans can only be degraded by highly specialized microbes such as the marine Verrucomicrobium ‘*Lentimonas*’ sp. CC4 employing over 100 enzymes (Sichert et al., in preparation). Consequently, fucoidans accumulate in the water column, for example over a diatom spring bloom, and have a high potential to sequester carbon in the ocean (Vidal et al., in preparation). Although previous studies identified potential degradation pathways for fucoidan, we lack the biochemical characterization of fucoidan-active enzymes that would help us understand why fucoidans are difficult to turn-over in the environment.

The enzymatic degradation of fucoidan is likely a multi-step reaction with several interlocked enzymes only active with their cognate enzyme partner. The activity of

### Chapter III

characterized fucoidanases is typically low, yielding only a few percent degradation, but the yield can be improved by combining glycoside hydrolases with ancillary enzymes (Schultz-Johansen et al., 2018; Vickers et al., 2018). For example, the carbohydrate esterase (CE) increases the activity of an endo-enzyme and sulfatase the activity of a GH29 exo-fucosidases (Berteau et al., 2004; Nagao et al., 2017). This synergistic effect of enzymes complicates the biochemical analyses of a single fucoidanase without its cognate partner. Enzymes that act together on a polysaccharide are regulated in polysaccharide utilization loci (PUL) and therefore, PULs provide an opportunity to identify cognate enzymatic partners. For example, the marine Bacteroidetes *Wenyinzhuangia fucanilytica* CZ1127<sup>T</sup> has a PUL encoding a S1\_17 and S1\_25 exo-sulfatases that stepwise degrade 2,3-di-O-sulfated fucooligosaccharides (A. S. Silchenko et al., 2018). The Verrucomicrobium '*Lentimonas*' sp. CC4 organizes its enzymes in operons, and therefore, these operons represent a resource to identify enzymes that act in synergy on fucoidan.

The degradation of fucoidan or fucoidan-derived oligosaccharides is catalysed by exo-acting fucosidases and sulfatases. Proteomics on the marine Verrucomicrobium '*Lentimonas*' sp. CC4 revealed each 20 homologs of GH29 fucosidases and S1\_15 sulfatases, suggesting those enzymes are key to degrade fucoidans. GH29 hydrolyse terminal  $\alpha$ -1,2/3/4 or /6-linked fucose using a retaining mechanism (White Jr. et al., 1987; Eneyskaya et al., 2001; Cobucci-Ponzano et al., 2003; Lombard, Ramulu, et al., 2014). The catalytic active site is highly conserved in a  $(\beta/\alpha)_8$  triosephosphate isomerase (TIM) barrel domain (Sulzenbacher et al., 2004; Sela et al., 2012; Summers et al., 2016). Typically, the catalytic residue Asp acts as nucleophile and Glu as Brønsted acid/base (Sulzenbacher et al., 2004). Since the catalytic residues are located on different loops up to 50 amino acids apart, they are difficult to identify and these insights can only be derived from protein structures. Only recently, the first substrate-complex of GH29 with Lewis<sup>X</sup>, Lewis<sup>Y</sup> and Lewis<sup>A</sup> oligosaccharides revealed unusual substrate binding pockets with a selectivity for Gal in the +2 subsite, GlcNAc in the +1 subsite and flexible cleavage of  $\alpha$ 1,3 and  $\alpha$ 1,4 L-fucose in the -1 subsite (Hobbs et al., 2019). Notably, no marine GH29 was crystallized with fucoidan as substrate, illustrating our limited understanding of marine fucosidases.

Similar to GH, sulfatases are specific for the targeted carbohydrate backbone and grouped into homologous enzyme families (Barbeyron, Brillet-Guéguen, et al., 2016; Hettle, Vickers, Robb, Liu, Withers, Hehemann, & Boraston, 2018). S1 family consist of small C-terminal and a large N-terminal domain harbouring the active site. The active site is consisting

of ten conserved residues: five basic and four acidic/polar amino acids as well as a formylglycine (FGly), which derives from post-translational oxidation of a Cys or Ser (Schmidt et al., 1995; Dierks et al., 1998; Lukatela et al., 1998). To date, one sulfatase from the marine mollusc *Pecten maximus* and two sulfatases from *Wenyingshuangia fucanilytica* CZ1127<sup>T</sup> are the only known sulfatases that act on fucoidan (Berteau et al., 2002; A. S. Silchenko et al., 2018). So far, there are no biochemical and structural characterized members of the subfamily S1\_15 known.

In this study, we characterize a two gene operon consisting of 22\_GH29 and 21\_S1\_15 from '*Lentimonas*' sp. CC4 that act in synergy on fucoidan. We show that the 22\_GH29 is an active fucosidase specific for  $\alpha$ 1,3-linked fucose and on fucoidan, this enzyme produces a so far uncharacterized component. The 21\_S1\_15 was produced in soluble form, but screening for activity remained unsuccessful. To understand the mode of action of both enzymes, we determined the structure of 22\_GH29 and 21\_S1\_15 using X-ray crystallography at 1.8 Å and 1.7 Å, which showed their small substrate binding pockets suggesting an exo-active mode. Additionally, we identified Asp259 as novel catalytical residues of 22\_GH29, which was confirmed as Bronsted acid/base by mutagenesis of 259Asp/Ala. The structure of S1\_15 is the first reported structure of subfamily S1\_15. Those results establish a basis to further elucidate the biochemistry of fucoidan active enzymes from '*Lentimonas*' sp. CC4.

## Material and methods

### Identification of target genes

The proteome expression data provided by Sichert et al., was filtered for glycoside hydrolase with the highest expression value (riBAQ). In this way, we identified the genes with the locus tag LCC4\_21\_S1\_15 and LCC4\_2\_22\_GH29, from now on called 21\_S1\_15 and 22\_GH29. To analyze their gene transcription, we obtain the single end reads for growth on iota-carrageenan and fucoidan from *Fucus vesiculosu* from ENA under the accession number SAMEA6101978 and SAMEA6101979. Reads were aligned to the genome CC4 using Bowtie2 v (Langmead & Salzberg, 2012). Next, we used samtools to first sort the alignment file with "samtools sort" and then calculate the coverage per bp "samtools depth" (Li et al., 2009). We then calculated the reads per transcript million (TPM) per 10 bp.

## Chapter III

### Production and cloning of recombinant plasmids

The N-terminal signal peptide (Supplement Table 2) was predicted using the SingalP V4.1 server (Nielsen, 2017) with default options. The forward and reverse primers for 22\_GH29, 21\_S1\_15 and 2701\_GH29 (Supplement Table 2) were designed with a single N-terminal 6-His-Tag and a ~30 bp overhang and complementary to the pet28a(+) expression plasmid (69864, Merck Millipore). Genes were amplified with Q5 High-Fidelity DNA Polymerase (M0492, New England Biolabs) from genomic DNA of '*Lentimonas*' sp. CC4. Recombinant plasmids were assembled with Gibson Assembly (E2611, New England Biolabs). Purified plasmids were transformed into *Escherichia coli* NEB5 $\alpha$  for subcloning and into *Escherichia coli* BL21(DE3) for overexpression according to the manufacturer's instructions (C2987I+C2527H, New England Biolabs). For activate sulfatase via posttranslational modification of Cys into FGly, pet28a(+) constructs were co-transformed with pBAD/myc-his A Rv0712 (FGE) (Hettle, Vickers, Robb, Liu, Withers, Hehemann, Hettle, et al., 2018). Transformed cells were grown on lysogeny broth (LB) agar plates with 50  $\mu$ g/mL kanamycin (Sigma Aldrich) for pet28a(+) constructs or 50  $\mu$ g/mL kanamycin and 50  $\mu$ g/mL chloramphenicol for pet28a/pBAD constructs at 37 °C overnight.

### Mutagenesis of catalytic residues from 22\_GH29

The putative catalytic residues were identified via structural alignment as Asp210 and Asp259 with 2wvs. Single-side directed mutagenesis of each catalytic residue into a Ala residue was performed according to Liu & Naismith (2008) using purified recombinant plasmid of 22\_GH29 (Supplement Table 2). Mutated recombinant plasmids were verified by gel electrophoresis and Sanger-sequencing prior to transformation into *E. coli* BL21(DE3).

### Protein production

22\_GH29 cultures were grown in 5 L Erlenmeyer flasks with 1 L of ZYP5052 auto-induction medium (Studier, 2005) and 100  $\mu$ g/mL kanamycin for four days at 20 °C and 150 rpm. 21\_S1\_15 was overexpressed in 5 L Erlenmeyer flasks with 1 L of LB, 2  $\mu$ M CuSO<sub>4</sub>, 50  $\mu$ g/mL kanamycin and 50  $\mu$ g/mL chloramphenicol at 37 °C until OD<sub>600nm</sub> ~ 0.5. The expression of FGE was induced by 0.1 % L-arabinose for 2-5 h at 20 °C, followed by the induction of the sulfatase using 1 mM (IPTG) at 16 °C overnight. Bacterial cultures were harvested at 4900 g

and 4 °C for 15 minutes. For cell lysis, the pellet was resuspended in 20 mL buffer (25 % sucrose, 50 mM Tris pH 8), 30 mg of lysozyme (~ 7000 U mg<sup>-1</sup>, Sigma Aldrich) was added and the mixture was incubated at room temperature (~ 25 °C) for 10 minutes while stirring. Then, 40 mL of deoxycholate solution (20 mM Tris pH 8, 1 % w/v deoxycholate, 100 mM NaCl, 1 % w/v Triton X-100), MgSO<sub>4</sub> (5 mM final concentration) and 100 µL of 10 mg ml<sup>-1</sup> DNase I (≥ 400 Kunitz mg<sup>-1</sup>, Sigma Aldrich) were added. The mixture was incubated at room temperature (~ 25 °C) until it was no longer viscous and centrifuged at 30966 g and 4 °C for 45 minutes.

### Protein purification

Immobilized metal affinity chromatography (IMAC) was carried out in ÄKTA™ start chromatography system (29-0220-94, GE Healthcare Life Sciences) with a 5 mL cobalt column (HiTrap™ Talon crude, 28953766, GE Healthcare Life Sciences). The supernatant from chemical lysis was applied to the column equilibrated in binding buffer (20 mM Tris pH 8, 500 mM NaCl) at a flow rate of 5 mL min<sup>-1</sup>. The column was subsequently washed with 40 mL binding buffer followed by elution with a linear gradient of 0 – 100 % elution buffer (20 mM Tris pH 8, 0.5 M NaCl, 0.5 M imidazole) over 25 mL. Size exclusion chromatography (SEC) was performed for concentrated IMAC fractions in NGC™ Chromatography System (Biorad) using a HiPrep 16/60 Sephacryl™ S-200 HR column (17116601, GE Healthcare Life Sciences) and 20 mM Tris pH 8 250 mM NaCl elution buffer.

IMAC and SEC fractions were verified for purity via sodium dodecyl sulfate polyacrylamide gel electrophoresis (SDS-PAGE) for soluble proteins (Laemmli, 1970). The 1 mm polyacrylamide gel was run at constant 200 V for 40 minutes in 1x Tris-Glycine-SDS (TGS) buffer. Purified protein fractions were concentrated in a stirred ultrafiltration unit (Amicon) using 50 psi nitrogen pressure and a 10 kDa membrane (Biomax®). The concentration was determined by measuring the absorbance at 280 nm (BioSpectrophotometer basic, Eppendorf) using the calculated molar extinction coefficient.

### Analytical size exclusion chromatography

In order to determine the molecular size of the protein, analytical size exclusion chromatography (SEC) was performed using pooled and concentrated SEC fractions containing protein. SEC was carried out in NGC™ Chromatography System (Bio Rad) using

## Chapter III

a high resolution column ENrich™ SEC 650 10 x 300 (Bio Rad) and 1 mL/min flow rate with 20 mM Tris pH 8, 250 mM NaCl. The absorbance at 280 nm of 60 µL Gel Filtration Standard (1511901, Bio Rad) and protein sample was measured.

### Thermal stability

Dynamic light scattering (DLS) was performed to determine the thermal stability of the protein. Triplicates of 30 µL of SEC-purified protein were transferred into a microtiter plate (Aurora), centrifuged at 4500 g and 4 °C for 10 min and analyzed in a DynaPro plate reader-II (Wyatt Technology). Thermal stability was monitored using a temperature gradient of 25 – 80 °C with an increase of 0.1 °C min<sup>-1</sup> and 5 acquisitions per sample each measured for 5 seconds.

### Enzyme activity assay

The physiochemical properties of 22\_GH29 were determined spectrophotometric using pNP- $\alpha$ -L-Fuc (Sigma Aldrich) by measuring enzyme activity at 410 nm in FLUOstar Omega microplate reader (BMG Labtech GmbH). The influence of pH 2-11, 0-1 M NaCl, 1 mM divalent cations and temperature, respectively, were investigated in triplicates in a total reaction volume of 100 µL. Kinetic parameters were measured in triplicates using 0.1 M Na-cacodylate pH 6, 1 mg/ml BSA, 0.1 M NaCl and 0-0.1 mM pNP- $\alpha$ -L-Fuc or MU- $\alpha$ -L-Fuc (Zellbio) at 30 °C. Similar to 22\_GH29, the activity of 21\_S1\_15 was tested on pNP-S (Sigma Aldrich).

### Substrate specificity and HPAEC-PAD analysis of 22\_GH29

Substrate specificity and linkage specificity was analyzed via high-performance anion exchange chromatography with pulsed amperometric detection (HPAEC-PAD). The following substrates were tested: Lewis<sub>y</sub> tetraose (Le<sub>y</sub>, Elicityl), Lewis<sub>b</sub> tetraose (Le<sub>b</sub>, Elicityl), Lewis<sub>x</sub> triaose (Le<sub>x</sub>, Elicityl), Lewis<sub>a</sub> triaose (Le<sub>a</sub>, Elicityl), 3-fucosyllactose (3-FL, Elicityl), reduced XFG xyloglucan (XFGol, Elicityl) and 2'-fucosyllactose (2'-FL, Carbosynth). 10 µM enzyme were incubated with 0.1 mg/mL substrate, 0.1 M Na-cacodylate pH 6, 1 mg/ml BSA, 0.1 M NaCl at 30 °C and 250 rpm and the reaction was terminated at 99 °C for 10 min. Prior HPAEC-PAD, the samples were filtered through 0.2 µm Spin-X centrifuge filter (Sigma Aldrich). HPAEC-PAD was carried out on a Dionex ICS5000+ system (Dionex) using a CarboPac PA10 (2 mm x 250 mm, Dinoex) analytical column and a CarboPac PA10 (2 mm x 50 mm, Dinoex)



guard column. Separation of neutral and acidic monomers was carried out using a previous described protocol (Engel & Händel, 2011). In short, neutral monosaccharides were separated by a linear flow of 18 mM NaOH for 20 minutes, followed by a gradient of to 100 mM NaOH and 500 mM NaAc for 15 minutes to elute acidic sugars. To quantify the released monosaccharides, we used an external standard mixture composed of fucose, rhamnose, galactosamine, arabinose, glucosamine, galactose, glucose, mannose, xylose, muramic acid, galacturonic acid, glucuronic acid and mannuronic acid.

### Multiple sequence alignment

Closely related sulfatases were found by NCBI pBLAST using the PDB data base (Berman et al., 2000). Protein sequences of structurally characterized  $\alpha$ -L-fucosidases were retrieved from CAZY database (Lombard et al., 2014). The catalytic nucleophile of 22\_GH29 was identified by multiple alignment using MUSCLE (Edgar, 2004) in ESPript V3.0 (Robert & Gouet, 2014). The acid/base catalytic residue of 22\_GH29 as well as the residues of the active site from 21\_S1\_15 were identified by superimposition of available structures in PyMOL Version 2.0 (Schrödinger, LLC).

### Protein crystallization and X-ray data collection

Sitting-drop vapour diffusion was set up with 96-well sparse matrix and grid screens at 16 °C to find conditions, which allow the protein to crystallize. Conditions that showed crystallized protein were repeated and, optimized with slight modifications to the original recipe using hanging-drop vapour diffusion at 16 °C. 24-well hanging drop crystal trials were set up containing 500  $\mu$ L mother liquor and three different dilutions (1:2, 2:1 and 1:1) of protein and crystallization solution with a total volume of 3  $\mu$ L.

Protein crystals were soaked in 25-30 % glycerol in the mother liquor and flash-frozen to cryo-temperatures using liquid nitrogen. Data collection was done at the PETRAIII (Burkhardt *et al.*, 2016) at the beam line P13 (Cianci *et al.*, 2017) from European Molecular Biology Laboratory (EMBL, Hamburg) and beam line P11 (Meents *et al.*, 2013) from Deutsches Elektronen Synchrotron (DESY, Hamburg).

## Chapter III

### Structure solution and refinement

Diffraction data were processed in CCP4i (Winn et al., 2011) using AIMLESS (Evans, 2011) and iMOSFLM (Battye *et al.*, 2011). The structures were solved by molecular replacement with PHASER (McCoy *et al.*, 2007) and the structural homologue PDB:2WVS (Lammerts van Bueren *et al.*, 2010) for 22\_GH29 and PDB: (REFERNCE) for 21\_S1\_15. The models were built in AUTOBUILD and REFINE in the Phenix crystallography suite (Adams *et al.*, 2010). Refinement was done based on a Maximum Likelihood method using REFMAC V5.5 (Murshudov *et al.*, 1997) and manually finalized in COOT V0.8.7.1 (Emsley *et al.*, 2010).

## Results

### Operon of '*Lentimonas*' sp. CC4 targeting sulfated fucans

To identify candidate enzymes that act on fucoidan, we extended on a transcriptomic and proteome study on '*Lentimonas*' sp. CC4. We identified two genes (22\_GH29 and 21\_S1\_15) that reached up to 0.5% and 0.25% of the total '*Lentimonas*' proteome during growth on fucoidan from *Fucus vesiculosus*. Both genes are only separated by a three bp intergenic distance and read mapping of the RNA-seq data shows that both genes and the intergenic region have similar expression values (Figure 16: **Operon structure for the degradation sulfated fucans.**). Both genes are potentially regulated by one promotor, since we identified an AT-rich -10 and -35 region upstream of the 22\_GH29 gene but not upstream of 21\_S1\_15. This indicates that both genes are transcribed as polycistronic mRNA and this transcriptional wiring suggests that both enzymes act together on fucoidan.

The 22\_GH29 and 21\_S1\_15 enzymes are also found in other fucoidan degrading bacteria, suggesting that they are essential to degrade fucoidan. 21\_S1\_15 and 22\_GH29 share both above 77 % identity (99 % coverage) with a S1\_15 (WP\_136078751) and GH29 (WP\_136078752) from *Kiritimatiella* F21. This strain is an anaerobic degrader of sulfated polysaccharides including fucoidan from *Fucus vesiculosus* (van Vliet *et al.*, 2019b). *Kiritimatiella* F21 and '*Lentimonas*' sp. CC4 are highly specialized fucoidan degraders and both strains encode more than 30 copies of GH29 and S1\_15. This suggest a key function of S1\_15 and GH29 in degrading fucoidan, yet both enzymes are biochemically not characterized.

## Biochemical characterization of 22\_GH29 and 21\_S1\_15

22\_GH29 is a monomer of approximately 47.8 kDa size measured via analytical SEC (Figure 17A), which matches with SDS-PAGE results (data not shown) as well as the theoretical size of the recombinant plasmid including the N-terminal signal peptide (54.4 kDa). The enzyme is highly active of pNP- $\alpha$ -L-Fuc with a  $K_m$  of  $0.265 \pm 0.098$  mM and  $K_{cat}$  of  $0.085 \text{ min}^{-1}$  as well as MU- $\alpha$ -L-Fuc with a  $K_m$  of  $0.359 \pm 0.145$  mM and  $K_{cat}$  of  $0.187 \text{ min}^{-1}$  (Supplement Figure 11). 22\_GH29 is stable and active to about  $\sim 38$  °C (Figure 17B, D) in a pH range from 5 to 8 with an optimum of pH 6 using sodium citrate buffer (Figure 17C). Based on the signal peptide prediction, 22\_GH29 is probably excreted and located in the periplasm or extracellular space. Therefore, we tested the effect of sodium chloride on enzyme activity. However, no significant effect was observed (Figure 17E). A screening of co-factors, shows that only Cu(II)SO<sub>4</sub> reduced the enzyme activity by factor 4, whereas the activity was unaffected by other potential co-factors (Figure 17F), which suggests, that the enzyme does not require any co-factors to be active.

To determine the substrate and linkage specificity, we tested 22\_GH29 on seven oligosaccharides which were varying in the monosaccharide composition, linkage type and degree of polymerization (DP). Besides pNP substrates, GH29 was exclusively active on Lewis<sup>X</sup> antigen triose (Table 5), which is composed of  $\beta$ -D-Gal-1 $\rightarrow$ 4( $\alpha$ -L-Fuc-1 $\rightarrow$ 3) $\beta$ -GlcNAc. Notably, the enzyme was not active on 3-fucosyllactose which differs from Lewis<sup>X</sup> only in having a Glc instead of GlcNAc. Also, the enzyme was not active on any 1-4-linked fucose substrate, suggesting that is a fucosidase specific for the 1-3 linkage.

On fucoidan, 22\_GH29 releases an unidentified component. HPAEC-PAD analysis of reaction products shows a peak eluting at 7.6 min after 30 minutes of enzyme digest (Figure 18). We were unable to identify this compound, since none of our standard monosaccharides eluted together with this compound. To exclude the possibility of an experimental artifact, we cloned and expressed another fucosidase (2701\_GH29) from '*Lentimonas*'. 2701\_GH29 produced fucose from fucoidan, suggesting that 22\_GH29 is indeed a new catalytic activity on fucoidan. 2701\_GH29 produced 3 mg L<sup>-1</sup> fucose, which is a degradation yield of about 0.1% from initial fucoidan. The peak area of 22\_GH29 was slightly higher, but the yield is still below 1%. The low yield suggests that other enzymes are required to increase the catalytic activity of 22\_GH29.

Since it was previously reported that sulfatases increase the activity of exo-fucosidases, we tested if the adjacent sulfatase 21\_S1\_15 increases the yield of 22\_GH29 (Berteau et al.,

### Chapter III

2002). Like the 22\_GH29, the 21\_S1\_15 is a monomer of 45.2 kDa size, which is stable to about 40 °C (Figure 19). 21\_S1\_15 was neither active on pNP-S nor fucoidan (data not shown).

#### Overall structure of 22\_GH29 and 21\_S1\_15

Needle-like crystals of 22\_GH29 which crystallized at 33 mg/mL in 0.045 M ammonium acetate, 0.1 M Bis-Tris pH 6.5, and 20% (w/v) PEG 3350 were analyzed via X-ray crystallography. The holo structure of 22\_GH29 (PDB: INSERT) was solved at 1.8 Å resolution from a  $P2_1$  crystal (Table S2) with a two domain-fold and overall dimensions of about 71x39x38 Å (Figure 20A). A  $Mg^{2+}$  molecule was found at the N-terminal domain above the active site. X-ray crystallography confirms the monomeric structure determined by analytical size exclusion chromatography. 22\_GH29 adopts a two domain-fold composed of a  $\beta$ -sandwich domain consisting of 7 antiparallel  $\beta$ -strands packed in two  $\beta$ -sheets at the C-terminus and the N-terminal  $(\beta/\alpha)_{8/6}$  TIM-barrel domain containing the active site. Compared to other GH29 structures, 22\_GH29 possess an additional loop at the very C-terminus consisting of 48 aa, which is stretching above the  $\beta$ -sandwich and facing towards the active site (Supplement Figure 12A).

The highly active site is formed as a small pocket consisting of twelve highly conserved residues (Supplement Figure 12B), which were identified via structural and multiple-sequence alignment. Superimposition with Lewis<sup>x</sup> antigen triose (from PDB: 6ORF) shows the binding of fucose in the -1 subsite, GlcNAc in the pseudo +1\* subsite (Hobbs *et al.*, 2019) and galactose which is clashing in the +1 subsite (Supplement Figure 13A). Based on the negative electrostatic charge of the -1 subsite as well as the little space, we hypothesise that 22\_GH29 is an exo-acting enzyme.

21\_S1\_15 crystallized at 4, 9 and 12 mg/ml in various conditions covering a wide range of concentrations (4 – 20 %) and molecular weight of PEGs (2000 MME, 3350, 4000, 6000, 8000, 10000, 20000). The conditions contained different buffer system of 0.1 M pH 5.6 – 9, as well as 0.1 – 0.2 M cations (MgCl, CaCl, NaCl) or sodium iodide, ammonium sulfate, lithium sulfate, calcium acetate or sodium acetate. In total, 10 data sets from 1.3 – 2.5 Å of different conditions were collected for needle-like and cubic crystals. The holo structure of 21\_S1\_15 was solved at 1.7 Å (PDB: INSERT) with two molecules in the asymmetric unit at 45.89 % solvent and overall dimensions of about 60x60x47 Å (Figure 20B). Like 22\_GH29, 21\_S1\_15 also assembles as a monomer of a  $P2_1$  crystal. This is the first structure of the subfamily S1\_15 adopting a heart-like overall fold consisting of 12 helices and 12 strands. A parallel  $\beta$ -sheet of

four strands is located close to the N-terminus. Sulfatase 21\_S1\_15 shares 27.5 % sequence identity (with 93 % coverage) with an undescribed arylsulfatase of family S1-23 from *E. coli* CFT073 (PDB:3ED4) and 30 % sequence identity (with 86 % coverage) of family S1-1 from *H. sapiens* (PDB:1E2S). The active site of family S1 is composed of 10 highly conserved residues, which were also found in 21\_S1\_15. Comparable to 22\_GH29, the highly conserved active site is formed as a small pocket, which is known for exo-acting enzymes. In the positively charged active site (Figure 20B), electron density for a Ca<sup>2+</sup> molecule was found (Figure 20D). Sulfatases of family S1 are known to acquire divalent cations such as Mg<sup>2+</sup> or Ca<sup>2+</sup>, which are coordinated by negatively charged amino acids, whereas positively charged amino acids are responsible for substrate binding (Hanson et al., 2004).

### Structure of 22\_GH29 reveals aspartate as novel catalytic residue

Previous studies reported the catalytical residues to be a highly conserved nucleophile Asp and Glu as Bronsted acid/base (Sulzenbacher *et al.*, 2004). In the 22\_GH29 from '*Lentimonas*' sp. CC4, the catalytic residues were identified as nucleophile Asp210 and Bronsted acid/base Asp259 with a distance of 6.2 Å (Figure 20C). To corroborate those findings, the structural alignment of 22\_GH29 with all ten available structures of GH29 shows that Asp259 is sterically conserved at the same position in the active side as the catalytic Glu from other GH29s (Supplement Figure 12). To verify both catalytic residues, we constructed the mutants 22\_GH29<sub>D210A</sub> and 22\_GH29<sub>D259A</sub>. Compared to the wild type, both mutants have between 20-30% residual activity, strongly suggesting that 259Asp is indeed a new catalytic Bronsted acid/base (Figure 21). The DNA base triplet of the 22\_GH29 gene encoding the Asp259 is GAC, and might have evolved by a single point mutation from GAA or GAG encoding Glu to GAC encoding Asp. This is the first study reporting the Bronsted acid/base to be an Asp instead of a Glu.

### Discussion

Only few fucoidan enzymes are characterized, here we provide a structure and biochemical characterization of 22\_GH29 fucosidase and 21\_S1\_15 sulfatase from '*Lentimonas*' sp. CC4. Both enzymes are transcribed in an operon induced by fucoidan from *Fucus vesiculosus*, suggesting they act together on the polysaccharide. The GH29 is an  $\alpha$ -1,3 specific fucosidase with an pH optimum at pH 6 and a temperature optimum at 37 °C. The structure of GH29 at 1.8 Å shows an active side typical for exo-acting enzymes. Additionally, we identified Asp259

### Chapter III

as novel catalytic acid/base of GH29 fucosidases. On fucoidan, the GH29 produces a yet uncharacterized compound. Despite activity screening for the S1\_15 remained unsuccessful, the structure of S1\_15 at 1.7 Å is the first structure of this subfamily and shows a small active suggesting an exo lytic mode of action. Together, these insights demonstrate how '*Lentimonas*' sp. CC4 uses exo-enzymes to degrade fucoidans.

The 22\_GH29 uses two aspartates as unusual catalytic pair, whereas most other GH29 use one aspartate and one glutamate. The two mutants 22\_GH29<sub>D210A</sub> and 22\_GH29<sub>D259A</sub> have a residual activity of 20-30% and likely a double mutant of both residues would lead to complete loss of activity. Likely, the new catalytic residue (Asp259) is a conservative mutation with little effect on the function of the enzyme. A single point mutation in the last base of the glutamate triplet (GAC or GAG) could result in aspartate (GAC). Therefore, the new catalytic base pair could be considered an oddity of evolution. Also, other glycoside hydrolases use a catalytic base pair with two identical amino acids, e.g., the GH16 use a conserved glutamate/glutamate catalytic pair (Viladot et al., 1998; Labourel et al., 2014). The identification of Asp259 as catalytic acid/base in 22\_GH29 facilitates the identification of catalytic residues of other GH29s.

The 22\_GH29 is a fucosidase with an unusual activity on fucoidan. Our screening of various fucose-containing oligosaccharides revealed that GH29 produces fucose from Lewis<sup>X</sup>, but not other oligosaccharides. Thus, the 22\_GH29 is an  $\alpha$ -1,3 specific fucosidase. On fucoidan, the enzyme did not release fucose, but another a yet unidentified compound. A direct comparison with 2701\_GH29 shows that this enzyme produces fucose from fucoidan, indicating that the production of the unknown compound is a feature specific to 22\_GH29. As this compound eluted after fucose, it could be i) sulfated fucose, ii) acetylated fucose, iii) fucose disaccharide, iv) fucose in another form such as fucofuranose instead of fucopyranose or v) any other carbohydrate. A superimposed Lewis<sup>X</sup> into the structure of 22\_GH29, shows that acetyl from GlcNac in the +1 site fits into a pocket between the -1 and +1 subsite (Supplement Figure 13). This shows a small space to potentially accommodate a small modification such as sulfate or acetate of fucose in the active side. Indeed, at least two fucosidases (of unknown sequence) can produce sulfate fucose from fucoidan, suggesting that the product of 22\_GH29 might be sulfated fucose (Tanaka & Sorai, 1970; Sasaki et al., 1996). The yield of this compound is ~0.1% of initial fucoidan, thus the product of 22\_GH29 could be purified via SEC from a large batch digest for structural elucidation. Potentially, this could be tested as substrate for the 21\_S1\_15.

‘*Lentimonas*’ sp. CC4 is a valuable resource for the discovery of enzymes with a high biochemical and biotechnological novelty. Our characterization of 22\_GH29 and 21\_S1\_15 shows that these are indeed exo-acting enzymes. Especially, the 22\_GH29 uses an unusual catalytic residue pair and produces novel compounds from fucoidan. This underpins that ‘*Lentimonas*’ sp. CC4 can be further explored to obtain new fucoidan-active enzymes.

### **Acknowledgments and funding**

We acknowledge EMBL and DESY (Hamburg, Germany), a member of the Helmholtz Association HGF, for the provision of experimental facilities. Parts of this research were carried out at PETRAIII and we would like to thank Guillaume Pompidor and Eva Crosas for assistance in using the beamline P13 and P11. AS is member of the International Max Planck Research School of Marine Microbiology (MarMic). JHH, AS and NG acknowledges funding from the Max-Planck-Gesellschaft and from the Emmy Noether Program of the DFG, grant number HE 7217/1-1 and from the DFG in the framework of the research unit FOR2406 “Proteogenomics of Marine Polysaccharide Utilization” (POMPU). We also thank Alek Bolte for assistance with HPEAC-PAD.

### **Conflict of interest**

The authors declare no conflict of interest.

### **Author’s contributions**

JHH and AS initiated the study. Protein crystallization: AS, NG, TvR. Structure determination: CR, NG. Primer design and cloning: AS, NG, TvR. Biochemical experiments: AS, NG. AS, NG, JHH wrote the manuscript and received input from all authors.

## Figures and Tables

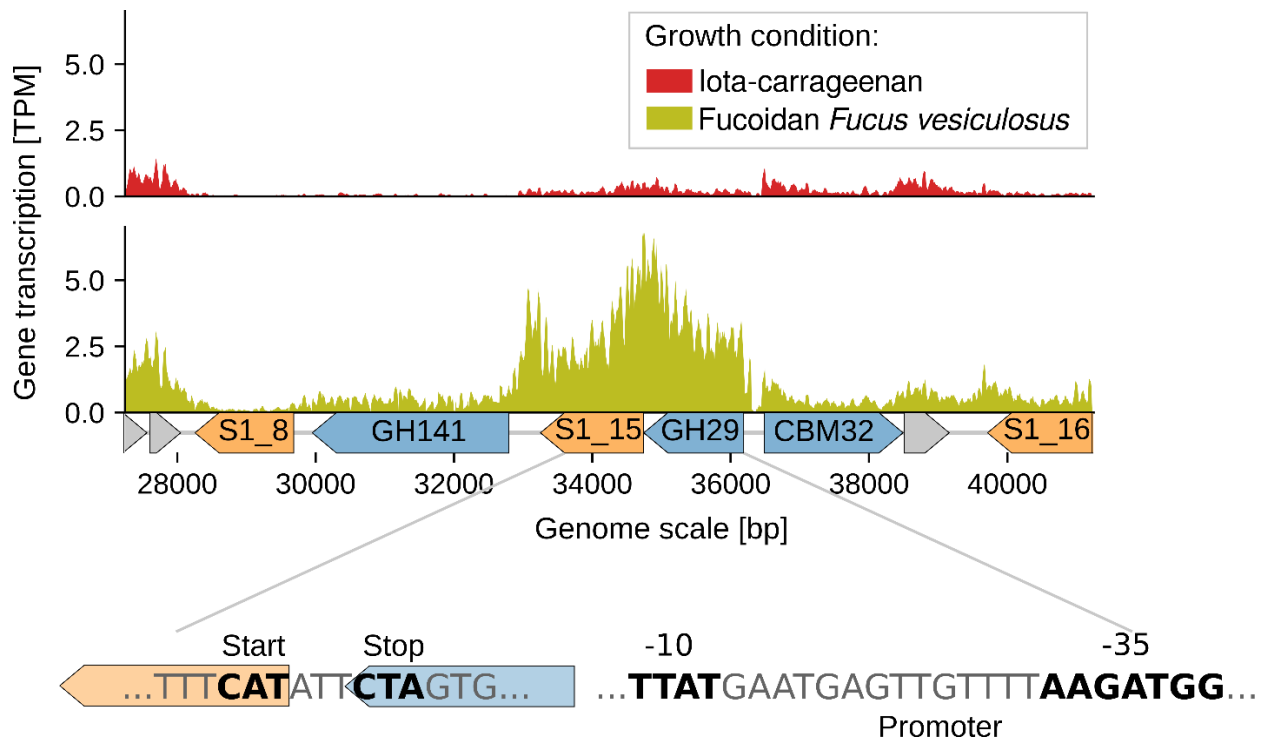


Figure 16: **Operon structure for the degradation sulfated fucans.** The genomic region surrounding the 21\_S1\_15 sulfatase and the 22\_GH29 fucosidase located on the plasmid of ‘*Lentimonas*’ sp. CC4 is shown. Sulfatases, CAZymes, and hypothecital proteins are shown in orange, blue and grey. Gene transcription from cells grown on iota-carrageenan or fucoidan from *Fucus vesiculosus* is represented as transcript per million (TPM) averaged over 10 bp.



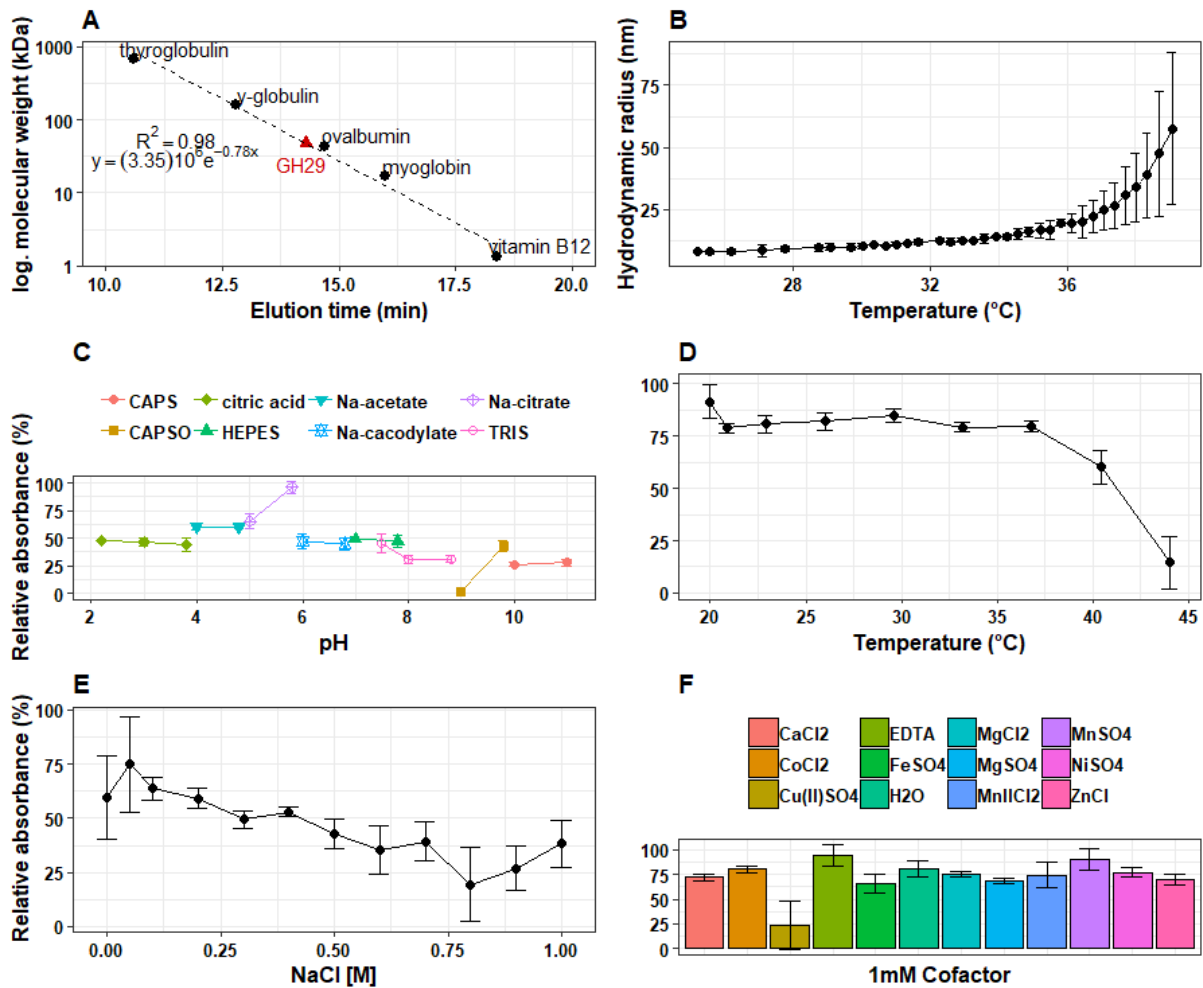
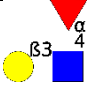
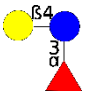
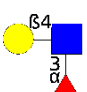
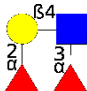
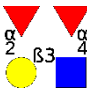
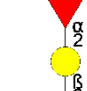
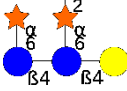
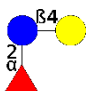


Figure 17: **Biochemical characterization of 22\_GH29.** (A) Determination of molecular weight by analytical SEC and (B) thermal protein stability indicated by a constant hydrodynamic radius (nm). Relative activity of 22\_GH29 in screens to find (C) optimal pH, (D) optimal temperature, (E) salt concentration and (F) required co-factors.

### Chapter III

Table 5: Substrate specificity of 22\_GH29 against fucose-containing oligosaccharides. Release of fucose was analysed via HPAEC-PAD and enzyme activity is represented as absent (–) and present (+). The structure of each oligosaccharide is drawn according to the symbol nomenclature of glycans including fucose (red triangle), galactose (yellow circle), glucose (blue circle), glucosamine (blue square) and xylose (orange star) (Varki et al., 2015).

Substrate	Structure	Activity
Lewis <sup>a</sup> triaose		–
3-fucosyllactose		–
Lewis <sup>x</sup> triaose		+
Lewis <sup>y</sup> tetraose		–
Lewis <sup>b</sup> tetraose		–
Reduced XFG		–
xyloglucan		–
2'-fucosyllactose		–

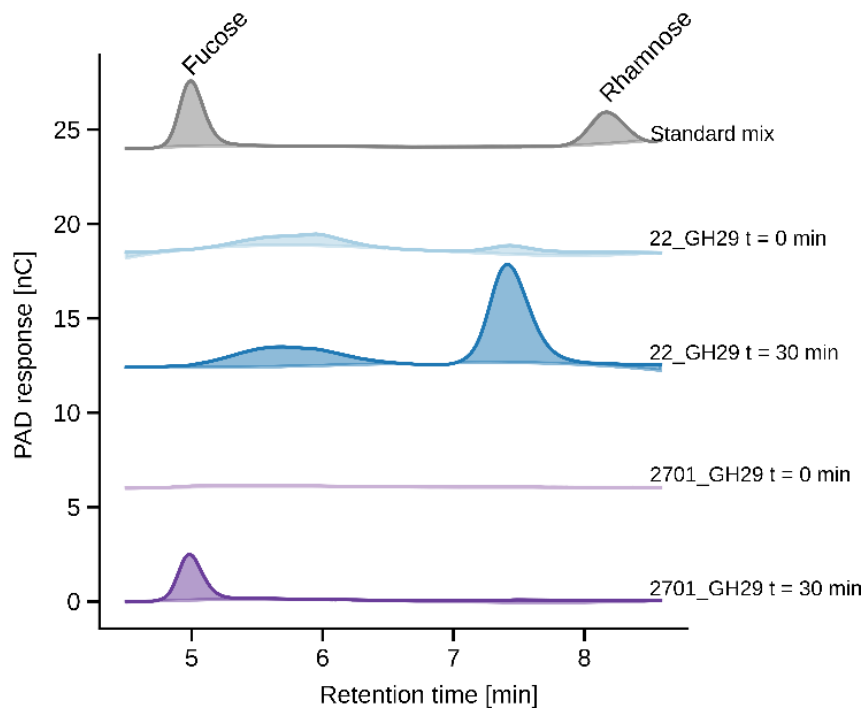


Figure 18: **Activity of 22\_GH29 on fucoidan.** The HPAEC-PAD chromatogram shows a reference standard mixture and the hydrolysis products of 22\_GH29 and 2701\_GH29 on fucoidan from *Fucus vesiculosus*. While 2701\_GH29 produces fucose, 22\_GH29 produces a compound eluting at 7.6 min that remained unidentified due to the lack of reference standards.

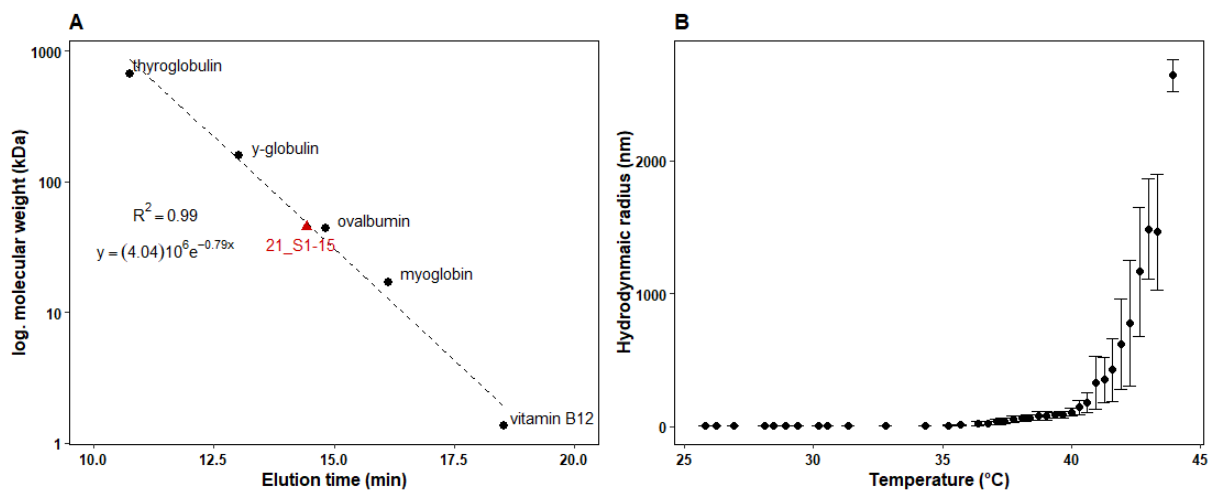


Figure 19: **Size and stability of 22\_S1\_15.** (A) Determination of molecular weight by analytical SEC and (B) thermal protein stability indicated by a constant hydrodynamic radius (nm).

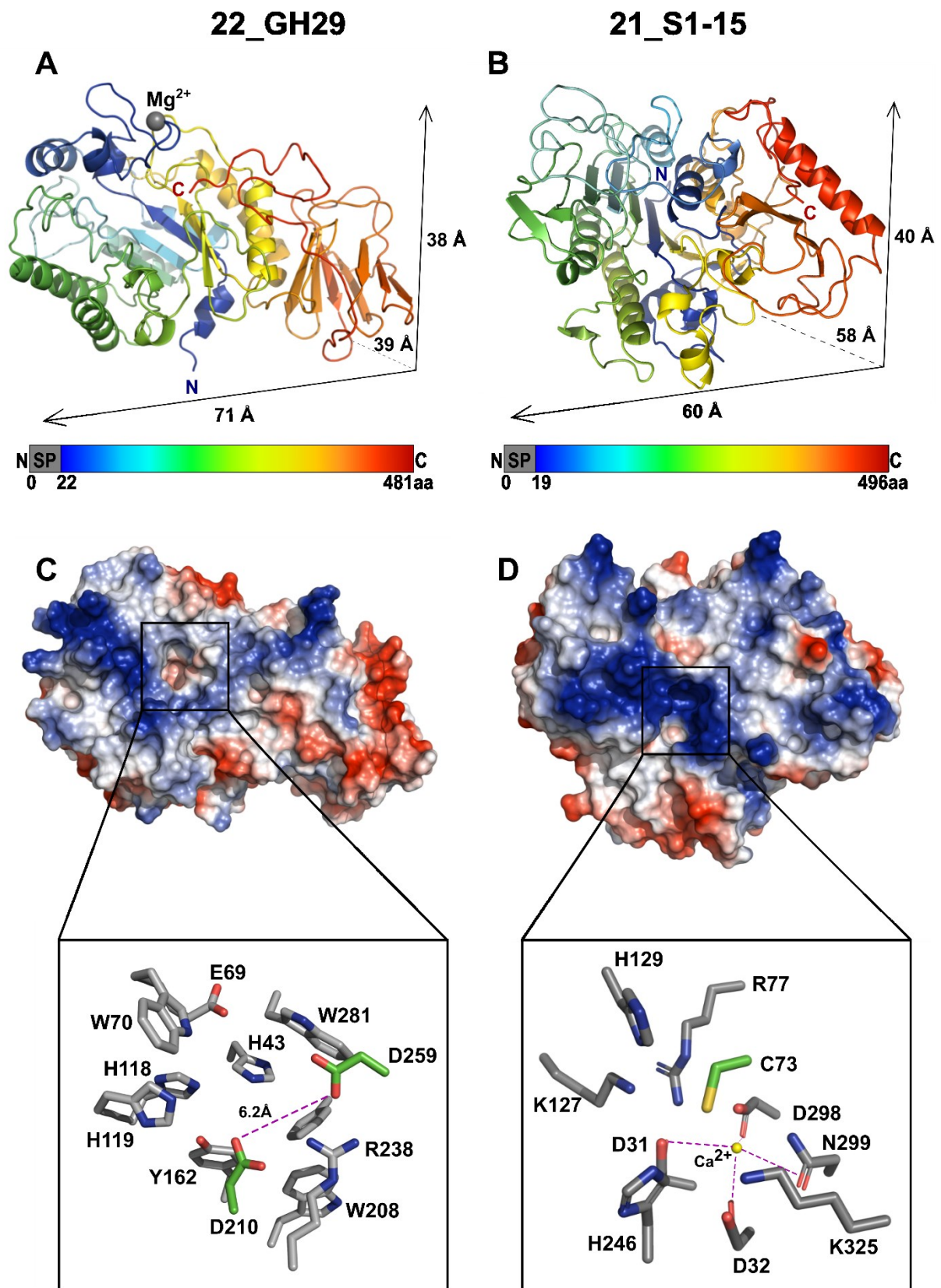


Figure 20: Overall structure of 22\_GH29 and 21\_S1\_15. Cartoon view and overall dimensions (Å) of (A) 22\_GH29:  $\beta$ -sandwich domain consisting of 7 antiparallel  $\beta$ -strands

packed in two  $\beta$ -sheets at the C-terminus and the N-terminal  $(\beta/\alpha)_{8/6}$  TIM-barrel domain containing the active site and (B) 21\_S1\_15: heart-like overall fold consisting of 12 helices and 12 strands. Surface view colour coded according to electrostatic potential ranging from positive (blue) to negative (red) and zoom into active site of (C) 22\_GH29: highly conserved residues, catalytic pair is coloured in green (D) 21\_S1\_15: highly conserved residues, catalytic nucleophile Cys colored in green, calcium ion which binds and activates the sulfate group of the substrate.

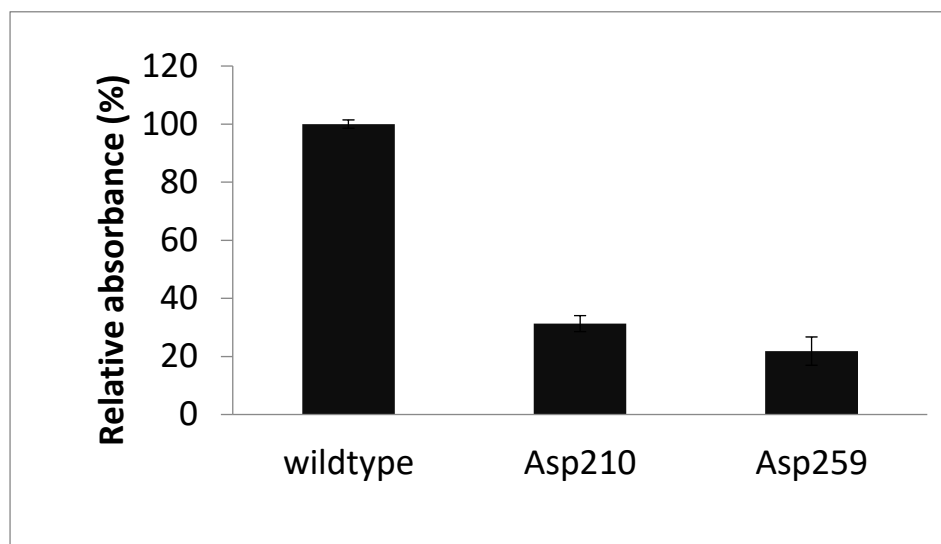


Figure 21: **New catalytic pair of 22\_GH29.** Relative activity of 22\_GH29<sub>D210A</sub> and 22\_GH29<sub>D259A</sub> on pNP- $\alpha$ -L-Fuc.



## Chapter IV.

# Fucose polysaccharide from diatoms may sequester carbon in the ocean

Silvia Vidal-Melgosa<sup>1,2</sup>, Andreas Sichert<sup>1,2</sup>, Ben Francis<sup>1</sup>, Daniel Bartosik<sup>3,4</sup>, Pier Luigi Buttigieg<sup>1</sup>, Jutta Niggemann<sup>5</sup>, Antje Wichels<sup>6</sup>, Thomas Schweder<sup>3,4</sup>, Dörte Becher<sup>7</sup>, Rudolf Amann<sup>1</sup>, Hanno Teeling<sup>1</sup>, Jan-Hendrik Hehemann<sup>1,2\*</sup>

<sup>1</sup> Max Planck-Institute for Marine Microbiology, 28359 Bremen, Germany.

<sup>2</sup> University of Bremen, Center for Marine Environmental Sciences, MARUM, 28359 Bremen, Germany.

<sup>3</sup> Pharmaceutical Biotechnology, Institute of Pharmacy, University of Greifswald, 17489 Greifswald, Germany.

<sup>4</sup> Institute of Marine Biotechnology, 17489 Greifswald, Germany.

<sup>5</sup> University of Oldenburg, Institute for Chemistry and Biology of the Marine Environment, 26129 Oldenburg, Germany.

<sup>6</sup> Biologische Anstalt Helgoland, Alfred Wegener Institute for Polar and Marine Research, 27498 Helgoland, Germany.

<sup>7</sup> Institute of Microbiology, University of Greifswald, 17489, Greifswald, Germany.

\* Corresponding author





## Summary

The ocean is a major sink of the greenhouse gas carbon dioxide (CO<sub>2</sub>); its microscopic algae annually absorb vast amounts of CO<sub>2</sub> and fix it through photosynthesis into sugar monomers. Algae polymerize these monomers into polysaccharides, the majority of which are enzymatically depolymerized and metabolized back into CO<sub>2</sub> by bacteria. However, a minor fraction of polysaccharides persist enzymatic degradation storing carbon in the ocean, thus removing it from the atmosphere for geological time scales. We do not know which polysaccharide structures are degraded or persist owing to the challenge to measure them in complex matrices, such as marine organic matter. Here we used highly specific monoclonal antibodies to measure polysaccharide structural types during a three month diatom bloom in the North Sea. We traced the presence of these microalgal polysaccharides in dissolved and particulate organic matter, monitored their degradation by bacterial digestive enzymes and identified labile and stable structural types. Glucans, among others, were rapidly degraded providing fast food for bacteria, while fucose-containing sulfated polysaccharide, or FCSP, accumulated during the three-month bloom. FCSP was synthesized and secreted by diatoms, appeared stable, aggregated into particles that can sink and thereby store carbon in deeper waters. Altogether, our results show that different polysaccharide structural types in freshly produced algal matter are not equally biodegradable, which must be considered if we are to predict their contribution to carbon sequestration in a warming and acidifying ocean.

## Introduction

Growth of microalgae in the surface ocean is responsible for about half of the global biological CO<sub>2</sub> fixation and generates about 45 gigatonnes of organic carbon per year (Field, 1998). Most of the biomass synthesized by microalgae consists of polysaccharides, which contribute up to 70% of the freshly produced organic carbon in algal particulate and dissolved organic matter (POM and DOM) (Myklestad, 1995). Microalgal polysaccharides serve as cell wall components, energy storage or as secreted exudates but the fate of these structurally diverse molecules in the carbon cycle remains currently unknown.

Polysaccharides are thought to belong to the labile carbon pool (Loh et al., 2004) as they are prime food for heterotrophic bacteria, which digest them with carbohydrate active enzymes (CAZymes) (Lombard, Golaconda Ramulu, et al., 2014); yet they are also found to accumulate in surface waters suggesting that some are more stable taking months or longer to degrade (Lihini I. Aluwihare et al., 1997). This stability is intriguing because CAZymes belong

## Chapter IV

to the most expressed proteins of bacteria that thrive during algal blooms (Hedges et al., 2001) indirectly pointing at the importance of polysaccharides for microbial growth and carbon cycling. However, individual polysaccharide structures have rarely been measured in the ocean as they remain difficult to analyse with current methods due to their complexity; with numerous permutations with diverse linkages connecting a wide variety of monosaccharides, which are often substituted with a range of chemical groups (Hofmann et al., 2015).

Common techniques used for marine glycan analysis, such as monosaccharide composition by acid hydrolysis and HPLC or NMR, examine bulk properties of the polysaccharide pool without distinguishing different structural types. This lack of molecular resolution renders our understanding of the cycling or sequestration of glyco-carbon incomplete (Hedges et al., 2001; Engel et al., 2004; Becker et al., 2017). Consequently we do not know labile polysaccharides that fuel microbial metabolism or stable ones that accumulate in the sea surface or drive the aggregation of particles (Chin et al., 1998) that can sink to the deep ocean and transport carbon via the biological pump into marine sediments (Alldredge & Gotschalk, 1989; Lihini I. Aluwihare et al., 1997; Buchan et al., 2014). These processes have profound implications to the CO<sub>2</sub> fixation and the global carbon cycle at present and limits our capabilities to predict future ocean scenarios in a changing climate, where phytoplankton communities producing different types of polysaccharides are bound to change.

To reconcile the marine polysaccharides lability/stability conundrum, new approaches to obtain detailed structural information are urgently needed. Here, by using monoclonal antibodies we show specific polysaccharide structures present in DOM and POM during a phytoplankton bloom. Our data reveal fluctuations in the abundance of specific polysaccharide structural types during the algal bloom and suggest selective grazing preserves aggregating polysaccharides.

## Results

### Compositional monosaccharide analysis in DOM

We first performed compositional monomer analysis in DOM polysaccharides, which showed minor longitudinal variation during the bloom. We monitored polysaccharides in the North Sea (54°11.3'N, 7°54.0'E) near the island of Helgoland, Germany, for about three months during a spring diatom bloom. The bloom developed from the 10<sup>th</sup> of March until the 17<sup>th</sup> of May 2016. During the field campaign chlorophyll *a* fluctuated forming multiple maxima and minima

ranging between 2.1 and 11.8 mg/m<sup>3</sup> (Supplement Figure 14) provided by three, consecutive diatom peaks as well as by flagellates and additional phytoplankton species of lower abundance (Supplement Figure 15). During this time series the dissolved organic carbon (DOC) concentrations of DOM (< 0.2 µm) ranged between 96 and 133 µmol/L. High molecular weight DOM (HMWDOM) was sampled twice per week by concentrating 100 L of 0.2 µm filtered seawater using tangential flow filtration (TFF) on 1 KDa membranes. A total of 21 samples were isolated. We first quantified the polysaccharides in HMWDOM using monosaccharide analysis, which is the commonly used method to analyse marine glycans, to investigate if potential polysaccharide fluctuations over time can be resolved. The HMWDOM samples were hydrolyzed with acid and resulting monomers were quantified by high performance anionic exchange chromatography with pulsed amperometric detection (HPAEC-PAD). Our measurements showed that, except for the relative decrease of glucosamine and the peak in arabinose at the end of the bloom, the monomer composition was relatively constant during the time series (Supplement Figure 16). Monosaccharide composition therefore does not suffice to resolve the putative fluctuation of unique polysaccharide structural types underlying the monosaccharide signal. These fluctuations are indicated by previously observed successions of microbes and their expressed CAZymes that respond timely and to various polysaccharide structural types during algal blooms (Teeling et al., 2012). Therefore, in order to uncover polysaccharide structures present in DOM and POM we turned to bioanalytic tools that have not yet been used in the ocean.

### **Polysaccharide fine structure characterization**

Carbohydrate microarrays combined with glycan-specific antibodies and analytic enzymes enabled the detection and traced the evolution of various polysaccharide structural types within DOM and POM. The use of carbohydrate microarrays, technique that is established in the fields of biomedicine and plant cell wall research (Willats et al., 2002; Moller et al., 2008), and monoclonal antibodies (mAbs) that are specific for particular glycan epitopes (unique stereochemistry) allowed a broad polysaccharide chemical characterisation of the HMWDOM. We also studied polysaccharides in POM samples from the diatom bloom, which were collected by filtration including three size fractions: POM over 10 µm, between 10 and 3 µm, and between 3 and 0.2 µm (Figure 22a). POM samples were harvested in parallel to the HMWDOM (size fraction between 0.2 µm and 1 kDa), hence the 21 sampling days resulted in a total of 84 samples. Polysaccharides from all HMWDOM and POM samples were

## Chapter IV

sequentially extracted using the solvents H<sub>2</sub>O, EDTA and NaOH and these organic matter extracts were printed onto nitrocellulose microarrays (see scheme in Figure 22). Each single microarray was incubated individually with one of 51 polysaccharide-specific mAbs and carbohydrate binding modules (CBMs), which specifically bind one of the many different polysaccharide structural types present in the extracts from the microalgae bloom. Binding of the primary mAbs or CBMs to the cognate polysaccharide on the microarray is detected with a secondary antibody coupled to alkaline phosphatase. This is used in combination with the enzymes substrate yielding a colored product the amount of which is proportional to epitope abundance (Moller et al., 2008; Vidal-Melgosa, Pedersen, Schückerl, et al., 2015). We detected diverse polysaccharide structures including the energy storage  $\beta$ -1,3-glucan, as well as cell wall  $\beta$ -1,4-mannan,  $\beta$ -1,4-xylan,  $\alpha$ -arabinan,  $\beta$ -galactan, pectin, cellulose, arabinogalactan and fucose-containing sulfated polysaccharide (FCSP) among others (data subset shown in Figure 23, complete dataset in Supplement Figure 17). In cases where specific enzymes were available to us we used these to verify the presence of the polysaccharides (Øbro et al., 2007) in HMWDOM and POM extracts. Enzymatic treatment of individual microarrays (populated with HMWDOM or POM polysaccharide extracts) with structure-specific glycoside hydrolases (GHs) prior to incubation with the mAb, resulted in epitope deletion ( $P < 0.0001$ ) for  $\beta$ -1,4-mannan and  $\beta$ -1,3(1,4)-glucan in HMWDOM and homogalacturonan (pectin) and  $\beta$ -1,3-glucan in POM (Figure 24a). Overall, we identified 27 polysaccharide epitopes (Supplement Figure 17) on the microarrays most of which have not been described in the ocean before.

We used carbohydrate microarrays with non-covalent immobilization, which is a semi-quantitative method proven to be highly reproducible, robust and specific (Moller et al., 2008; Vidal-Melgosa, Pedersen, Schückerl, et al., 2015). The correlation between epitope concentration and antibody signal intensity has been previously shown (Øbro et al., 2007) and we ensured it by printing polysaccharide standards with several dilutions, which resulted in mAb signal that vary with epitope concentration (Figure 24b). Since different antibodies have different avidities, the signal intensities obtained with two different probes cannot be used to infer different abundances of the corresponding epitopes. By contrast, the signal intensities from a single antibody can be used to determine the relative abundance of its recognized polysaccharide structure and can be applied to monitor changes in epitope abundance by time. As DOM and POM samples were isolated differently, their data sets were normalized independently and therefore absolute values from DOM and POM should not be compared but the trends. Our data (Supplement Figure 17) present the relative abundance of specific

polysaccharide epitopes in HMWDOM and POM revealing fluctuations in their abundance during the diatom bloom.

Our microarray data suggest chemical structure drives reactivity of polysaccharides. As we sampled during a microalgae bloom we assume, even though some glycans of bacterial or macroalgal origin might be present, the vast majority of polysaccharides in our samples were produced by microalgae. About 40% of the POM and DOM from diatoms consists of laminarin making it one of the most abundant polysaccharides in the ocean. As expected this  $\beta$ -1,3-glucan diatom storage glycan was detected in POM (recognized by the mAb BS-400-2), but was barely detected in HMWDOM with microarray analysis (Figure 23) or with a recently developed laminarin-specific biocatalytic assay (Becker et al., 2017) (data now shown). This indicates that as soon as laminarin reached the DOM pool (by microalgae grazing or decay) free-living bacteria consumed it. Degradation of this structurally simple, glucose-based polysaccharide requires only three types of depolymerizing enzymes, rendering laminarin one of the most labile and for microbes most profitable carbon-energy source (Becker et al., 2017). Homogalacturonan, a carboxylated pectic polysaccharide targeted by mAb LM19, was detected in POM and not detected in DOM (Figure 23). The structure of homogalacturonan is relatively simple and its depolymerization would require pectinesterases and lyase or hydrolase activity to degrade the de-esterified backbone. The absence of this polymer in HMWDOM may be due to its rapid consumption by bacteria (lability) but it can also be due to its acidic structure nature. Carboxylated polysaccharides can crosslink with high concentrations of calcium and other divalent cations in seawater. This ionic interaction decreases solubility and maintains presence in particles (Hehemann et al., 2017; Koch et al., 2019). In contrast, numerous polysaccharide structural types such as  $\beta$ -1,4-mannan, arabinogalactan,  $\beta$ -1-3(1-4)-glucan,  $\alpha$ -1,5-arabinan, rhamnogalacturonan I backbone and  $\beta$ -1,4-glucan were detected in both pools in several data points. Showing that these molecules can move between the particulate and dissolved carbon pool where they are accessed by both, particle-attached and free-living bacterioplankton. The fact that several polysaccharides are found in both pools may be associated to having structures with higher amounts of different sugar monomers (compared to laminarin) and additional branching and chemical modifications delaying rapid access by microbes since more enzymes are needed for their degradation (Cartmell et al., 2018; J. Chen et al., 2018; Leth et al., 2018). FCSP are a class of highly complex, anionic, cell wall and secreted polysaccharides (Koch et al., 2019) of brown macroalgae. They have many different linkage types, various monosaccharides and chemical modifications (Deniaud-Bouët et al., 2017), which likely require a set of diverse, mostly unknown digestive enzymes (Colin et al.,

## Chapter IV

2006; Schultz-Johansen et al., 2018). FCSP was present at all-time points in DOM, detected by the recently developed anti-fucan mAb BAM1 (Torode et al., 2015). Moreover, FCSP accumulated in POM during weeks (Figure 23). The continuous presence in DOM and its accumulation in POM indicate high stability extending the “shelf life” of FCSP. The structural complexity of a polysaccharide type might be the cause of extended permanence in a bloom compared to more simple structures. On the other hand, some of the epitopes detected in both pools correspond to homopolymers with one single linkage type, for instance  $\alpha$ -1,5-arabinan. Recent laboratory experiments have shown the marine bacteria *Alteromonas macleodii* presents polysaccharide substrate prioritization when exposed to a polysaccharide mixture (Koch et al., 2019), which proposes different degradation trends among different structures. The homopolymer epitopes that we find in both pools, might be part of a structurally complex polymer or might be present in the bloom as structurally simple polymers but nonetheless bacteria selectively chose to feed from other polysaccharide structures continuously available during the diatom bloom - selective degradation. Together, these results reveal that there is glycan structure-specific reactivity, which may be a result of structural complexity, selective degradation or a combination of both.

We created a filter to classify the polysaccharide epitopes detected in the bloom into: labile, semi-labile and stable based on their abundance trends and applied it to our microarray data. We define *labile polysaccharide epitopes* are rapidly consumed in DOM - mostly not detected in DOM. Up to 20% of bacterioplankton may be particle-attached but the bulk are free-living (Azam & Graf, 1983) and we expect a labile epitope to be consumed once accessible at the dissolved pool. An example is the abundances detected for  $\beta$ -1,3-glucan and homogalacturonan. In the case of negatively charged polymers we cannot conclude if the absence in DOM is due to its lability or aggregation properties. *Semi-labile epitopes with transient presence or sudden increase* like the shown by arabinogalactan. *Semi-labile epitopes with no prominent variation* do not display a notable change through the bloom as the one presented by a  $\beta$ -1,4-mannan epitope recognized by mAb BS-400-4. This behaviour mimics a steady state system of production and degradation. *Stable polysaccharide epitopes* accumulate during the bloom in time spans of over weeks to months, here observed for the FCSP in POM. On the basis of our data we categorized different behaviours among the structures present on the here studied phytoplankton bloom.

## **Bacteria consume laminarin but no FCSP enabling its accumulation**

To understand why laminarin was rapidly degraded while FCSP accumulated, we investigated the presence of glycan-degrading heterotrophic microbes and their enzymes with metagenomics and proteomics. The total bacteria counts increased more than 2 fold during the bloom by degrading and growing on the algal molecules. Our metagenomics results, together with previous reports (Teeling et al., 2012), showed bacterial taxa present during blooms display a vast repertoire of CAZymes with relevance for carbohydrate degradation. Some examples of the GH families found during the bloom are GH16, GH17, GH30 and GH3, which are classified as families which corresponding genes mainly target  $\beta$ -glucan; and GH29, GH95 and GH141 that mainly encode fucosidases (exo-acting) (Figure 25). GH107 is the only known fucanase (endo-acting) family and was rarely found in the bacterial genomes (only in some *Verrucomicrobiae*). The bacterial community found during our study encoded polysaccharide-degrading genes that would putatively allow degradation of most glycan structures detected during the bloom, but our microarray data does not suggest that all of the structures were degraded during the course of the bloom. To further investigate the degradation of polysaccharides by marine bacteria we analyzed the presence of CAZymes during the campaign. GH families that mediate polysaccharide degradation were expressed with distinct expression levels during the course of the bloom, as revealed by proteomics (Supplement Figure 18). Previous studies have shown the extensive expression of laminarinases, which are among the most abundant enzymes in proteomic datasets during microalgal blooms, thus supporting selective degradation of laminarin by Flavobacteria and Gammaproteobacteria (Teeling et al., 2012; Unfried et al., 2018). We also identified laminarinases from family GH16 as the highest expressed CAZymes by marine bacteria. They had expression maxima at the beginning of the bloom but their expression level was high through the time series, indicative of selective degradation of laminarin during the bloom here studied (Figure 25b). The GH16 expression maxima did not overlap with the highest diatom abundance peaks and did not have a visible effect in the laminarin abundance detected in that date. From the above stated fucosidase families only GH29 was detected a single time at the end of the bloom (coinciding with the end of the diatom bloom) but with no perceptible effect in the FCSP abundance detected in any of both pools. Expression of the GH107 fucanase family was not detected. We cannot exclude that GH families containing not yet characterized fucanases and other FCSP-degrading enzymes were expressed during the bloom with lower expression levels compared to laminarinases. Even if this was the case, we can conclude that degradation of FCSP in the

## Chapter IV

bloom was either at a slower pace or not occurring and FCSP could therefore store carbon longer time compared to the labile polysaccharides. Moreover, reduced degradability of FCSP is a global phenomenon since experiments performed with externally-introduced-polysaccharides showed the lowest degradation rates for macroalgal FCSP in various oceanic regions (Carol Arnosti et al., 2011); yet the presence of fucan, and its accumulation, during a microalgal bloom had hitherto not been revealed. The mechanism of selective degradation, which enables accumulation of FCSPs, is reminiscent of Monods Diauxie where bacteria sequentially consume carbohydrates rather than simultaneously (Koch et al., 2019). Continuous growth of diatoms occupied bacteria with a steady source of labile laminarin and other less “complicated” polysaccharides ultimately leading to the accumulation of FCSP. This hypothesis extends the dynamics observed for simple carbohydrates in the test tube to polysaccharides in the ocean which might regulate large scale organic matter degradation.

### Source of FCSP

The stability of FCSP proposes a mechanism for carbon sequestration; hence we asked which organisms create this polysaccharide during the microalgal bloom. To visualize FCSP we used fluorescence microscopy. This phytoplankton bloom was dominated by flagellates and the centric diatom *Chaetoceros socialis* (Supplement Figure 15). We immunolabeled filters from the bloom that contained the entire POM size range (all organic matter > 0.2  $\mu\text{m}$ ) with the mAb BAM1, and found FCSP occurred abundantly on the cells of the chain-forming diatom *C. socialis*. *In situ* localization of the FCSP in samples from the beginning of the bloom was mainly restricted to the exterior of the diatoms cell walls and their spines (Figure 26a). Towards the end of the bloom FCSP extensively covered the diatom cell surfaces; moreover it was also present in particles (Figure 26b). Quantification of the FCSP signal intensity on the diatom cells confirmed that its abundance on diatom cells markedly increased at the end compared to the beginning of the bloom ( $P < 0.0001$ ) (Figure 26c). Moreover, its presence in particles (areas not containing diatom cells) also increased between March to May ( $P < 0.0001$ ) (Figure 26d). Both fluorescence microscopy and microarray analyses indicate that FCSP abundance increased in POM during the bloom. The identified increase of FCSP in particles at the end of the bloom (Figure 26d) point to aggregation processes similar to the previously described aggregation of negatively charged microalgal polysaccharides into transparent exopolymer particles (TEP) during coccolithophore blooms in mesocosms (Alldredge & Gotschalk, 1989; Engel et al., 2004) that drive particle mediated carbon export. A likely polyanion driven



aggregation mechanism was confirmed by anion exchange chromatography wherein FCSP isolated from the bloom eluted with high NaCl concentrations confirming its anionic nature (Figure 26e). We also investigated the production of FCSP by the diatom strain *C. socialis* that was present in the bloom, which was isolated on the sampling site during the campaign. We grew a monospecific laboratory culture of *C. socialis*, harvested the biomass and performed polysaccharide extraction. The extract was analyzed by the recently developed method epitope detection chromatography (Cornuault et al., 2014) and our data confirmed that the diatom *C. socialis* produced negatively charged FCSP (Figure 26f). The FCSP-enriched chromatographic fractions from POM and *C. socialis* were analysed by monosaccharide analysis showing that about 10% of the monomer content was fucose (Figure 26g). We explored the source of FCSP and found they were exopolysaccharides secreted by diatoms.

## Discussion

The presented data show that polysaccharide degradation and aggregation processes are structure-specific, which led here to the selected degradation of laminarin and other glycans and to the formation of FCSP particles. We demonstrate diatoms produced FCSP that accumulated in POM during time storing carbon in the course of the bloom. This observed FCSP stability to bacterial degradation and its presence on the diatom surface implies biological function protecting the cells from pathogens or predation. FCSP from brown algae have indeed antiviral properties (Ponce et al., 2003), and in diatoms may act as a barrier to pathogens akin to the role of mucins in human gut epithelia cells (Corfield, 2015). Interestingly, in human gut when dietary polysaccharides such as  $\beta$ -glucans that serve as food for gut microbes are removed from the diet, gut bacteria start to digest and deteriorate the mucin layer. Hence labile polysaccharides help to conserve the mucin in the gut (Martens et al., 2018) in a similar way that is proposed here for FCSP in the wild. In addition, owing to their surface reactive chemical nature mediated by sulfate and potentially carboxyl groups, we observed the diatom-secreted FCSP coagulated and formed aggregates that may act as precursors of marine snow. Notably, marine snow particles fabricated from diatoms with roller tanks in the laboratory (Gärdes et al., 2011) are, indeed similar to what we saw in the bloom, stable for month despite the presence of associated microbial communities. Additionally, the same chemical groups that drive aggregation via inorganic bonding also capture metal ions. Anionic, algal polysaccharides are used for metal ion removal in the laboratory with affinities comparable to the strongest metal chelators EDTA and chelex resins providing a chemical

## **Chapter IV**

explanation for the extensive removal of trace metals from surface waters by diatoms (Zaferani et al., 2018).

The geographical distribution and abundance of microalgal species is currently being pushed by climate change. Our study shows microalgae produce different types of polysaccharides, each of which have their unique reactivity and aggregation potentials. Understanding how climate changes microalgae-driven carbon and trace metal export must thus involve the structural and quantitative study of these underexplored polysaccharides in the ocean.

## **Online Content**

Methods, along with any additional Extended Data display items and Source Data, are available in the online version of the paper; references unique to these sections appear only in the online paper.

## **Acknowledgements**

This work was funded by the Max Planck Society and supported by the Deutsche Forschungsgemeinschaft (DFG) grant HE 7217/1-1 to J.-H.H. and the DFG research unit FOR2406. We thank K. Wiltshire from the Alfred Wegener Institute in Helgoland for provision of physicochemical and algae biodiversity data; T. Harder laboratory for providing the diatom strain isolated in the bloom.

## **Author contributions**

S.V.-M. and J.-H.H. designed the study. S.V.-M performed the polysaccharide extractions, microarray analyses, immunolabeling and epitope detection chromatography; A.S. performed monosaccharide analysis and statistical analyses; J.N. executed DOC measurements; A.W. supported with the TFF processing during the sampling campaign; B.F. performed metagenome analysis; D.B. performed metaproteome analysis; P.L.B. executed the filter classification analysis to the microarray data. S.V-M, A.S. and B.F. prepared graphical illustrations. All authors discussed the results. SV-M and J-HH wrote the manuscript. All authors commented and approved the manuscript.

## **Competing interests:**

The authors declare no competing interests.

## METHODS

### Sampling for POM and HMWDOM.

Sampling was carried out from the 15.03 to the 26.05 in 2016 during a phytoplankton bloom at the station Kabeltonne at the North Sea (54°11.3'N, 7°54.0'E) near the island of Helgoland, Germany. Two times per week 100 L of surface seawater (1 m depth) were collected in the morning with the research vessel Aade. See sampling scheme in Fig 1a. For harvesting POM samples, the 100 L seawater were directly transported to the lab in 25 L carboys and sequentially filtered through 10 µm, 3 µm and 0.2 µm pore size polycarbonate filters with 142 mm diameter (filter codes were TCTP14250; TSTP14250 and GTTP14250, respectively; Merck Millipore). To reduce the filtration time filtration was performed sequentially but in parallel using three filtration units with air pressure pumps by <2 bar. The filters were replaced for new filters when clogged. The entire filtration was normally completed in less than four hours after the sampling. Filters were stored at -80 °C until further analysis.

For harvesting DOM samples, the 100 L of 0.2 µm-filtered seawater (that were obtained after the sequential filtration described above) were concentrated to 0.5 L by tangential flow filtration (TFF) using three membranes with a cut-off of 1kDa (Cat. Nr 3051460901E--SG, Sartocoon® Slice PESU Cassette, Sartorius Stedim). These samples correspond to high molecular weight-dissolved organic matter (HMWDOM). TFF concentrates molecules by molecular size and is therefore less chemically selective than other concentration techniques, such as solid phase extraction, allowing the recovery of a broad representative fraction of DOM (Benner et al 1992). The TFF system (X) was run with an air pressure pump using feed and retentate pressures of < 4 bar and with the permeate valve opened. Once the retentate had a volume of approximately 0.5 L the TFF was stopped and the retentate sample (containing molecules < 0.2 µm and > 1 KDa) was stored at -80 °C until further analysis. In between runs the TFF system and the membranes were washed with 4 L of 1 M NaOH at 50 °C for 1 h, afterwards the system was flushed and permeated with 0.2 µm-filtered tap water until the pH of the permeate was neutral. The TFF system was stored in 0.1 M NaOH and before starting a new sample the system was flushed and permeated with 0.2 µm-filtered tap water until neutral pH.

## Chapter IV

### **Dissolved organic carbon (DOC) analysis.**

Samples for DOC quantification were collected from the 0.2  $\mu\text{m}$ -filtered seawater. Four replicate samples of 10 ml were acidified to pH 2 (HCl, p.a.) in pre-combusted glass vials (400 °C, 4 h) and stored in the dark at 4 °C until analysis. DOC was analyzed on a Shimadzu TOC-VCPH instrument via high temperature catalytic oxidation. Analytical accuracy and precision were tested with deep-sea reference material (D. Hansell, University of Miami, USA) and were better than 5%. Standard deviation for replicates was on average 2.8 +/- 1.6 %. DOC content of 1 ml aliquots of the TFF concentrated HMWDOM samples was as well quantified. Based on the DOC content of the HMWDOM compared to the 0.2  $\mu\text{m}$ -filtered seawater we calculated our TFF concentration had an average extraction efficiency of about 5.5 %.

### **Monosaccharide analysis.**

Aliquots (1 ml) of the 0.5 L concentrated HMWDOM samples were acid hydrolyzed using a final concentration of 1 M HCl at 100 °C for 24 h. Afterwards the samples were dried using a Speed-Vac, redissolved in MilliQ and analysed by high-performance anion exchange chromatography (HPAEC) coupled with a pulsed amperometric detector (PAD). We used a Dionex ICS5000 system equipped with a CarboPac PA10 analytical column (2 x 250 mm) and a CarboPac PA10 guard column (2 x 50 mm). The operation procedure was performed as described (Engel et al 2011).

For the chromatographic fractions enriched with FCSP (mAb BAM1 absorbance peak), the 1 ml fractions were dialysed in 1 KDa dialysis bags and then acid hydrolyzed and analyzed as described above (Figure 26g).

### **Processing of POM samples.**

For POM samples, the material retained on the 10, 3 and 0.2  $\mu\text{m}$  filters was scrapped out from the filters with a flat spatula. The scrapped material was washed out from the filter surface with pure ethanol and collected in 50 ml Falcon tubes. To ensure the removal of the filters content this procedure was repeated three times per each filter. Per each sample (one specific pore size and date) material was extracted from three different filters and collected together. The collected material corresponds to particulate organic matter (POM) with the equivalent molecular sizes of > 10  $\mu\text{m}$ , between 10 and 3  $\mu\text{m}$ , and between 3 and 0.2  $\mu\text{m}$ . The alcohol

insoluble residue (AIR) was performed for all POM samples. The scrapped out, ethanol washed material that was collected in 50 ml Falcon tubes was rotated at room temperature for 10 min. Afterwards samples were spun down at 4500 rpm for 15 min at 15 °C. Supernatants were discarded and pellets were re-suspended (6:1 volume solvent:volume pellet) in chloroform:methanol (1:1). Samples were vortexed and rotated for 10 min and then spun down as described above. Pellets were re-suspended in pure acetone (6 volumes acetone to 1 volume pellet), vortexed and rotated for 10 min and spun down as depicted above. The pellets were left to air dry under the fume hood overnight.

### **Processing of HMWDOM samples.**

The TFF concentrated HMWDOM samples were further concentrated from 0.5 L to approximately 40 ml by using an Amicon® stirred ultrafiltration cell (Merck Millipore) with a 1 KDa membrane using nitrogen for gas pressure. In order to get rid of the salt, the concentrated sample was collected and placed inside a 1 KDa dialysis tubing (Spectra/Por®, Spectrum Laboratories) and then dialysed overnight against 5 L milliQ water in a beaker with stirring. After overnight stirring, the milliQ water was replaced for new 5 L of milliQ and left stirring for 4 h. The water was replaced a third time and after 4 h stirring the dialysed HMW-DOM sample was transferred into a Falcon tube, frozen and freeze dried.

### **Polysaccharide extraction.**

As polysaccharides have different extractability and solubility we extracted the polysaccharides with 3 different solvents. The HMWDOM freeze dried samples and the POM AIR samples were individually well-homogenised with a spatula. Samples were weighed out in an 8-strip tube (approximately 10 mg of each sample were weighed out). A small stainless steel bead was added in each tube. Polysaccharides were sequentially extracted with: autoclaved milliQ water, 50 mM EDTA pH 7.5 and 4 M NaOH with 0.1% NaBH<sub>4</sub>. Per each of the extracting solvents the following was performed: for every 10 mg of sample 300 µl of solvent were added (volume of solvent was adjusted to the weight i.e. the sample extractions were normalized by weight). The tubes were placed in an appropriate holder and placed on a tissue lyser. Samples were shaken at 30/s for 2 min and then at 6/s for 2 h. Afterwards samples were spun down at 4500 rpm for 15 min at 15 °C. Extracts (supernatants) were collected and stored at 4 °C and the pellets were resuspended in the next extracting solvent.

## Chapter IV

### **Carbohydrate microarray analysis.**

All the HMWDOM and POM polysaccharide extracts were added into wells of 384-microwell plates. For each sample a 2-fold dilution followed by a 5-fold dilution was performed in printing buffer (55.2% glycerol, 44% water, 0.8% Triton X-100). Plates containing the samples were spun down at 4500 rpm for 10 min to get rid of bubbles. The content of the plates was printed onto nitrocellulose membrane with a pore size of 0.45  $\mu\text{m}$  (Whatman) using a microarray robot (Sprint, Arrayjet, Roslin, UK) under controlled conditions of 20 °C and 50% humidity. A replicate was included per each extract and therefore each sample was represented by a total of 4 spots in the microarray (duplicates and two different concentrations for each). Note: the HMWDOM water extracts presented very high viscosity, probably due to the high polysaccharide content. Solutions with very high viscosity have a negative effect on the quality of the microarray print (appearance of satellites). To warranty a good quality print, the HMWDOM water extracts were 3-fold diluted in milliQ water before being 2-fold diluted in printing buffer. Therefore a direct comparison of the total abundance of polysaccharides in the HMWDOM water extracts with the EDTA or NaOH extracts cannot be performed. But comparison of the result from one probe within HMWDOM water extracts can be done. Once printed, the microarrays were individually probed with 51 polysaccharide-specific monoclonal antibodies and carbohydrate binding modules (in EDTable. 1) as previously described in (Vidal-Melgosa, Pedersen, Schückerl, et al., 2015). The developed arrays were scanned at 2400 dots per inch and the binding of each probe (probe signal intensity) against each spotted sample was quantified using the software Array-Pro Analyzer 6.3 (Media Cybernetics). Per each sample the mean antibody signal intensity (derived from 4 spots) was calculated. The maximum mean spot signal detected in the data set was set to 100 and all other values were normalized accordingly. As DOM and POM samples were isolated differently, their data sets were normalized independently and therefore absolute values from DOM and POM should not be compared but the trends. Polysaccharide epitope abundance within HMWDOM samples (water independently from EDTA and NaOH) and within all POM samples can be compared. A cutoff of 5 arbitrary units was applied. Some data are shown in Figure 23 and Supplement Figure 17 shows all profiles where an antibody positive signal (value > 5) was detected.

### **Epitope deletion and substrate concentration effect experiment.**

Epitope deletion –

Microarrays containing particular extracts from HMWDOM or POM were printed. Epitope deletion was performed as described in (Feng, T. et al. 2014) with some modifications. Briefly, individual arrays were blocked for 1 h in PBS (140 mM NaCl, 2.7 mM KCl, 10 mM Na<sub>2</sub>HPO<sub>4</sub>, 1.7 mM KH<sub>2</sub>PO<sub>4</sub>, pH 7.5) with 5% (w/v) low fat milk powder, MPBS. Arrays were washed with PBS and then they were individually incubated either with a specific glycoside hydrolase (GH) at 2 U/ml or with only buffer for 2 h at 37 °C and 50 rpm. The different commercial enzymes used in the experiments were: endo-1,4- $\beta$ -Xylanase (E-XYAN4), endo-1,4  $\beta$ -Mannanase (E-BMATM), Lichenase (endo-1,3:1,4- $\beta$ -D-Glucanase) (E-LICHN), endo-Polygalacturonase (E-PGALUSP) and endo-1,3- $\beta$ -D-Glucanase (E-LAMSE ) from Megazyme (Bray, Ireland). Enzyme solutions at 2 U/ml were prepared in 100 mM sodium acetate buffer pH 5.0 or 100 mM sodium phosphate buffer pH 7.0 depending on the enzymes optimal pH. The negative control (array not treated with enzyme) was always done with the same buffer used for the GH. After incubation, the arrays were thoroughly washed in PBS and then incubated with specific monoclonal antibodies (microarray probing, quantification and data analysis was performed as described above). Microarrays were probed with antibodies that would recognise the epitope to which the GH was specific for (except for the control, that showed that pre-treatment with an endo-1,4- $\beta$ -Xylanase did not hydrolyze the  $\beta$ -1,4-mannan from HMWDOM extracts. Results (Figure 24a) are presented in box plot pares. If the GH digested the polysaccharide from the POM or DOM extract, the epitope recognised by the antibody was modified or destroyed and the binding signal of the antibody was either diminished or completely abolished. Results were analysed with a paired t-test that compared the antibody signal obtained for each extract with the two treatments (enzyme and buffer).

### **Substrate concentration effect**

To corroborate the correlation between epitope concentration and probe signal intensity the following commercial defined polysaccharides were used: Fucoidan (Laminaria, PSa13) from Glycomix; and galactomannan (carob), glucomannan (konjac) and polygalacturonic acid (PGA, citrus pectin) from Megazyme. The defined polysaccharides were dissolved in milliQ water to 2 mg/ml. The polysaccharide solutions were added into wells of 384-microwell plates including eight successive 2-fold dilutions in printing buffer. Each polysaccharide solution had twelve replicates for each of the 8 different concentrations to also assess the spot reproducibility. Microarray printing, probing and data analysis was performed as described above.

## Chapter IV

### Metagenomics.

Metagenomic samples were collected and sequenced as described previously (Teeling et al., 2016). Specifically, samples were sequenced from the following dates: 2016/03/16; 2016/03/21; 2016/03/31; 2016/04/12; 2016/04/19; 2016/04/26; 2016/05/02; 2016/05/12; 2016/05/17. Briefly, water was pre-filtered to remove eukaryotes using both 10  $\mu\text{m}$  and 3  $\mu\text{m}$  pore-size filters, and then bacterioplankton was collected on 0.2  $\mu\text{m}$  pore-size polycarbonate filters.

DNA was sequenced at the DOE Joint Genome Institute (JGI) on the Illumina HiSeq 2500 platform with  $2 \times 150$  bp reads. Raw reads were quality filtered and trimmed using BBDuk v35.14 (<http://bbtools.jgi.doe.gov>) and the following parameters:  $k_{\text{trim}} = r_{\text{k}} = 28$   $m_{\text{ink}} = 12$   $h_{\text{dist}} = 1$   $t_{\text{bo}} = t_{\text{tpe}} = t_{\text{qtrim}} = r_{\text{l}} \text{ trimq} = 20$   $\text{minlength} = 100$ . Reads were assembled with metaSPAdes v3.10.0, with kmer lengths of 21, 33, 55, 77, and 99. Contigs longer than 2500 bp were kept for further analyses. Assemblies are available under the accession PRJEB28156.

Gene prediction and translation was done with Prodigal v2.6.3 (Hyatt et al., 2010) in metagenomic mode. Amino acid sequences were then initially placed into CAZyme families using the hmmscan function of HMMer v3.2.1 (Finn et al., 2011) and the dbCAN v6 database and using the hmmscan-parser.sh script to select the best hit (Yin et al., 2012). Predicted CAZymes were then confirmed via DIAMOND-BLAST comparison (Buchfink et al., 2014) selecting the top hit against the CAZy database v07312018 (Lombard, Golaconda Ramulu, et al., 2014), using –sensitive mode, an e-value cutoff of 1-20, minimum query cover of 40%, and minimum sequence identity of 30% (Krüger et al., 2019). CAZymes were assigned to taxonomic groups based on their presence in MAGs from PRJEB28156. MAGs were classified using GTDB-Tk v0.3.1 and GTDB v89 (Parks et al., 2018).

In order to estimate abundance of different gene families, reads were mapped to the individual CAZyme gene sequences using BBDuk v35.14 (<http://bbtools.jgi.doe.gov>), with minimum mapping identity of 0.99, and identity filter for reporting mappings of 0.97. Reads per kilobase per million ( $\text{RPKM} = 1,000,000 \times (\text{number of reads mapped} \div \text{gene length in kilobase pairs}) \div \text{number of reads in sample}$ ) values were calculated to estimate the normalised relative abundance of individual gene families.



### **Physicochemical parameters and phytoplankton taxa measurements.**

These data were assessed from subsurface water samples as part of the Helgoland Roads LTER time series. The chlorophyll a concentration was measured using an algal group analyzer (bbe moldaenke).

### **Immunolabelling.**

Subsurface seawater was sampled (in parallel with the 100 L to get the same water body) and 1 L was fixed without pre-filtration with 37 % formaldehyde to a final concentration of 1 % (v/v) for 1 h at room temperature. Once fixed, triplicates of 100 ml were filtered onto polycarbonate filters with 0.2 µm pore size and 47 mm diameter (GTTP, Merck Millipore) with a manual vacuum pump with < 5 mm Hg. Filters were stored at -80 °C until analysis. For microscopy analyses, immunolabeling of filters from the beginning and end of the bloom was performed a number of times independently (including filters from the dates 2016/03/24, 2016/03/29, 2016/03/31, 2016/05/10, 2016/05/12 and 2016/05/19). Sections of the filters were cut and added in separate eppendorf tubes. Filter sections were blocked in PBS with 3% (w/v) bovine serum albumin (BSA-PBS) for 1 h. Next, sections were incubated for 1.5 h with the anti-rat mAb BAM1 (PlantProbes) diluted 1:5 in BSA-PBS. Then they were washed four times with PBS and incubated with anti-rat secondary antibody conjugated to FITC (F1763, Sigma Aldrich) diluted 1:100 in BSA-PBS for 1.5 h in darkness. The thorough washing step with PBS was repeated. Afterwards, filter sections were incubated with 4',6-diamidino-2-phenylindole (DAPI, at 1 µg/ml) for 10 min in the dark, flushed with MilliQ and in 96 % ethanol. Filter sections were mounted on glass slides with the antifading reagents Citifluor:Vectashield as 4:1 (v/v). Negative controls without BAM1 incubation were included. In the controls mAb BAM1 incubation was replaced by incubation with only BSA-PBS and afterwards the secondary antibody anti-rat-FITC incubation and DAPI staining was performed to detect any unspecific binding of the secondary antibody.

### **Super-resolution microscopy by Airyscan.**

The immunolabelled filter samples were examined on a Zeiss LSM 780 with Airyscan (Leica) equipped with an inverted microscope and a supercontinuum light source. The instrument was controlled by using the ZEN black software. Z-stack images were taken using a 63x/1.4 oil

## Chapter IV

objective. Images were collected and processed with the ZEN black software. Movement of the sample during acquisition was corrected by Z-stack alignment (with 2Dslices, highest resolution, translation and linear) with the ZEN blue software. Images (Figure 26a,b) were projected as maximum intensity projection (ZEN black).

### **Quantification of the BAM1 antibody signal intensity in filters.**

Immunolabeling of filters with no pre-filtration (containing all POM fraction  $> 0.2 \mu\text{m}$ ) revealed *C. socialis* cells in filters from the end of the bloom presented a stronger BAM1 signal than filters from the beginning of the bloom. The mAb BAM1 intensity was quantified by the software ZEN blue. Triplicate filters from the sampling dates 2016/03/31 and 2016/05/16 were chosen (sampling dates with the highest chlorophyll a value of March and May, 9.0 and 7.0  $\mu\text{g/l}$ , respectively) from which five fields of view were analysed. Immunolabeling was performed as described above and filters were examined on a Zeiss Axioplan II Imaging epifluorescence microscope (Carl Zeiss MicroImaging GmbH, Göttingen, Germany) using the ZEN black software with the same laser power and exposure time for all the filter sections. All images were analysed on the same day. The Intensity Mean Value was quantified by using the ZEN blue software. BAM1 intensity was quantified both on the diatom cells and on regions of the filter with no diatoms. Negative control filters with no BAM1 incubation and with only BSA-PBS (i.e. no incubation with BAM1, secondary ant-rat-FITC neither DAPI) were included.

### **FCSP separation by chromatography**

Polysaccharide extraction from POM 3  $\mu\text{m}$  filter material (from dates 2016/03/31 and 2016/05/12) and *C. socialis* biomass was performed as described above. The FCSP from MilliQ extracts was separated by anion-exchange chromatography using the method epitope detection chromatography as described in (Cornuault et al., 2014). The chromatographic fractions containing FCSP were identified by using the mAbs BAM1.

## Figures

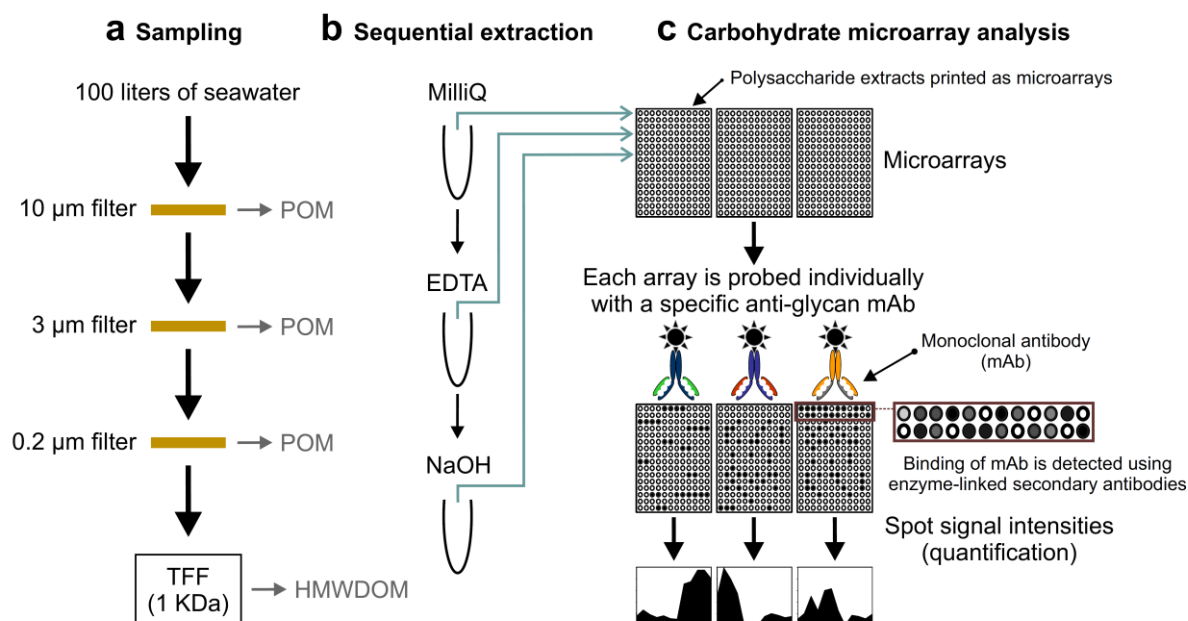


Figure 22: **Schematic overview of the polysaccharide sampling, extraction and analysis.** **a**, Scheme of the sampling. TFF, Tangential flow filtration. **b**, Polysaccharides from each POM and HMWDOM sample are sequentially extracted with MilliQ water, EDTA and NaOH. **c**, Polysaccharide extracts are printed on microarrays (each extract represented by 4 spots) and each individual array is probed with one specific mAb. Binding of a mAb to the extracts is detected colorimetrically with a secondary antibody conjugated to an enzyme that yields a colored product when in conjunction with its substrate. Signal intensities of each spotted sample against each mAb are quantified displaying the relative abundance of specific polysaccharide epitopes in the samples.

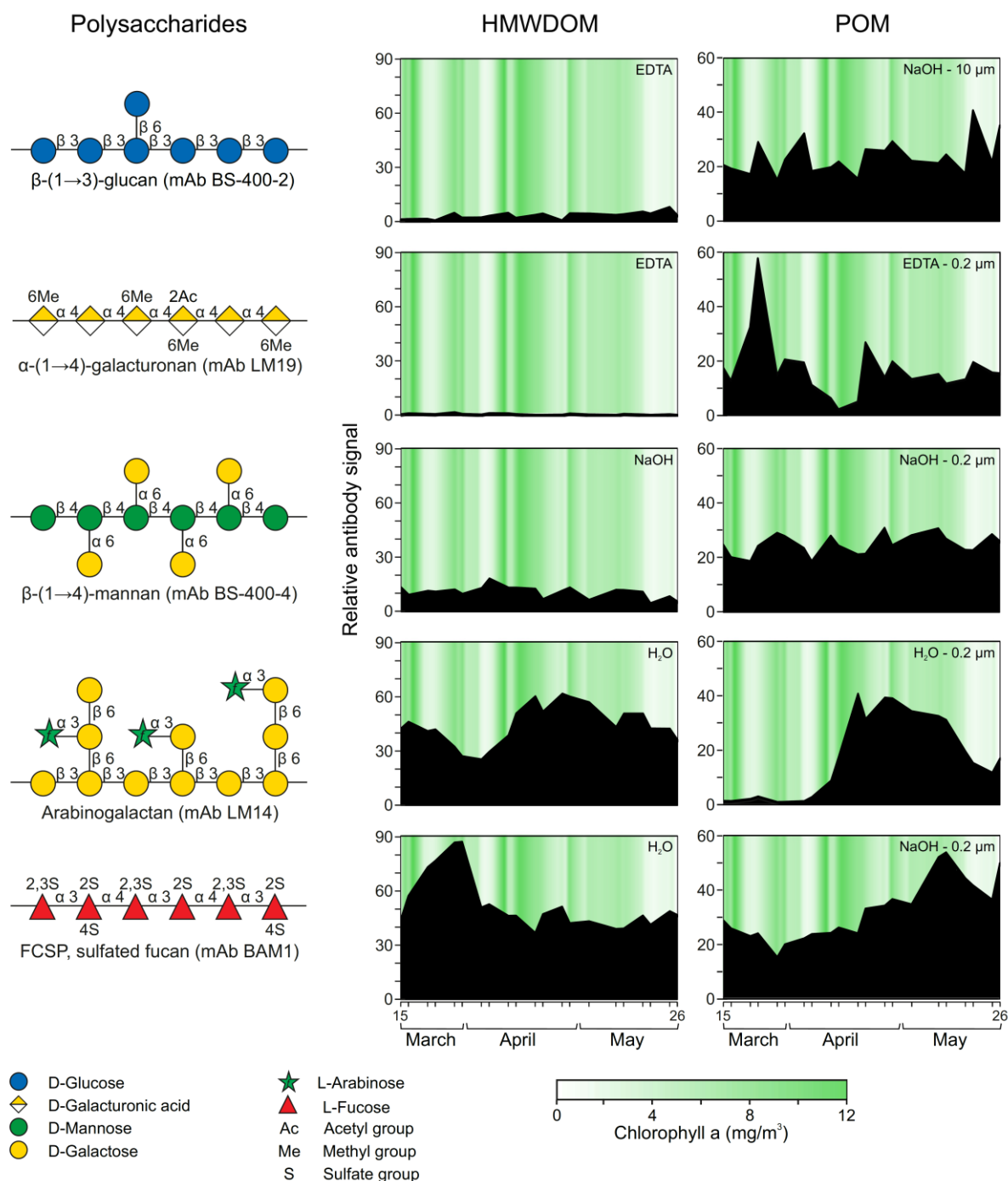


Figure 23: **Different polysaccharide structural types are present in HMWDOM and POM and show fluctuations in their abundance during the diatom bloom.** Example of five selected polysaccharides, complete microarray data set is shown in Supplement Figure 17. At the left, sketch of the polysaccharide structures that the corresponding mAbs, which are depicted in parentheses, would bind to. Plots show the relative abundance of these particular polysaccharide epitopes (antibody signal intensity, y axis) detected in HMWDOM and POM during the bloom (21 sampling dates marked at the *bottom*). For each mAb only the HMWDOM and the POM extracts that presented highest signal are shown as example. Spot signal intensities for each extract against each probe were quantified and the highest mean signal value in the data set was set to 100 and all other values were normalized accordingly.

HMWDOM and POM microarray data were normalized independently hence the trend but not the absolute number should be compared between the two pools. Chlorophyll a values ( $\text{mg}/\text{m}^3$ ) are shown as green background. HMWDOM, between  $0.2 \mu\text{m}$  and  $1 \text{ KDa}$ ; POM,  $> 0.2 \mu\text{m}$ ; *f*, furanose form.

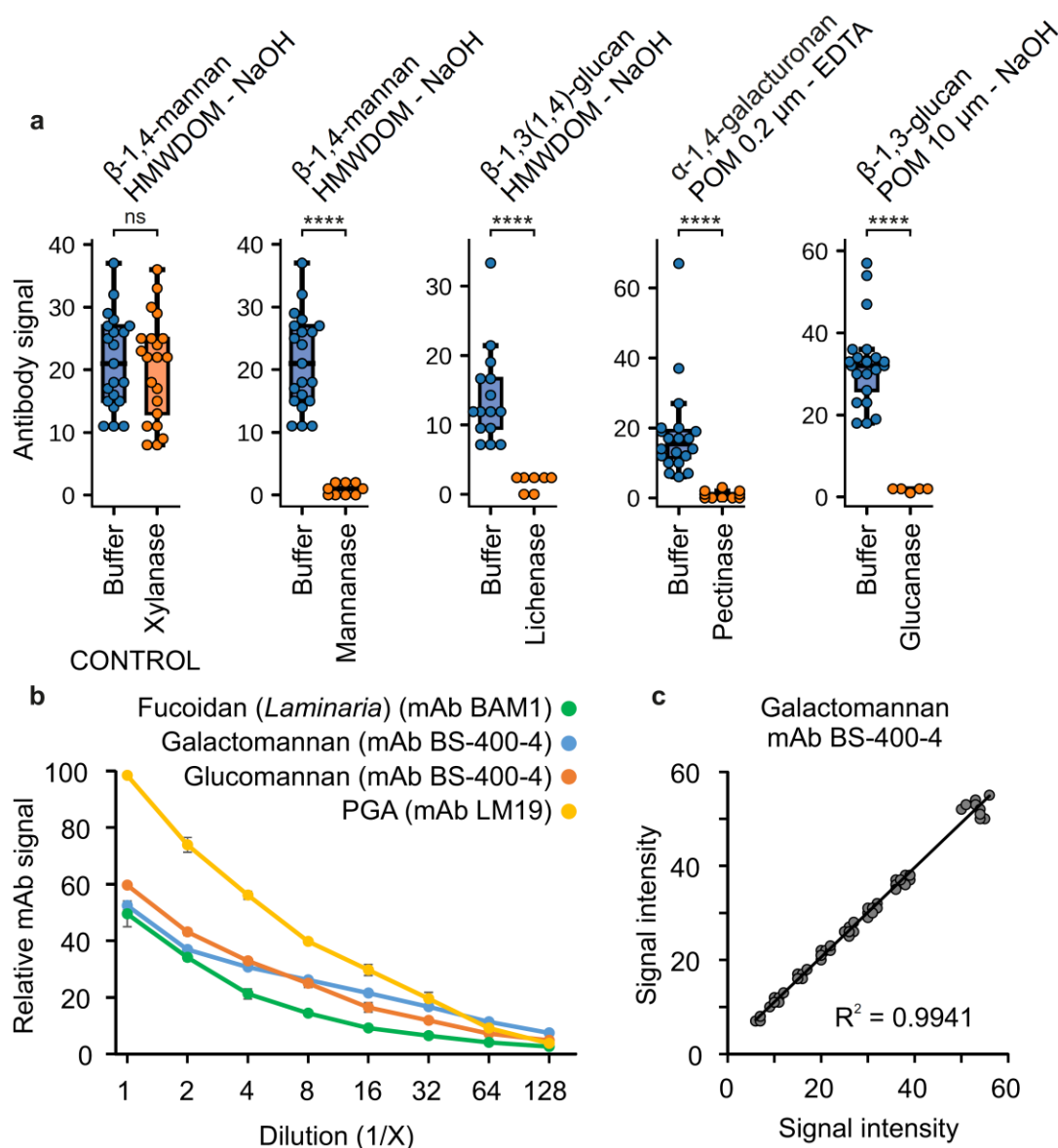
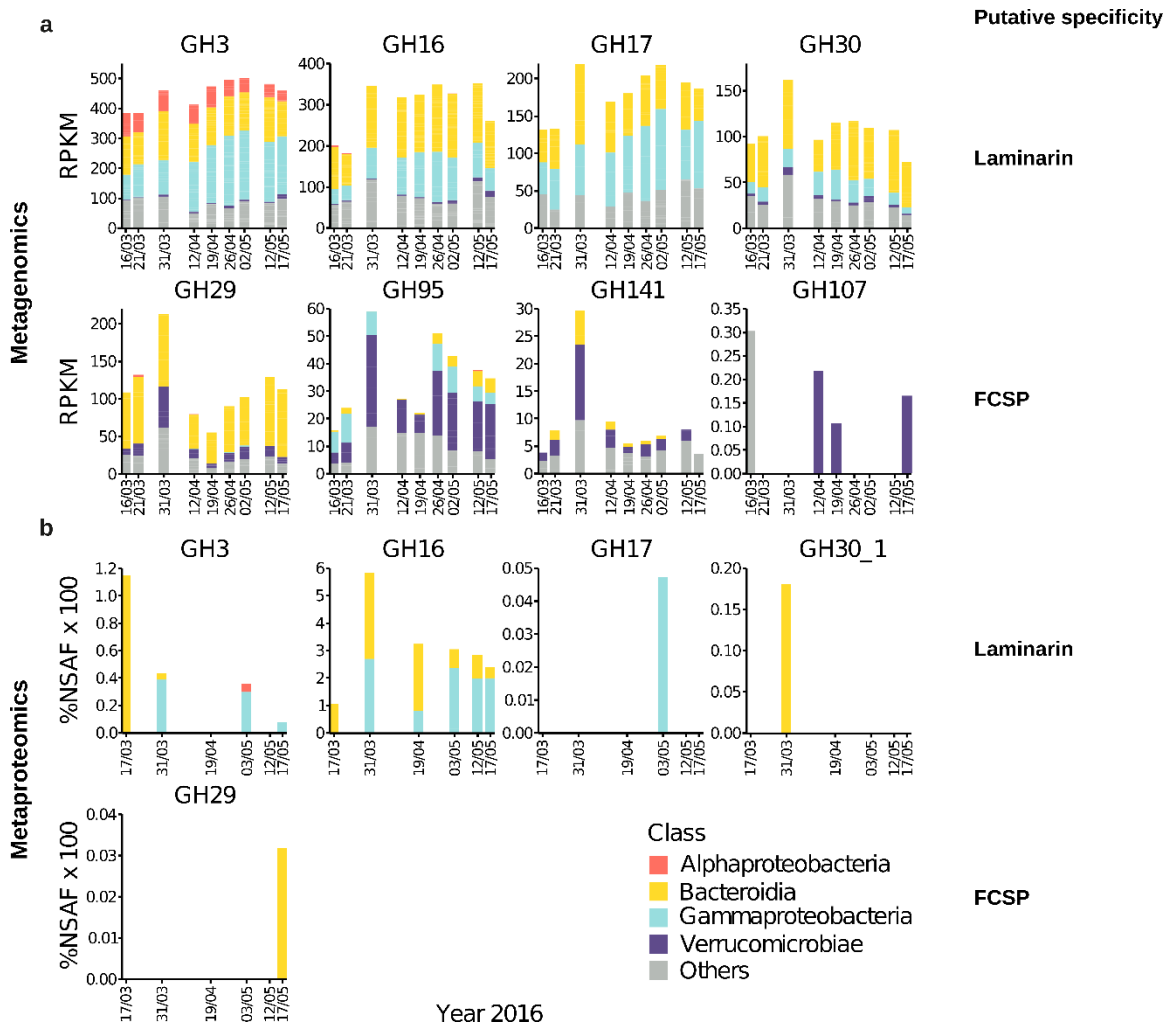
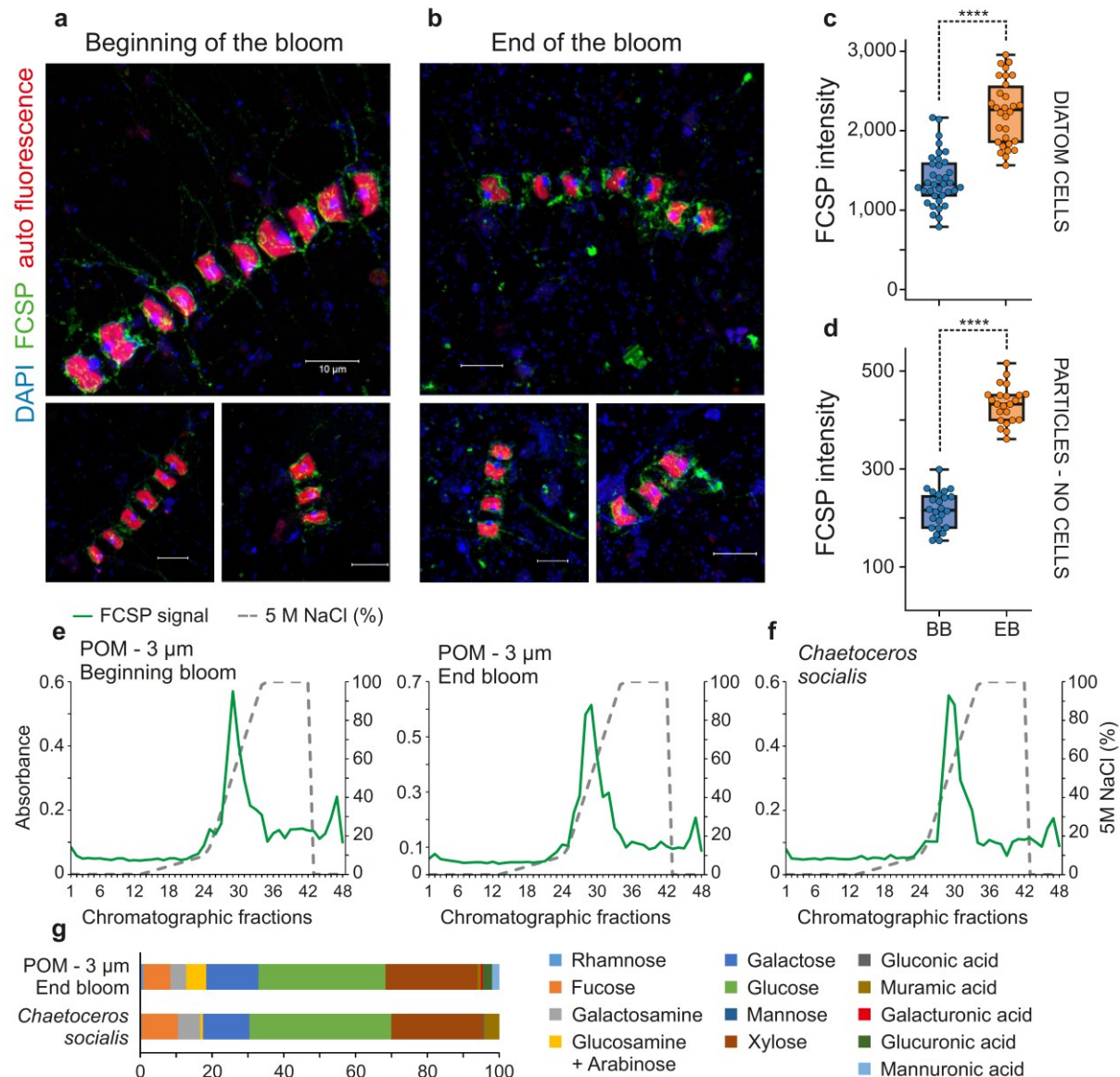


Figure 24. **Enzymatic epitope deletion, substrate concentration effect and reproducibility.** **a**, Comparison of antibody signal intensity ( $y$  axis) detected in arrays populated with HMWDOM or POM extracts treated with a glycoside hydrolase (GH) to arrays treated with buffer. After treatment arrays were probed with (pairs from left to right) the mAb: LM21, LM21, BS-400-3, LM19 and BS-4002. GH treatment resulted in reduction of mAb signal to background levels ( $< 5$ ), i.e. the epitope recognized by the probe was degraded by the GH. From the 21 sampling days the dates where signal was detected on the untreated samples are shown, resulting in (from left to right)  $n = 21$ ,  $n = 21$ ,  $n = 15$ ,  $n = 20$  and  $n = 21$ . *ns*: not significant, \*\*\*\* $P < 0.0001$  (paired two-sided  $t$ -test). See Methods for GH details. For boxplots, the middle line indicates the median, the box designates the interquartile range (IQR) and the whiskers denote 1.5 times the IQR. **b**, Plot presents the correlation between standard polysaccharides concentration and mAb signal intensity, which progressively decreases with decreasing epitope concentration. Dots and error bars represent mean and standard deviation of  $n = 12$  replicates per each concentration. For the four polysaccharides first dilution was 1 mg/ml. **c**, Reproducibility of the microarrays tested by comparing the spot mAb signals

obtained from two microarrays probed with the same antibody. The four polysaccharides from section b were tested and all resulted in  $R^2 > 0.99$  indicating a low level of variability. Representative graph shows the plotted galactomannan signals detected with mAb BS-400-4 in two arrays,  $n = 96$  spotted galactomannan samples in each array.



**Figure 25: Content and expression of particular CAZymes by marine bacteria during the bloom.** **a**, Abundances of CAZymes with relevance for degradation of two selected glycan substrates ( $\beta$ -(1 $\rightarrow$ 3)-glucan and fucose-containing sulfated polysaccharide, FCSP) in the genomes of marine bacteria. **b**, Expression of CAZymes, with relevance for laminarin and FCSP degradation, by marine bacteria during the bloom (Supplement Figure 18). Proteome data were analyzed in a semiquantitative manner based on normalized spectral abundance factors (NSAF). Both analyses include class-level taxonomic classifications. GH, glycoside hydrolase family.



**Figure 26: FCSP is produced by diatoms and increases abundance in POM during the bloom.** **a-b**, Representative images of FCSP localisation in POM ( $> 0.2 \mu\text{m}$ ) from the diatom bloom. Airyscan super-resolution images demonstrate FCSP occurred around the cells of the chain forming diatom *Chaetoceros socialis* at the beginning of the bloom (**a**) and on the diatoms cells as well as on particles at the end of the bloom (**b**). DAPI (blue), FCSP (green) and diatom auto fluorescence (red). Scale bars,  $10 \mu\text{m}$ . **c**, Quantification of FCSP signal (mAb BAM1) on diatom cells. BB: Beginning bloom  $n = 36$  cells, EB: end bloom  $n = 30$  cells. **d**, FCSP quantification on particles (areas not including cells). BB  $n = 24$  areas, EB  $n = 23$  areas. In **c-d**,  $****P < 0.0001$  (two-sided  $t$ -test). For boxplots, the middle line indicates the median, the box designates the interquartile range (IQR) and the whiskers denote 1.5 times the IQR. **e**, Chromatographic separation of FCSP in POM extracts by anion exchange chromatography confirms its acidic nature. **f**, Negatively charged FCSP is produced by the diatom *C. socialis*. **e-f**, epitope detection chromatography (EDC) with the mAb BAM1. **g**, Monosaccharide composition of the FCSP-enriched chromatographic fraction (EDC fraction with BAM1 absorbance peak) shows the fucose content.



## General Discussion

The primary goal of this dissertation was to elucidate the biochemical pathway of fucoidan metabolism by marine bacteria. *En route*, I established routine purification and quantification protocols for fucoidans and greatly enhanced our handling and understanding of diversity within this class of polysaccharides (Chapter I). Next, I characterized the degradation of fucoidan by the marine Verrucomicrobium ‘*Lentimonas*’ sp. CC4 and found excessive metabolic requirements of over 100 enzymes to degrade fucoidans showing why fucoidans are recalcitrant to most microbes (Chapter II). Subsequently, we provided a structural and biochemical characterization of a fucosidase and sulfatase from ‘*Lentimonas*’ sp. CC4 and identified new catalytic residues and activity (Chapter III). Tracing the production and recycling of polysaccharides over a diatom bloom revealed that fucoidans indeed accumulate and play a key role in aggregate formation and therefore fucoidans drive marine carbon sequestration. (Chapter IV).

### Verrucomicrobia are important polysaccharide degraders

This work has greatly advanced our genetic and physiological understanding of how Verrucomicrobia degrade polysaccharides. We identified a PUL structure for iota-carrageenan in ‘*Lentimonas*’ sp. CC4. This locus is upregulated by iota-carrageenan and encodes the enzymes GH82, GH16, GH29, GH127, S1\_19 and S1\_7, which represent a canonical iota-carrageenan pathway (Ficko-Blean et al., 2017). Additionally, this locus encodes a highly expressed TonB dependent uptake system that could potentially take up oligosaccharides in a selfish manner. The uptake of HMW-carrageenan by ‘*Lentimonas*’ sp. CC4 could be experimentally tested with fluorescently labelled carrageenan. This method is commonly used to infer the substrate uptake of Planctomycetes, Bacteroidetes or Gammaproteobacteria and also showed the uptake of xylan by Verrucomicrobia in an arctic fjord (Cardman et al., 2014; Boedeker et al., 2017; Reintjes et al., 2017, 2018; Unfried et al., 2018). Altogether, the genetic architecture of iota-carrageenan degradation in ‘*Lentimonas*’ sp. CC4 is similar to the previously described architecture for Bacteroidetes or Gammaproteobacteria (Ficko-Blean et al., 2017) underpinning broadly shared features across phyla.

Verrucomicrobia appear to specialize in the degradation of few, but complex polysaccharides. ‘*Lentimonas*’ sp. CC4 carries about 300 enzymes for the degradation of

## General Discussion

fucoidans, iota-carrageenan and sulfated mannans and does not grow on any other polysaccharide tested. In comparison, marine and human gut Bacteroidetes with similar amounts of enzymes degrade a broader range of up to 40 different substrates (Martens et al., 2011; Terrapon et al., 2015; Barbeyron, Thomas, et al., 2016). ‘*Lentimonas*’ sp. CC4 specializes in degrading various fucoidans with more than 50 exo-enzymes of family GH29, GH95 and GH141. Such a specialization of a few substrates with many gene copies of a few exo-enzymes families has also been observed in the Verrucomicrobium *Akkermansia muciniphila*, which degrades mucins (Seekatz et al., 2016). We observed that this expanded repertoire of exo-enzymes is a general trend in available genomes of Verrucomicrobia. Therefore, we suggest that Verrucomicrobia are polysaccharide specialists using an expanded set of exo-enzymes to degrade complex polysaccharides.

Fucoidan hydrolysis is a trait with a broad phylogenetic distribution among Verrucomicrobia. The phylum ‘Verrucomicrobia’ is grouped into six monophyletic subdivisions (Hugenholtz et al., 1998), of which three distinct clades are capable of fucoidan hydrolysis. *Luteolibacter algae* H18 (Subdivision 1, family Verrucomicrobiaceae), ‘*Lentimonas*’ sp. CC4 (Subdivision 4, family Puniceicoccaceae) and *Kiritimatiella* sp. F21 (formerly subdivision 5, now phylum Kiritimatiellaeota) can degrade fucoidan (Choo et al., 2007; Ohshiro et al., 2012; Spring et al., 2016; van Vliet et al., 2019a). Kiritimatiellaeota are anaerobic heterotrophs and are highly abundant on settling marine aggregates, suggesting that Kiritimatiellaeota thrive in the microaerophilic or anaerobic microniches of particles and contribute to polysaccharide degradation *in situ* (Ploug & Bergkvist, 2015; Bachmann et al., 2018). Genomic analysis of *Kiritimatiella* sp. F21 shows a similarly expanded repertoire of exo-enzymes to ‘*Lentimonas*’ sp. CC4, suggesting a similar metabolic strategy. In contrast, subdivision 1 and 4 are aerobic heterotrophs and are enriched in sediments or water column, respectively (Freitas et al., 2012). Therefore, fucoidan degrading Verrucomicrobia are widespread in marine habitats and are important primary degraders.

## Biotechnological potential of ‘*Lentimonas*’ sp. CC4

‘*Lentimonas*’ sp. CC4 is the first well characterized fucoidan degrader and represents a resource for discovery of fucoidan modifying enzymes. The bacterial strain, genome and expression data are publicly available and the strain can be systematically explored to discover novel enzymes and activities. In Chapter II, we identified operon structures and speculated that they act together on different branches of fucoidan. As a proof of principle, we started to

characterize a two-gene operon consisting of one GH29 and one S1\_15. The LCC4\_2\_22\_GH29 is an exo-acting fucosidase, potentially producing sulfated fucose from fucoidan, which is a novel feature of GH29s since these were considered to only produce fucose. This demonstrates that the CAZymes are biochemically interesting and further targets could be enzymes of family GH95, GH141 or S1\_16.

To dissect the full enzymatic degradation of fucoidan with over 100 candidate enzymes is a major challenge, which I will explain in the following example. The fucoidan from *C. okamurans* has an alpha  $\alpha$ 1,2-linked glucuronic acid (GlcA), which I verified to be present in the IEX-purified fucoidan from *C. okamurans* and accounts for ~15% (w/w) (Nagaoka et al., 1999). During growth of '*Lentimonas*' sp. CC4 on fucoidan from *C. okamurans*, I observed a decrease of GlcA by 50%, showing that the strain has the ability to use this sugar. By generating a batch enzyme extract, I confirmed the release of GlcA, indicating the production of a monomer by an exo-acting enzyme. In the genome of '*Lentimonas*' sp. CC4, I identified one homolog of a GH115, which are known exo-acting glucuronidases acting on xylan (Aalbers et al., 2015). This enzyme was highly expressed during growth on fucoidan from *C. okamurans*, but not on fucoidan from *F. vesiculosus*, which does not contain GlcA. This strongly indicates that the GH115 removes GlcA from fucoidan from *C. okamurans*. The enzyme was heterologously produced in soluble form, however, the release of GlcA from any of the fucoidans could not be detected with HPAEC-PAD (Mikkel Schultz-Johansen, personal communication). This stresses the difficulties of working with fucoidan-active enzymes. It was then shown, that the activity of GH115 depends on a carbohydrate esterase which removes acetate from xylan prior to cleavage by GH115 (Razeq et al., 2018). This suggests that the depolymerization of fucoidan is a complex cascade of interlocked enzymes similar to degradation of xylan and pectin (Rogowski et al., 2015; Biely et al., 2016; Labourel et al., 2016; Ndeh et al., 2017). Therefore, it is difficult to study individual fucoidan-acting enzymes without their appropriate enzymatic partner.

To circumvent this, I propose to focus on the analysis of operons that were identified in Chapter II and III, as well as on the reduction of macromolecular diversity of fucoidans to obtain simpler structures. I identified co-regulated and co-located genes organized in operons up to 15 genes, which are likely to synergistically degrade branches of fucoidan. These loci could be amplified by PCR and cloned into an expression vector to simultaneously produce multiple enzymes in *E. coli*. This library of operons can be screened for activity on various fucoidans and HPAEC-PAD. Recently, a similar metagenomic library was screened using only

## General Discussion

crude cell extracts without enzyme purification to identify novel enzymes (Rahfeld et al., 2019). Alternatively, the potential of individual enzymes can be unlocked by chemically simplifying the structure of fucoidans. For example, mild acid hydrolysis (0.01 M HCl, 6 h, 60 °C) produces smaller oligosaccharides that can serve as substrate for exo-enzymes (Queiroz et al., 2015). Another possibility is to selectively remove sulfate groups through solvolytic desulfation without changing the molecular weight (Usov et al., 1971; Torode et al., 2015).

With the identification of Verrucomicrobia as powerful fucoidan degraders, it is now possible to unlock major parts of brown algal biomass and use it as a resource. One application of '*Lentimonas*' sp. CC4 or close relatives could be for direct biorefinement of brown algal biomass into valuable fermentation products. The strain uses a bacterial microcompartment to convert ~20% of metabolized fucose into 1,2-propanediol. With an annual production of 2.6 million tons, 1,2 propanediol is a valuable chemical for the food, pharma and polymer industry (Sullivan et al., 2018). An interesting application would be to convert the increasing bloom biomass of *Sargassum fluitans* or *S. natans* into propanediol, since this biomass represents an untapped renewable resource. Compared to wood, dead macroalgal tissue is more accessible to microbial degradation, since phlorotannins, the algal pendant to lignin, are more soluble and chemically less complex (Koivikko et al., 2005; Fang Chen & Dixon, 2007). Consequently, bacteria such as *Zobellia galactanivorans* can directly digest alginate from the tissue, suggesting that extensive pre-treatment of algal biomass is unnecessary (Zhu et al., 2017). Yet, strain CC4 did not grow on the heterofucan from *Sargassum fusiforme* and likely, novel strains would be required for the hydrolysis of fucoidan from *S. fluitans* or *S. natans*. Fucoidan can be extracted from *S. fluitans* or *S. natans* and purified via IEX and used as sole carbon source for isolation of new strains.

## Complete degradation of fucoidan is community controlled

Previously, it was thought that single microbial strains can digest any complex polysaccharide. For example, *Bacteroides thetaiotaomicron* encodes 25 enzymes to digest pectin – the most complex plant polysaccharide (Ndeh et al., 2017). By contrast, '*Lentimonas*' sp. CC4 employs over 100 exo-enzymes to generally debranch various fucoidans but leaves the backbone largely untouched. '*Lentimonas*' sp. CC4 barely expressed endo-lytic GH107 enzymes and also lacked enzymes to effectively remove xylose and galactose residues from the backbone. Likely, those enzymatic functions are encoded by other particle-associated bacteria such as Bacteroidetes, Planctomycetes or Gammaproteobacteria. The debranching of fucoidan by '*Lentimonas*' sp.

CC4 potentially opens up the substrate for endo-hydrolysis by other bacteria, e.g., *Mariniflexile fucanivorans* or *Wenyngzhuangia fucanilytica*. Therefore, I suggest that ‘*Lentimonas*’ are important primary degraders that initiate the degradation cascade of fucoidan and make it accessible to other microbes for complete degradation.

The activity of ‘*Lentimonas*’ spp. and overall fucoidan turnover is potentially driven by interactions within the degrading community, specifically competition for available nitrogen and production of secondary metabolites. When growing on fucoidan, ‘*Lentimonas*’ sp. CC4 needs to invest more nitrogen to build up a threefold larger proteome compared to growth on iota-carrageenan. Therefore, the degradation of complex polysaccharides such as fucoidan has a nitrogen cost resulting in a growth disadvantage. Since nitrogen is typically limited in aquatic environments, microbes growing on simpler polysaccharides would outgrow fucoidan degraders and, consequently, fucoidan is recycled more slowly. Additionally, the production of free fucose, lactate and propanediol enable the growth of secondary consumers that lack enzymes to hydrolyse fucoidan (Datta et al., 2016; Enke et al., 2019). These secondary consumers potentially further restrict the growth of fucoidan degrading microbes. Therefore, the apparent stability of fucoidan emerges from limitations of the primary degrader within the microbial community.

### **Fucoidan forms particles in the environment**

For the first time, we show conclusively that diatoms produce fucoidans. We identified this polysaccharide in *Chaetoceros socialis*. by binding of the fucoidan specific antibody BAM1 (Torode et al., 2015). Similar to brown algal fucoidan, these molecules bind to an ion exchange column demonstrating their charge, which is likely conferred by sulfate groups. The monosaccharide composition shows high concentration of other monosaccharides, suggesting that the fucoidan from *Chaetoceros socialis* could be a heterofucan. The purification of larger amounts is ongoing for subsequent structural elucidation (Silvia-Vidal Melgossa, personal communication).

In the Helgoland time series, we observed a decrease of fucoidan in DOM and increase in POM, suggesting a coupling between both processes. In the beginning of the bloom, *Chaetoceros socialis*. secrete fucoidan in dissolved form, as well as EPS attached to their cell surface. Over the course of one month, fucoidan particles appear detached from the cell. Those particles could simply be dislodged EPS from the cell surface, however the DOM-POM dynamics suggest that dissolved fucoidan assembled over time into particles (Chin et al., 1998).

## **General Discussion**

Metagenomic and metaproteomic analysis of the bacterioplankton community showed no free-living fucoidan degrader. This explains the high abundance of fucoidan in DOM and slow aggregation into POM. Due to their stickiness fucoidan particles act as aggregation nuclei and accelerate carbon export from the surface to the deep ocean.

## **Concluding remarks**

With the insights presented in this thesis, it appears a major reason for the recalcitrance of fucoidans in the marine environment is the complex microbial machinery required to digest this complex molecule. Only few highly specialized Verrucomicrobia with a high metabolic burden can slowly hydrolyse fucoidan from the cell wall of brown algae, explaining the high stability of brown algal deposits. In microalgae, the slow bacterial turn-over of fucoidan enables a transition from dissolved fucoidan into particulate form which potentially promotes aggregation of organic matter and increases carbon export. This shows how the remarkable diversity of sulfated polysaccharides leads to a complex microbial metabolism, ultimately regulating the marine carbon cycle.

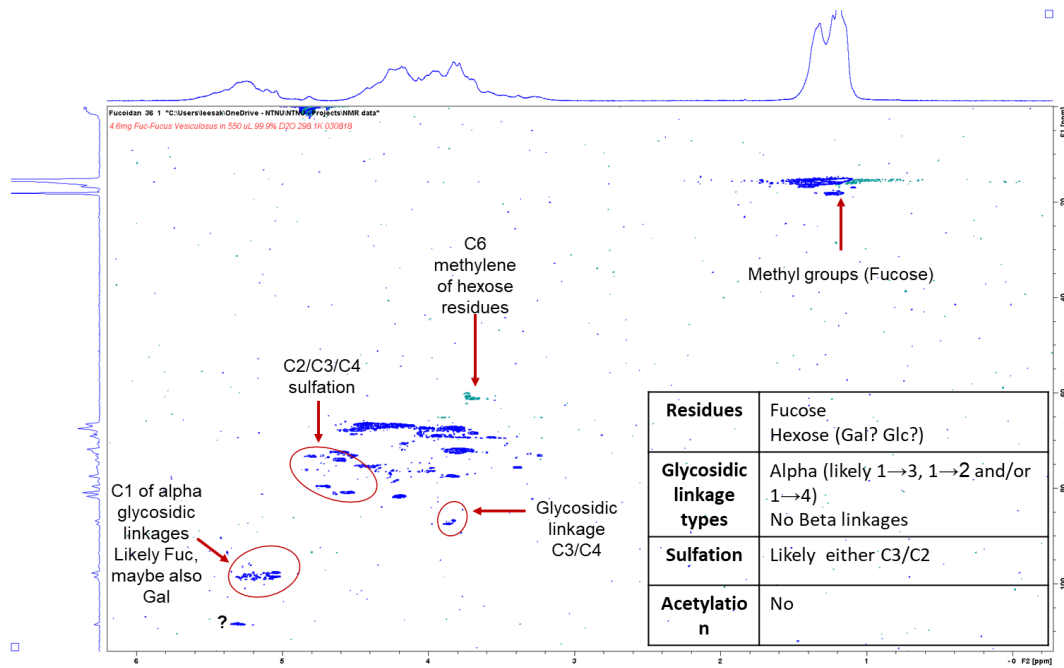
## Appendix

## Supplementary Figures and Tables for Chapter I

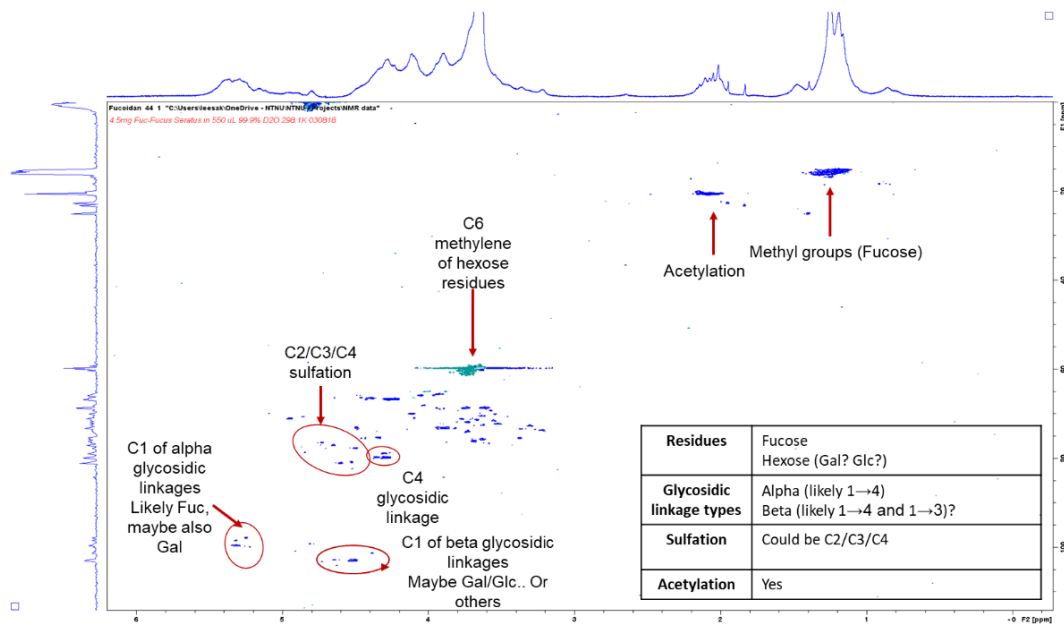


Supplement Figure 1: **A simple medium-scale setup for the purification of fucoidans.** The peristaltic pump was manually controlled to load, wash or elute fucoidans onto the column packed with ANX-FF resin. The duration of one run, including column wash was approximately 45 minutes and yielded up to 350 mg of purified fucoidans per 500 mg starting material.

# Appendix

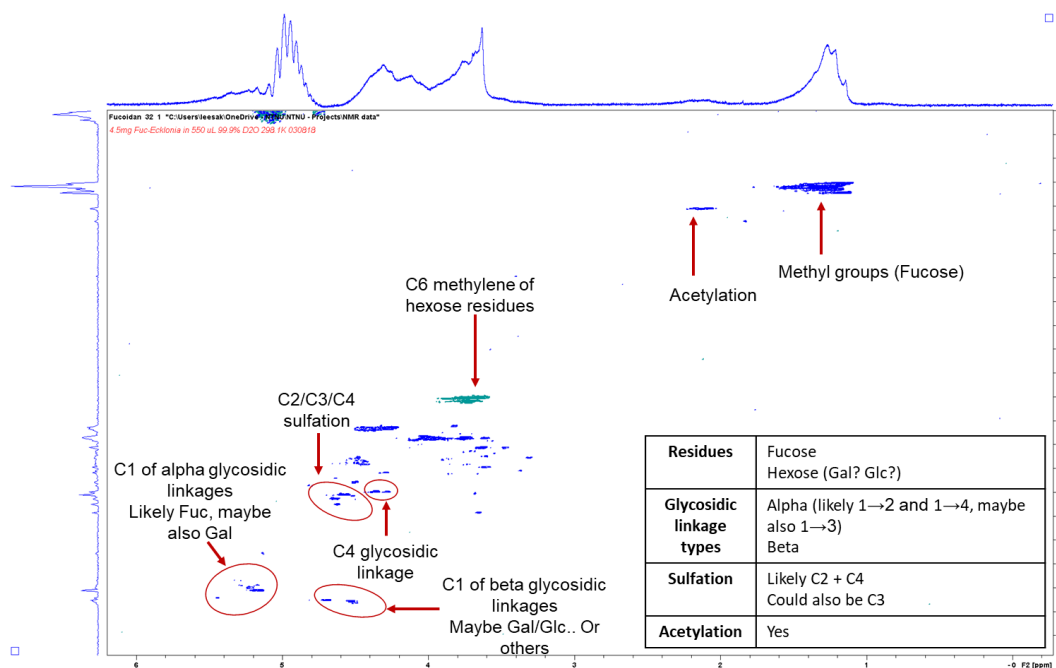


Supplement Figure 2: 2D HSQC NMR spectrum of fucoidan from *Fucus vesiculosus*.

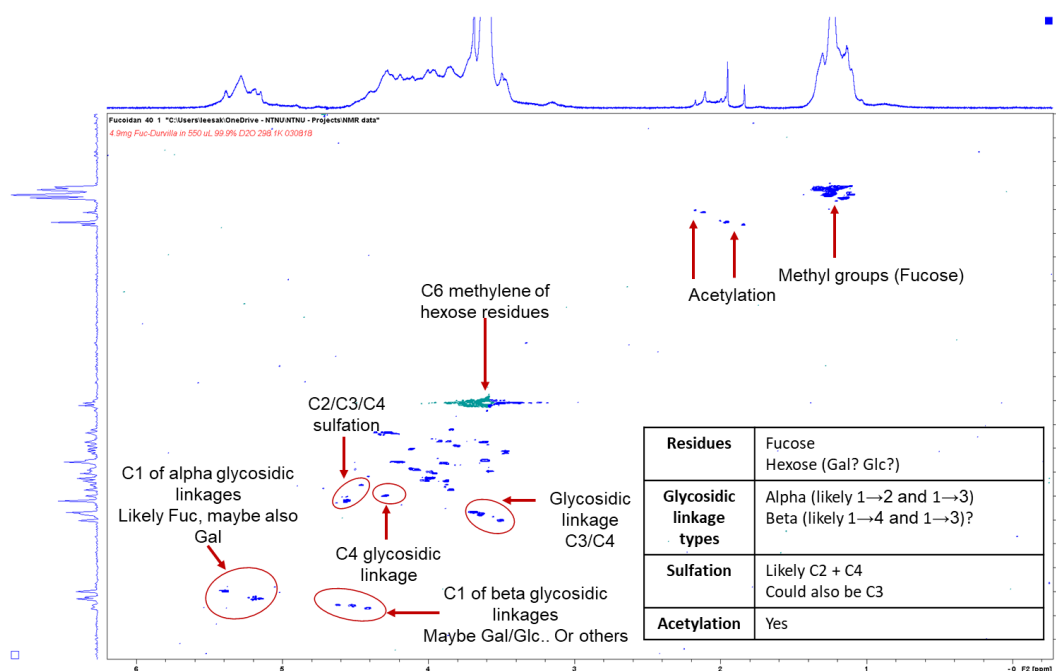


Supplement Figure 3: 2D HSQC NMR spectrum of fucoidan from *Fucus serratus*.



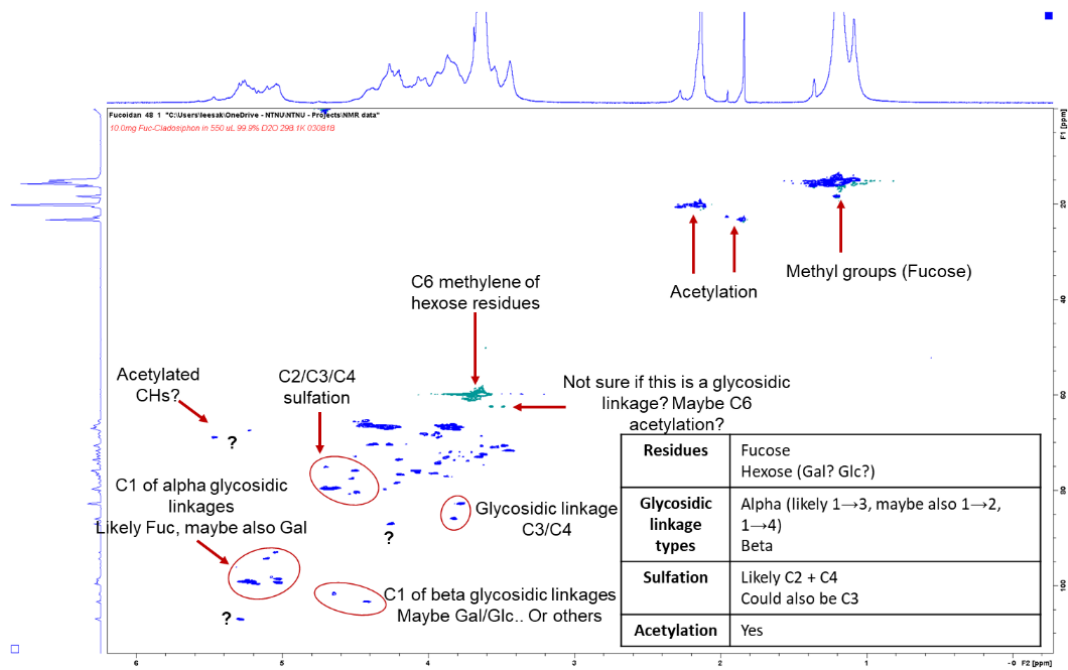


Supplement Figure 4: 2D HSQC NMR spectrum of fucoidan from *Ecklonia maxima*.



Supplement Figure 5: 2D HSQC NMR spectrum of fucoidan from *Durvillea potatorum*.

# Appendix

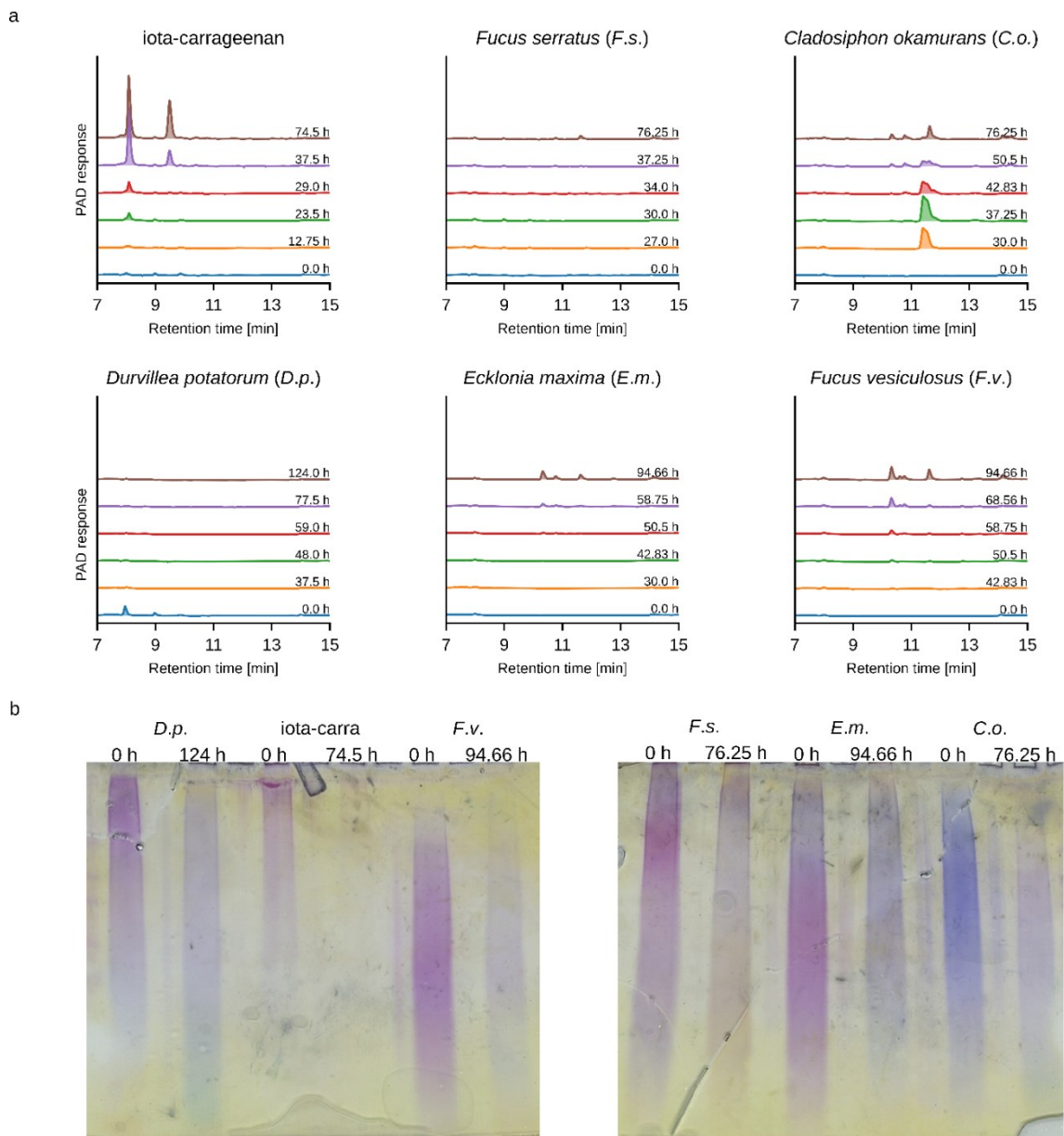


Supplement Figure 6: 2D HSQC NMR spectrum of fucoidan from *Cladosiphon okamurans*.

Supplement Table 1: Building block composition of purified fucoidans and *Fucus vesiculosus* as reference. The concentration of each building block is reported in  $\mu\text{g L}^{-1}$  as mean and standard deviation from three triplicated acid hydrolysis of 50  $\mu\text{g}$  of each polysaccharide.

	<i>Cladosiphon okamurae</i>	<i>Durvillea potatorum</i>	<i>Ecklonia maxima</i>	<i>Fucus serratus</i>	<i>Fucus vesiculosus</i>	<i>Macrocystis pyrifera</i>	<i>Undaria pinnatifida</i>
Fucose	20408 $\pm$ 44	16432 $\pm$ 1434	8799 $\pm$ 191	10501 $\pm$ 305	22649 $\pm$ 1102	12576 $\pm$ 475	11467 $\pm$ 464
Rhamnose	0 $\pm$ 0	206 $\pm$ 21	609 $\pm$ 43	258 $\pm$ 18	4 $\pm$ 8	63 $\pm$ 5	37 $\pm$ 8
Galactosamine	0 $\pm$ 0	44 $\pm$ 4	63 $\pm$ 7	10 $\pm$ 18	12 $\pm$ 22	30 $\pm$ 3	156 $\pm$ 25
Glucosamine	99 $\pm$ 4	424 $\pm$ 17	291 $\pm$ 22	305 $\pm$ 47	121 $\pm$ 10	90 $\pm$ 3	88 $\pm$ 7
Galactose	917 $\pm$ 61	5833 $\pm$ 301	7656 $\pm$ 275	3737 $\pm$ 84	1648 $\pm$ 118	1870 $\pm$ 52	12537 $\pm$ 636
Glucose	41 $\pm$ 57	458 $\pm$ 32	546 $\pm$ 22	340 $\pm$ 97	136 $\pm$ 85	153 $\pm$ 45	0 $\pm$ 0
Mannose	51 $\pm$ 9	408 $\pm$ 44	1328 $\pm$ 51	1156 $\pm$ 59	278 $\pm$ 24	166 $\pm$ 11	104 $\pm$ 5
Xylose	399 $\pm$ 10	731 $\pm$ 45	951 $\pm$ 14	876 $\pm$ 21	1224 $\pm$ 28	225 $\pm$ 31	681 $\pm$ 36
Muramic acid	266 $\pm$ 6	0 $\pm$ 0	123 $\pm$ 14	111 $\pm$ 8	0 $\pm$ 0	0 $\pm$ 0	0 $\pm$ 0
Galacturonic acid	4468 $\pm$ 290	136 $\pm$ 9	0 $\pm$ 0	143 $\pm$ 13	95 $\pm$ 10	86 $\pm$ 15	85 $\pm$ 27
Glucuronic acid	7541 $\pm$ 299	1396 $\pm$ 58	4482 $\pm$ 246	6194 $\pm$ 176	954 $\pm$ 92	802 $\pm$ 36	708 $\pm$ 34
Mannuronic acid	0 $\pm$ 0	673 $\pm$ 75	0 $\pm$ 0	0 $\pm$ 0	48 $\pm$ 29	0 $\pm$ 0	37 $\pm$ 6
Iduronic acid	191 $\pm$ 14	0 $\pm$ 0	189 $\pm$ 6	198 $\pm$ 6	0 $\pm$ 0	0 $\pm$ 0	0 $\pm$ 0
Sulfate	6480 $\pm$ 153	10351 $\pm$ 130	8850 $\pm$ 111	10651 $\pm$ 53	12120 $\pm$ 602	13247 $\pm$ 299	12403 $\pm$ 356

## Supplementary Figures and Tables for Chapter II

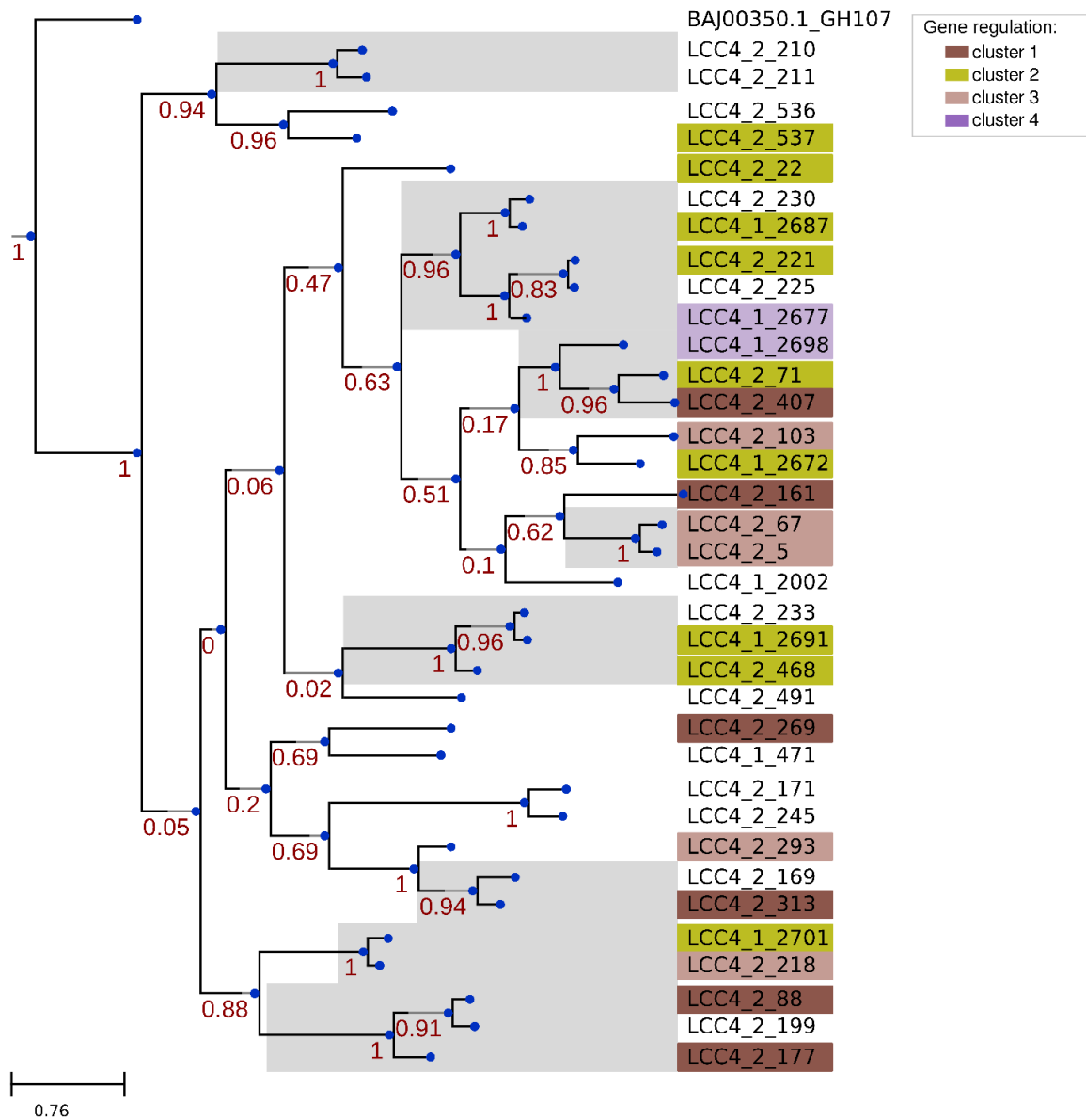


Supplement Figure 7: **Depolymerization of fucoidans and iota-carrageenan by ‘*Lentimonas*’ sp. CC4.** **a**, Profiling of oligosaccharides produced during the degradation process. **b**, C-PAGE analysis of first and last-time point shows incomplete degradation. Cultures were grown in triplicates and representative chromatograms and gel images are shown.

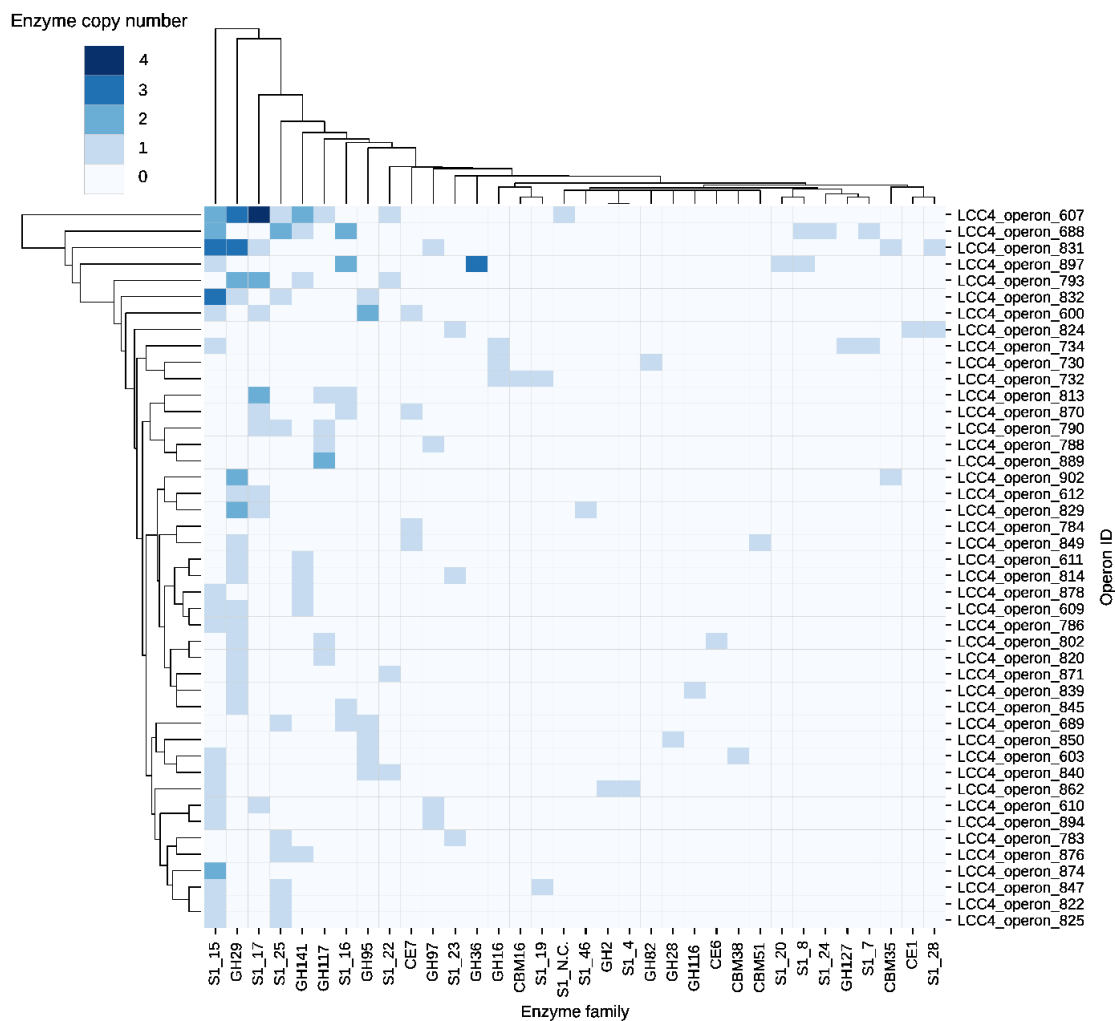
LCC4 genome	100 [100]	99 [97]	99 [97]	99 [97]	99 [97]	98 [86]	98 [86]	98 [86]	74 [2]	78 [2]	80 [2]	79 [2]	79 [2]	77 [2]	77 [2]	70 [32]
LCC151 genome	99 [98]	100 [100]	99 [98]	99 [97]	99 [98]	98 [86]	98 [87]	98 [86]	78 [2]	76 [2]	80 [2]	80 [2]	80 [2]	78 [2]	78 [2]	70 [32]
LCC6 genome	99 [98]	99 [99]	100 [100]	99 [98]	99 [98]	98 [86]	98 [87]	98 [86]	74 [2]	75 [2]	75 [2]	75 [2]	75 [2]	74 [2]	74 [2]	70 [32]
LCC21 genome	99 [97]	100 [98]	99 [97]	100 [100]	99 [97]	98 [86]	98 [86]	98 [86]	75 [2]	75 [2]	76 [2]	75 [2]	75 [2]	75 [2]	74 [2]	70 [32]
LCC8 genome	100 [97]	100 [98]	99 [97]	100 [97]	100 [100]	98 [86]	98 [86]	98 [86]	76 [2]	76 [2]	77 [2]	76 [2]	74 [2]	77 [2]	76 [2]	70 [32]
LCC10 genome	98 [87]	98 [88]	98 [87]	98 [87]	98 [87]	100 [100]	99 [98]	99 [98]	74 [2]	74 [2]	75 [2]	75 [2]	75 [2]	74 [2]	74 [2]	70 [33]
LCC11 genome	98 [87]	98 [88]	98 [87]	98 [87]	98 [87]	99 [98]	100 [100]	99 [98]	76 [2]	76 [2]	77 [2]	76 [2]	76 [2]	76 [2]	77 [2]	70 [32]
LCC19 genome	97 [83]	97 [84]	97 [83]	97 [83]	97 [83]	99 [94]	99 [94]	100 [100]	87 [5]	87 [5]	87 [5]	87 [5]	87 [5]	88 [5]	88 [5]	70 [31]
LCC4 plasmid	70 [12]	73 [13]	70 [12]	70 [12]	73 [13]	71 [12]	71 [12]	84 [26]	100 [100]	99 [93]	99 [96]	99 [94]	99 [93]	96 [84]	96 [84]	67 [2]
LCC151 plasmid	73 [14]	69 [12]	68 [12]	69 [12]	71 [13]	70 [11]	70 [11]	83 [27]	99 [96]	100 [100]	99 [98]	99 [97]	99 [97]	96 [87]	96 [87]	63 [2]
LCC6 plasmid	75 [14]	74 [13]	70 [11]	70 [12]	73 [13]	72 [12]	72 [12]	84 [26]	99 [95]	99 [95]	100 [100]	99 [95]	99 [94]	96 [84]	96 [84]	67 [3]
LCC21 plasmid	76 [15]	75 [13]	71 [11]	71 [11]	74 [13]	73 [12]	73 [12]	84 [27]	99 [94]	99 [96]	99 [97]	100 [100]	99 [96]	96 [86]	96 [86]	68 [3]
LCC8 plasmid	75 [14]	74 [13]	70 [11]	70 [11]	71 [11]	71 [12]	71 [12]	84 [28]	99 [96]	99 [97]	99 [99]	99 [98]	100 [100]	96 [87]	96 [87]	67 [2]
LCC10 plasmid	73 [14]	73 [13]	71 [12]	71 [12]	73 [13]	70 [11]	71 [11]	85 [27]	96 [80]	96 [81]	96 [82]	96 [81]	96 [80]	100 [100]	99 [98]	68 [3]
LCC11 plasmid	73 [13]	73 [13]	71 [11]	71 [12]	73 [13]	71 [11]	71 [11]	85 [27]	96 [80]	96 [81]	96 [82]	96 [81]	96 [80]	99 [98]	100 [100]	67 [3]
LCC19 plasmid	75 [13]	75 [12]	73 [10]	73 [10]	75 [12]	73 [10]	74 [10]	72 [11]	96 [77]	96 [78]	96 [79]	96 [79]	96 [78]	99 [97]	99 [97]	67 [3]
<i>Coralimargarita akajimensis</i>	70 [33]	70 [33]	70 [33]	70 [33]	70 [33]	70 [33]	70 [33]	70 [33]	70 [0]	64 [0]	70 [0]	70 [0]	70 [0]	70 [0]	70 [0]	100 [100]

Supplement Figure 8: Genome comparison of isolated ‘*Lentimonas*’ strain to closest reference genome of *Coralimargarita akajimensis* DSM 45221. Contigs of Illumina sequenced genomes (LCC4 to LCC19) were aligned to the PacBio genome of LCC4. The heatmap shows their average nucleotide identity based on Blast (ANIb). The text inside each cell denotes the identity value and the percent of aligned sequences.

## Appendix



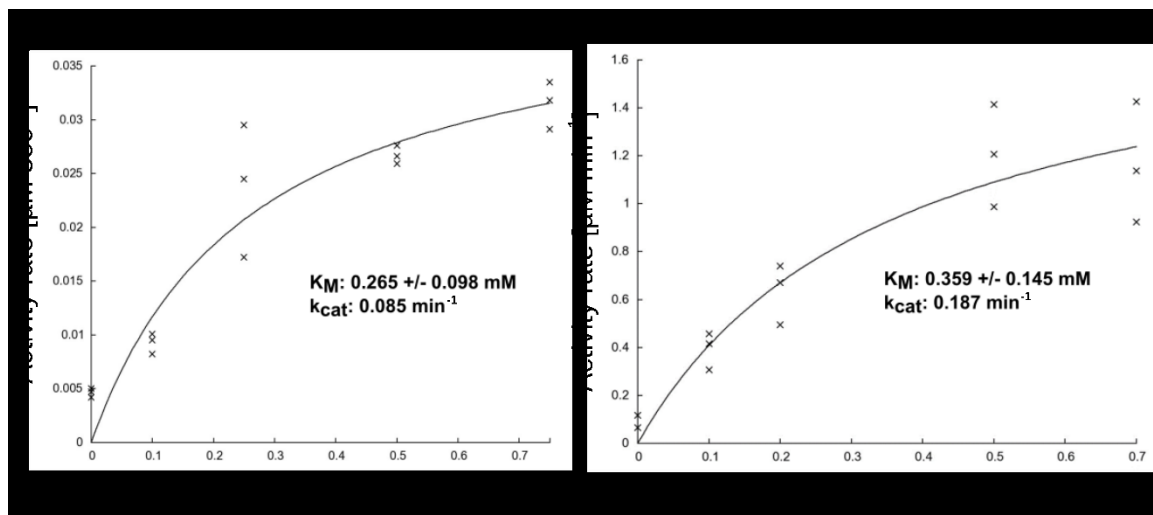
Supplement Figure 9: **Phylogenetic tree of GH29 enzymes from *'Lentimonas' sp. CC4***. Grey colored areas represent clusters of 50% identical proteins and the leaf coloring denotes the gene regulation according to the color scheme of clusters of co-expressed enzymes (Figure 12). Node labels indicate the bootstrap support value and as outgroup, we used a GH107 enzyme which display structural similarities to GH29 enzymes (Vickers et al., 2018).



Supplement Figure 10: **CAZyme and sulfatase content of operons of ‘*Lentimonas*’ sp. CC4.** The heatmap shows the copy number of each enzyme family per operon. Rows and columns are arranged according to hierarchical clustering using the ‘cityblock’ distance metric. Only operons with at least one differentially expressed enzyme are shown.

## Supplementary Figures and Tables for Chapter III

## Appendix



Supplement Figure 11: **Kinetic parameters of 22\_GH29**. Michaelis-Menten kinetics using (A) pNP- $\alpha$ -L-Fuc and (B) 4-MU- $\alpha$ -L-Fuc. Kinetic parameters were derived from three replicates and represented as mean and standard deviation.



Supplement Table 2: Overview over cloned constructs.

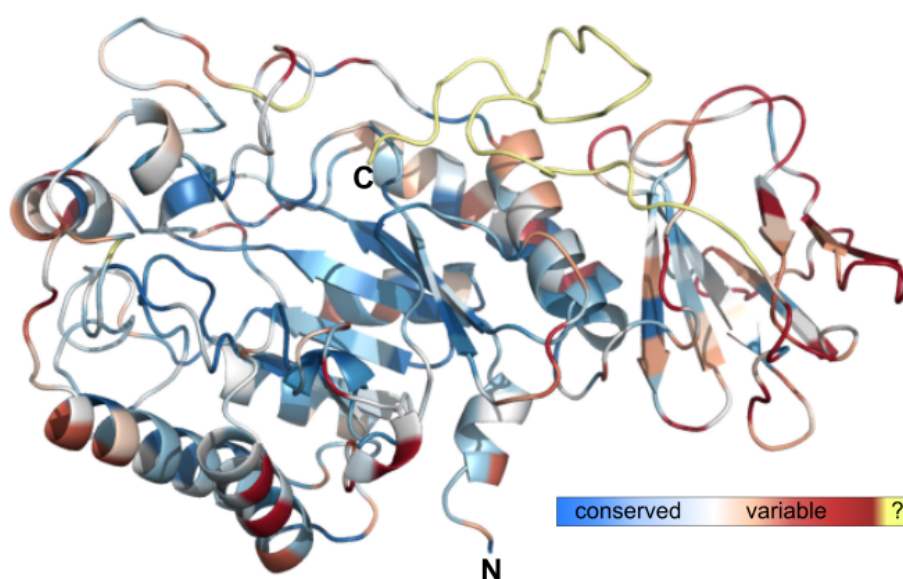
	22_GH29	21_S1_15	2701_GH29
Locus tag	LCC4_2_22	LCC4_2_21	LCC4_1_2701
Signal peptide	0-22	0-19	0-23
molar extinction coefficient	2.021	1.364	2.249
F primer (5'→'3)	CTG GTG CCG CGC GGC AGC CAT ATG GCT AGC GCC GAC CAG ACG GAC GAT	CTG GTG CCG CGC GGC AGC CAT ATG GCT AGC CCA AAT GTT ATC TAT ATC CTC GCC	CTG GTG CCG CGC GGC AGC CAT ATG GCT AGC TCT GGA ACA CCT TAT GAC GG
R primer (5'→'3)	ATC TCA GTG GTG GTG GTG GTG GTG CTC GAG CTA GTG ACG TGC GGC TTT AAC	ATC TCA GTG GTG GTG GTG GTG GTG CTC GAG CTA TTT GAA GCG TTT CTT GAA ATT TAC ATT	ATC TCA GTG GTG GTG GTG GTG GTG CTC GAG TTA ACG ATA CGG TTC GAG CGT
F primer Asp210 (5'→'3)	TGG TTC GCT GTC GGT GGT AAT AAT GTC GTC GAA GCC	-	
R primer Asp210 (5'→'3)	CGA CAG CGA ACC ACA ACA CGG CCA TAT CGC	-	
F primer Asp259 (5'→'3)	CTT CCA GCC CGC ATG CTA CCA GCG AAG CGT AT	-	
R primer Asp259 (5'→'3)	GCG GGC TGG AAG GGA GTT AAA GTC AGC ATA TTT TTG CTG	-	

## Appendix

Supplement Table 3: Data collection and refinement statistics.

Data collection	22_GH29	21_S1_15
PDB	Not submitted yet	Not submitted yet
Data set	GH29 1018	
X-ray source	PETRA III, EMBL P13	PETRA III, DESY P11
Wavelength (Å)	1.033	1.0332
Resolution range, Å	59.63-1.778	48.94 - 1.70
Space group	P212121	P212121
Unit cell (Å)	74.99 76.03 96.09 90 90 90	61.72 80.31 97.25 90.00 90.00 90.00
$R_{\text{sym}}$ (%)	0.167 (0.652)	0.072 (0.486)
Completeness (%)	98.5 (98.9)	99.4 (92.6)
Redundancy	7.2 (7.5)	12.8 (12.6)
$\langle I/\sigma(I) \rangle$	7.9 (3.3)	20.0 (4.2)
No. of Reflections	377820 (22268)	687391 (33048)
No. Unique	52571 (2959)	53780 (2627)
Mosaicity	0.44	0.16
Wilson B.-factor		20.6
Refinement		
$R_{\text{work}}/R_{\text{free}}$ (%)	0.148/0.180	
No. Of Atoms	4070	
Protein	3545	
Magnesium	1	
Water	525	
B factors		
Overall	14.32	
Protein	12.26	
Magnesium	12.88	
Water	28.17	
R.m.s. deviations		
Bond Lengths (Å)	0.021	
Bond Angles (°)	1.994	
Ramachandran Statistics (%)		
Favored	95.52	
Allowed	3.59	
Outliers	0.90	

A

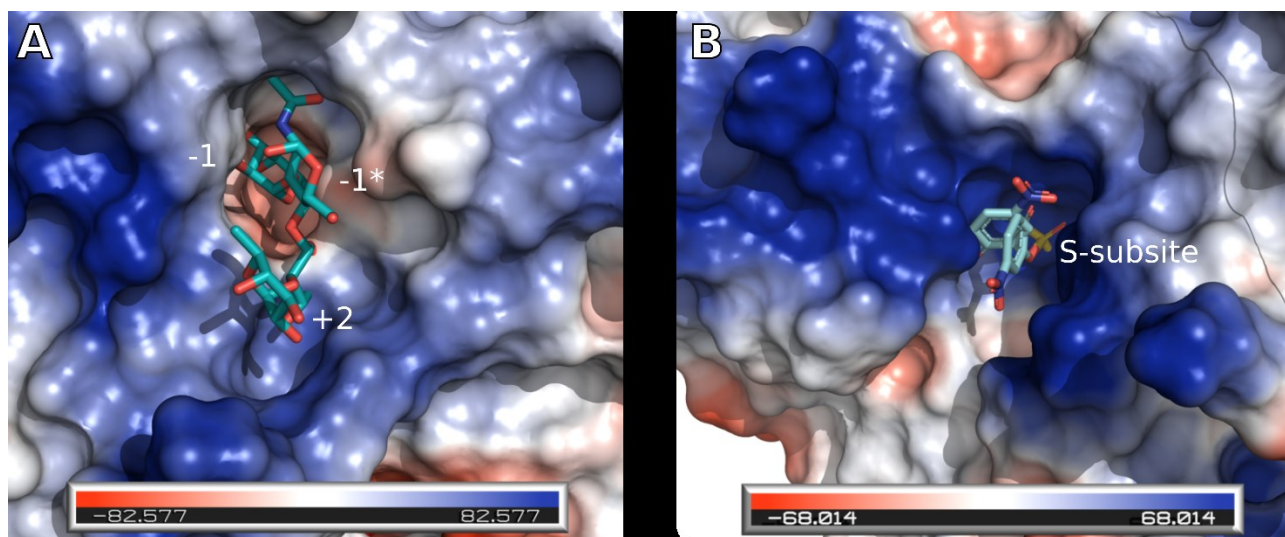


B

Organism	Conserved residues of active site												Reference
<i>Lentimonassp.</i> CC151	Phe41	His43	Glu69	Trp70	His118	His119	Tyr162	Trp208	Asp210	Arg238	Asp259	Trp281	PDB: 5 This st
Unknown rumen bacterium	Phe25	His27	Glu37	Trp38	His76	His77	Tyr122	Trp160	Asp162	Asp206	Glu220	Trp266	PDB: 5 (Summe al., 20
<i>Bacteroides</i> <i>ovatus</i> ATCC 8483	Phe66	His68	Glu78	Trp79	His117	His118	Tyr163	Trp202	Asp204	Mse236	Glu249	Trp314	PDB: 4 (unpubl
<i>Bacteroides</i> <i>thetaiotaomicron</i>	Phe47	His49	Asn60	Glu61	His99	-	Tyr145	Trp186	Asp188	Thr219	Glu234	Trp284	PDB: 3 (unpubl
<i>Bacteroides</i> <i>thetaiotaomicron</i> VPI-5482	Val42	His44	Tyr55	Gln57	His99	-	Tyr145	Trp197	Asp199	His227	Glu240	Trp300	PDB: 3 (unpubl
<i>Bifidobacterium</i>													PDB: 3

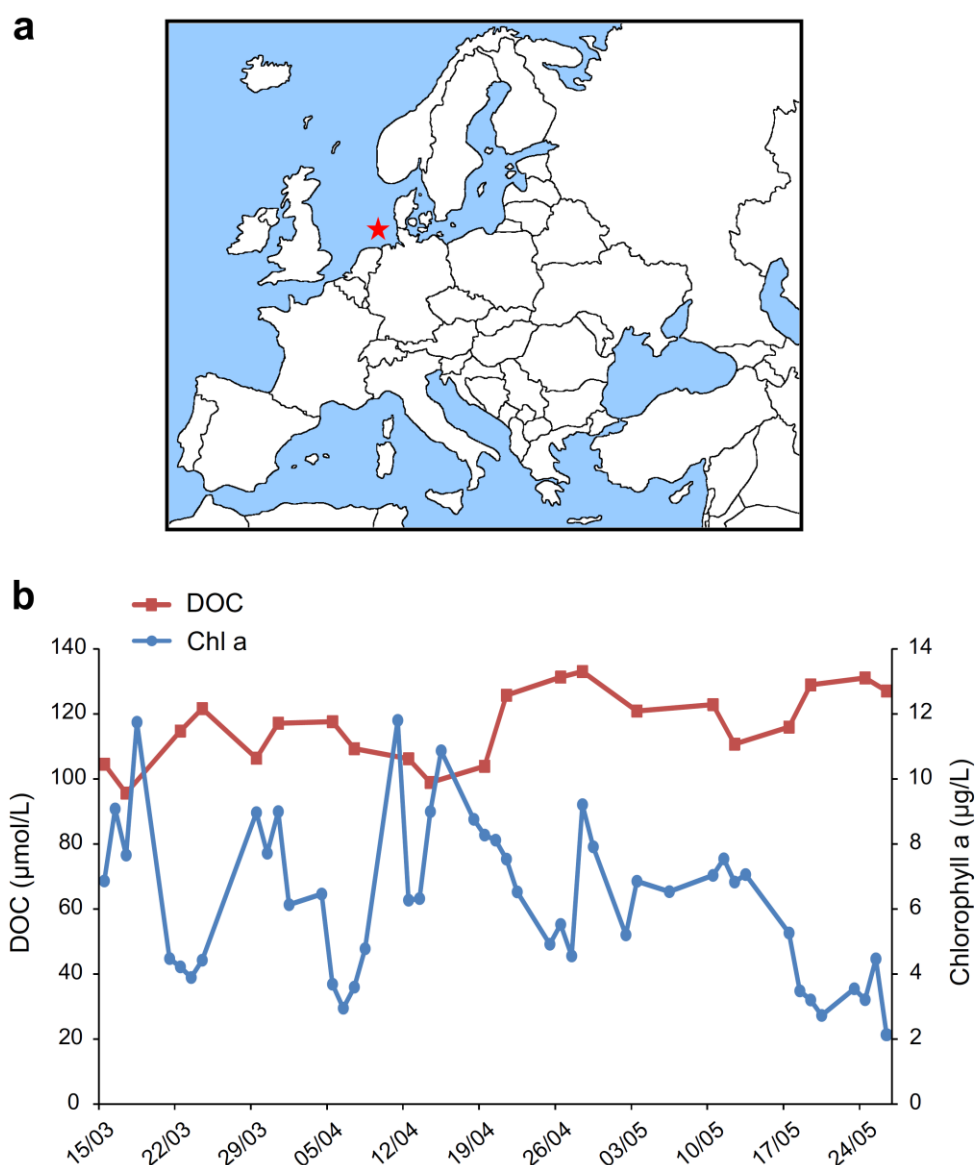
Supplement Figure 12: **Conserved residues of active site detected by structural and multiple sequence alignment.** Conservation of amino acids in 22\_GH29 and 150 homologues with a minimal sequence identity of 35 %. (B) Table modified after (Summers et al., 2016). \*: residue in active site but facing outside. – : residue not found.

## Appendix



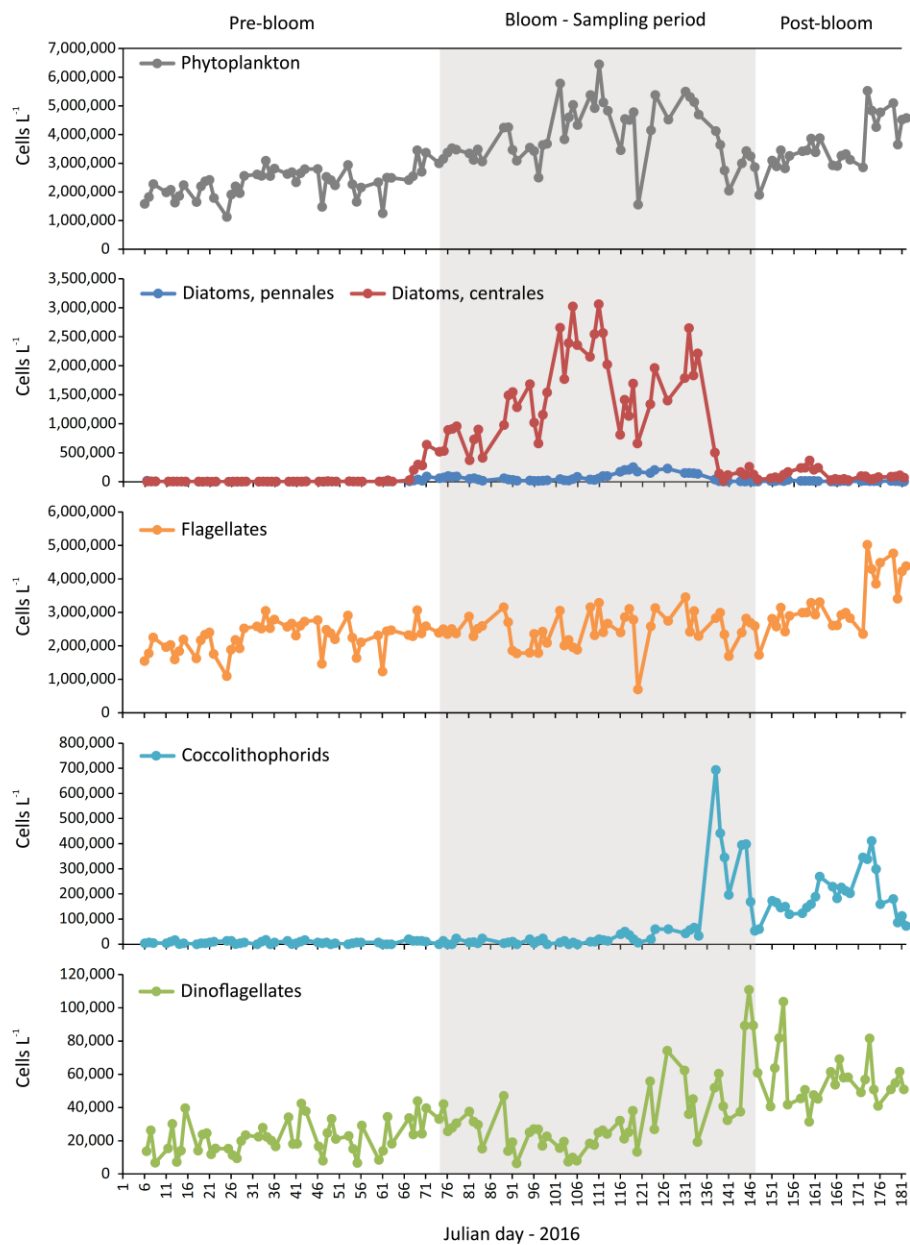
Supplement Figure 13: **Substrate binding into pocket-like active site confirms exo-activity motif.** Superimposition of (A) Lewis<sup>X</sup> antigen triose (coloured in cyan) from PDB: 6ORF (Hobbs *et al.*, 2019) into 22\_GH29 and (B) *p*-nitrophenyl sulfate (coloured in cyan and yellow) from PDB: 1E2S (Von Bülow *et al.*, 2001) into 21\_S1\_15.

## Supplementary Figures and Tables for Chapter IV

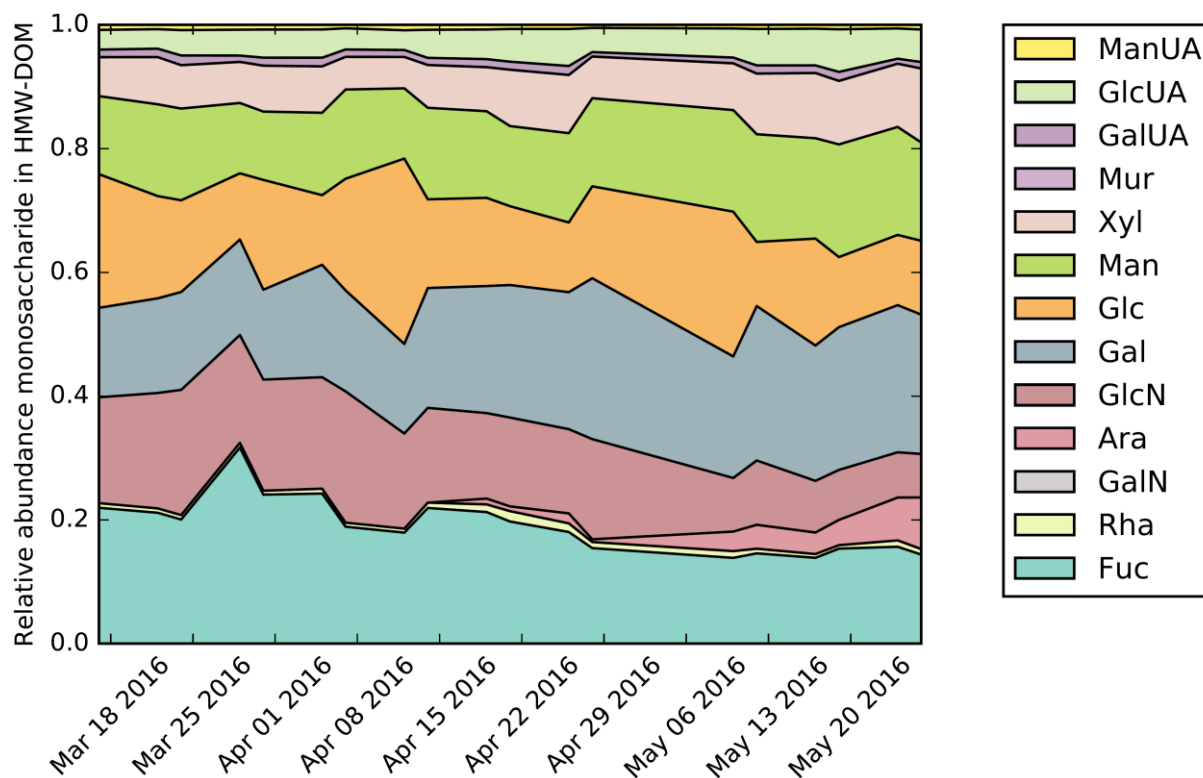


Supplement Figure 14: **Sampling site, chlorophyll a and DOC values.** **a**, Sampling site ( $54^{\circ}11.3'N$ ,  $7^{\circ}54.0'E$ ) indicated in the map with a red star. **b**, Values obtained from the analysis of dissolved organic carbon (DOC) in the DOM pool ( $< 0.2 \mu\text{m}$ ) during the spring bloom in 2016. Chlorophyll a concentrations detected from mid-March until end of May are shown as well.

## Appendix

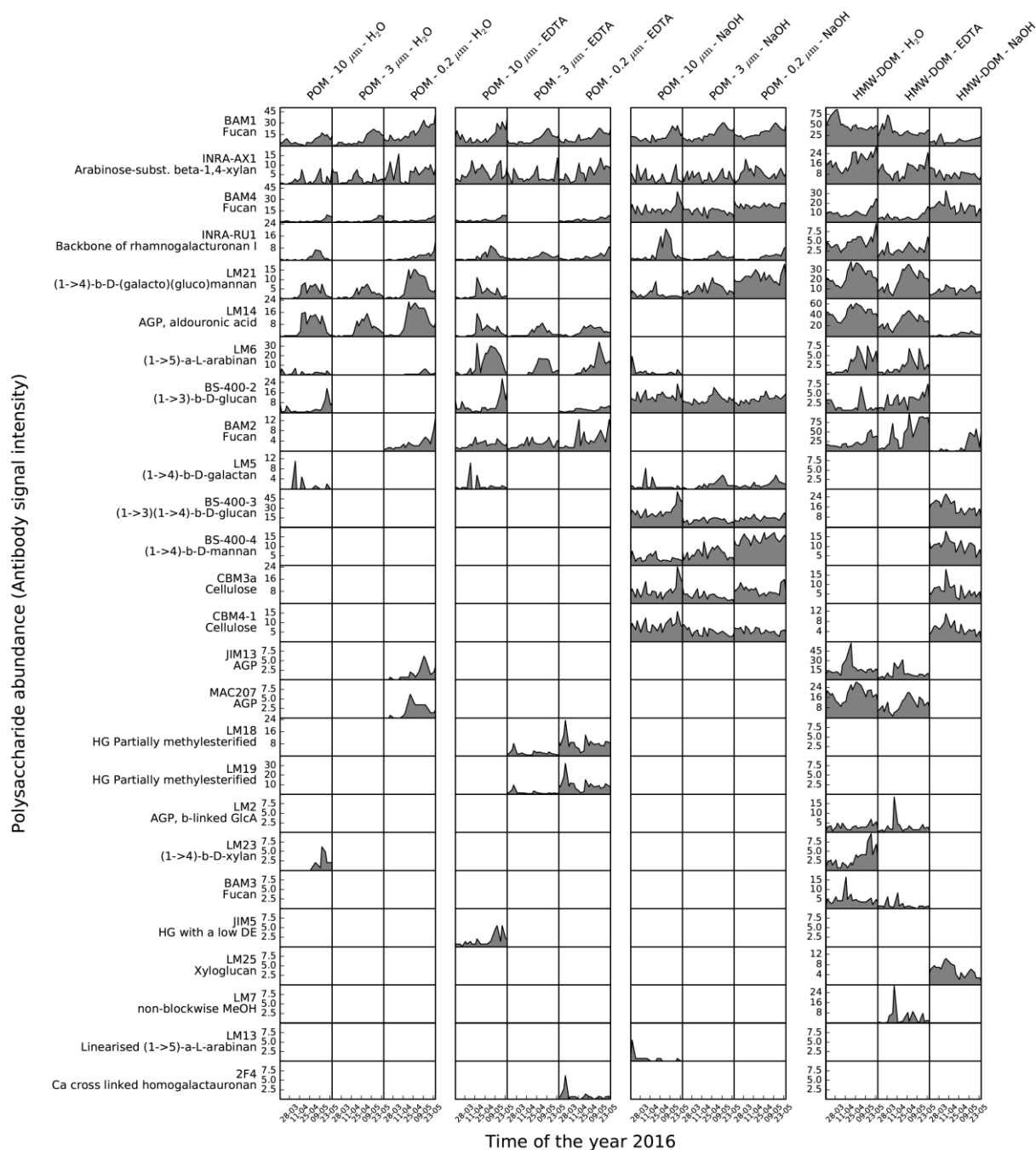


Supplement Figure 15: **The most abundant phytoplankton taxa present during the spring bloom.** Phytoplankton (on top) represents the sum of all taxa detected from beginning of January to end of June 2016. Note that the diatom bloom initiated one week before the start of the sampling period.



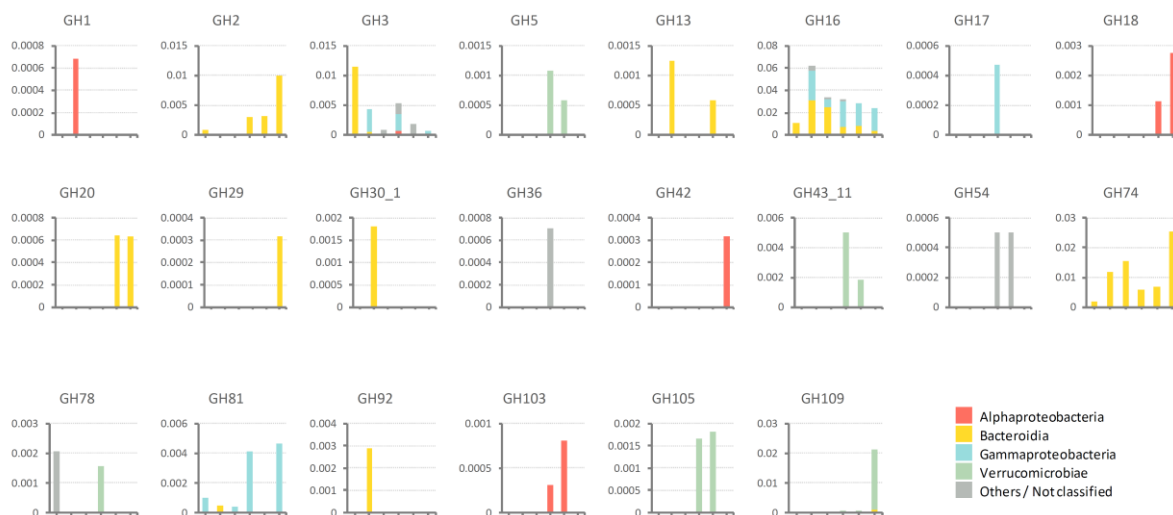
Supplement Figure 16: **Compositional monosaccharide analysis of HMWDOM.** Analysis of 19 HMWDOM samples from the bloom was performed by acid hydrolysis followed by HPAEC-PAD detection. Concentration of monosaccharides are presented as relative abundance.

## Appendix



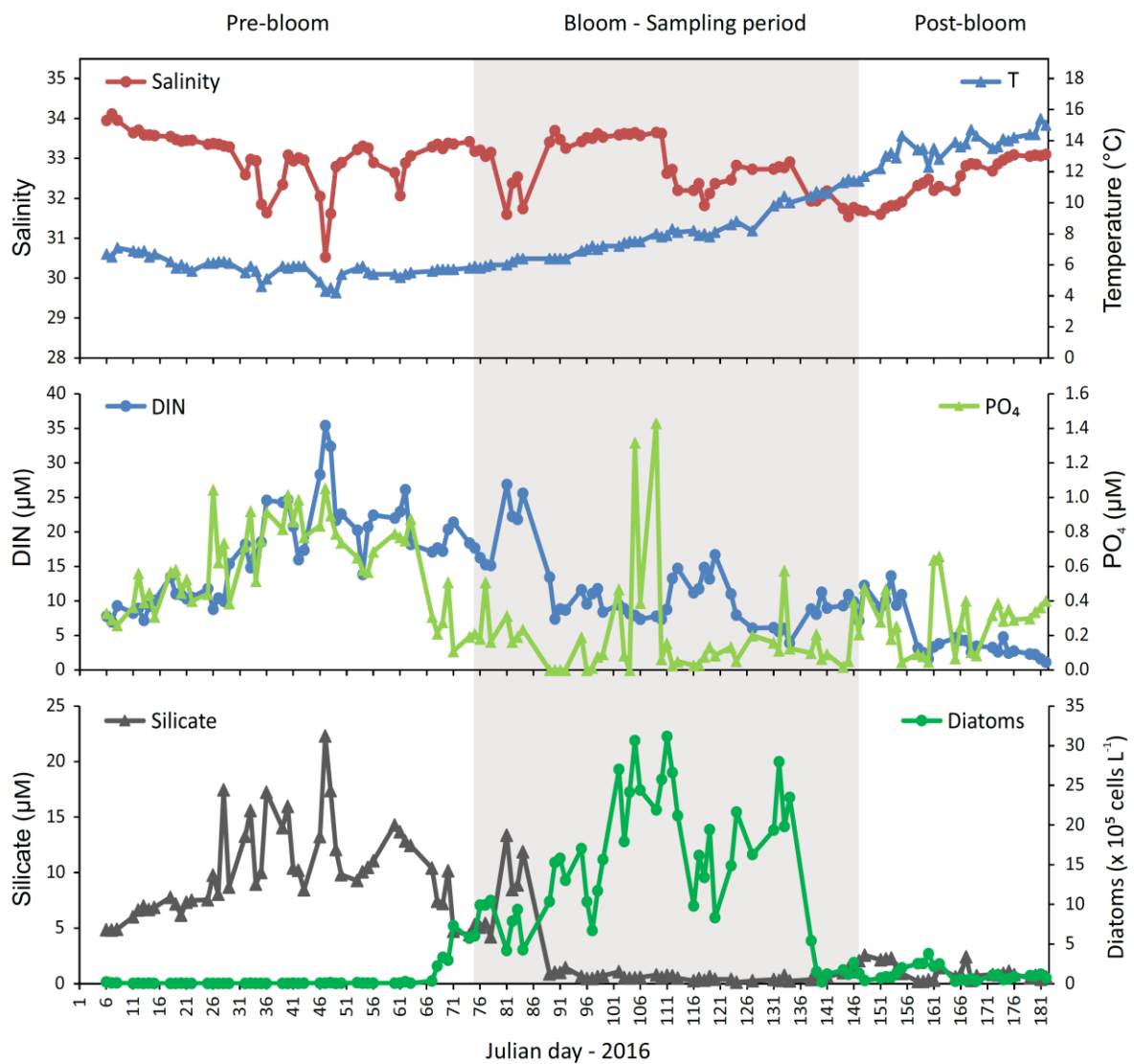
Supplement Figure 17: **Polysaccharide structural types detected in HMWDON and POM by microarray analysis.** Carbohydrate microarray data showing the relative polysaccharide abundance (y axes indicate antibody signal intensity) detected in the different extracts (specific size fraction and extraction solvent depicted at the top) throughout the spring phytoplankton bloom (x axes). Binding for a total of 27 probes specific for particular polysaccharide epitopes (listed to the left) was detected. Antibodies are arranged from most to least abundant epitope. Details of probes used are provided in EDTable1.





Supplement Figure 18: **CAZymes expression found by proteomics analysis during the phytoplankton bloom.** Proteome data were analyzed in a semiquantitative manner based on normalized spectral abundance factors (NSAF). GH: glycoside hydrolase.

## Appendix



Supplement Figure 19: **Major physicochemical parameters from beginning of January to end of June 2016.** Diatom abundance is shown together with silicate concentration to highlight the silicate decrease during the diatom bloom.

## References

- Aalbers, F., Turkenburg, J. P., Davies, G. J., Dijkhuizen, L., & Lammerts Van Bueren, A. (2015). Structural and Functional Characterization of a Novel Family GH115 4-O-Methyl- $\alpha$ -Glucuronidase with Specificity for Decorated Arabinogalactans. *Journal of Molecular Biology*, 427(24), 3935–3946. <https://doi.org/10.1016/j.jmb.2015.07.006>
- Adams, P. D., Afonine, P. V., Bunkóczi, G., Chen, V. B., Davis, I. W., Echols, N., ... Zwart, P. H. (2010). PHENIX : a comprehensive Python-based system for macromolecular structure solution. *Acta Crystallographica Section D Biological Crystallography*, 66(2), 213–221. <https://doi.org/10.1107/S0907444909052925>
- Ale, M. T., Mikkelsen, J. D., & Meyer, A. S. (2011). Important Determinants for Fucoidan Bioactivity: A Critical Review of Structure-Function Relations and Extraction Methods for Fucose-Containing Sulfated Polysaccharides from Brown Seaweeds. *Marine Drugs*, 9(12), 2106–2130. <https://doi.org/10.3390/md9102106>
- Allredge, A. L., & Gotschalk, C. C. (1989). Direct observations of the mass flocculation of diatom blooms: characteristics, settling velocities and formation of diatom aggregates. *Deep Sea Research Part A, Oceanographic Research Papers*, 36(2), 159–171. [https://doi.org/10.1016/0198-0149\(89\)90131-3](https://doi.org/10.1016/0198-0149(89)90131-3)
- Aluwihare, L., & Repeta, D. (1999). A comparison of the chemical characteristics of oceanic DOM and extracellular DOM produced by marine algae. *Marine Ecology Progress Series*, 186, 105–117. <https://doi.org/10.3354/meps186105>
- Aluwihare, L. I., Repeta, D. J., & Chen, R. F. (1997). A major biopolymeric component to dissolved organic carbon in surface sea water. *Nature*, Vol. 387, pp. 166–169. <https://doi.org/10.1038/387166a0>
- Amicucci, M. J., Galermo, A. G., Guerrero, A., Treves, G., Nandita, E., Kailemia, M. J., ... Lebrilla, C. B. (2019). Strategy for Structural Elucidation of Polysaccharides: Elucidation of a Maize Mucilage that Harbors Diazotrophic Bacteria [Research-article]. *Analytical Chemistry*, 91, 7254–7265. <https://doi.org/10.1021/acs.analchem.9b00789>
- Aranda-Martinez, A., Lenfant, N., Escudero, N., Zavala-Gonzalez, E. A., Henrissat, B., & Lopez-Llorca, L. V. (2016). CAZyme content of pochonia chlamydosporia reflects that chitin and chitosan modification are involved in nematode parasitism. *Environmental Microbiology*, 18(11), 4200–4215. <https://doi.org/10.1111/1462-2920.13544>
- Arnosti, C., Durkin, S., & Jeffrey, W. H. (2005). Patterns of extracellular enzyme activities

## References

- among pelagic marine microbial communities: Implications for cycling of dissolved organic carbon. *Aquatic Microbial Ecology*, 38(2), 135–145.  
<https://doi.org/10.3354/ame038135>
- Arnosti, Carol. (2011). Microbial extracellular enzymes and the marine carbon cycle. *Annual Review of Marine Science*, 3, 401–425. <https://doi.org/10.1146/annurev-marine-120709-142731>
- Arnosti, C., Steen, A. D., Ziervogel, K., Ghobrial, S., & Jeffrey, W. H. (2011). Latitudinal Gradients in Degradation of Marine Dissolved Organic Carbon. *PLoS ONE*, 6(12), e28900. <https://doi.org/10.1371/journal.pone.0028900>
- Axen, S. D., Erbilgin, O., & Kerfeld, C. A. (2014). A Taxonomy of Bacterial Microcompartment Loci Constructed by a Novel Scoring Method. *PLoS Computational Biology*, 10(10). <https://doi.org/10.1371/journal.pcbi.1003898>
- Azam, F., Fenchel, T., Field, J., Gray, J., Meyer-Reil, L., & Thingstad, F. (1983). The Ecological Role of Water-Column Microbes in the Sea. *Marine Ecology Progress Series*, 10, 257–263. <https://doi.org/10.3354/meps010257>
- Bachmann, J., Heimbach, T., Hassenrück, C., Kopprio, G. A., Iversen, M. H., Grossart, H. P., & Gärdes, A. (2018). Environmental Drivers of Free-Living vs. Particle-Attached Bacterial Community Composition in the Mauritania Upwelling System. *Frontiers in Microbiology*, 9(November), 1–13. <https://doi.org/10.3389/fmicb.2018.02836>
- Baldocchi, D. D., Vogel, C. A., & Hall, B. (1997). Seasonal variation of carbon dioxide exchange rates above and below a boreal jack pine forest. *Agricultural and Forest Meteorology*, 83(1–2), 147–170. [https://doi.org/10.1016/S0168-1923\(96\)02335-0](https://doi.org/10.1016/S0168-1923(96)02335-0)
- Baldomà, L., & Aguilar, J. (1988). Metabolism of L-fucose and L-rhamnose in *Escherichia coli*: aerobic-anaerobic regulation of L-lactaldehyde dissimilation. *Journal of Bacteriology*, 170(1), 416–421.
- Barbeyron, T., Brillet-Guéguen, L., Carré, W., Carrière, C., Caron, C., Czjzek, M., ... Michel, G. (2016). Matching the Diversity of Sulfated Biomolecules: Creation of a Classification Database for Sulfatases Reflecting Their Substrate Specificity. *PLOS ONE*, 11(10), e0164846. <https://doi.org/10.1371/journal.pone.0164846>
- Barbeyron, T., L'Haridon, S., Michel, G., & Czjzek, M. (2008). Mariniflexile fucanivorans sp. nov., a marine member of the Flavobacteriaceae that degrades sulphated fucans from brown algae. *International Journal Of Systematic And Evolutionary Microbiology*, 58(9), 2107–2113. <https://doi.org/10.1099/ijs.0.65674-0>
- Barbeyron, T., Thomas, F., Barbe, V., Teeling, H., Schenowitz, C., Dossat, C., ... Michel, G.

- (2016). Habitat and taxon as driving forces of carbohydrate catabolism in marine heterotrophic bacteria: example of the model algae-associated bacterium *Zobellia galactanivorans* Dsij<sup>T</sup>. *Environmental Microbiology*, 00(12), 4610–4627.  
<https://doi.org/10.1111/1462-2920.13584>
- Basan, M., Hui, S., Okano, H., Zhang, Z., Shen, Y., Williamson, J. R., & Hwa, T. (2015). Overflow metabolism in *Escherichia coli* results from efficient proteome allocation. *Nature*, 528(7580), 99–104. <https://doi.org/10.1038/nature15765>
- Battye, T. G. G., Kontogiannis, L., Johnson, O., Powell, H. R., & Leslie, A. G. W. (2011). iMOSFLM: A new graphical interface for diffraction-image processing with MOSFLM. *Acta Crystallographica Section D: Biological Crystallography*, 67(4), 271–281.  
<https://doi.org/10.1107/S0907444910048675>
- Becker, S., Scheffel, A., Polz, M. F., & Hehemann, J.-H. (2017). Accurate Quantification of Laminarin in Marine Organic Matter with Enzymes from Marine Microbes. *Applied and Environmental Microbiology*, 83(9). <https://doi.org/10.1128/AEM.03389-16>
- Berman, H. M., Westbrook, J., Feng, Z., Gilliland, G., Bhat, T. N., Weissig, H., ... Bourne, P. E. (2000). The Protein Data Bank. *Nucleic Acids Research*, 28(1), 235–242.  
<https://doi.org/10.1093/nar/28.1.235>
- Berteau, O., Bielicki, J., Kilonda, A., Machy, D., Anson, D. S., & Kenne, L. (2004).  $\alpha$ -L-Fucosidases: Exoglycosidases with unusual transglycosylation properties. *Biochemistry*, 43(24), 7881–7891. <https://doi.org/10.1021/bi036066z>
- Berteau, O., McCort, I., Goasdoué, N., Tissot, B., & Daniel, R. (2002). Characterization of a new alpha-L-fucosidase isolated from the marine mollusk *Pecten maximus* that catalyzes the hydrolysis of alpha-L-fucose from algal fucoidan (*Ascophyllum nodosum*). *Glycobiology*, 12(4), 273–282. <https://doi.org/10.1093/glycob/12.4.273>
- Biely, P., Singh, S., & Puchart, V. (2016). Towards enzymatic breakdown of complex plant xylan structures: State of the art. *Biotechnology Advances*, 34(7), 1260–1274.  
<https://doi.org/10.1016/j.biotechadv.2016.09.001>
- Bilan, M. I., Grachev, A. a., Shashkov, A. S., Kelly, M., Sanderson, C. J., Nifantiev, N. E., & Usov, A. I. (2010). Further studies on the composition and structure of a fucoidan preparation from the brown alga *Saccharina latissima*. *Carbohydrate Research*, 345(14), 2038–2047. <https://doi.org/10.1016/j.carres.2010.07.009>
- Bilan, M. I., Grachev, A. A., Shashkov, A. S., Nifantiev, N. E., & Usov, A. I. (2006). Structure of a fucoidan from the brown seaweed *Fucus serratus* L. *Carbohydrate Research*, 341(2), 238–245. <https://doi.org/10.1016/j.carres.2005.11.009>

## References

- Bilan, M. I., Grachev, A. A., Shashkov, A. S., Thuy, T. T. T., Thanh Van, T. T., Ly, B. M., ... Usov, A. I. (2013). Preliminary investigation of a highly sulfated galactofucan fraction isolated from the brown alga *Sargassum polycystum*. *Carbohydrate Research*, 377, 48–57. <https://doi.org/10.1016/j.carres.2013.05.016>
- Bilan, M. I., Grachev, A. A., Ustuzhanina, N. E., Shashkov, A. S., Nifantiev, N. E., & Usov, A. I. (2004). A highly regular fraction of a fucoidan from the brown seaweed *Fucus distichus* L. *Carbohydrate Research*, 339(3), 511–517. <https://doi.org/10.1016/j.carres.2003.10.028>
- Bilan, M. I., Shashkov, A. S., & Usov, A. I. (2014). Structure of a sulfated xylofucan from the brown alga *Punctaria plantaginea*. *Carbohydrate Research*, 393, 1–8. <https://doi.org/10.1016/j.carres.2014.04.022>
- Bilan, M. I., Ustyuzhanina, N. E., Shashkov, A. S., Thanh, T. T. T., Bui, M. L., Tran, T. T. Van, ... Usov, A. I. (2017). Sulfated polysaccharides of the Vietnamese brown alga *Sargassum aquifolium* (Fucales, Sargassaceae). *Carbohydrate Research*, 449, 23–31. <https://doi.org/10.1016/j.carres.2017.06.016>
- Bo, T. H., Dysvik, B., & Jonassen, I. (2004). LSImpute: accurate estimation of missing values in microarray data with least squares methods. *Nucleic Acids Research*, 32(3), 34e – 34. <https://doi.org/10.1093/nar/gnh026>
- Boedeker, C., Schüler, M., Reintjes, G., Jeske, O., van Teeseling, M. C. F., Jogler, M., ... Jogler, C. (2017). Determining the bacterial cell biology of Planctomycetes. *Nature Communications*, 8, 14853. <https://doi.org/10.1038/ncomms14853>
- Böhm, M., Bohne-Lang, A., Frank, M., Loss, A., Rojas-Macias, M. A., & Lütteke, T. (2019). Glycosciences.DB: an annotated data collection linking glycomics and proteomics data (2018 update). *Nucleic Acids Research*, 47(D1), D1195–D1201. <https://doi.org/10.1093/nar/gky994>
- Boyd, P. W., Claustre, H., Levy, M., Siegel, D. A., & Weber, T. (2019). Multi-faceted particle pumps drive carbon sequestration in the ocean. *Nature*, 568(7752), 327–335. <https://doi.org/10.1038/s41586-019-1098-2>
- Buchan, A., LeCleir, G. R., Gulvik, C. a, & González, J. M. (2014). Master recyclers: features and functions of bacteria associated with phytoplankton blooms. *Nat Rev Microbiol*, 12(August), 686–698. <https://doi.org/10.1038/nrmicro3326>
- Buchfink, B., Xie, C., & Huson, D. H. (2014). Fast and sensitive protein alignment using DIAMOND. *Nature Methods*, 12(1), 59–60. <https://doi.org/10.1038/nmeth.3176>
- Buffetto, F., Cornuault, V., Rydahl, M. G., Ropartz, D., Alvarado, C., Echasserieau, V., ...

- Guillon, F. (2015). The Deconstruction of Pectic Rhamnogalacturonan I Unmasks the Occurrence of a Novel Arabinogalactan Oligosaccharide Epitope. *Plant and Cell Physiology*, 56(September), pcv128. <https://doi.org/10.1093/pcp/pcv128>
- Burkhardt, A., Pakendorf, T., Reime, B., Meyer, J., Fischer, P., Stübe, N., ... Meents, A. (2016). Status of the crystallography beamlines at PETRA III. *European Physical Journal Plus*, 131(3), 0–8. <https://doi.org/10.1140/epjp/i2016-16056-0>
- Cardman, Z., Arnosti, C., Durbin, A., Ziervogel, K., Cox, C., Steen, a. D., & Teske, A. (2014). Verrucomicrobia are candidates for polysaccharide-degrading bacterioplankton in an Arctic fjord of Svalbard. *Applied and Environmental Microbiology*, 80(12), 3749–3756. <https://doi.org/10.1128/AEM.00899-14>
- Cartmell, A., Muñoz-Muñoz, J., Briggs, J. A., Ndeh, D. A., Lowe, E. C., Baslé, A., ... Gilbert, H. J. (2018). A surface endogalactanase in *Bacteroides thetaiotaomicron* confers keystone status for arabinogalactan degradation. *Nature Microbiology*, 3(11), 1314–1326. <https://doi.org/10.1038/s41564-018-0258-8>
- Chai, C. L. L., Loughlin, W. A., & Lowe, G. (1992). The stereochemical course of sulphuryl transfer catalysed by arylsulphatase II from *Aspergillus oryzae*. *Biochemical Journal*, 287(3), 805–812. <https://doi.org/10.1042/bj2870805>
- Chen, F., Chang, Y., Dong, S., & Xue, C. (2016). *Wenyingshuangia fucanilytica* sp. nov., a sulfated fucan utilizing bacterium isolated from shallow coastal seawater. *International Journal of Systematic and Evolutionary, In press*, 3270–3275. <https://doi.org/10.1099/ijsem.0.001184>
- Chen, F., & Dixon, R. A. (2007). Lignin modification improves fermentable sugar yields for biofuel production. *Nature Biotechnology*, 25(7), 759–761. <https://doi.org/10.1038/nbt1316>
- Chen, J., Robb, C. S., Unfried, F., Kappelmann, L., Markert, S., Song, T., ... Teeling, H. (2018). Alpha- and beta-mannan utilization by marine Bacteroidetes. *Environmental Microbiology*, 20(11), 4127–4140. <https://doi.org/10.1111/1462-2920.14414>
- Chevolot, L., Mulloy, B., Ratiskol, J., Foucault, A., & Collic-Jouault, S. (2001). A disaccharide repeat unit is the major structure in fucoidans from two species of brown algae. *Carbohydrate Research*, 330(4), 529–535. [https://doi.org/10.1016/S0008-6215\(00\)00314-1](https://doi.org/10.1016/S0008-6215(00)00314-1)
- Chin, W. C., Orellana, M. V., & Verdugo, P. (1998). Spontaneous assembly of marine dissolved organic matter into polymer gels. *Nature*, 391(6667), 568–572. <https://doi.org/10.1038/35345>

## References

- Choo, Y. J., Lee, K., Song, J., & Cho, J. C. (2007). *Puniceicoccus vermicola* gen. nov., sp. nov., a novel marine bacterium, and description of *Puniceicoccaceae* fam. nov., *Puniceicoccales* ord. nov., *Opitutaceae* fam. nov., *Opitutaes* ord. nov. and *Opitutae* classis nov. in the phylum “Verrucomicrobia.” *International Journal of Systematic and Evolutionary Microbiology*, 57(3), 532–537. <https://doi.org/10.1099/ijms.0.64616-0>
- Chung, I. K., Oak, J. H., Lee, J. A., Shin, J. A., Kim, J. G., & Park, K. (2013). Installing kelp forests/seaweed beds for mitigation and adaptation against global warming: Korean Project Overview. *ICES Journal of Marine Science*, 70(5), 1038–1044. <https://doi.org/10.1093/icesjms/fss206>
- Cianci, M., Bourenkov, G., Pompidor, G., Karpics, I., Kallio, J., Bento, I., ... Schneider, T. R. (2017). P13, the EMBL macromolecular crystallography beamline at the low-emittance PETRA III ring for high- and low-energy phasing with variable beam focusing. *Journal of Synchrotron Radiation*, 24(1), 323–332. <https://doi.org/10.1107/S1600577516016465>
- Clément, M.-J., Tissot, B., Chevolut, L., Adjadj, E., Du, Y., Curmi, P. A., & Daniel, R. (2010). NMR characterization and molecular modeling of fucoidan showing the importance of oligosaccharide branching in its anticomplementary activity. *Glycobiology*, 20(7), 883–894. <https://doi.org/10.1093/glycob/cwq046>
- Cobucci-Ponzano, B., Trincone, A., Giordano, A., Rossi, M., & Moracci, M. (2003). Identification of an archaeal  $\alpha$ -L-fucosidase encoded by an interrupted gene: Production of a functional enzyme by mutations mimicking programmed -1 frameshifting. *Journal of Biological Chemistry*, 278(17), 14622–14631. <https://doi.org/10.1074/jbc.M211834200>
- Cole, J., Findlay, S., & Pace, M. (1988). Bacterial production in fresh and saltwater ecosystems: a cross-system overview. *Marine Ecology Progress Series*, 43, 1–10. <https://doi.org/10.3354/meps043001>
- Colin, S., Deniaud, E., Jam, M., Descamps, V., Chevolut, Y., Kervarec, N., ... Kloareg, B. (2006). Cloning and biochemical characterization of the fucanase FcnA: definition of a novel glycoside hydrolase family specific for sulfated fucans. *Glycobiology*, 16(11), 1021–1032. <https://doi.org/10.1093/glycob/cwl029>
- Cong, Q., Chen, H., Liao, W., Xiao, F., Wang, P., Qin, Y., ... Ding, K. (2016). Structural characterization and effect on anti-angiogenic activity of a fucoidan from *Sargassum fusiforme*. *Carbohydrate Polymers*, 136, 899–907. <https://doi.org/10.1016/j.carbpol.2015.09.087>



- Corfield, A. P. (2015). Mucins: A biologically relevant glycan barrier in mucosal protection. *Biochimica et Biophysica Acta (BBA) - General Subjects*, 1850(1), 236–252. <https://doi.org/10.1016/j.bbagen.2014.05.003>
- Cornuault, V., Manfield, I. W., Ralet, M.-C., & Knox, J. P. (2014). Epitope detection chromatography: a method to dissect the structural heterogeneity and inter-connections of plant cell-wall matrix glycans. *The Plant Journal*, 78(4), 715–722. <https://doi.org/10.1111/tpj.12504>
- Corzett, C. H., Elsherbini, J., Chien, D. M., Hehemann, J.-H., Henschel, A., Preheim, S. P., ... Polz, M. F. (2018). Evolution of a Vegetarian *Vibrio*: Metabolic Specialization of *Vibrio breoganii* to Macroalgal Substrates. *Journal of Bacteriology*, 200(15). <https://doi.org/10.1128/JB.00020-18>
- Darling, A. C. E. (2004). Mauve: Multiple Alignment of Conserved Genomic Sequence With Rearrangements. *Genome Research*, 14(7), 1394–1403. <https://doi.org/10.1101/gr.2289704>
- Datta, M. S., Sliwerska, E., Gore, J., Polz, M., & Cordero, O. X. (2016). Microbial interactions lead to rapid micro-scale successions on model marine particles. *Nature Communications*, 7(May), 11965. <https://doi.org/10.1038/ncomms11965>
- Davies, G., & Henrissat, B. (1995). Structures and mechanisms of glycosyl hydrolases. *Structure*, 3(9), 853–859. [https://doi.org/10.1016/S0969-2126\(01\)00220-9](https://doi.org/10.1016/S0969-2126(01)00220-9)
- Davies, G., Wilson, K. S., & Henrissat, B. (1997). Nomenclature for sugar-binding subsites in glycosyl hydrolases. *Biochemical Journal*, 321(2), 557–559. <https://doi.org/10.1042/bj3210557>
- de Baar, H. J. W., de Jong, J. T. M., Bakker, D. C. E., Löscher, B. M., Veth, C., Bathmann, U., & Smetacek, V. (1995). Importance of iron for plankton blooms and carbon dioxide drawdown in the Southern Ocean. *Nature*, 373(6513), 412–415. <https://doi.org/10.1038/373412a0>
- Deniaud-Bouët, E., Hardouin, K., Potin, P., Kloareg, B., & Hervé, C. (2017). A review about brown algal cell walls and fucose-containing sulfated polysaccharides: Cell wall context, biomedical properties and key research challenges. *Carbohydrate Polymers*, 175(2), 395–408. <https://doi.org/10.1016/j.carbpol.2017.07.082>
- Deniaud-Bouët, E., Kervarec, N., Michel, G., Tonon, T., Kloareg, B., & Hervé, C. (2014). Chemical and enzymatic fractionation of cell walls from *Fucales*: Insights into the structure of the extracellular matrix of brown algae. *Annals of Botany*, 114(6), 1203–1216. <https://doi.org/10.1093/aob/mcu096>

## References

- Diepenbroek, M., & Glöckner, F. O. (2014). Towards an Integrated Biodiversity and Ecological Research Data Management and Archiving Platform : The .... *Informatik 2014 – Big Data Komplexität Meistern. GI-Edition: Lecture Notes in Informatics (LNI) – Proceedings 232*, (November), 1711–1721 <https://dl.gi.de/handle/20.500.12116/2782>
- Dierks, T., Miech, C., Hummerjohann, J., Schmidt, B., Kertesz, M. A., & Von Figura, K. (1998). Posttranslational formation of formylglycine in prokaryotic sulfatases by modification of either cysteine or serine. *Journal of Biological Chemistry*, *273*(40), 25560–25564. <https://doi.org/10.1074/jbc.273.40.25560>
- Dillehay, T. D., Ramirez, C., Pino, M., Collins, M. B., Rossen, J., & Pino-Navarro, J. D. (2008). Monte Verde: Seaweed, Food, Medicine, and the Peopling of South America. *Science*, *320*(5877), 784–786. <https://doi.org/10.1126/science.1156533>
- Drescher, K., Nadell, C. D., Stone, H. A., Wingreen, N. S., & Bassler, B. L. (2014). Solutions to the Public Goods Dilemma in Bacterial Biofilms. *Current Biology*, *24*(1), 50–55. <https://doi.org/10.1016/j.cub.2013.10.030>
- Duarte, C M, Middelburg, J. J., & Caraco, N. (2005). Major role of marine vegetation on the oceanic carbon cycle. *Biogeosciences*, *2*(1), 1–8. <https://doi.org/10.5194/bg-2-1-2005>
- Duarte, C. M. (2017). Reviews and syntheses: Hidden forests, the role of vegetated coastal habitats in the ocean carbon budget. *Biogeosciences*, *14*(2), 301–310. <https://doi.org/10.5194/bg-14-301-2017>
- Dubois, M., Gilles, K. A., Hamilton, J. K., Rebers, P. A., & Smith, F. (1956). Colorimetric Method for Determination of Sugars and Related Substances. *Analytical Chemistry*, *28*(3), 350–356. <https://doi.org/10.1021/ac60111a017>
- Ducklow, H. W., Kirchman, D. L., Quinby, H. L., Carlson, C. A., & Dam, H. G. (1993). Stocks and dynamics of bacterioplankton carbon during the spring bloom in the eastern North Atlantic Ocean. *Deep-Sea Research Part II*, *40*(1–2), 245–263. [https://doi.org/10.1016/0967-0645\(93\)90016-G](https://doi.org/10.1016/0967-0645(93)90016-G)
- Edgar, R. C. (2004). MUSCLE: Multiple sequence alignment with high accuracy and high throughput. *Nucleic Acids Research*, *32*(5), 1792–1797. <https://doi.org/10.1093/nar/gkh340>
- El-Gebali, S., Mistry, J., Bateman, A., Eddy, S. R., Luciani, A., Potter, S. C., ... Finn, R. D. (2019). The Pfam protein families database in 2019. *Nucleic Acids Research*, *47*(D1), D427–D432. <https://doi.org/10.1093/nar/gky995>
- Emsley, P., Lohkamp, B., Scott, W. G., & Cowtan, K. (2010). Features and development of Coot. *Acta Crystallographica Section D: Biological Crystallography*, *66*(4), 486–501.

- <https://doi.org/10.1107/S0907444910007493>
- Eneyskaya, E. V., Kulminskaya, A. A., Kalkkinen, N., Nifantiev, N. E., Arbatskii, N. P., Saenko, A. I., ... Neustroev, K. N. (2001). An  $\alpha$ -L-fucosidase from *Thermus* sp. with unusually broad specificity. *Glycoconjugate Journal*, *18*(10), 827–834.  
<https://doi.org/10.1023/A:1021163720282>
- Engel, A., & Händel, N. (2011). A novel protocol for determining the concentration and composition of sugars in particulate and in high molecular weight dissolved organic matter (HMW-DOM) in seawater. *Marine Chemistry*, *127*(1–4), 180–191.  
<https://doi.org/10.1016/j.marchem.2011.09.004>
- Engel, A., Thoms, S., Riebesell, U., Rochelle-Newall, E., & Zondervan, I. (2004). Polysaccharide aggregation as a potential sink of marine dissolved organic carbon. *Nature*, *428*(6986), 929–932. <https://doi.org/10.1038/nature02453>
- Enke, T. N., Datta, M. S., Schwartzman, J., Cermak, N., Schmitz, D., Barrere, J., ... Cordero, O. X. (2019). Modular Assembly of Polysaccharide-Degrading Marine Microbial Communities. *Current Biology*, 1–8. <https://doi.org/10.1016/j.cub.2019.03.047>
- Enke, T. N., Leventhal, G. E., Metzger, M., Saavedra, J. T., & Cordero, O. X. (2018). Microscale ecology regulates particulate organic matter turnover in model marine microbial communities. *Nature Communications*, *9*(1), 2743.  
<https://doi.org/10.1038/s41467-018-05159-8>
- Erbilgin, O., McDonald, K. L., & Kerfeld, C. A. (2014). Characterization of a Planctomycetal Organelle: a Novel Bacterial Microcompartment for the Aerobic Degradation of Plant Saccharides. *Applied and Environmental Microbiology*, *80*(7), 2193–2205.  
<https://doi.org/10.1128/AEM.03887-13>
- Evans, P. R. (2011). An introduction to data reduction: Space-group determination, scaling and intensity statistics. *Acta Crystallographica Section D: Biological Crystallography*, *67*(4), 282–292. <https://doi.org/10.1107/S090744491003982X>
- Ficko-Blean, E., Préchoux, A., Thomas, F., Rochat, T., Larocque, R., Zhu, Y., ... Michel, G. (2017). Carrageenan catabolism is conferred by a complex regulon in marine heterotrophic bacteria. *Nature Communications*, *in press*.  
<https://doi.org/10.1038/s41467-017-01832-6>
- Field, C. B. (1998). Primary Production of the Biosphere: Integrating Terrestrial and Oceanic Components. *Science*, *281*(5374), 237–240.  
<https://doi.org/10.1126/science.281.5374.237>
- Finn, R. D., Clements, J., & Eddy, S. R. (2011). HMMER web server: Interactive sequence

## References

- similarity searching. *Nucleic Acids Research*, 39(SUPPL. 2), 29–37.  
<https://doi.org/10.1093/nar/gkr367>
- Fitton, J. H., Stringer, D. N., & Karpiniec, S. S. (2015). Therapies from fucoidan: An update. *Marine Drugs*, 13(9), 5920–5946. <https://doi.org/10.3390/md13095920>
- Fletcher, H. R., Biller, P., Ross, A. B., & Adams, J. M. M. (2017). The seasonal variation of fucoidan within three species of brown macroalgae. *Algal Research*, 22, 79–86.  
<https://doi.org/10.1016/j.algal.2016.10.015>
- Freitas, S., Hatosy, S., Fuhrman, J. A., Huse, S. M., Mark Welch, D. B., Sogin, M. L., & Martiny, A. C. (2012). Global distribution and diversity of marine Verrucomicrobia. *The ISME Journal*, 6(8), 1499–1505. <https://doi.org/10.1038/ismej.2012.3>
- Galperin, M. Y., Makarova, K. S., Wolf, Y. I., & Koonin, E. V. (2015). Expanded microbial genome coverage and improved protein family annotation in the COG database. *Nucleic Acids Research*, 43(D1), D261–D269. <https://doi.org/10.1093/nar/gku1223>
- Gärdes, A., Iversen, M. H., Grossart, H.-P., Passow, U., & Ullrich, M. S. (2011). Diatom-associated bacteria are required for aggregation of *Thalassiosira weissflogii*. *The ISME Journal*, 5(3), 436–445. <https://doi.org/10.1038/ismej.2010.145>
- Glöckner, F. O., Kube, M., Bauer, M., Teeling, H., Lombardot, T., Ludwig, W., ... Reinhardt, R. (2003). Complete genome sequence of the marine planctomycete *Pirellula* sp. strain 1. *Proceedings of the National Academy of Sciences*, 100(14), 8298–8303.  
<https://doi.org/10.1073/pnas.1431443100>
- Gogou, A., & Repeta, D. J. (2010). Particulate-dissolved transformations as a sink for semi-labile dissolved organic matter: Chemical characterization of high molecular weight dissolved and surface-active organic matter in seawater and in diatom cultures. *Marine Chemistry*, 121(1–4), 215–223. <https://doi.org/10.1016/j.marchem.2010.05.001>
- Grachev, A., Gerbst, A., Ustyuzhanina, N., Shashkov, A., Usov, A., & Nifantiev, N. (2006). NMR investigation of the influence of sulfate groups at C-2 and C-4 on the conformational behavior of fucoidan fragments with homo-(1→3)-linked backbone. *Journal of Carbohydrate Chemistry*, 25(4), 315–330.  
<https://doi.org/10.1080/07328300600770493>
- Graham, M. H., Kinlan, B. P., Druehl, L. D., Garske, L. E., & Banks, S. (2007). Deep-water kelp refugia as potential hotspots of tropical marine diversity and productivity. *Proceedings of the National Academy of Sciences of the United States of America*, 104(42), 16576–16580. <https://doi.org/10.1073/pnas.0704778104>
- Gügi, B., Costauuec, T. Le, Burel, C., Lerouge, P., Helbert, W., & Bardor, M. (2015).

- Diatom-specific oligosaccharide and polysaccharide structures help to unravel biosynthetic capabilities in diatoms. *Marine Drugs*, 13(9), 5993–6018.  
<https://doi.org/10.3390/md13095993>
- Hahn, T., Lang, S., Ulber, R., & Muffler, K. (2012). Novel procedures for the extraction of fucoidan from brown algae. *Process Biochemistry*, 47(12), 1691–1698.  
<https://doi.org/10.1016/j.procbio.2012.06.016>
- Hahn, T., Zayed, A., Kovacheva, M., Stadtmüller, R., Lang, S., Muffler, K., & Ulber, R. (2016). Dye affinity chromatography for fast and simple purification of fucoidan from marine brown algae. *Engineering in Life Sciences*, 16(1), 78–87.  
<https://doi.org/10.1002/elsc.201500044>
- Hanson, S. R., Best, M. D., & Wong, C.-H. (2004). Sulfatases: Structure, Mechanism, Biological Activity, Inhibition, and Synthetic Utility. *Angewandte Chemie International Edition*, 43(43), 5736–5763. <https://doi.org/10.1002/anie.200300632>
- Haroun-Bouhedja, F., Ellouali, M., Siquin, C., & Boisson-Vidal, C. (2000). Relationship between Sulfate Groups and Biological Activities of Fucans. *Thrombosis Research*, 100(5), 453–459. [https://doi.org/10.1016/S0049-3848\(00\)00338-8](https://doi.org/10.1016/S0049-3848(00)00338-8)
- Harris, P. J., Henry, R. J., Blakeney, A. B., & Stone, B. A. (1984). An improved procedure for the methylation analysis of oligosaccharides and polysaccharides. *Carbohydrate Research*, 127(1), 59–73. [https://doi.org/10.1016/0008-6215\(84\)85106-X](https://doi.org/10.1016/0008-6215(84)85106-X)
- Harrison, P. W., Alako, B., Amid, C., Cerdeño-Tárraga, A., Cleland, I., Holt, S., ... Cochrane, G. (2019). The European Nucleotide Archive in 2018. *Nucleic Acids Research*, 47(D1), D84–D88. <https://doi.org/10.1093/nar/gky1078>
- He, S., Stevens, S., Chan, L., Bertilsson, S., Glavina del Rio, T., Tringe, S. G., ... McMahon, K. D. (2017). Ecophysiology of Freshwater Verrucomicrobia Inferred from. *MSphere*, 2(5), 1–17.
- Hedges, J. I., Baldock, J. A., Gélinas, Y., Lee, C., Peterson, M., & Wakeham, S. G. (2001). Evidence for non-selective preservation of organic matter in sinking marine particles. *Nature*, 409(6822), 801–804. <https://doi.org/10.1038/35057247>
- Hehemann, J.-H., Arevalo, P., Datta, M. S., Yu, X., Corzett, C. H., Henschel, A., ... Polz, M. F. (2016). Adaptive radiation by waves of gene transfer leads to fine-scale resource partitioning in marine microbes. *Nature Communications*, 7, 12860.  
<https://doi.org/10.1038/ncomms12860>
- Hehemann, J.-H., Correc, G., Thomas, F., Bernard, T., Barbeyron, T., Jam, M., ... Czjzek, M. (2012). Biochemical and Structural Characterization of the Complex Agarolytic Enzyme

## References

- System from the Marine Bacterium *Zobellia galactanivorans*. *Journal of Biological Chemistry*, 287(36), 30571–30584. <https://doi.org/10.1074/jbc.M112.377184>
- Hehemann, J.-H., Truong, L. Van, Unfried, F., Welsch, N., Kabisch, J., Heiden, S. E., ... Schweder, T. (2017). Aquatic adaptation of a laterally acquired pectin degradation pathway in marine gammaproteobacteria. *Environmental Microbiology*, 19(6), 2320–2333. <https://doi.org/10.1111/1462-2920.13726>
- Hemmingson, J. A., Falshaw, R., Furneaux, R. H., & Thompson, K. (2006). Structure and antiviral activity of the galactofucan sulfates extracted from *Undaria pinnatifida* (Phaeophyta). *Journal of Applied Phycology*, 18(2), 185–193. <https://doi.org/10.1007/s10811-006-9096-9>
- Hettle, A. G., Vickers, C., Robb, C. S., Liu, F., Withers, S. G., Hehemann, J.-H., & Boraston, A. B. (2018). The Molecular Basis of Polysaccharide Sulfatase Activity and a Nomenclature for Catalytic Subsites in this Class of Enzyme. *Structure*, 26(5), 747–758.e4. <https://doi.org/10.1016/j.str.2018.03.012>
- Hobbs, J. K., Pluinage, B., Robb, M., Smith, S. P., & Boraston, A. B. (2019). Two complementary  $\alpha$ -fucosidases from *Streptococcus pneumoniae* promote complete degradation of host-derived carbohydrate antigens. *Journal of Biological Chemistry*, 294(34), 12670–12682. <https://doi.org/10.1074/jbc.RA119.009368>
- Hofmann, J., Hahm, H. S., Seeberger, P. H., & Pagel, K. (2015). Identification of carbohydrate anomers using ion mobility-mass spectrometry. *Nature*, 526(7572), 241–244. <https://doi.org/10.1038/nature15388>
- Holtkamp, A. D. (2009). Isolation , Characterisation , Modification and Application of Fucoidan from *Fucus vesiculosus*. *Analysis*, 179.
- Hugenholtz, P., Goebel, B. M., & Pace, N. R. (1998). Impact of culture-independent studies on the emerging phylogenetic view of bacterial diversity. *Journal of Bacteriology*, 180(18), 4765–4774. Retrieved from <https://jb.asm.org/content/180/18/4765>
- Jackson, G. A. (1987). Modelling the growth and harvest yield of the giant kelp *Macrocystis pyrifera*. *Marine Biology*, 95(4), 611–624. <https://doi.org/10.1007/BF00393105>
- Kadam, S. U., Tiwari, B. K., & O'Donnell, C. P. (2015). Extraction, structure and biofunctional activities of laminarin from brown algae. *International Journal of Food Science and Technology*, 50(1), 24–31. <https://doi.org/10.1111/ijfs.12692>
- Kammers, K., Cole, R. N., Tiengwe, C., & Ruczinski, I. (2015). Detecting significant changes in protein abundance. *EuPA Open Proteomics*, 7, 11–19. <https://doi.org/10.1016/j.euprot.2015.02.002>

- Kappelmann, L., Krüger, K., Hehemann, J.-H., Harder, J., Markert, S., Unfried, F., ... Teeling, H. (2019). Polysaccharide utilization loci of North Sea *Flavobacteriia* as basis for using SusC/D-protein expression for predicting major phytoplankton glycans. *The ISME Journal*, 13(1), 76–91. <https://doi.org/10.1038/s41396-018-0242-6>
- Kjørboe, T., & Hansen, J. L. s. (1993). Phytoplankton aggregate formation: observations of patterns and mechanisms of cell sticking and the significance of exopolymeric material. *Journal of Plankton Research*, 15(9), 993–1018. <https://doi.org/10.1093/plankt/15.9.993>
- Koch, H., Dürwald, A., Schweder, T., Noriega-Ortega, B., Vidal-Melgosa, S., Hehemann, J.-H., ... Wietz, M. (2019). Biphasic cellular adaptations and ecological implications of *Alteromonas macleodii* degrading a mixture of algal polysaccharides. *The ISME Journal*, 13(1), 92–103. <https://doi.org/10.1038/s41396-018-0252-4>
- Koivikko, R., Loponen, J., Honkanen, T., & Jormalainen, V. (2005). Contents Of Soluble, Cell-Wall-Bound And Exuded Phlorotannins In The Brown Alga *Fucus vesiculosus*, With Implications On Their Ecological Functions. *Journal of Chemical Ecology*, 31(1), 195–212. <https://doi.org/10.1007/s10886-005-0984-2>
- Kopf, A., Bicak, M., Kottmann, R., Schnetzer, J., Kostadinov, I., Lehmann, K., ... Glöckner, F. O. (2015). The ocean sampling day consortium. *GigaScience*, 4(1). <https://doi.org/10.1186/s13742-015-0066-5>
- Kopplin, G., Rokstad, A. M., Mérida, H., Bulone, V., Skjåk-Bræk, G., & Achmann, F. L. (2018). Structural Characterization of Fucoïdan from *Laminaria hyperborea* : Assessment of Coagulation and Inflammatory Properties and Their Structure–Function Relationship . *ACS Applied Bio Materials*, 1(6), 1880–1892. <https://doi.org/10.1021/acsabm.8b00436>
- Koshland, D. E. (1953). Stereochemistry and the Mechanism of Enzymatic Reactions. *Biological Reviews*, 28(4), 416–436. <https://doi.org/10.1111/j.1469-185X.1953.tb01386.x>
- Kotak, M., Isanapong, J., Goodwin, L., Bruce, D., Chen, A., Han, C. S., ... Rodrigues, J. L. M. (2015). Complete Genome Sequence of the *Opitutaceae* Bacterium Strain TAV5, a Potential Facultative Methylophile of the Wood-Feeding Termite *Reticulitermes flavipes*. *Genome Announcements*, 3(2), e00060-15. <https://doi.org/10.1128/genomeA.00060-15>. Copyright
- Krause-Jensen, D., & Duarte, C. M. (2016). Substantial role of macroalgae in marine carbon sequestration. *Nature Geoscience*, 9(10), 737–742. <https://doi.org/10.1038/ngeo2790>
- Krüger, K., Chafee, M., Ben Francis, T., Glavina del Rio, T., Becher, D., Schweder, T., ...

## References

- Teeling, H. (2019). In marine Bacteroidetes the bulk of glycan degradation during algae blooms is mediated by few clades using a restricted set of genes. *The ISME Journal*, 1–17. <https://doi.org/10.1038/s41396-019-0476-y>
- Labourel, A., Crouch, L. I., Brás, J. L. A., Jackson, A., Rogowski, A., Gray, J., ... Cuskin, F. (2016). The mechanism by which arabinoxylanases can recognise highly decorated xylylans. *Journal of Biological Chemistry*, 291(2), jbc.M116.743948. <https://doi.org/10.1074/jbc.M116.743948>
- Labourel, A., Jam, M., Jeudy, A., Hehemann, J. H., Czjzek, M., & Michel, G. (2014). The  $\beta$ -glucanase ZgLamA from *Zobellia galactanivorans* evolved a bent active site adapted for efficient degradation of algal laminarin. *Journal of Biological Chemistry*, 289(4), 2027–2042. <https://doi.org/10.1074/jbc.M113.538843>
- Laemmli, U. K. (1970): (1970). Cleavage of Structural Proteins during Assembly of Head of Bacteriophage-T4. *Nature*, 227. <https://doi.org/10.1038/227680a0>
- Laine, R. A. (1994). Invited Commentary: A calculation of all possible oligosaccharide isomers both branched and linear yields  $1.05 \times 10^{12}$  structures for a reducing hexasaccharide: the Isomer Barrier to development of single-method saccharide sequencing or synthesis systems. *Glycobiology*, 4(6), 759–767. <https://doi.org/10.1093/glycob/4.6.759>
- Lammerts van Bueren, A., Ardèvol, A., Fayers-Kerr, J., Luo, B., Zhang, Y., Sollogoub, M., ... Davies, G. J. (2010). Analysis of the reaction coordinate of alpha-L-fucosidases: a combined structural and quantum mechanical approach. *Journal of the American Chemical Society*, 132(6), 1804–1806. <https://doi.org/10.1021/ja908908q>
- Langmead, B., & Salzberg, S. L. (2012). Fast gapped-read alignment with Bowtie 2. *Nature Methods*, 9(4), 357–359. <https://doi.org/10.1038/nmeth.1923>
- Le Quéré, C., Andrew, R. M., Friedlingstein, P., Sitch, S., Hauck, J., Pongratz, J., ... Zheng, B. (2018). Global Carbon Budget 2018. *Earth System Science Data*, 10(4), 2141–2194. <https://doi.org/10.5194/essd-10-2141-2018>
- Leth, M. L., Ejby, M., Workman, C., Ewald, D. A., Pedersen, S. S., Sternberg, C., ... Hachem, M. A. (2018). Differential bacterial capture and transport preferences facilitate co-growth on dietary xylan in the human gut. *Nature Microbiology*, 3(5), 570–580. <https://doi.org/10.1038/s41564-018-0132-8>
- Li, H., Handsaker, B., Wysoker, A., Fennell, T., Ruan, J., Homer, N., ... Durbin, R. (2009). The Sequence Alignment/Map format and SAMtools. *Bioinformatics*, 25(16), 2078–2079. <https://doi.org/10.1093/bioinformatics/btp352>



- Linger, J. G., Vardon, D. R., Guarnieri, M. T., Karp, E. M., Hunsinger, G. B., Franden, M. A., ... Beckham, G. T. (2014). Lignin valorization through integrated biological funneling and chemical catalysis. *Proceedings of the National Academy of Sciences*, *111*(33), 12013–12018. <https://doi.org/10.1073/pnas.1410657111>
- Liu, H., & Naismith, J. H. (2008). An efficient one-step site-directed deletion, insertion, single and multiple-site plasmid mutagenesis protocol. *BMC Biotechnology*, *8*(1), 91. <https://doi.org/10.1186/1472-6750-8-91>
- Loh, A. N., Bauer, J. E., & Druffel, E. R. M. (2004). Variable ageing and storage of dissolved organic components in the open ocean. *Nature*, *430*(7002), 877–881. <https://doi.org/10.1038/nature02780>
- Lombard, V., Golaconda Ramulu, H., Drula, E., Coutinho, P. M., & Henrissat, B. (2014). The carbohydrate-active enzymes database (CAZy) in 2013. *Nucleic Acids Research*, *42*(D1), 490–495. <https://doi.org/10.1093/nar/gkt1178>
- Lukatela, G., Krauss, N., Theis, K., Selmer, T., Gieseimann, V., Von Figura, K., & Saenger, W. (1998). Crystal structure of human arylsulfatase A: The aldehyde function and the metal ion at the active site suggest a novel mechanism for sulfate ester hydrolysis. *Biochemistry*, *37*(11), 3654–3664. <https://doi.org/10.1021/bi9714924>
- Ly, M., Laremore, T. N., Toida, T., Jonathan, I., Linhardt, R. J., Engineering, B., ... Studies, I. (2012). The proteoglycan bikunin has a defined sequence. *Nature Chemical Biology* *7*(11), 827–833. <https://doi.org/10.1038/nchembio.673>.The
- Maier-Reimer, E., Mikolajewicz, U., & Winguth, A. (1996). Future ocean uptake of CO<sub>2</sub>: interaction between ocean circulation and biology. *Climate Dynamics*, *12*(10), 711–722. <https://doi.org/10.1007/s003820050138>
- Mak, W., Hamid, N., Liu, T., Lu, J., & White, W. L. (2013). Fucoidan from New Zealand *Undaria pinnatifida*: Monthly variations and determination of antioxidant activities. *Carbohydrate Polymers*, *95*(1), 606–614. <https://doi.org/10.1016/j.carbpol.2013.02.047>
- Martens, E. C., Chiang, H. C., & Gordon, J. I. (2008). Mucosal Glycan Foraging Enhances Fitness and Transmission of a Saccharolytic Human Gut Bacterial Symbiont. *Cell Host and Microbe*, *4*(5), 447–457. <https://doi.org/10.1016/j.chom.2008.09.007>
- Martens, E. C., Lowe, E. C., Chiang, H., Pudlo, N. A., Wu, M., McNulty, N. P., ... Gordon, J. I. (2011). Recognition and degradation of plant cell wall polysaccharides by two human gut symbionts. *PLoS Biology*, *9*(12). <https://doi.org/10.1371/journal.pbio.1001221>
- Martens, E. C., Neumann, M., & Desai, M. S. (2018). Interactions of commensal and

## References

- pathogenic microorganisms with the intestinal mucosal barrier. *Nature Reviews Microbiology*, 16(8), 457–470. <https://doi.org/10.1038/s41579-018-0036-x>
- Mavromatis, K., Abt, B., Brambilla, E., Lapidus, A., Copeland, A., Deshpande, S., ... Kyrpides, N. C. (2010). Complete genome sequence of *Coralimargarita akajimensis* type strain (04OKA010-24). *Standards in Genomic Sciences*, 2, 290–299. <https://doi.org/10.4056/sigs.952166>
- McCarthy, M., Hedges, J., & Benner, R. (1996). Major biochemical composition of dissolved high molecular weight organic matter in seawater. *Marine Chemistry*, 55(3–4), 281–297. [https://doi.org/10.1016/S0304-4203\(96\)00041-2](https://doi.org/10.1016/S0304-4203(96)00041-2)
- McClure, R., Balasubramanian, D., Sun, Y., Bobrovskyy, M., Sumby, P., Genco, C. A., ... Tjaden, B. (2013). Computational analysis of bacterial RNA-Seq data. *Nucleic Acids Research*, 41(14), 1–16. <https://doi.org/10.1093/nar/gkt444>
- McCoy, A. J., Grosse-Kunstleve, R. W., Adams, P. D., Winn, M. D., Storoni, L. C., & Read, R. J. (2007). Phaser crystallographic software. *Journal of Applied Crystallography*, 40(4), 658–674. <https://doi.org/10.1107/S0021889807021206>
- Meents, A., Reime, B., Stuebe, N., Fischer, P., Warmer, M., Goeries, D., ... David, C. (2013). Development of an in-vacuum X-ray microscope with cryogenic sample cooling for beamline P11 at PETRA III. *X-Ray Nanoimaging: Instruments and Methods*, 8851, 1–7. <https://doi.org/10.1117/12.2027303>
- Megson, Z. A., Koerdt, A., Schuster, H., Ludwig, R., Janesch, B., Frey, A., ... Schäffer, C. (2015). Characterization of an  $\alpha$ -L-fucosidase from the periodontal pathogen *Tannerella forsythia*. *Virulence*, 6(3), 282–292. <https://doi.org/10.1080/21505594.2015.1010982>
- Mewis, K., Lenfant, N., Lombard, V., & Henrissat, B. (2016). Dividing the large glycoside hydrolase family 43 into subfamilies: A motivation for detailed enzyme characterization. *Applied and Environmental Microbiology*, 82(6), 1686–1692. <https://doi.org/10.1128/AEM.03453-15>
- Moller, I., Marcus, S. E., Haeger, A., Verhertbruggen, Y., Verhoef, R., Schols, H., ... Willats, W. (2008). High-throughput screening of monoclonal antibodies against plant cell wall glycans by hierarchical clustering of their carbohydrate microarray binding profiles. *Glycoconjugate Journal*, 25(1), 37–48. <https://doi.org/10.1007/s10719-007-9059-7>
- Morelle, W., Faïd, V., Chirat, F., & Michalski, J. C. (2009). Analysis of N- and O-linked glycans from glycoproteins using MALDI-TOF mass spectrometry. In *Methods in Molecular Biology* (Vol. 534). [https://doi.org/10.1007/978-1-59745-022-5\\_1](https://doi.org/10.1007/978-1-59745-022-5_1)
- Murshudov, G. N., Vagin, A. A., & Dodson, E. J. (1997). Refinement of macromolecular

- structures by the maximum-likelihood method. *Acta Crystallographica Section D: Biological Crystallography*, 53(3), 240–255.  
<https://doi.org/10.1107/S0907444996012255>
- Myklestad, S. M. (1995). Release of extracellular products by phytoplankton with special emphasis on polysaccharides. *Science of the Total Environment*, 165(1–3), 155–164.  
[https://doi.org/10.1016/0048-9697\(95\)04549-G](https://doi.org/10.1016/0048-9697(95)04549-G)
- Nagao, T., Kumabe, A., Komatsu, F., Yagi, H., Suzuki, H., & Ohshiro, T. (2017). Gene identification and characterization of fucoidan deacetylase for potential application to fucoidan degradation and diversification. *Journal of Bioscience and Bioengineering*, 124(3), 277–282. <https://doi.org/10.1016/j.jbiosc.2017.04.002>
- Nagaoka, M., Shibata, H., Kimura-Takagi, I., Hashimoto, S., Kimura, K., Makino, T., ... Yokokura, T. (1999). Structural study of fucoidan from *Cladosiphon okamuranus* TOKIDA. *Glycoconjugate Journal*, 16(1), 19–26.  
<https://doi.org/10.1023/A:1006945618657>
- Ndeh, D., Rogowski, A., Cartmell, A., Luis, A. S., Baslé, A., Gray, J., ... Gilbert, H. J. (2017). Complex pectin metabolism by gut bacteria reveals novel catalytic functions. *Nature*. <https://doi.org/10.1038/nature21725>
- Needham, D. M., Fichot, E. B., Wang, E., Berdjeb, L., Cram, J. A., Fichot, C. G., & Fuhrman, J. A. (2018). Dynamics and interactions of highly resolved marine plankton via automated high-frequency sampling. *The ISME Journal*, 12(10), 2417–2432.  
<https://doi.org/10.1038/s41396-018-0169-y>
- Needham, D. M., & Fuhrman, J. A. (2016). Pronounced daily succession of phytoplankton, archaea and bacteria following a spring bloom. *Nature Microbiology*, 1(4), 16005.  
<https://doi.org/10.1038/NMICROBIOL.2016.5>
- Nelson, C. E., Goldberg, S. J., Wegley Kelly, L., Haas, A. F., Smith, J. E., Rohwer, F., & Carlson, C. A. (2013). Coral and macroalgal exudates vary in neutral sugar composition and differentially enrich reef bacterioplankton lineages. *The ISME Journal*, 7(5), 962–979. <https://doi.org/10.1038/ismej.2012.161>
- Nielsen, H. (2017). Predicting Secretory Proteins with SignalP. In D. Kihara (Ed.), *Protein Function Prediction: Methods and Protocols* (pp. 59–73). [https://doi.org/10.1007/978-1-4939-7015-5\\_6](https://doi.org/10.1007/978-1-4939-7015-5_6)
- Nishino, T., Nagumo, T., Kiyohara, H., & Yamada, H. (1991). Structural characterization of a new anticoagulant fucan sulfate from the brown seaweed *Ecklonia kurome*. *Carbohydrate Research*, 211(1), 77–90. [https://doi.org/10.1016/0008-6215\(91\)84147-7](https://doi.org/10.1016/0008-6215(91)84147-7)

## References

- Nishino, T., Nishioka, C., Ura, H., & Nagumo, T. (1994). Isolation and partial characterization of a novel amino sugar-containing fucan sulfate from commercial *Fucus vesiculosus* fucoidan. *Carbohydrate Research*, 255(4), 213–224. [https://doi.org/10.1016/S0008-6215\(00\)90980-7](https://doi.org/10.1016/S0008-6215(00)90980-7)
- Øbro, J., Sørensen, I., Møller, I., Skjøt, M., Mikkelsen, J. D., & Willats, W. G. T. (2007). High-throughput microarray analysis of pectic polymers by enzymatic epitope deletion. *Carbohydrate Polymers*, 70(1), 77–81. <https://doi.org/10.1016/j.carbpol.2007.03.008>
- Ohshiro, T., Harada, N., Kobayashi, Y., Miki, Y., & Kawamoto, H. (2012). Microbial Fucoidan Degradation by *Luteolibacter algae* H18 with Deacetylation. *Bioscience, Biotechnology, and Biochemistry*, 76(3), 620–623. <https://doi.org/10.1271/bbb.110911>
- Otto, A., Bernhardt, J., Meyer, H., Schaffer, M., Herbst, F. A., Siebourg, J., ... Becher, D. (2010). Systems-wide temporal proteomic profiling in glucose-starved *Bacillus subtilis*. *Nature Communications*, 1(9). <https://doi.org/10.1038/ncomms1137>
- Overbeek, R. (2005). The Subsystems Approach to Genome Annotation and its Use in the Project to Annotate 1000 Genomes. *Nucleic Acids Research*, 33(17), 5691–5702. <https://doi.org/10.1093/nar/gki866>
- Parks, D. H., Chuvochina, M., Waite, D. W., Rinke, C., Skarshewski, A., Chaumeil, P.-A., & Hugenholtz, P. (2018). A standardized bacterial taxonomy based on genome phylogeny substantially revises the tree of life. *Nature Biotechnology*, 36(10), 996–1004. <https://doi.org/10.1038/nbt.4229>
- Passow, U. (2002). Transparent exopolymer particles (TEP) in aquatic environments. *Progress in Oceanography*, 55(3–4), 287–333. [https://doi.org/10.1016/S0079-6611\(02\)00138-6](https://doi.org/10.1016/S0079-6611(02)00138-6)
- Passow, U., & Carlson, C. (2012). The biological pump in a high CO<sub>2</sub> world. *Marine Ecology Progress Series*, 470(2), 249–271. <https://doi.org/10.3354/meps09985>
- Paulsen, B. S., & Myklesstad, S. (1978). Structural studies of the reserve glucan produced by the marine diatom *Skeletonema costatum* (grev.) Cleve. *Carbohydrate Research*, 62(2), 386–388. [https://doi.org/10.1016/S0008-6215\(00\)80888-5](https://doi.org/10.1016/S0008-6215(00)80888-5)
- Peters, C., Schmidt, B., Rommerskirch, W., Rupp, K., Zühlendorf, M., Vingron, M., ... von Figura, K. (1990). Phylogenetic conservation of arylsulfatases. cDNA cloning and expression of human arylsulfatase B. *The Journal of Biological Chemistry*, 265(6), 3374–3381. Retrieved from <http://www.ncbi.nlm.nih.gov/pubmed/2303452>
- Petit, E., LaTouf, W. G., Coppi, M. V., Warnick, T. A., Currie, D., Romashko, I., ... Blanchard, J. L. (2013). Involvement of a Bacterial Microcompartment in the

- Metabolism of Fucose and Rhamnose by *Clostridium phytofermentans*. *PLoS ONE*, 8(1), 1–12. <https://doi.org/10.1371/journal.pone.0054337>
- Ploug, H., & Bergkvist, J. (2015). Oxygen diffusion limitation and ammonium production within sinking diatom aggregates under hypoxic and anoxic conditions. *Marine Chemistry*, 176, 142–149. <https://doi.org/10.1016/j.marchem.2015.08.012>
- Pluvinage, B., Grondin, J. M., Amundsen, C., Klassen, L., Moote, P. E., Xiao, Y., ... Abbott, D. W. (2018). Molecular basis of an agarose metabolic pathway acquired by a human intestinal symbiont. *Nature Communications*, 9(1). <https://doi.org/10.1038/s41467-018-03366-x>
- Pomin, V. H., Valente, A. P., Pereira, M. S., & Mourão, P. A. S. (2005). Mild acid hydrolysis of sulfated fucans: A selective 2-desulfation reaction and an alternative approach for preparing tailored sulfated oligosaccharides. *Glycobiology*, 15(12), 1376–1385. <https://doi.org/10.1093/glycob/cwj030>
- Ponce, N. M. A., Pujol, C. A., Damonte, E. B., Flores, M. L., & Stortz, C. A. (2003). Fucoidans from the brown seaweed *Adenocystis utricularis*: Extraction methods, antiviral activity and structural studies. *Carbohydrate Research*, 338(2), 153–165. [https://doi.org/10.1016/S0008-6215\(02\)00403-2](https://doi.org/10.1016/S0008-6215(02)00403-2)
- Popper, Z. A., Michel, G., Herve, C., Domozych, D. S., Willats, W. G. T., Tuohy, M. G., ... Stengel, D. B. (2011). Evolution and Diversity of Plant Cell Walls: From Algae to Flowering Plants. *Annual Review of Plant Biology*, Vol 62, 62, 567–588. <https://doi.org/10.1146/annurev-arplant-042110-103809>
- Pruesse, E., Peplies, J., & Glöckner, F. O. (2012). SINA: Accurate high-throughput multiple sequence alignment of ribosomal RNA genes. *Bioinformatics*, 28(14), 1823–1829. <https://doi.org/10.1093/bioinformatics/bts252>
- Quast, C., Pruesse, E., Yilmaz, P., Gerken, J., Schweer, T., Yarza, P., ... Glöckner, F. O. (2013). The SILVA ribosomal RNA gene database project: Improved data processing and web-based tools. *Nucleic Acids Research*, 41(D1), 590–596. <https://doi.org/10.1093/nar/gks1219>
- Queiroz, I. N., Wang, X., Glushka, J. N., Santos, G. R., Valente, A. P., Prestegard, J. H., ... Pomin, V. H. (2015). Impact of sulfation pattern on the conformation and dynamics of sulfated fucan oligosaccharides as revealed by NMR and MD. *Glycobiology*, 25(5), 535–547. <https://doi.org/10.1093/glycob/cwu184>
- Rahfeld, P., Sim, L., Moon, H., Constantinescu, I., Morgan-Lang, C., Hallam, S. J., ... Withers, S. G. (2019). An enzymatic pathway in the human gut microbiome that

## References

- converts A to universal O type blood. *Nature Microbiology*.  
<https://doi.org/10.1038/s41564-019-0469-7>
- Razeq, F. M., Jurak, E., Stogios, P. J., Yan, R., Tenkanen, M., Kabel, M. A., ... Master, E. R. (2018). A novel acetyl xylan esterase enabling complete deacetylation of substituted xylans. *Biotechnology for Biofuels*, *11*(1), 74. <https://doi.org/10.1186/s13068-018-1074-3>
- Reintjes, G., Arnosti, C., Fuchs, B., & Amann, R. (2018). Selfish, sharing and scavenging bacteria in the Atlantic Ocean: a biogeographical study of bacterial substrate utilisation. *The ISME Journal*. <https://doi.org/10.1038/s41396-018-0326-3>
- Reintjes, G., Arnosti, C., Fuchs, B. M., & Amann, R. (2017). An alternative polysaccharide uptake mechanism of marine bacteria. *The ISME Journal*, 1–11.  
<https://doi.org/10.1038/ismej.2017.26>
- Reisky, L., Préchoux, A., Zühlke, M.-K., Bäumgen, M., Robb, C. S., Gerlach, N., ... Hehemann, J.-H. (2019). A marine bacterial enzymatic cascade degrades the algal polysaccharide ulvan. *Nature Chemical Biology*, *15*(8), 803–812.  
<https://doi.org/10.1038/s41589-019-0311-9>
- Richter, M., Rosselló-Móra, R., Oliver Glöckner, F., & Peplies, J. (2016). JSpeciesWS: a web server for prokaryotic species circumscription based on pairwise genome comparison. *Bioinformatics*, *32*(6), 929–931. <https://doi.org/10.1093/bioinformatics/btv681>
- Rioux, L. E., Turgeon, S. L., & Beaulieu, M. (2009). Effect of season on the composition of bioactive polysaccharides from the brown seaweed *Saccharina longicruris*. *Phytochemistry*, *70*(8), 1069–1075. <https://doi.org/10.1016/j.phytochem.2009.04.020>
- Robert, X., & Gouet, P. (2014). Deciphering key features in protein structures with the new ENDscript server. *Nucleic Acids Research*, *42*(W1), 320–324.  
<https://doi.org/10.1093/nar/gku316>
- Rocha, H. A. O., Moraes, F. A., Trindade, E. S., Franco, C. R. C., Torquato, R. J. S., Veiga, S. S., ... Dietrich, C. P. (2005). Structural and hemostatic activities of a sulfated galactofucan from the brown alga *Spaghtoglossum schroederi*: An ideal antithrombotic agent? *Journal of Biological Chemistry*, *280*(50), 41278–41288.  
<https://doi.org/10.1074/jbc.M501124200>
- Rogowski, A., Briggs, J. A., Mortimer, J. C., Tryfona, T., Terrapon, N., Lowe, E. C., ... Bolam, D. N. (2015). Glycan complexity dictates microbial resource allocation in the large intestine. *Nature Communications*, *6*(May), 7481.  
<https://doi.org/10.1038/ncomms8481>

- Ropartz, D., Li, P., Jackson, G. P., & Rogniaux, H. (2017). Negative Polarity Helium Charge Transfer Dissociation Tandem Mass Spectrometry: Radical-Initiated Fragmentation of Complex Polysulfated Anions. *Analytical Chemistry*, 89(7), 3824–3828. <https://doi.org/10.1021/acs.analchem.7b00473>
- Rothäusler, E., Gutow, L., & Thiel, M. (2012). *Floating Seaweeds and Their Communities*. [https://doi.org/10.1007/978-3-642-28451-9\\_17](https://doi.org/10.1007/978-3-642-28451-9_17)
- Sakai, T., Ishizuka, K., & Kato, I. (2003). Isolation and Characterization of a Fucoidan-Degrading Marine Bacterium. *Marine Biotechnology*, 5(5), 409–416. <https://doi.org/10.1007/s10126-002-0118-6>
- Sarmiento, J. L., & Gruber, N. (2002). Sinks for anthropogenic carbon. *Physics Today*, 55(8), 30. <https://doi.org/10.1063/1.1510279>
- Sasaki, K., Sakai, T., Kojima, K., Nakayama, S., Nakanishi, Y., & Kato, I. (1996). Partial purification and characterization of an enzyme releasing 2-sulfo- $\alpha$ -l-fucopyranose from 2-sulfo- $\alpha$ -l-fucopyranosyl-(1 $\rightarrow$ 2) pyridylaminated fucose from a sea urchin, *strongylocentrotus nudus*. *Bioscience, Biotechnology and Biochemistry*, 60(4), 666–668. <https://doi.org/10.1271/bbb.60.666>
- Schmidt, B., Selmer, T., Ingendoh, A., & Figurat, K. von. (1995). A novel amino acid modification in sulfatases that is defective in multiple sulfatase deficiency. *Cell*, 82(2), 271–278. [https://doi.org/10.1016/0092-8674\(95\)90314-3](https://doi.org/10.1016/0092-8674(95)90314-3)
- Schultz-Johansen, M., Cueff, M., Hardouin, K., Jam, M., Larocque, R., Glaring, M. A., ... Stougaard, P. (2018). Discovery and screening of novel metagenome-derived GH107 enzymes targeting sulfated fucans from brown algae. *The FEBS Journal*. <https://doi.org/10.1111/febs.14662>
- Seekatz, A. M., Terrapon, N., Kamada, N., Henrissat, B., Muller, A., Young, V. B., ... Koropatkin, N. M. (2016). A Dietary Fiber-Deprived Gut Microbiota Degrades the Colonic Mucus Barrier and Enhances Pathogen Susceptibility. *Cell*, 167(5), 1339–1353.e21. <https://doi.org/10.1016/j.cell.2016.10.043>
- Sela, D. A., Garrido, D., Lerno, L., Wu, S., Tan, K., Eom, H. J., ... Mills, D. A. (2012). *Bifidobacterium longum* subsp. *infantis* ATCC 15697  $\alpha$ -fucosidases are active on fucosylated human milk oligosaccharides. *Applied and Environmental Microbiology*, 78(3), 795–803. <https://doi.org/10.1128/AEM.06762-11>
- Shachrai, I., Zaslaver, A., Alon, U., & Dekel, E. (2010). Cost of Unneeded Proteins in *E. coli* Is Reduced after Several Generations in Exponential Growth. *Molecular Cell*, 38(5), 758–767. <https://doi.org/10.1016/j.molcel.2010.04.015>

## References

- Shimanaka, K., Ikai, K., Kato, I., Sakai, T., & Ishizuka, K. (2003). Structures of Oligosaccharides Derived from *Cladosiphon okamuranus* Fucoidan by Digestion with Marine Bacterial Enzymes. *Marine Biotechnology*, *5*(6), 536–544. <https://doi.org/10.1007/s10126-002-0107-9>
- Shin, J. B., Krey, J. F., Hassan, A., Metlagel, Z., Tauscher, A. N., Pagana, J. M., ... Barr-Gillespie, P. G. (2013). Molecular architecture of the chick vestibular hair bundle. *Nature Neuroscience*, *16*(3), 365–374. <https://doi.org/10.1038/nn.3312>
- Silberfeld, T., Leigh, J. W., Verbruggen, H., Cruaud, C., de Reviers, B., & Rousseau, F. (2010). A multi-locus time-calibrated phylogeny of the brown algae (Heterokonta, Ochrophyta, Phaeophyceae): Investigating the evolutionary nature of the “brown algal crown radiation.” *Molecular Phylogenetics and Evolution*, *56*(2), 659–674. <https://doi.org/10.1016/j.ympev.2010.04.020>
- Silchenko, A., Kusaykin, M., Kurilenko, V., Zakharenko, A., Isakov, V., Zaporozhets, T., ... Zvyagintseva, T. (2013). Hydrolysis of Fucoidan by Fucoidanase Isolated from the Marine Bacterium, *Formosa algae*. *Marine Drugs*, *11*(7), 2413–2430. <https://doi.org/10.3390/md11072413>
- Silchenko, A. S., Rasin, A. B., Zueva, A. O., Kusaykin, M. I., Zvyagintseva, T. N., Kalinovsky, A. I., ... Ermakova, S. P. (2018). Fucoidan Sulfatases from Marine Bacterium *Wenyngzhuangia fucanilytica* CZ1127<sup>T</sup>. *Biomolecules*, *8*(4), 98. <https://doi.org/10.3390/biom8040098>
- Silchenko, A. S., Ustyuzhanina, N. E., Kusaykin, M. I., Krylov, V. B., Shashkov, A. S., Dmitrenok, A. S., ... Zvyagintseva, T. N. (2017). Expression and biochemical characterization and substrate specificity of the fucoidanase from *Formosa algae*. *Glycobiology*, *27*(3), 254–263. <https://doi.org/10.1093/glycob/cww138>
- Skriptsova, A. V., Shevchenko, N. M., Zvyagintseva, T. N., & Imbs, T. I. (2010). Monthly changes in the content and monosaccharide composition of fucoidan from *Undaria pinnatifida* (Laminariales, Phaeophyta). *Journal of Applied Phycology*, *22*(1), 79–86. <https://doi.org/10.1007/s10811-009-9438-5>
- Smetacek, V., & Zingone, A. (2013). Green and golden seaweed tides on the rise. *Nature*, *504*(7478), 84–88. <https://doi.org/10.1038/nature12860>
- Smith, S. V. (1981). Marine Macrophytes as a Global Carbon Sink. *Science*, *211*(4484), 838–840. <https://doi.org/10.1126/science.211.4484.838>
- Sogin, E. M., Puskas, E., Dubilier, N., & Liebeke, M. (2019). Revealing the ocean metabolome with mass spectrometry. *BioRxiv*, 528307. <https://doi.org/10.1101/528307>



- Spring, S., Bunk, B., Spröer, C., Schumann, P., Rohde, M., Tindall, B. J., & Klenk, H.-P. (2016). Characterization of the first cultured representative of Verrucomicrobia subdivision 5 indicates the proposal of a novel phylum. *The ISME Journal*, *10*(12), 2801–2816. <https://doi.org/10.1038/ismej.2016.84>
- Sprockett, D. D., Piontkivska, H., & Blackwood, C. B. (2011). Evolutionary analysis of glycosyl hydrolase family 28 (GH28) suggests lineage-specific expansions in necrotrophic fungal pathogens. *Gene*, *479*(1–2), 29–36. <https://doi.org/10.1016/j.gene.2011.02.009>
- Stam, M. R., Danchin, E. G. J., Rancurel, C., Coutinho, P. M., & Henrissat, B. (2006). Dividing the large glycoside hydrolase family 13 into subfamilies: towards improved functional annotations of alpha-amylase-related proteins. *Protein Engineering, Design & Selection : PEDS*, *19*(12), 555–562. <https://doi.org/10.1093/protein/gzl044>
- Steinberger, M., Mirdita, M., & Söding, J. (2019). Protein-level assembly increases protein sequence recovery from metagenomic samples manifold. *Nature Methods*, *16*(7), 603–606. <https://doi.org/10.1038/s41592-019-0437-4>
- Steinberger, M., & Söding, J. (2017). MMseqs2 enables sensitive protein sequence searching for the analysis of massive data sets. *Nature Biotechnology*, *35*(11), 1026–1028. <https://doi.org/10.1038/nbt.3988>
- Stocker, R. (2012). Marine microbes see a sea of gradients. *Science*, Vol. 338, pp. 628–633. <https://doi.org/10.1126/science.1208929>
- Studier, F. W. (2005). Protein production by auto-induction in high-density shaking cultures. *Elsevier Protein Expression and Purification*, *41*, 207–234. <https://doi.org/10.1016/j.pep.2005.01.016>
- Sullivan, C. J., Kuenz, A., & Vorlop, K.-D. (2018). Propanediols. In *Ullmann's Encyclopedia of Industrial Chemistry* (pp. 1–15). [https://doi.org/10.1002/14356007.a22\\_163.pub2](https://doi.org/10.1002/14356007.a22_163.pub2)
- Sulzenbacher, G., Bignon, C., Nishimura, T., Tarling, C. A., Withers, S. G., Henrissat, B., & Bourne, Y. (2004). Crystal structure of *Thermotoga maritima*  $\alpha$ -L-fucosidase: Insights into the catalytic mechanism and the molecular basis for fucosidosis. *Journal of Biological Chemistry*, *279*(13), 13119–13128. <https://doi.org/10.1074/jbc.M313783200>
- Summers, E. L., Moon, C. D., Atua, R., & Arcus, V. L. (2016). The structure of a glycoside hydrolase 29 family member from a rumen bacterium reveals unique, dual carbohydrate-binding domains. *Acta Crystallographica Section F Structural Biology Communications*, *72*(10), 750–761. <https://doi.org/10.1107/S2053230X16014072>
- Sunagawa, S., Coelho, L. P., Chaffron, S., Kultima, J. R., Labadie, K., Salazar, G., ... Bork,

## References

- P. (2015). Structure and function of the global ocean microbiome. *Science*, 348(6237), 1261359. <https://doi.org/10.1126/science.1261359>
- Sverdrup, H. U. (1953). On conditions for the vernal blooming of phytoplankton. *ICES Journal of Marine Science*, 18(3), 287–295. <https://doi.org/10.1093/icesjms/18.3.287>
- Synytsya, A., Kim, W. J., Kim, S. M., Pohl, R., Synytsya, A., Kvasnička, F., ... Il Park, Y. (2010). Structure and antitumour activity of fucoidan isolated from sporophyll of Korean brown seaweed *Undaria pinnatifida*. *Carbohydrate Polymers*, 81(1), 41–48. <https://doi.org/10.1016/j.carbpol.2010.01.052>
- Tanaka, K., & Sorai, S. (1970). Hydrolysis of fucoidan by abalone liver  $\alpha$ -L-fucosidase. *FEBS Letters*, 9(1), 45–48. [https://doi.org/10.1016/0014-5793\(70\)80307-6](https://doi.org/10.1016/0014-5793(70)80307-6)
- Teeling, H., Fuchs, B. M., Becher, D., Klockow, C., Gardebrecht, A., Bennke, C. M., ... Amann, R. (2012). Substrate-Controlled Succession of Marine Bacterioplankton Populations Induced by a Phytoplankton Bloom. *Science*, 336(6081), 608–611. <https://doi.org/10.1126/science.1218344>
- Teeling, H., Fuchs, B. M., Bennke, C. M., Krüger, K., Chafee, M., Kappelmann, L., ... Amann, R. I. (2016). Recurring patterns in bacterioplankton dynamics during coastal spring algae blooms. *ELife*, 5(APRIL2016), 1–29. <https://doi.org/10.7554/eLife.11888>
- Tegtmeier, D., Belitz, A., Radek, R., Heimerl, T., & Brune, A. (2018). *Ereboglobus luteus* gen. nov. sp. nov. from cockroach guts, and new insights into the oxygen relationship of the genera *Opitutus* and *Didymococcus* (Verrucomicrobia: *Opitutaceae*). *Systematic and Applied Microbiology*, 41(2), 101–112. <https://doi.org/10.1016/j.syapm.2017.10.005>
- Terrapon, N., Lombard, V., Gilbert, H. J., & Henrissat, B. (2015). Automatic prediction of polysaccharide utilization loci in Bacteroidetes species. *Bioinformatics*, 31(5), 647–655. <https://doi.org/10.1093/bioinformatics/btu716>
- Thrash, J. C., Cho, J. C., Vergin, K. L., Morris, R. M., & Giovannoni, S. J. (2010). Genome sequence of *Lentisphaera araneosa* HTCC2155T, the type species of the order *Lentisphaerales* in the phylum Lentisphaerae. *Journal of Bacteriology*, 192(11), 2938–2939. <https://doi.org/10.1128/JB.00208-10>
- Tibbles, B. J., & Rawlings, D. E. (1994). Characterization of nitrogen-fixing bacteria from a temperate saltmarsh lagoon, including isolates that produce ethane from acetylene. *Microbial Ecology*. <https://doi.org/10.1007/BF00170115>
- Torode, T. A., Marcus, S. E., Jam, M., Tonon, T., Blackburn, R. S., Hervé, C., & Knox, J. P. (2015). Monoclonal Antibodies Directed to Fucoidan Preparations from Brown Algae. *Plos One*, 10(2), e0118366. <https://doi.org/10.1371/journal.pone.0118366>

- Tréguer, P., Legendre, L., Rivkin, R. T., Ragueneau, O., & Dittert, N. (2003). Water Column Biogeochemistry below the Euphotic Zone. In *Ocean Biogeochemistry* (pp. 145–156). [https://doi.org/10.1007/978-3-642-55844-3\\_7](https://doi.org/10.1007/978-3-642-55844-3_7)
- Trevathan-Tackett, S. M., Kelleway, J., Macreadie, P. I., Beardall, J., Ralph, P., & Bellgrove, A. (2015). Comparison of marine macrophytes for their contributions to blue carbon sequestration. *Ecology*, *96*(11), 3043–3057. <https://doi.org/10.1890/15-0149.1>
- Tyanova, S., Temu, T., & Cox, J. (2016). The MaxQuant computational platform for mass spectrometry-based shotgun proteomics. *Nature Protocols*, *11*(12), 2301–2319. <https://doi.org/10.1038/nprot.2016.136>
- Unfried, F., Becker, S., Robb, C. S., Hehemann, J.-H., Markert, S., Heiden, S. E., ... Schweder, T. (2018). Adaptive mechanisms that provide competitive advantages to marine bacteroidetes during microalgal blooms. *The ISME Journal*, *12*(12), 2894–2906. <https://doi.org/10.1038/s41396-018-0243-5>
- Usoltseva, R. V., Anastyuk, S. D., Ishina, I. A., Isakov, V. V., Zvyagintseva, T. N., Thinh, P. D., ... Ermakova, S. P. (2018). Structural characteristics and anticancer activity in vitro of fucoidan from brown alga *Padina boryana*. *Carbohydrate Polymers*, *184*, 260–268. <https://doi.org/10.1016/j.carbpol.2017.12.071>
- Usoltseva, R. V., Anastyuk, S. D., Shevchenko, N. M., Surits, V. V., Silchenko, A. S., Isakov, V. V., ... Ermakova, S. P. (2017). Polysaccharides from brown algae *Sargassum duplicatum*: the structure and anticancer activity in vitro. *Carbohydrate Polymers*, *175*(July), 547–556. <https://doi.org/10.1016/j.carbpol.2017.08.044>
- Usov, A. I., Adamyants, K. S., Miroshnikova, L. I., Shaposhnikova, A. A., & Kochetkov, N. K. (1971). Solvolytic desulphation of sulphated carbohydrates. *Carbohydrate Research*, *18*(2), 336–338. [https://doi.org/10.1016/S0008-6215\(00\)80360-2](https://doi.org/10.1016/S0008-6215(00)80360-2)
- van Vliet, D. M., Palakawong Na Ayudthaya, S., Diop, S., Villanueva, L., Stams, A. J. M., & Sánchez-Andrea, I. (2019b). Anaerobic Degradation of Sulfated Polysaccharides by Two Novel *Kiritimatiellales* Strains Isolated From Black Sea Sediment. *Frontiers in Microbiology*, *10*(February), 1–16. <https://doi.org/10.3389/fmicb.2019.00253>
- Varki, A., Cummings, R. D., Aebi, M., Packer, N. H., Seeberger, P. H., Esko, J. D., ... Kornfeld, S. (2015). Symbol nomenclature for graphical representations of glycans. *Glycobiology*, *25*(12), 1323–1324. <https://doi.org/10.1093/glycob/cwv091>
- Vasella, A., Davies, G. J., & Böhm, M. (2002). Glycosidase mechanisms. *Current Opinion in Chemical Biology*, *6*(5), 619–629. [https://doi.org/10.1016/S1367-5931\(02\)00380-0](https://doi.org/10.1016/S1367-5931(02)00380-0)
- Verdugo, P., Alldredge, A. L., Azam, F., Kirchman, D. L., Passow, U., & Santschi, P. H.

## References

- (2004). The oceanic gel phase: A bridge in the DOM-POM continuum. *Marine Chemistry*, 92(1-4 SPEC. ISS.), 67–85. <https://doi.org/10.1029/2002GL016046>
- Viborg, A. H., Terrapon, N., Lombard, V., Michel, G., Czjzek, M., Henrissat, B., & Brumer, H. (2019). A subfamily roadmap for functional glycomics of the evolutionarily diverse Glycoside Hydrolase Family 16 (GH16). *Journal of Biological Chemistry*, 16, jbc.RA119.010619. <https://doi.org/10.1074/jbc.RA119.010619>
- Vickers, C., Liu, F., Abe, K., Salama-Alber, O., Jenkins, M., Springate, C. M. K., ... Boraston, A. B. (2018). Endo-fucoidan hydrolases from glycoside hydrolase family 107 (GH107) display structural and mechanistic similarities to -L-fucosidases from GH29. *Journal of Biological Chemistry*, 293(47), 18296–18308. <https://doi.org/10.1074/jbc.RA118.005134>
- Vidal-Melgosa, S., Pedersen, H. L., Schückel, J., Arnal, G., Dumon, C., Amby, D. B., ... Willats, W. G. T. (2015). A new versatile microarray-based method for high throughput screening of carbohydrate-active enzymes. *Journal of Biological Chemistry*, 290(14), 9020–9036. <https://doi.org/10.1074/jbc.M114.630673>
- Viladot, J.-L., de Ramon, E., Durany, O., & Planas, A. (1998). Probing the Mechanism of Bacillus 1,3-1,4-β- d -Glucan 4-Glucanohydrolases by Chemical Rescue of Inactive Mutants at Catalytically Essential Residues †. *Biochemistry*, 37(32), 11332–11342. <https://doi.org/10.1021/bi980586q>
- Vishchuk, O. S., Ermakova, S. P., & Zvyagintseva, T. N. (2011). Sulfated polysaccharides from brown seaweeds *Saccharina japonica* and *Undaria pinnatifida*: Isolation, structural characteristics, and antitumor activity. *Carbohydrate Research*, 346(17), 2769–2776. <https://doi.org/10.1016/j.carres.2011.09.034>
- von Bülow, R., Schmidt, B., Dierks, T., von Figura, K., & Usón, I. (2001). Crystal Structure of an Enzyme-Substrate Complex Provides Insight into the Interaction between Human Arylsulfatase A and its Substrates During Catalysis. *Journal of Molecular Biology*, 305(2), 269–277. <https://doi.org/10.1006/jmbi.2000.4297>
- Wang, M., Hu, C., Barnes, B. B., Mitchum, G., Lapointe, B., & Montoya, J. P. (2019). The great Atlantic Sargassum belt. *Science*, 365(6448), 83–87. <https://doi.org/10.1126/science.aaw7912>
- Wang, Q., Garrity, G. M., Tiedje, J. M., & Cole, J. R. (2007). Naïve Bayesian classifier for rapid assignment of rRNA sequences into the new bacterial taxonomy. *Applied and Environmental Microbiology*, 73(16), 5261–5267. <https://doi.org/10.1128/AEM.00062-07>

- Wegner, C.-E., Richter-Heitmann, T., Klindworth, A., Klockow, C., Richter, M., Achstetter, T., ... Harder, J. (2013). Expression of sulfatases in *Rhodopirellula baltica* and the diversity of sulfatases in the genus *Rhodopirellula*. *Marine Genomics*, *9*, 51–61. <https://doi.org/10.1016/j.margen.2012.12.001>
- White Jr., W. J., Schray, K. J., Legler, G., & Alhadeff, J. A. (1987). Further studies on the catalytic mechanism of human liver  $\alpha$ -L-fucosidase. *Biochimica et Biophysica Acta (BBA) - Protein Structure and Molecular Enzymology*, *912*(1), 132–138. [https://doi.org/10.1016/0167-4838\(87\)90256-1](https://doi.org/10.1016/0167-4838(87)90256-1)
- Willats, W. G. T., Rasmussen, S. E., Kristensen, T., Mikkelsen, J. D., & Knox, J. P. (2002). Sugar-coated microarrays: A novel slide surface for the high-throughput analysis of glycans. *Proteomics*, *2*(12), 1666–1671. [https://doi.org/10.1002/1615-9861\(200212\)2:12<1666::AID-PROT1666>3.0.CO;2-E](https://doi.org/10.1002/1615-9861(200212)2:12<1666::AID-PROT1666>3.0.CO;2-E)
- Winn, M. D., Ballard, C. C., Cowtan, K. D., Dodson, E. J., Emsley, P., Evans, P. R., ... Wilson, K. S. (2011). Overview of the CCP4 suite and current developments. *Acta Crystallographica Section D: Biological Crystallography*, *67*(4), 235–242. <https://doi.org/10.1107/S0907444910045749>
- Yilmaz, P., Kottmann, R., Field, D., Knight, R., Cole, J. R., Amaral-Zettler, L., ... Glöckner, F. O. (2011). Minimum information about a marker gene sequence (MIMARKS) and minimum information about any (x) sequence (MIXS) specifications. *Nature Biotechnology*, *29*(5), 415–420. <https://doi.org/10.1038/nbt.1823>
- Yin, Y., Mao, X., Yang, J., Chen, X., Mao, F., & Xu, Y. (2012). DbCAN: A web resource for automated carbohydrate-active enzyme annotation. *Nucleic Acids Research*, *40*(W1), 445–451. <https://doi.org/10.1093/nar/gks479>
- Zaferani, S., Pérez-Rodríguez, M., & Biester, H. (2018). Diatom ooze—A large marine mercury sink. *Science*, *361*(6404), 797–800. <https://doi.org/10.1126/science.aat2735>
- Zayed, A., Muffler, K., Hahn, T., Rupp, S., Finkelmeier, D., Burger-Kentischer, A., & Ulber, R. (2016). Physicochemical and biological characterization of fucoidan from fucus vesiculosus purified by dye affinity chromatography. *Marine Drugs*, *14*(4), 1–15. <https://doi.org/10.3390/md14040079>
- Zhou, J., Mopper, K., Passow, U., & Zhou, J. (2011). The role of surface-active carbohydrates in the formation of transparent exopolymer of seawater particles by bubble adsorption. *Limnology*, *43*(8), 1860–1871.
- Zhou, J., Mopper, K., & Passow, U. (1998). The role of surface-active carbohydrates in the formation of transparent exopolymer particles by bubble adsorption of seawater.

## References

*Limnology and Oceanography*, 43(8), 1860–1871.

<https://doi.org/10.4319/lo.1998.43.8.1860>

Zhu, Y., Thomas, F., Larocque, R., Li, N., Duffieux, D., Cladière, L., ... McBride, M. J. (2017). Genetic analyses unravel the crucial role of a horizontally acquired alginate lyase for brown algal biomass degradation by *Zobellia galactanivorans*. *Environmental Microbiology*, 19(6), 2164–2181. <https://doi.org/10.1111/1462-2920.13699>

## Eidesstattliche Erklärung

### Versicherung an Eides Statt / *Affirmation in lieu of an oath*

gem. § 5 Abs. 5 der Promotionsordnung vom 18.06.2018 /  
*according to § 5 (5) of the Doctoral Degree Rules and Regulations of 18 June, 2018*

Ich / I, \_\_\_\_\_  
(Vorname / *First Name*, Name / *Name*, Anschrift / *Address*, ggf. Matr.-Nr. / *student ID no.*, if applicable)

versichere an Eides Statt durch meine Unterschrift, dass ich die vorliegende Dissertation selbständig und ohne fremde Hilfe angefertigt und alle Stellen, die ich wörtlich dem Sinne nach aus Veröffentlichungen entnommen habe, als solche kenntlich gemacht habe, mich auch keiner anderen als der angegebenen Literatur oder sonstiger Hilfsmittel bedient habe und die zu Prüfungszwecken beigelegte elektronische Version (PDF) der Dissertation mit der abgegebenen gedruckten Version identisch ist. / *With my signature I affirm in lieu of an oath that I prepared the submitted dissertation independently and without illicit assistance from third parties, that I appropriately referenced any text or content from other sources, that I used only literature and resources listed in the dissertation, and that the electronic (PDF) and printed versions of the dissertation are identical.*

Ich versichere an Eides Statt, dass ich die vorgenannten Angaben nach bestem Wissen und Gewissen gemacht habe und dass die Angaben der Wahrheit entsprechen und ich nichts verschwiegen habe. / *I affirm in lieu of an oath that the information provided herein to the best of my knowledge is true and complete.*

Die Strafbarkeit einer falschen eidesstattlichen Versicherung ist mir bekannt, namentlich die Strafandrohung gemäß § 156 StGB bis zu drei Jahren Freiheitsstrafe oder Geldstrafe bei vorsätzlicher Begehung der Tat bzw. gemäß § 161 Abs. 1 StGB bis zu einem Jahr Freiheitsstrafe oder Geldstrafe bei fahrlässiger Begehung. / *I am aware that a false affidavit is a criminal offence which is punishable by law in accordance with § 156 of the German Criminal Code (StGB) with up to three years imprisonment or a fine in case of intention, or in accordance with § 161 (1) of the German Criminal Code with up to one year imprisonment or a fine in case of negligence.*

\_\_\_\_\_  
Ort / *Place*, Datum / *Date*

\_\_\_\_\_  
Unterschrift / *Signature*